HR Wallingford
Working with water

Morlais Demonstration Zone

Coastal Processes

DER6261-RT001-R02-00 March 2020

Document information

Document permissions	Confidential - client
Project number	DER6261
Project name	Morlais Demonstration Zone
Report title	Coastal processes
Report number	RT001
Release number	R02-00
Report date	March 2020
Client	Menter Mon Morlais Limited
Client representative	James Orme
Project manager	Juliette Parisi
Project director	Graham Siggers

Document history

Date	Release	Prepared	Approved	Authorised	Notes
25 Mar 2020	02-00	MAK	JCP	GBS	
18 Mar 2020	01-00	NB/MK	JCP	GBS	

Document authorisation

Prepared

Approved

Authorised

Executive Summary

The Morlais Demonstration Zone (MDZ) is situated to the west of Holy Island on the Isle of Anglesey. The project will provide a consented area for the installation and commercial demonstration of multiple arrays of tidal energy devices, to a maximum installed capacity of 240 Megawatts (MW). The project will also provide permanent communal infrastructure through the provision of electrical infrastructure, including substation and onshore electrical cable route to grid connection. The project is being developed by Menter Môn Morlais Limited (hereafter “Menter Môn”).

The present study, which is based on and extends the previous work done in 2019 by HR Wallingford to assess tidal energy resources, was commissioned to provide the impact of the proposed development on coastal processes, including tidal currents, waves, and sediments. The results provide quantification of coastal process impacts as supplementary information to the Environmental Statement (ES) submitted in support of an application submitted in September 2019 for a Marine Licence under the Marine Planning and Coastal Access Act 2009 and a Transport and Works Act Order (TWAO).

HR Wallingford’s existing high resolution 2D (depth averaged) finite element model has been extensively validated in accordance with IEC TS 62600-201:2015. In particular the flow model is validated against 6 tide gauges (Gladstone Dock, Port St Mary, Workington, Barmouth, Holyhead and Trearddur Bay) and 4 ADCP datasets: location 1, location 2, location NE and location NW. All Mean Absolute Errors are between 4.5% and 6% of the peak currents measured, meeting the approximately 5% (“c. 5%”) recommended by the IEC TS 62600-201 guidelines.

The validated flow model was used to assess the direct impact of the worst case scenario (620 devices and the corresponding structures) on flow speeds. The difference in maximum speeds varies between a decrease of 0.7 m/s within the MDZ sub-zones and an increase of 0.3 m/s between the MDZ and the shore. The difference in average speeds is mostly a decrease up to 0.2 m/s within the MDZ sub-zones.

In order to assess the direct impact of the MDZ on the waves, a highly resolved SWAN wave model has been established. The wave model has been extensively validated for extreme wave conditions which have been measured by the SEACAMS wave buoy. In total, four storms were chosen to validate the wave model and predictions of Hs from the model have a Relative Bias (RB) of 0.9% to 1.5% and a Scatter Index (SI) of 13.7% to 14.3%. The wave model statistics meet the recommended RB up to 10% and a SI up to 20%, given by the Environment Agency guidelines.

The validated wave model was used to assess the direct impact of the worst case scenario (60 floating devices, 310 seabed-mounted devices and the corresponding structures) on wave heights. The differences in maximum Hs are mainly located within the MDZ and vary between a decrease of 0.4 m and an increase of 0.2 m.

The predicted changes to waves and flows are then used in a sediment transport model to assess the impact of the proposed development on sediment transport and in particular on key features such as the Gogarth Bay and Abraham’s Bosom sediment deposit zones; the South Stack Banner Bank and the pocket beaches on Holy Island. First, literature and data review were undertaken to assess the existing conditions.

The MDZ is located in an area where large parts of the coastline and seabed comprise exposed bedrock. The sediment modelling suggests that there is a northward potential residual transport to the west of Holy Island. Mobile areas of seabed include the “South Stack Banner Bank” and areas of sand waves to the north of this location.

The MDZ is predicted to have little impact on this residual sediment transport. There is some reduction of the residual transport over the sandwaves, which will move slightly slower as a result. Present day rates of movement of the sandwaves are about 30m per year (m/y), so a predicted 10 to 20% reduction in transport rate suggests a reduction of about 5m/y. This difference will not be discernible from the natural variation due to climatological variations. In addition this decrease may lead to a slightly different orientation of the South Stack banner bank. The offshore end may move slightly northward, but again, this is likely to be within the natural variation of this morphological feature, which is observed to move between consecutive surveys. In addition there may also be a small increase to the sediment volume of the bank, originating from sand deposits in front of Gogarth bay.

The changes in the wave height due to the MDZ lead to small changes in the littoral drift, the longshore residual sediment transport in Abraham's Bosom and Gogarth Bay. In Gogarth bay, the residual drift northwards is predicted to increase under predominant conditions, which implies that the rocky nature of the bay will be maintained with the devices in place.

In Abraham's Bosom, the wave driven sediment transport reduces, leading to a potentially more stable small pocket beach in this bay. There may be changes in the beach orientation, but these will be small compared to the natural changes due to climatological variations.

No changes in the sediment transport were predicted by the model outside of the direct neighbourhood of the MDZ.

Abbreviations

ADCP	Acoustic Doppler Current Profiler
CD	Chart Datum
EIA	Environmental Impact Assessment
LAT	Lowest Astronomical Tide
m	metre(s)
MAE	Mean Absolute Error
MBES	Multibeam Echosounder
MDZ	Morlais Demonstration Zone
MSL	Mean Sea Level
NOAA	National Oceanographic and Atmospheric Administration
NCDC	National Climatic Data Center
NRW	Natural Resources Wales
OD	Ordnance Datum
UTM	Universal Transverse Mercator
WCMC	Wales Coastal Monitoring Centre

Contents

Figures

Tables

1. Introduction

1.1. Background

The Morlais Demonstration Zone (MDZ) is situated to the west of Holy Island on the Isle of Anglesey. The MDZ will incorporate multiple tidal current device array projects from different project owners and with different technologies. Each will occupy a sub-zone (a geographically defined area of seabed) and will have a stated maximum capacity. Figure 1.1 shows the MDZ and eight subzones.

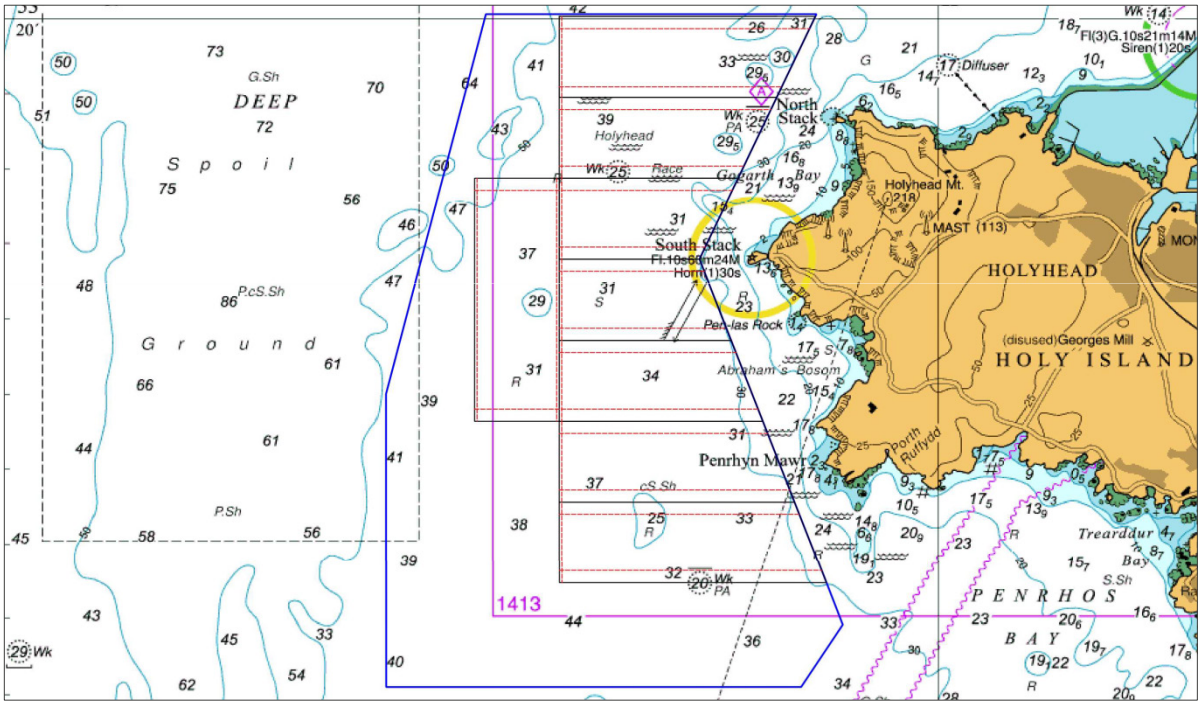

Figure 1.1: Morlais Demonstration Zone (MDZ), showing the eight proposed Sub-Zones

Source: UKHO (Chart), Menter Môn (Sub-Zones)

Interactions between projects will be governed by an agreement, which among other things will include details on the permitted levels of energy extraction for each project. The current form of agreement governing project interactions is the Welsh Waters Operators Agreement as provided by The Crown Estate. Owing to the close proximity of projects within the MDZ a specific Inter-Operators Agreement is being drafted which aims to manage the interactions in tidal energy resource extractions.

The present study, which is based on and extends the previous work done in 2019 to assess tidal energy resources, was commissioned to provide the impact of the proposed development on coastal processes, including tidal currents, waves, and sediments. The results provide quantification of coastal process impacts as supplementary information to the Environmental Statement submitted in September 2019.

HR Wallingford used for this study its existing high resolution 2D (depth averaged) finite element flow model, which has been extensively validated and in accordance with IEC TS 62600-201:2015. In particular the flow model has been calibrated against six tide gauges (Gladstone Dock, Port St Mary, Workington, Barmouth,

Holyhead and Trearddur Bay) and data from four Acoustic Doppler Current Profilers (ADCPs). A highly resolved SWAN wave model has been established and validated for this study to quantify potential changes to waves arising from the development. The predicted changes to waves and flows are then used in a sediment transport model (SISYPHE) to assess the impact of the proposed development on sediment transport and in particular on key features such as the Gogarth Bay and Abraham's Bosom sediment deposit zones; the South Stack Banner Bank and the pocket beaches on Holy Island.

1.2. Reference documents and data sources

This report should be read in conjunction with the following documents and data sets:

Table 1.1: Related HR Wallingford report

Reference	Title
DEM8387-RT001-R01	Morlais Demonstration Zone, Tidal Recource Modelling (2019)
Ocean Ecology Limited (2018)	Morlais Demonstration Zone (MDZ) Benthic Ecology Characterisation Survey 2018
Partrac (2018)	Morlais Demonstration Zone (MDZ) Hydrographic & Geophysical Survey
ADCP North West	Bangor University moored ADCP data, West Anglesey Demonstration Zone (North West), West Anglesey, 25/03/2015 to 28/05/2015
ADCP North East	Bangor University moored ADCP data, West Anglesey Demonstration Zone (North East), West Anglesey, 19/09/2014 to 03/11/2014
SEACAMS wave buoy	SEACAMS Datawell Waverider Mark III

1.3. Coordinate system and conventions

The coordinate system used in the report is WGS84 UTM Zone 30N. All depths/levels in this report are stated relative to Ordnance Datum (OD).

In accordance with normal meteorological and oceanographic conventions, winds come from the specified direction, while currents and water displacements are towards the specified direction.

1.4. Structure of the report

The report first introduces in Section 3 the worst case scenarios modelled and characteristics of the tidal energy devices. Next, Section 4 and Section 5 describe the setup, validation, results of the flow and wave modelling, respectively. Section 6 presents how the flow and wave modelling were combined in order to model the sediment transport.

2. Model bathymetry

Refined bathymetry data were delivered by SeaZone based on their Trudepth points data product, which itself is based on various UK Hydrographic Office surveys, supplemented by Charted Points where required. Local bathymetry survey data provided by Menter Môn (2015) and Partrac (2018) were also incorporated in the final seabed mapping. The survey data were received in Ordnance Datum (OD). The TruDepth, Charted Points and UKHO data were received in CD (Chart Datum) and were converted to OD by subtracting 3.05 m (the conversion for Holyhead).

Additionally LiDAR data were sourced from the Lle Geo-portal (Welsh Government and Natural Resources Wales) for a number of locations. These data were downloaded on a 2 m grid and were processed to remove areas of data return for the sea surface (keeping data for land / intertidal). UKHO MBES (2018) data was additionally used to represent bathymetry in the Menai Strait.

Figure 2.1 shows the coverage of each source of bathymetry data. Figure 2.2 shows the full extent of the tidal and sediment model bathymetry.

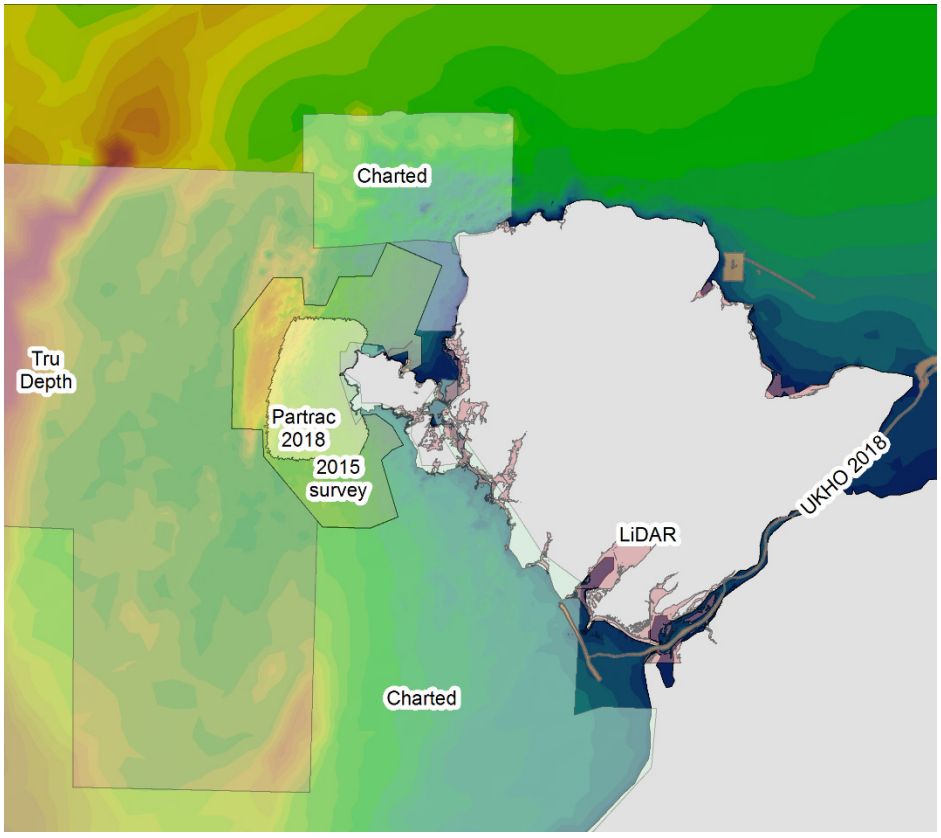

Figure 2.1: Bathymetry data coverage

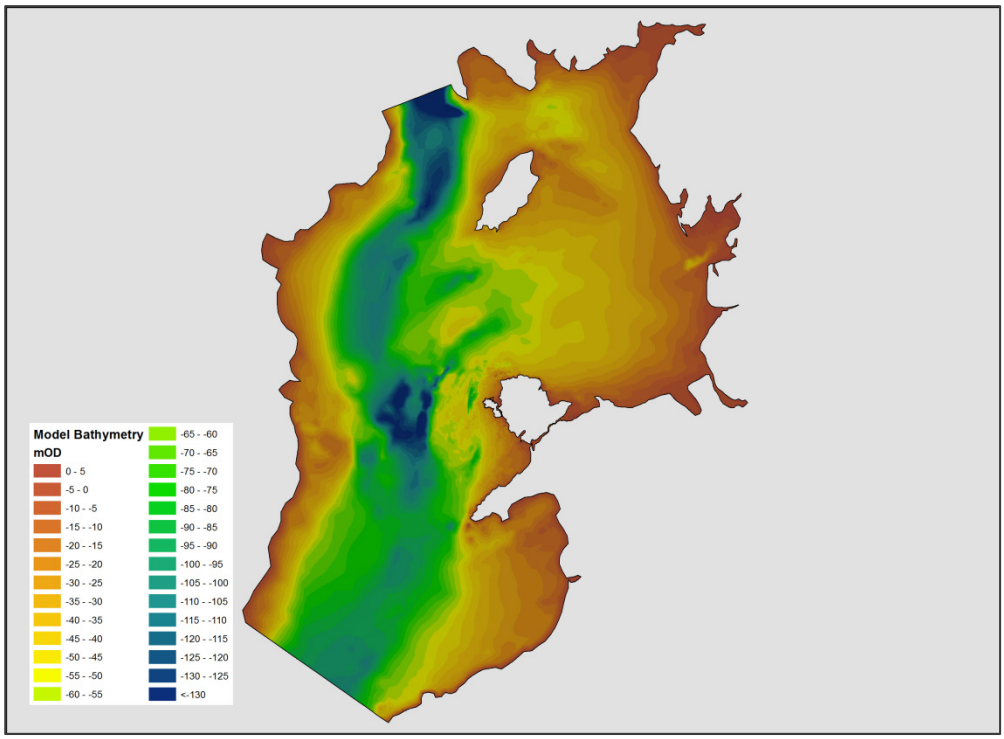

Figure 2.2: Full extent of model bathymetry

3. Tidal stream devices

Two types of tidal stream devices are considered in this study: seabed-mounted tidal devices and floating tidal devices. Two scenarios have been modelled: the worst case scenario in terms of impact on the tidal flows and the worst case scenario in terms of impact on the waves.

The characteristics for the different tidal devices and their locations are described in the following sub-sections.

3.1. Scenarios

3.1.1. Impact on tidal flows

The scenario assessed in terms of impact on tidal flows is the use of 620 seabed-mounted devices. This represents a worst case in terms of the reduction to current speeds caused by the tidal turbines arrays, their support structures, and associated structures.

The scenario with 620 seabed-mounted devices is illustrated in Figure 5.3 and includes the following:

- 112 electrical seabed hubs;
- 8 surface piercing electrical hubs, each of 6 m diameter;
- Rock bag protection along 9 cable routes.

Details of the method used to represent devices and structures in the flow model are given in Section 4.4.1.

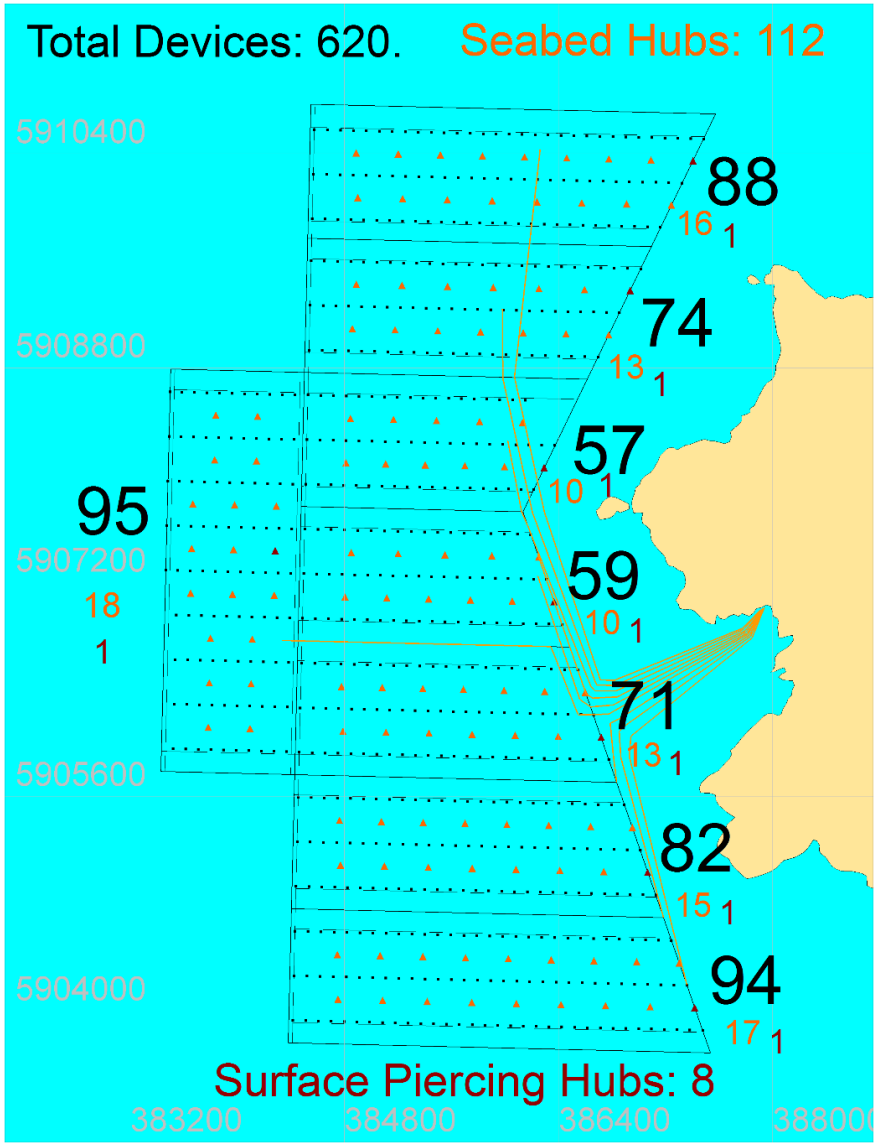

Figure 3.1: MDZ layout (scenario) for assessing impact on tidal currents

3.1.2. Impact on waves

The scenario represented to assess the potential impacts of the devices on waves includes the use of 60 floating devices located in the southern part of the Morlais Development Zone (MDZ). These floating devices cause more of a blockage to incident wave energy than the seabed-mounted devices and so this represents a worst case in terms of the direct impact on waves.

The impact on waves from the reduction of flow speeds caused by the array is also assessed. However this is done by using the changes to flow fields associated with 620 seabed-mounted devices.

The scenario for the assessing the direct impact on waves is illustrated in Figure 3.2 and includes the following:

- 60 floating devices;
- 310 seabed-mounted devices;
- 60 electrical seabed hubs;
- 8 surface piercing hubs.

Details of the method used to represent devices and structures in the wave model are given in Section 5.5.1.

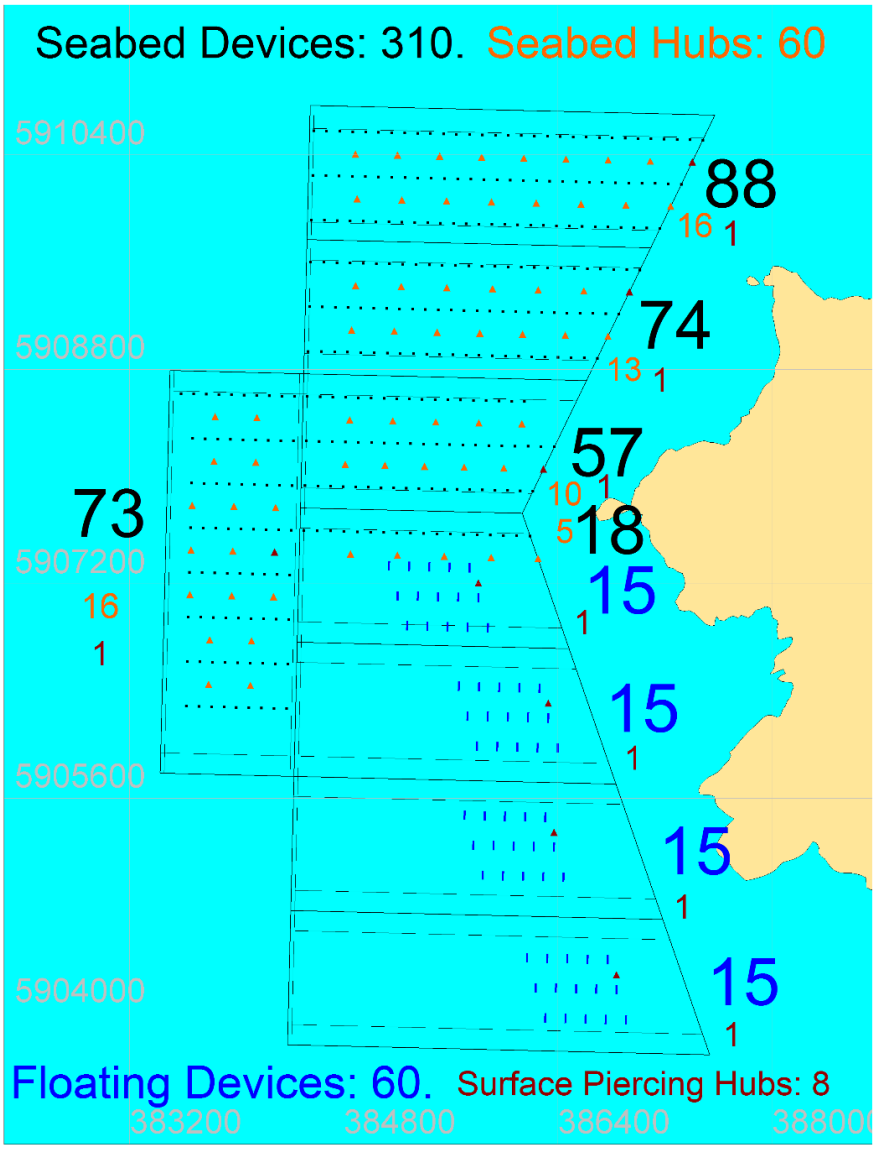

Figure 3.2: MDZ layout (scenario) for assessing impact on waves

3.2. Characteristics of seabed-mounted devices

The sea bed turbine characteristics are given in Table 3.1 below, with thrust and electrical power curves provided in Figure 3.3 and Figure 3.4 respectively.

Table 3.1: Sea bed Turbine Characteristics

Characteristic	Assumed Value
Rotor diameter (D)	16.13 m
Rated flow speed	2.015 m/s
Cut-in flow speed	0.5 m/s
Rated mechanical (electrical) power	429 kW (387 kW)
Power Curve	Variable with flow speed
Thrust Curve	Variable with flow speed
Position in water column	Mid depth

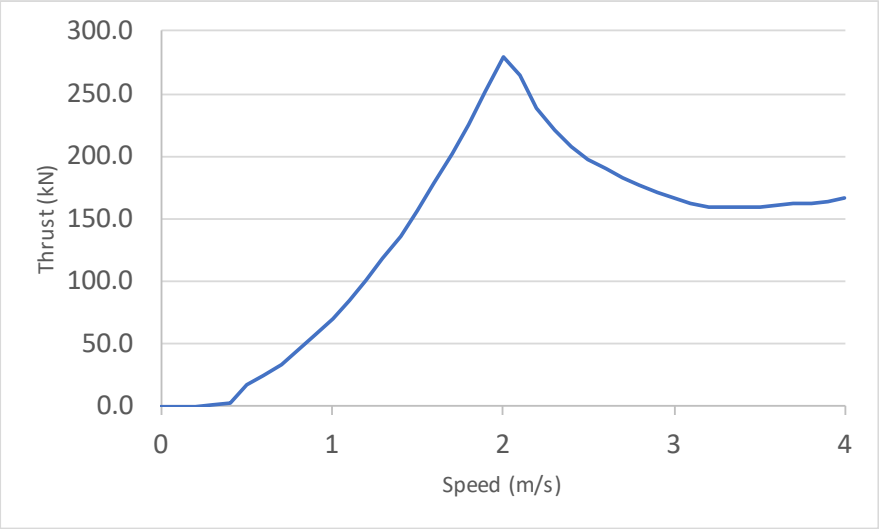

Figure 3.3: Thrust curve for seabed-mounted devices

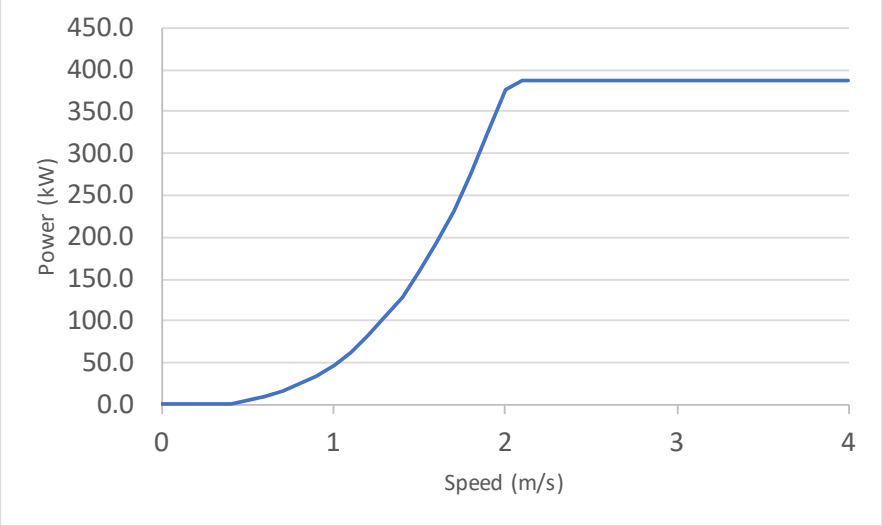

Figure 3.4: Electrical power curve for seabed-mounted devices

3.3. Characteristics of the floating devices

The Orbital device shown in the Figure 3.5, Figure 3.6 and Figure 3.7 below is implemented in the model for assessing the impact on waves. It is represented as an obstacle in the model and details of the method is given in Section 5.5. The device has the following dimensions:

- 20 m Rotor diameter
- 73 m long
- float extending to 2.5 m below the waterline.

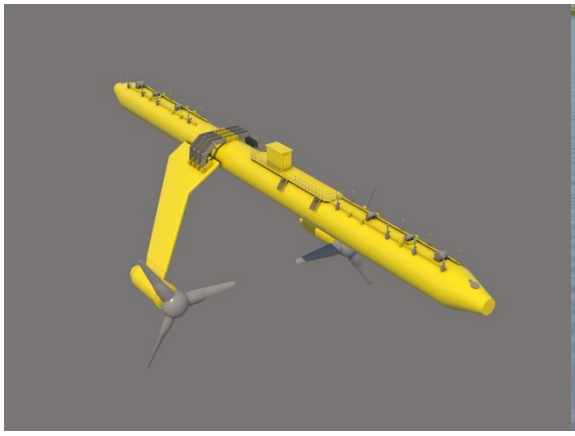

Figure 3.5: Orbital floating device (1)

Figure 3.6: Orbital floating device (2)

Source: Menter Môn

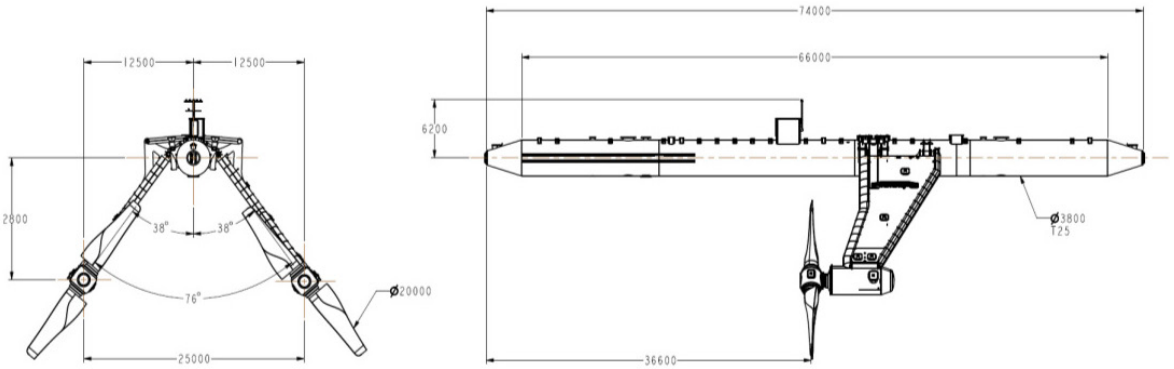

Figure 3.7: Orbital floating device dimensions

Source: Menter Môn

4. Hydrodynamic modelling (flows)

4.1. Methodology

The modelling is based on HR Wallingford's existing and well validated Irish Sea tidal flow model. This existing model is based on the 2D depth averaged flow component of the open source TELEMAC suite of scientific solvers, TELEMAC-2D. It has previously been used to provide rely-upon information for projects for various industries (e.g. nuclear, renewable energy, infrastructure, defence).

The flow modelling work described in this report expands on the previous studies done for Menter Môn (Ref. 9). The model was updated and further validated in order to model the worst case scenario of 620 devices (240 MW).

4.2. Hydrodynamic model Set-up

4.2.1. Hydrodynamic model mesh

The existing model, covering the Irish Sea (see Figure 4.1), has 395864 nodes and 782622 elements . The mesh resolution is 10 m in all zones of the MDZ and also along the cable routes (see Figure 4.2).

The resolution near beaches of interest (where the bathymetry was updated with LIDAR data, shown in Figure 2.1) was increased to 10-20 m. The mesh resolution grows gradually offshore, up to 10km near the southern open boundary.

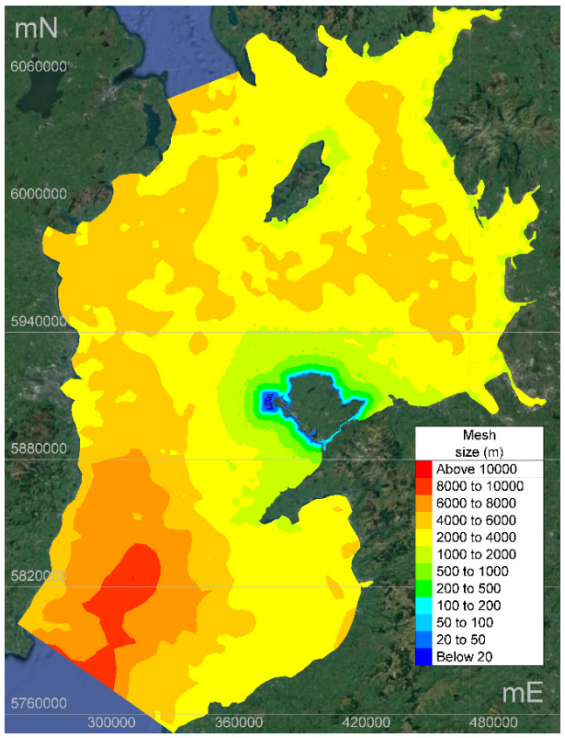

Figure 4.1: Extent of model and mesh resolution

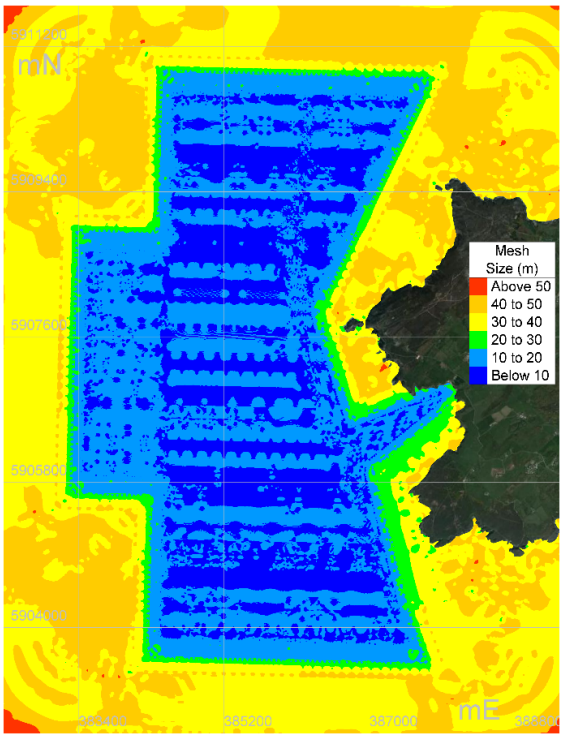

Figure 4.2: Model mesh in region of devices

4.2.2. Hydrodynamic model bathymetry

The bathymetry of the existing flow model was updated with the 2018 local survey carried out by Partrac (Ref. 15). The flow model bathymetry was also updated with LIDAR data along several beaches and with UKHO data in the Menai Strait (Section 2).

4.2.3. Hydrodynamic model boundary conditions

The 2D model is driven through its open boundaries, where the model extent opens up to the St George's Channel and the North Channel (south and north of the Irish Sea respectively). Tidal water levels have been computed based on the 12 harmonics available from the high resolution TPXO tidal model dataset distributed by the Oregon State University (http://volkov.oce.orst.edu/tides/tpxo8_atlas.html).

For the flow model validation (Section 4.3), spatially and time varying wind and pressure fields, obtained from ERA5 Reanalysis (Ref. 7), have been applied to the model. For the worst case scenario modelled (Section 4.4), the model is only driven by tidal water levels.

4.2.4. Hydrodynamic model parameters

In order to achieve the best fit of predicted data to the observed current and water level data described in Section 4.3, sensitivity tests to seabed friction coefficients were undertaken. Because comparisons are made against in-situ measurements in this case, the influence of the wind and the associated surge effects also contribute to the uncertainty and were assessed.

They parameters used are the following:

- The model friction was specified using the Nikuradse Roughness Length. The corresponding Chezy coefficient is given by the formula below (h is the water depth)

$$C = 7.83 \ln\left(12\frac{h}{k_s}\right)$$

  The friction varies spatially, with a roughness length varying from k_s of 0.2 m to the West of Anglesey to 0.035 m offshore.
- A constant turbulent viscosity was assumed: the flow is governed by the pressure gradient and the advection. This is usually used for modelling tide flow regime and especially for modelling oceanic circulation on a large scale. In 2D, this constant viscosity should include dispersion. After sensitivity tests, a velocity diffusivity of 2.0 m^2/s was selected.
- After sensitivity tests were undertaken a time step of 2.0 s was selected.

4.3. Hydrodynamic model validation

4.3.1. Previous flow model validation

HR Wallingford's existing high resolution 2D (depth averaged) finite element model has been extensively validated (Ref. 9) in accordance with IEC TS 62600-201:2015. In particular the flow model is validated against 6 tide gauges (Gladstone Dock, Port St Mary, Workington, Barmouth, Holyhead and Trearddur Bay) and 2 ADCPs, referred to as position 1 and position 2, provided by Mentor Môn in 2014 (Table 4.1, Figure 4.3).

The previous validation is very good, with a Mean Absolute Error about 6% of the peak current measured, meeting the guideline of approximately 5% (“c. 5%”) recommended by IEC TS 62600-201 (Ref 3).

4.3.2. Additional ADCP devices for further flow model validation

Two additional ADCP measurement datasets were made available for this assessment, which are referred to as position NE (North East) and position NW (North West). The coordinates of the previous and new ADCP devices are given in Table 4.1. and locations are plotted on Figure 4.3.

Table 4.1: Acoustic Doppler Current Profiler Locations

Position number	Latitude (decimal degrees)	Longitude (decimal degrees)	Bathymetry (m OD)
1	53.30413 N	4.71369 W	-39.6
2	53.29778 N	4.71558 W	-36.4
NE (North East)	53.30720 N	4.71871 W	-38.1
NW (North West)	53.28132 N	4.73792 W	-46.0

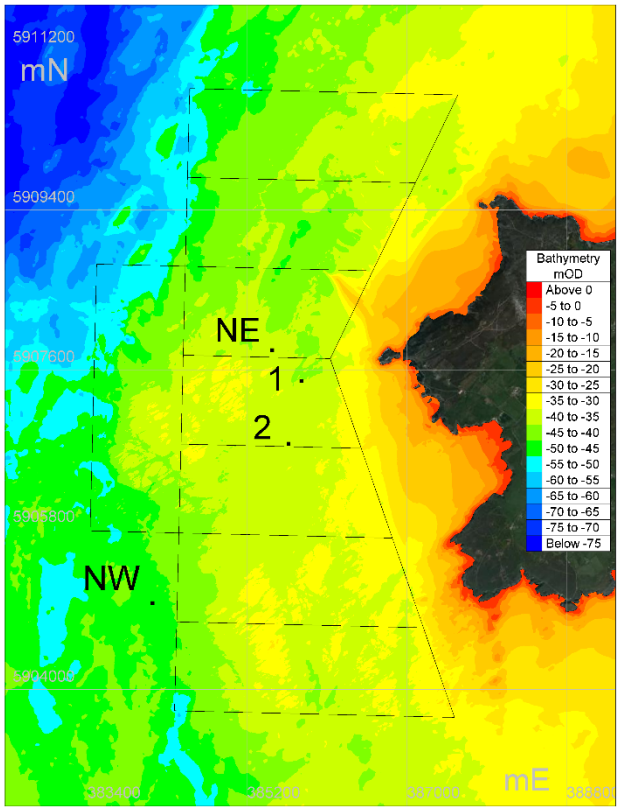

Figure 4.3: Locations of the four ADCP devices used for model validation

The model was run for two periods for comparison with the two new ADCP measurements:

- 49 days starting on 16 September 2014 for comparison with the North West ADCP (NW)
- 68 days starting on 21 March 2015 for comparison with the North East ADCP (NE).

The model bathymetry for these validation runs did not include the 2018 survey update (as the ADCP data were collected earlier). Instead, the 2015 local survey data was used as the date of this bathymetry was closest to the dates of the ADCP measurements.

4.3.3. Model validation, water levels

Figure 4.4 and Figure 4.5 below show comparisons of predicted water levels and measured water levels at ADCP NE and NW, for the whole period. Figure 4.6 and Figure 4.7 show the same comparison zooming in to a shorter period of time to show more detail. Winds and pressure fields were included in these model runs and the comparisons show modelled versus measured sea levels (i.e. without undertaking an harmonic analysis of the measured data).

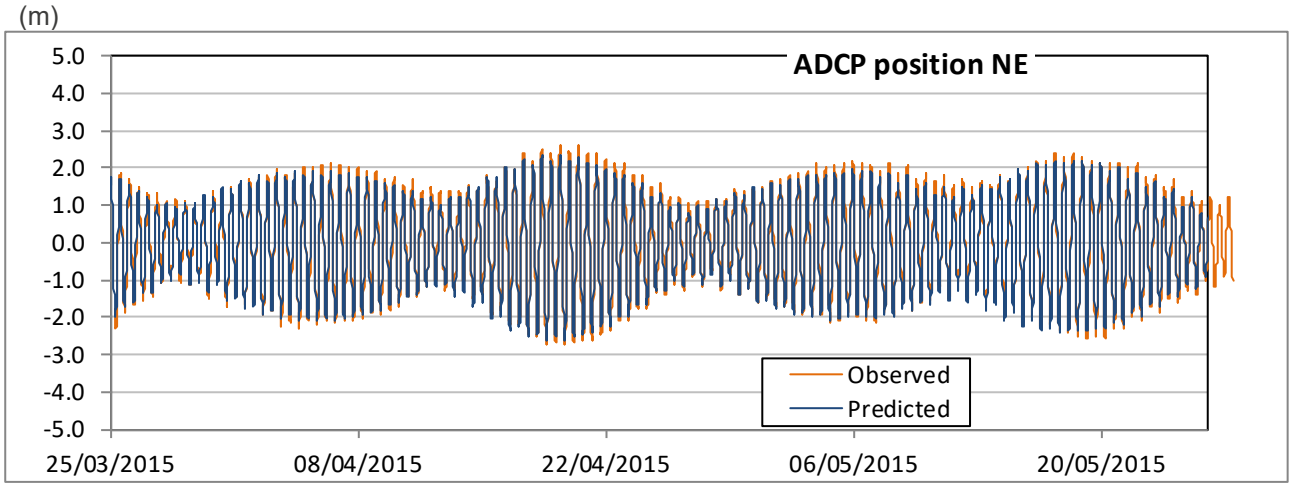

Figure 4.4: Overview comparison of model validation elevations at NE ADCP

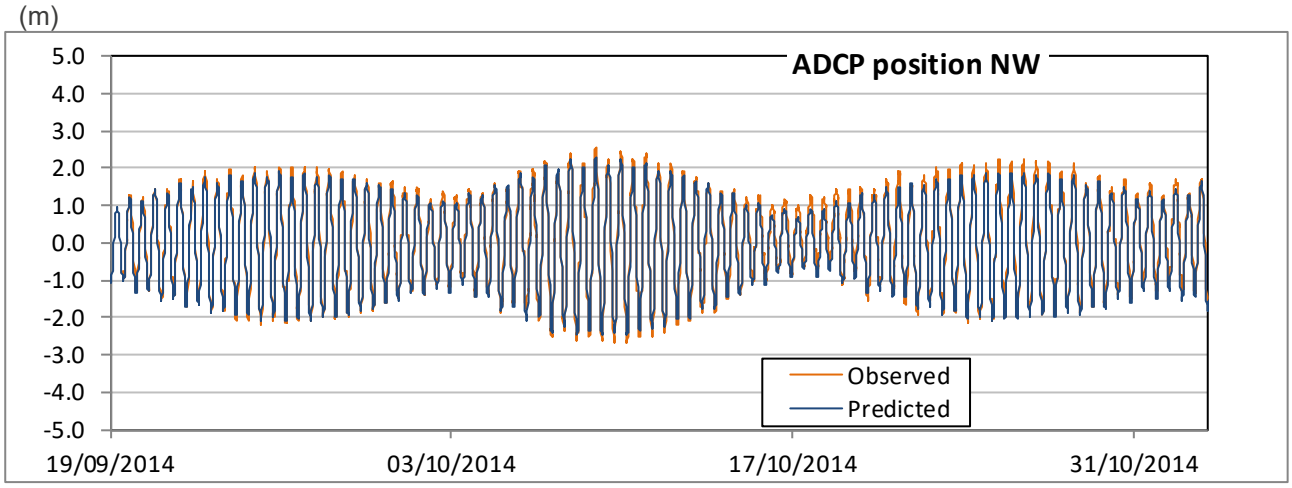

Figure 4.5: Overview comparison of model validation elevations at NW ADCP

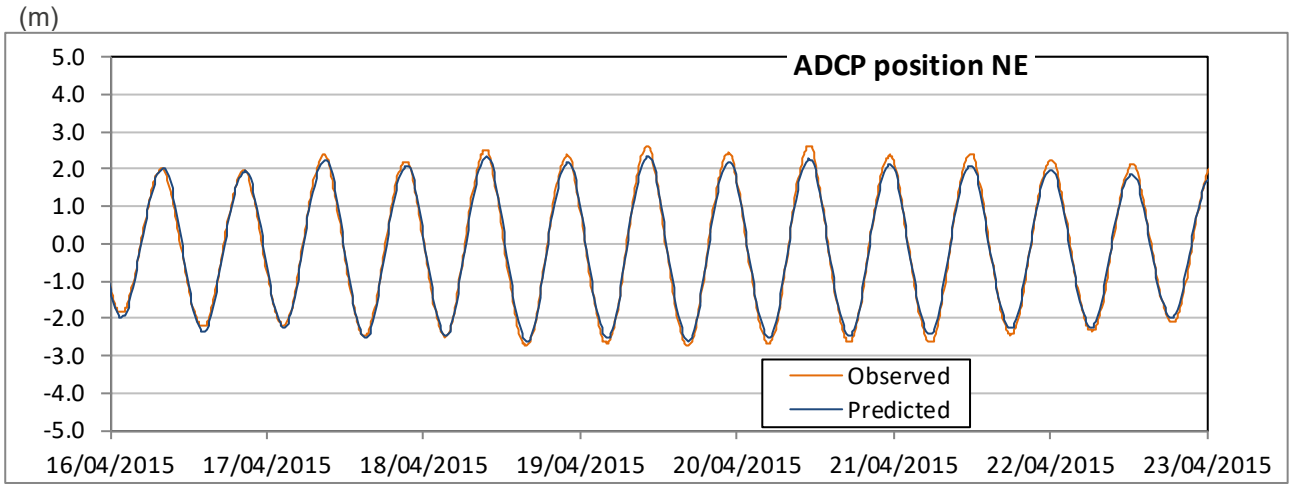

Figure 4.6: Highlighted comparison of model validation elevations at NE ADCP

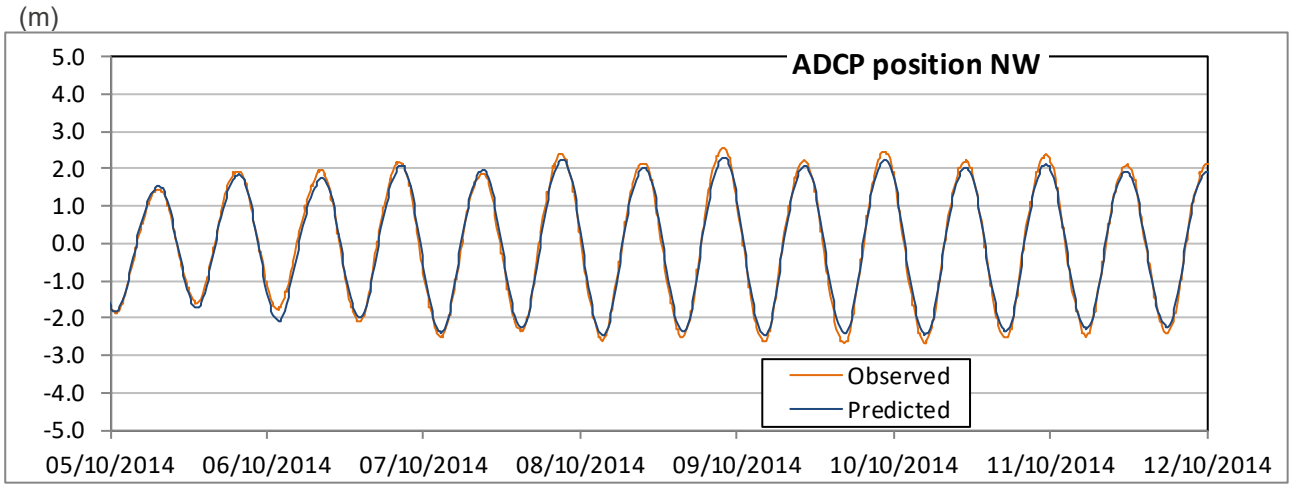

Figure 4.7: Highlighted comparison of model validation elevations at NW ADCP

A comparison of the model results to the ADCP water levels at the ADCP positions is reported in Table 4.2 as mean absolute error (MAE), normalised mean absolute error (NMAE) and phase shift (ΦE).

Table 4.2: Model validation results compared to observed water levels at NE and NW ADCP positions

Location	MAE (m)	NMAE (%)*	ΦE (min)
ADCP position NE	0.12	2.3	5
ADCP position NW	0.11	2.1	4

*Source: *MAE normalised by the maximum tidal range observed at location*

Performance of the flow model to predict water levels is very good, with levels within ± 0.1m, within 5% of spring tidal ranges and timing of high water within ± 15 minutes.

4.3.4. Model validation, current velocities

The model has been further validated against current velocities available from the two new ADCP deployments.

The comparison of the 2D model with the measured current speed and direction is shown in the next four figures, for the North East and the North West positions, as an overview over the whole period. Again, the predicted current patterns are shown in dark blue, the observed current patterns in orange.

Following these figures, four figures showing a shorter period are presented.

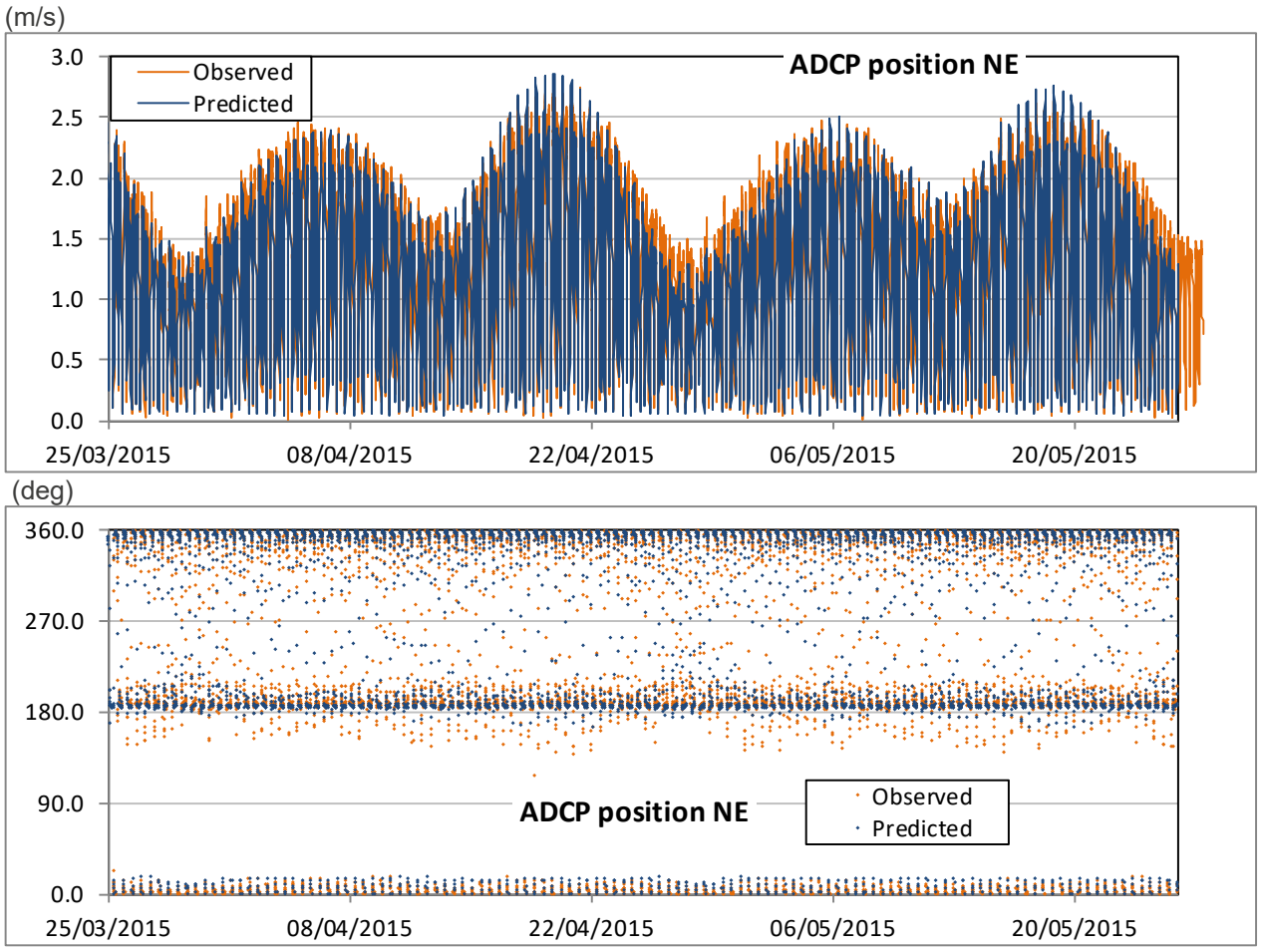

Figure 4.8: Overview comparison of model validation current speeds and directions at NE ADCP

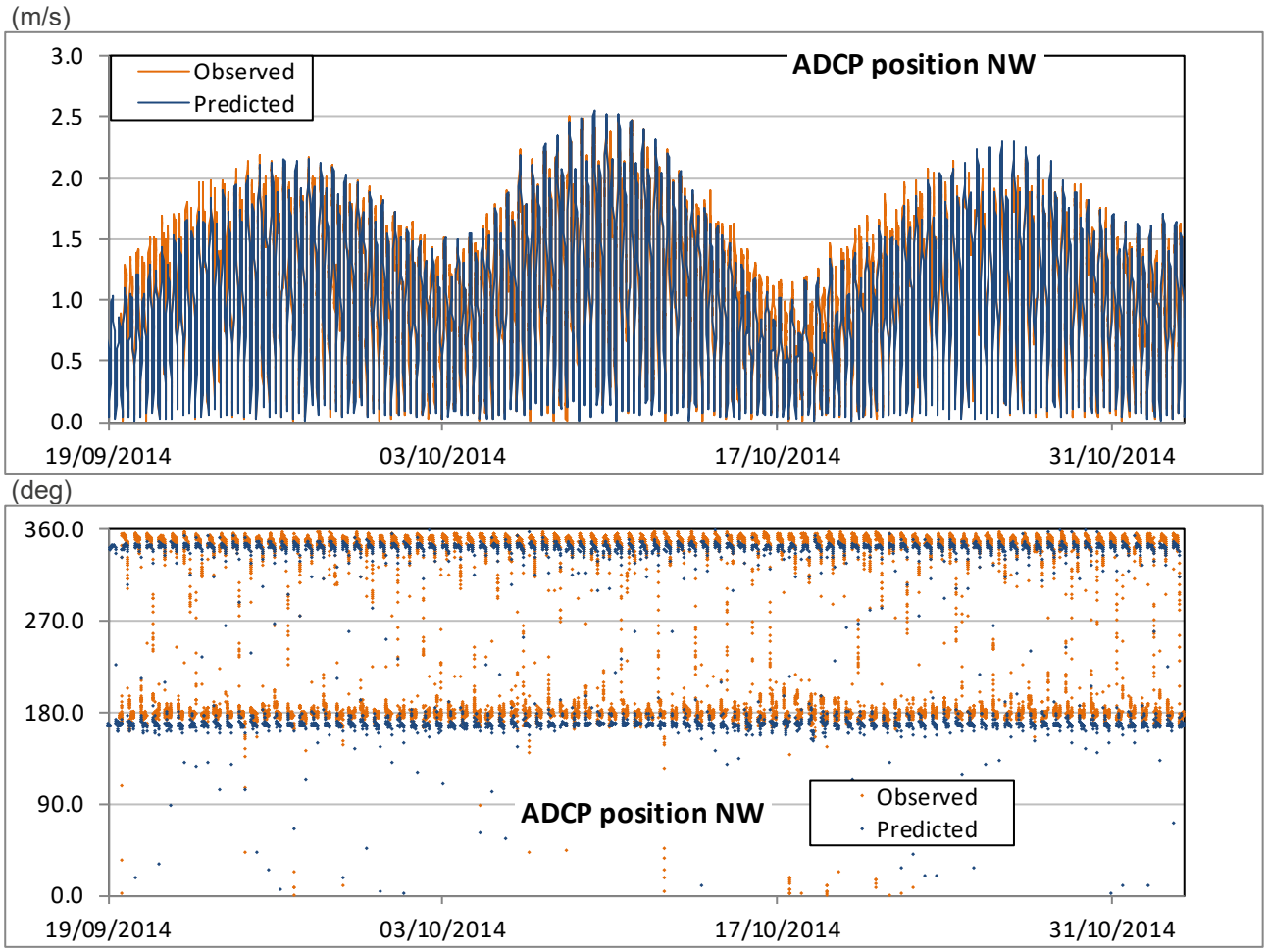

Figure 4.9: Overview comparison of model validation current speeds and directions at NW ADCP

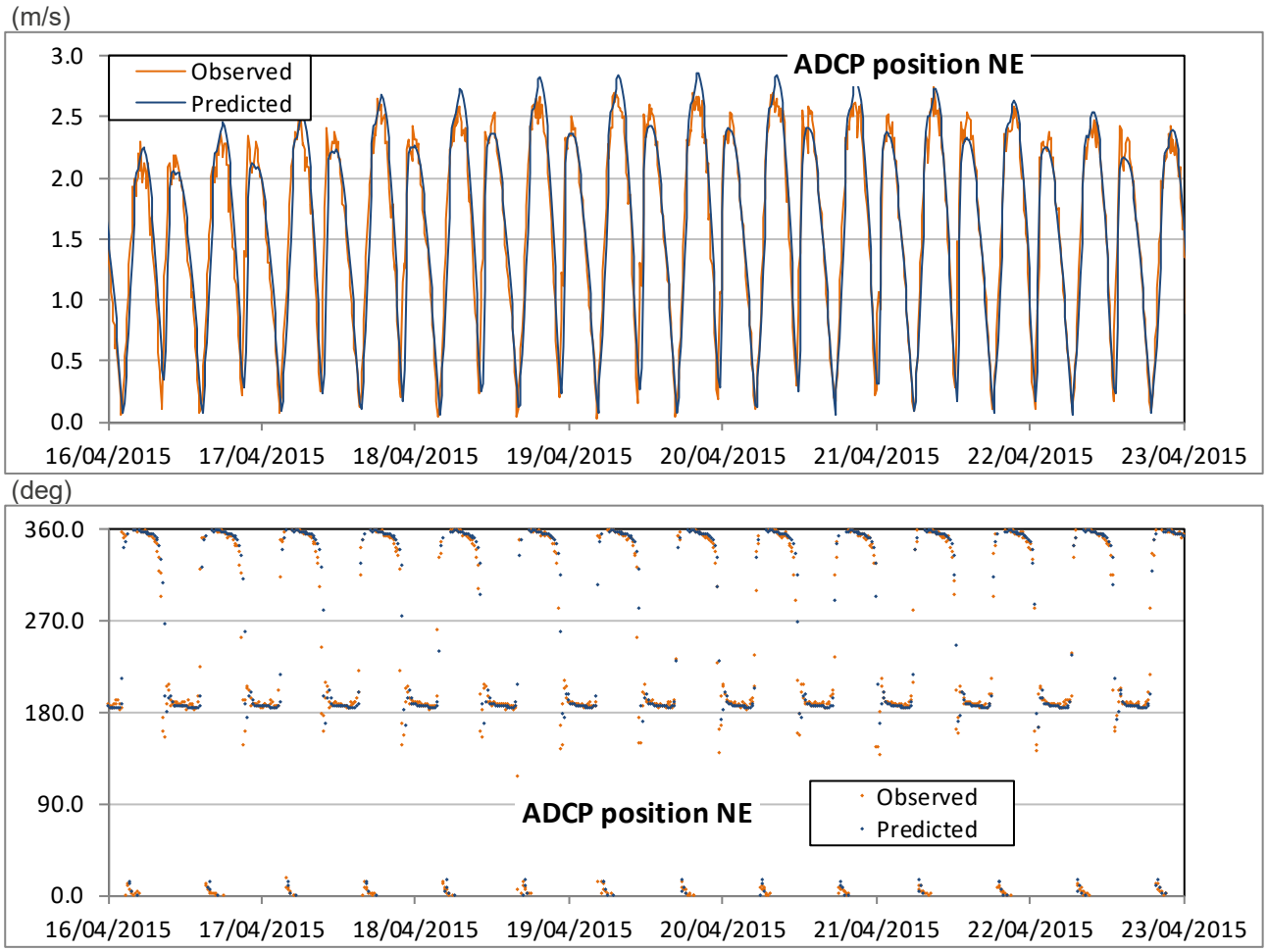

Figure 4.10: Highlighted comparison of model validation current speeds and directions at NE ADCP

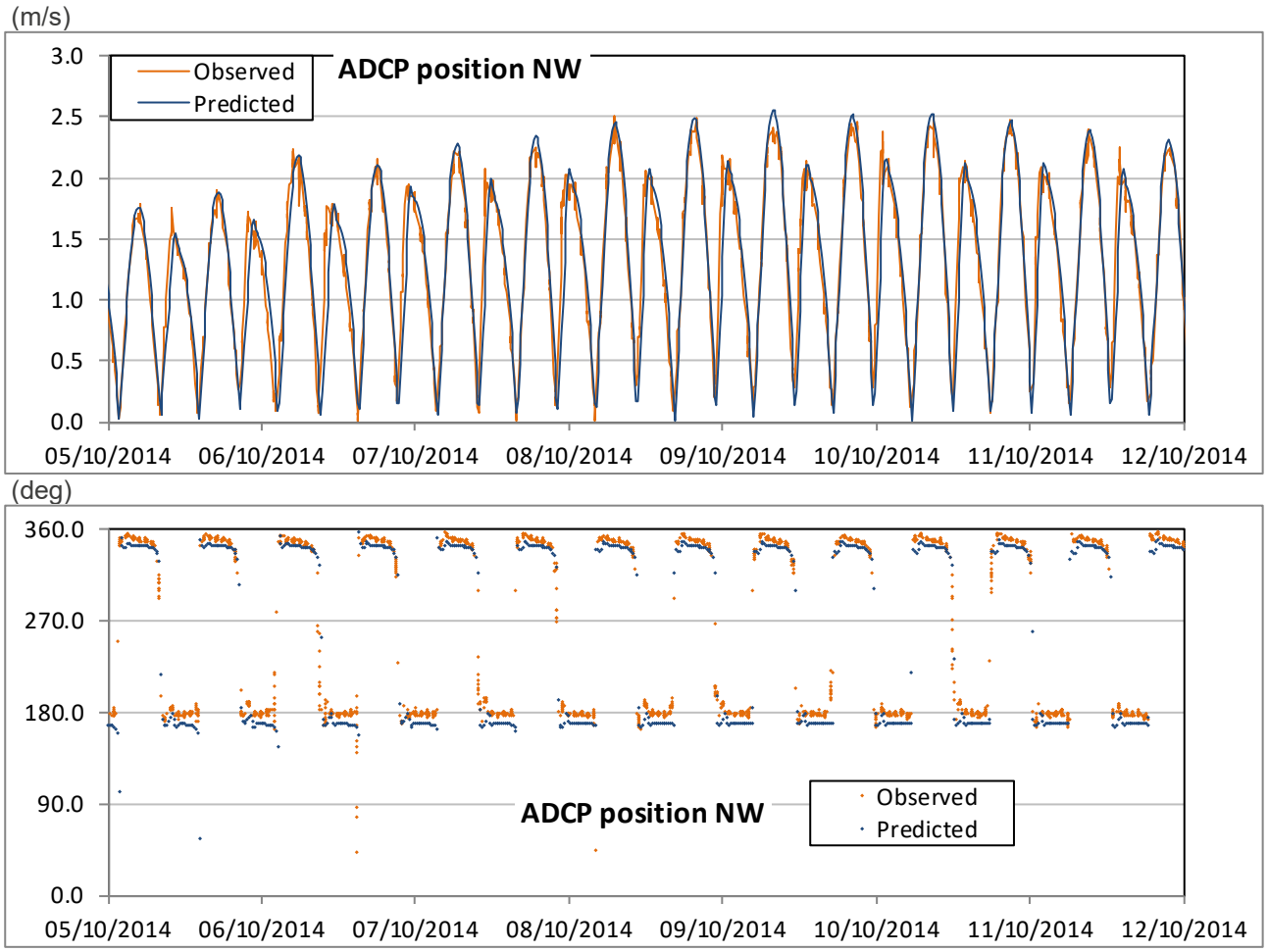

Figure 4.11: Highlighted comparison of model validation current speeds and directions at NW ADCP

The mean absolute error (MAE) on current speed), normalised mean absolute error (NMAE), tidal phase shift (ΦE), and current direction are reported in Table 4.3 below.

Table 4.3: Model validation results compared to observed data at NE and NW ADCP positions

Location	MAE (m/s)	NMAE(%)*	ΦE (min)	MAE (deg)
ADCP position NE	0.14	5.0	-13	16
ADCP position NW	0.11	4.5	-9	12

*Source: *MAE normalised by the maximum peak speed observed at location*

The performance of the flow model to predict tidal current speeds continues to meet the approximately 5% (“c 5%”) tolerance of observed current speeds, recommended by the IEC TS 62600-201 guidelines (Ref 3). Overall, the comparisons are very good and the flow model is considered fit for purpose.

4.3.5. Further model verification

Other types of analysis can be carried out to compare ADCP current velocities with model predictions. Two are presented here.

The first analysis is to create distributions of current speeds for the entire validation period, sorting speed values in bins (say 0.1 m/s in size). For consistency within this report, the predicted distribution is dark blue and the observed distribution is orange. Figure 4.12 relates to the North East ADCP; Figure 4.13 relates to the North West ADCP.

The analysis shows a good correspondence between predicted and observed, including the ranges of the current speeds contributing to the maximum power available (above 2.0 m/s), with the model results slightly higher at position NW and slightly lower at position NE.

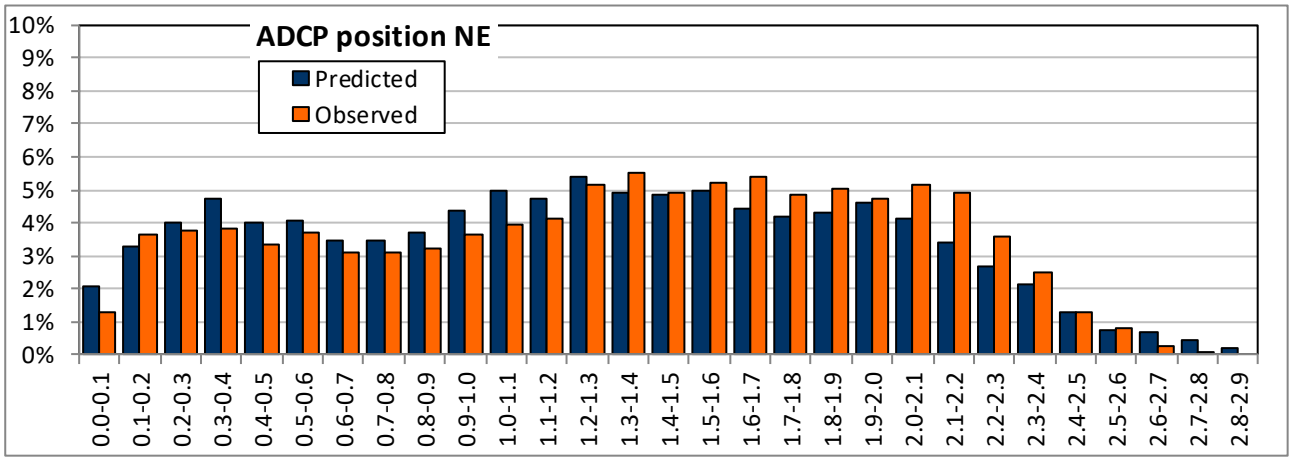

Figure 4.12: Model predicted and observed distribution of current speeds (m/s) at NE ADCP

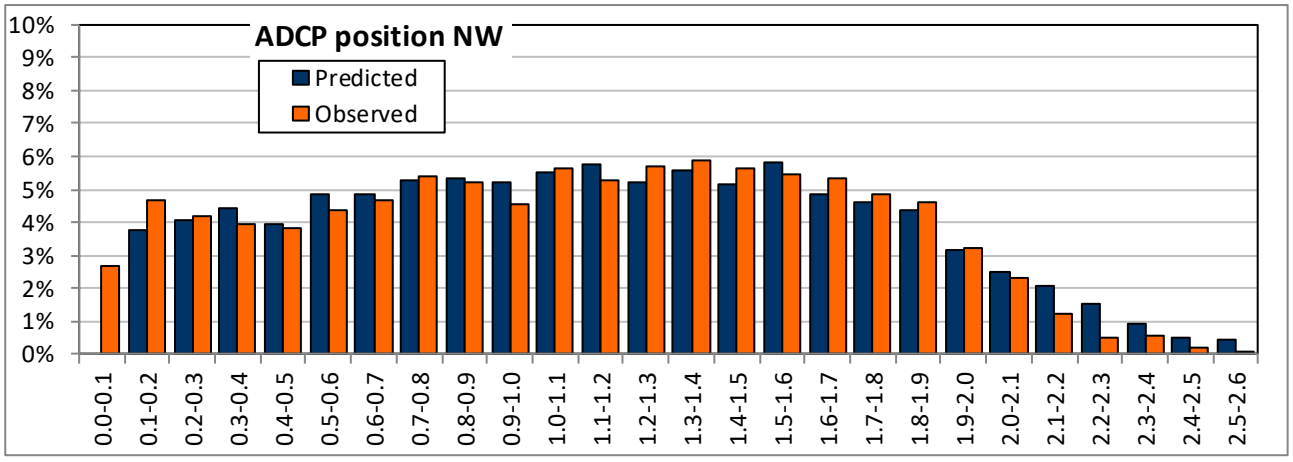

Figure 4.13: Model predicted and observed distribution of current speeds (m/s) at NW ADCP

The second analysis is to consider current tidal ellipses for the entire validation period. A tidal ellipse is a visual representation of the direction and strength of the flow throughout one or more tidal cycles and gives a good indication of the major current axis. The rings on the ellipse represent the current speed. Each point represents a time step in the model or an observation in the record. In this analysis the predicted current patterns are shown in dark blue, the observed current patterns in orange. Figure 4.14 relates to the North East ADCP; Figure 4.15 relates to the North West ADCP.

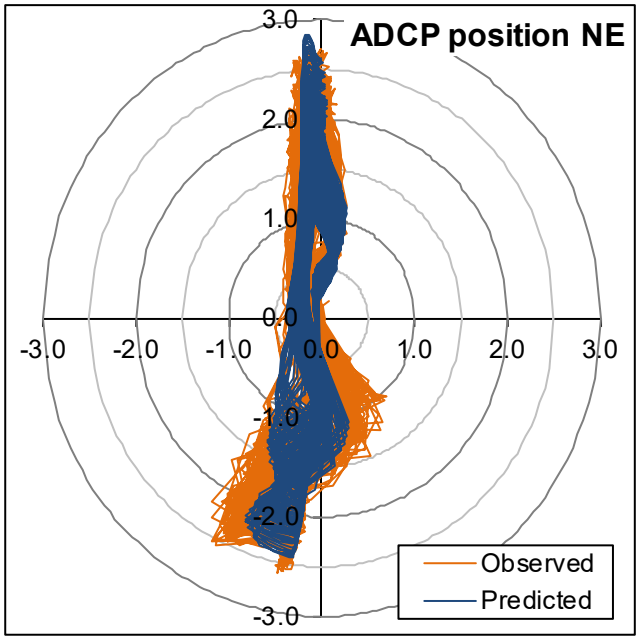

Figure 4.14: Predicted and observed tidal ellipse at NE ADCP

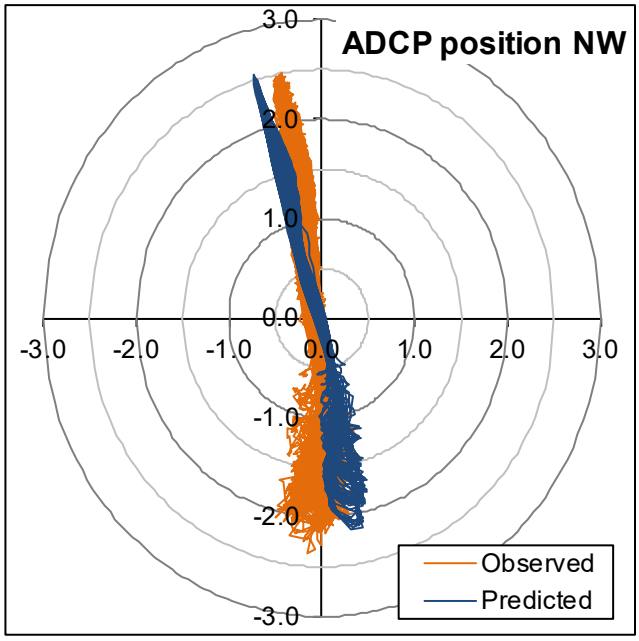

Figure 4.15: Predicted and observed tidal ellipse at NW ADCP

4.3.6. Hydrodynamic (flow) model validation conclusions

The flow model is validated against 6 tide gauges (Gladstone Dock, Port St Mary, Workington, Barmouth, Holyhead and Trearddur Bay) and 4 ADCP datasets, referred to as location 1, location 2, location NE and location NW.

All Mean Absolute Errors are between 4.5% and 6% of the peak currents measured, meeting the approximately 5% (“c. 5%”) recommended by the IEC TS 62600-201 guidelines (Ref 3).

The comparisons are very good and the flow model is considered fit for purpose.

4.4. Hydrodynamic (flow) model simulations

The flow model has been run for a 44 day period, starting on 15 November 2014 and for two cases:

- Baseline
- 620 seabed-mounted devices.

4.4.1. Representation of devices and corresponding structures

Each device and structure was modelled by applying a drag force at a single node at the location of the device.

Seabed-mounted tidal energy devices

The triangular finite element mesh used to represent the device area is further refined to provide a detailed representation of the tidal arrays and high-resolution flow information in the area of interest. The size of the

elements is approximately 10 m in the immediate vicinity of each individual device. An example of the mesh near tidal arrays is given in the Figure 4.16 below.

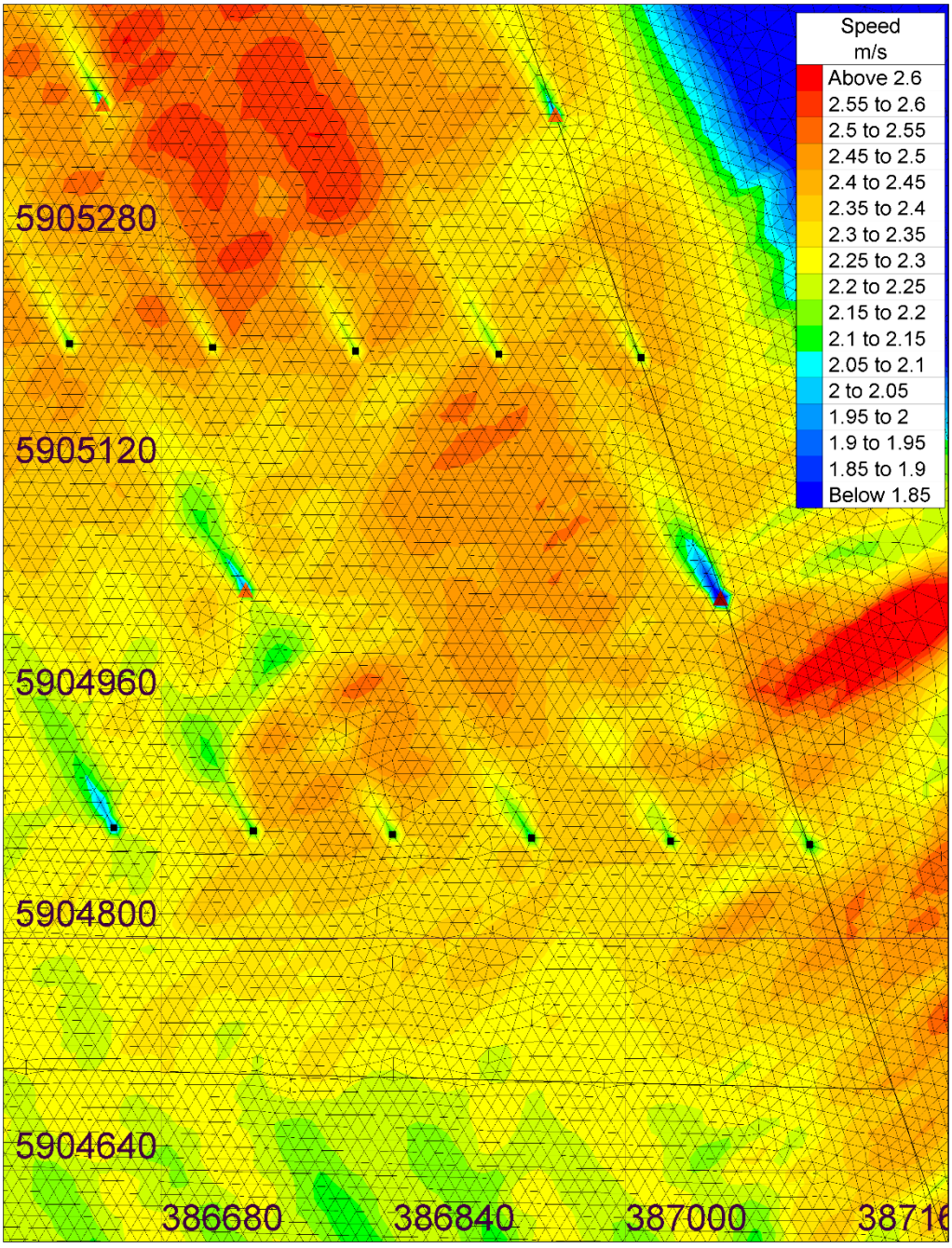

Figure 4.16: Flow model mesh near tidal arrays

The effect of the structures and rotor blades on the surrounding flows is simulated by applying sink terms F_x and F_y in the following two momentum equations on each set of model grid points representing a tidal device.

$$\rho h\frac{\partial u}{\partial t}+\rho hu\frac{\partial u}{\partial x}+\rho hv\frac{\partial u}{\partial y}=-\rho gh\frac{\partial (h+b)}{\partial x}+\frac{\partial}{\partial x}\left[h\nu_e\frac{\partial u}{\partial x}\right]+\frac{\partial}{\partial y}\left[h\nu_e\frac{\partial u}{\partial y}\right]+hF_x$$

$$\rho h\frac{\partial v}{\partial t}+\rho hu\frac{\partial v}{\partial x}+\rho hv\frac{\partial v}{\partial y}=-\rho gh\frac{\partial (h+b)}{\partial x}+\frac{\partial}{\partial x}\left[h\nu_e\frac{\partial v}{\partial x}\right]+\frac{\partial}{\partial y}\left[h\nu_e\frac{\partial v}{\partial y}\right]+hF_y$$

$$F_e+F_d=hA\sqrt{F_x^2+F_y^2}$$

Where *A* is the mesh element area and *h* is the water depth.

The total drag force is the sum of the drag caused by the device itself (F_e) and the drag due to the support structure (F_d).The device developer supplies an estimate of the mean structural drag force and rotor thrust figures. These are parameterised as sink terms proportional to either the current velocity squared, for the drag force, or cubed, for the power.

The drag force formula applied in the flow model to represent the seabed-mounted device support structure (Figure 6.17)is given below. The corresponding section area *S* is 44.4 m2 and the drag coefficient C_d is 0.305.

$$F_d=\frac{1}{2}\rho U^2SC_d$$

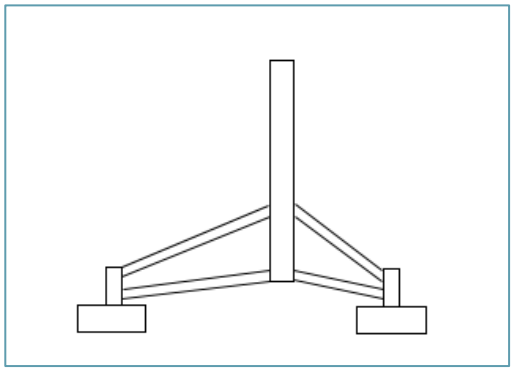

Figure 4.17: Support structure for the seabed mounted devices

- F_d is the drag force (kN);
- ρ is the water density (kg/m3);
- *U* is the depth-averaged current speed (m/s) 75m upstream;
- *S* is the surface area used for energy extraction (m2);
- C_d is the efficiency coefficient supplied by the device developer.

The power extraction is simulated in the model by applying another sink term F_e in the momentum equation, distributed to each set of model grid points representing the rotor blades. This term is based upon the power thrust curve, given by the device developer (Figure 3.3).

Characteristics of the seabed mounted devices used for flow model worst case scenarios are described in Section 5.

Seabed electrical hubs

Seabed electrical hubs are cuboid (10m x 10m x 8m) which are represented in the model with the drag force formula given above, where the section area *S* is 80 m^2 and the drag coefficient C_d is 1.5.

Surface piercing electrical hubs

Surface piercing electric hubs are a 6m diameter (*D*) pile throughout the water column. They are also represented in the flow model with the drag force where the section area *S* is *Dh* and the drag coefficient C_d is 1.0.

4.4.2. Modelled power extraction

The model was run for the same 44 day period as for the previous work (Ref 9) and the results were analysed for a full lunar month (29.5 days). The full model results showing simulated electrical power extraction is shown in Figure 4.18 below.

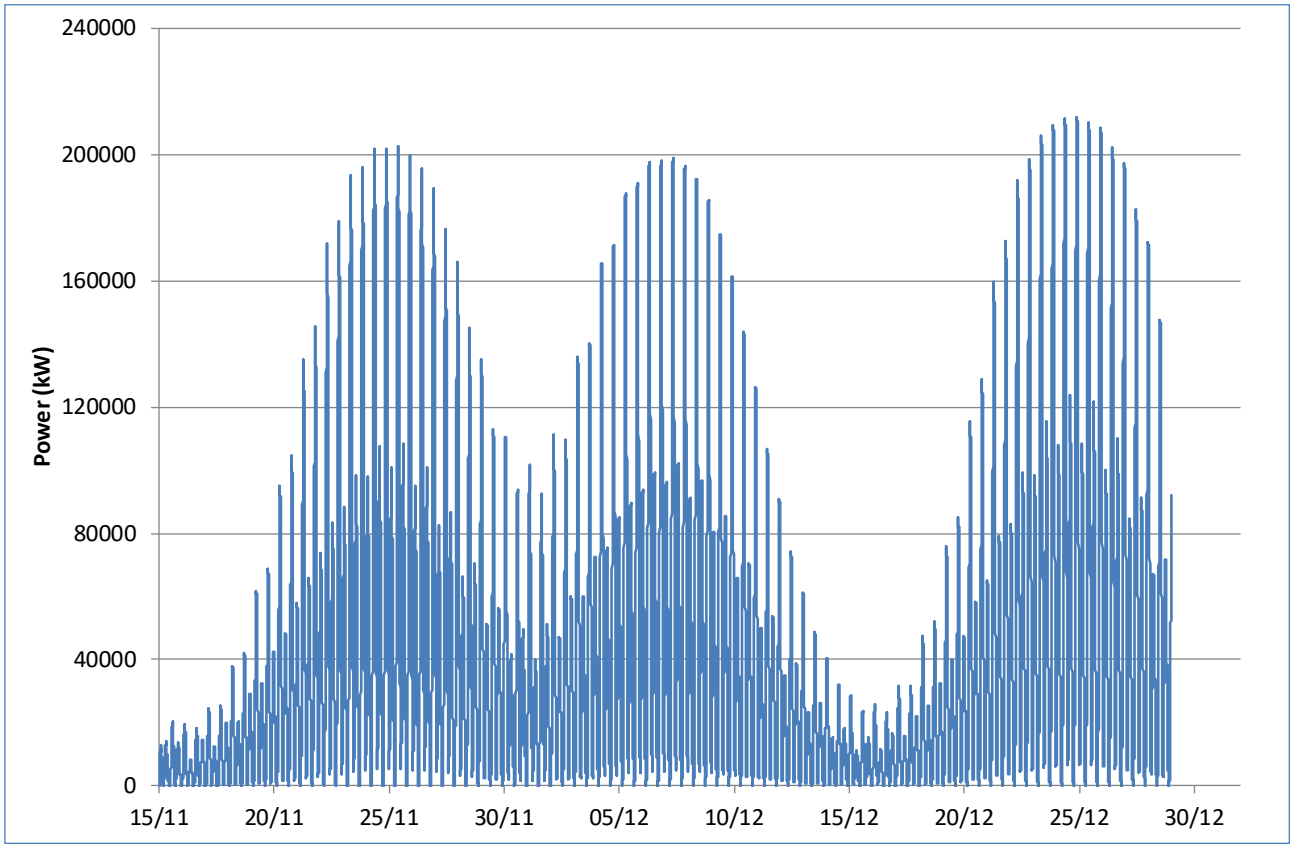

Figure 4.18: Modelled electrical power extraction

The figure shows the modelled power through three spring-neap cycles, starting on neap tides and showing three broad “peaks” corresponding to spring tide periods. For a date of stated mean spring tide range (4.9m) at Holyhead, the model predicts a peak total power of 202 MW. For neap tides, the peak total power is considerably less, reflecting the significantly lower tidal current speeds during neap tides.

Average power extraction

In accordance with IEC TS 62600-201:2015 recommendations it is also worth considering the average power over a lunar month and extrapolating through to a 19 year (nodal tidal cycle) long term average. The model computed the power produced by the array (with electrical conversion efficiency multiplier) for a 29.5 day simulation period (after model spin-up).

To extrapolate to a long period (19 years) we considered a single turbine at ADCP position 2. The table of power values as a function of current speed was used to compute a single turbine’s power output at this location for a 19 year period using a tidal synthesis of the currents at this location including the modelled period. The power produced on average for the 29.5 day and 19 year period (in MW) were obtained and the ratio of these values was then used to extrapolate the whole array production for the modelled period to the longer period. This method avoids the need for a very long continuous model simulation.

Position 2 was used, as a better tidal analysis was produced here. The ratio to extrapolate from the 29.5 days period to the 19 year period was 0.937 (the modelled period had a slightly greater than average energy production):

- Average power over simulated 29.5 day period: 42 MW;
- Estimated average power for 19 year period: 40 MW.

4.4.3. Modelled changes to peak and average flow speeds

The following series of figures shows the effects of the operating turbines on peak flows during a mean spring tide at Holyhead.

Figure 4.19, Figure 4.20 and Figure 4.21 show the baseline maximum flow speeds, the scheme maximum flow speeds and the difference in maximum flow speeds, respectively, over 29.5 days.

Figure 4.22, Figure 4.23 and Figure 4.24 show the baseline average flow speeds, the scheme average flow speeds and the difference in average flow speeds respectively, over 29.5 days.

Figure 4.25 and Figure 4.26 show changes to peak flood and ebb flows (respectively) for the scheme when compared against the baseline. Figure 4.27 and Figure 4.28 show the same results with a wider view over Anglesey.

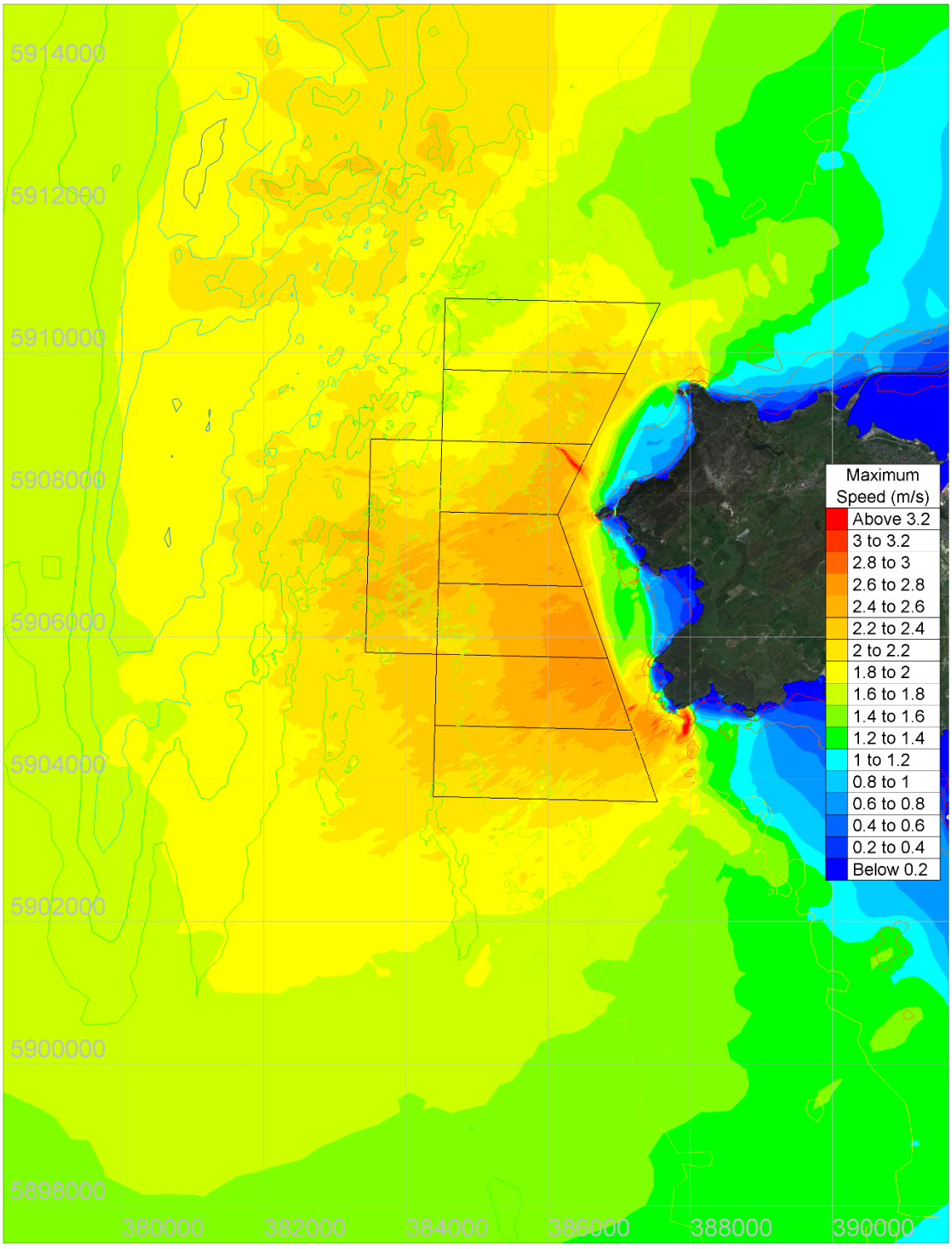

Figure 4.19: Baseline – Maximum speeds over 29.5 days

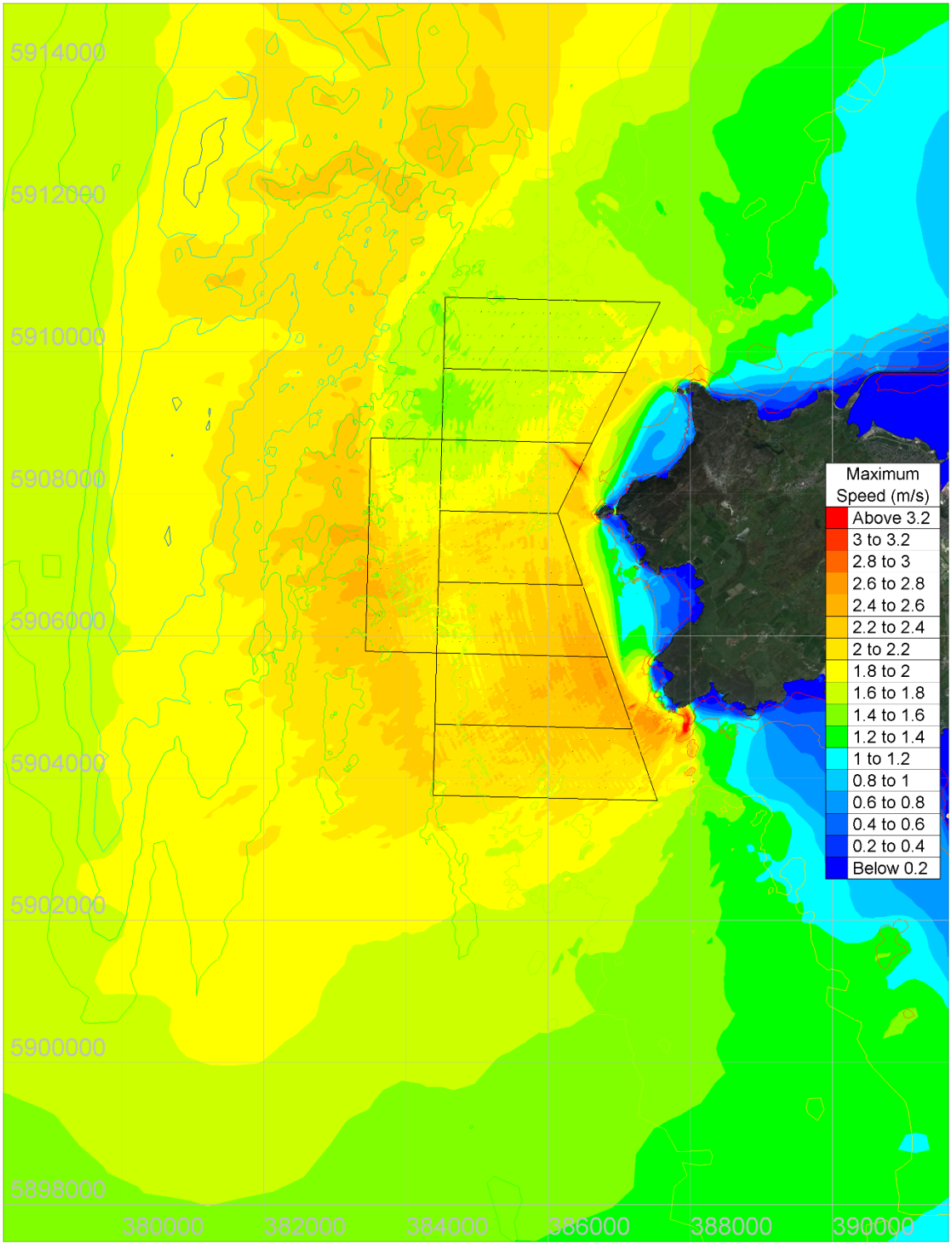

Figure 4.20: Scheme – Maximum speeds over 29.5 days

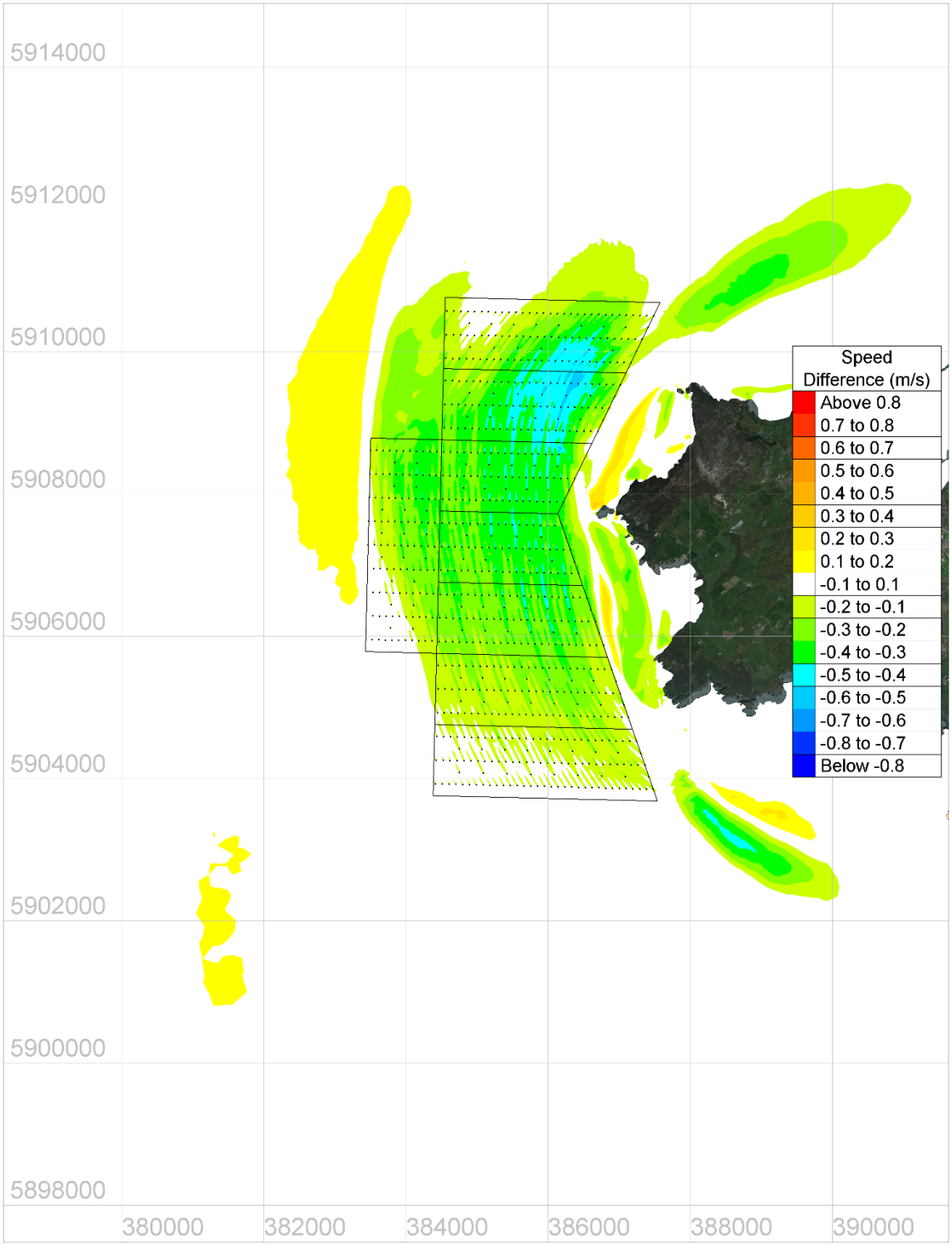

Figure 4.21: Difference of maximum speeds over 29.5 days (scheme minus baseline)

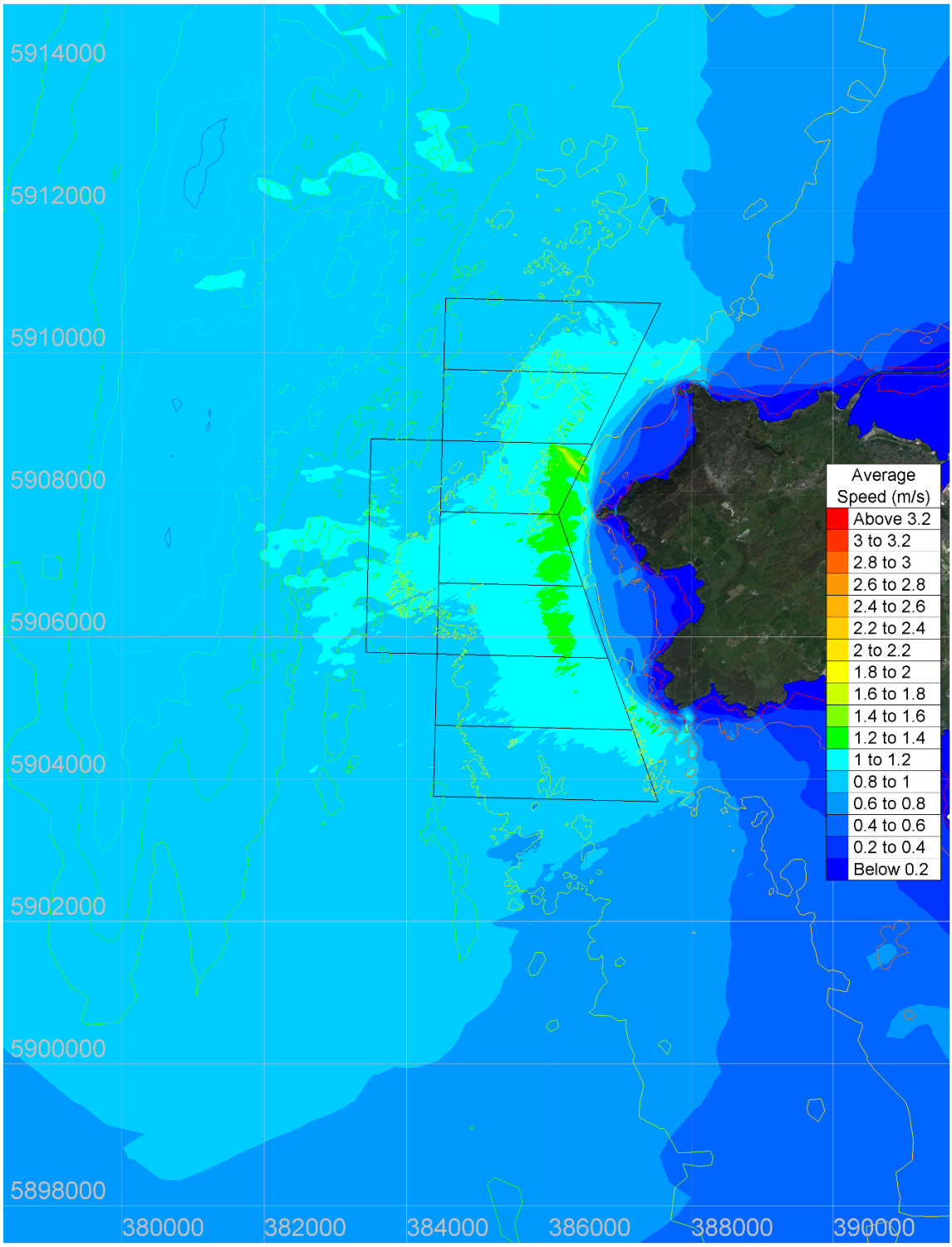

Figure 4.22: Baseline – Average flow speeds over 29.5 days

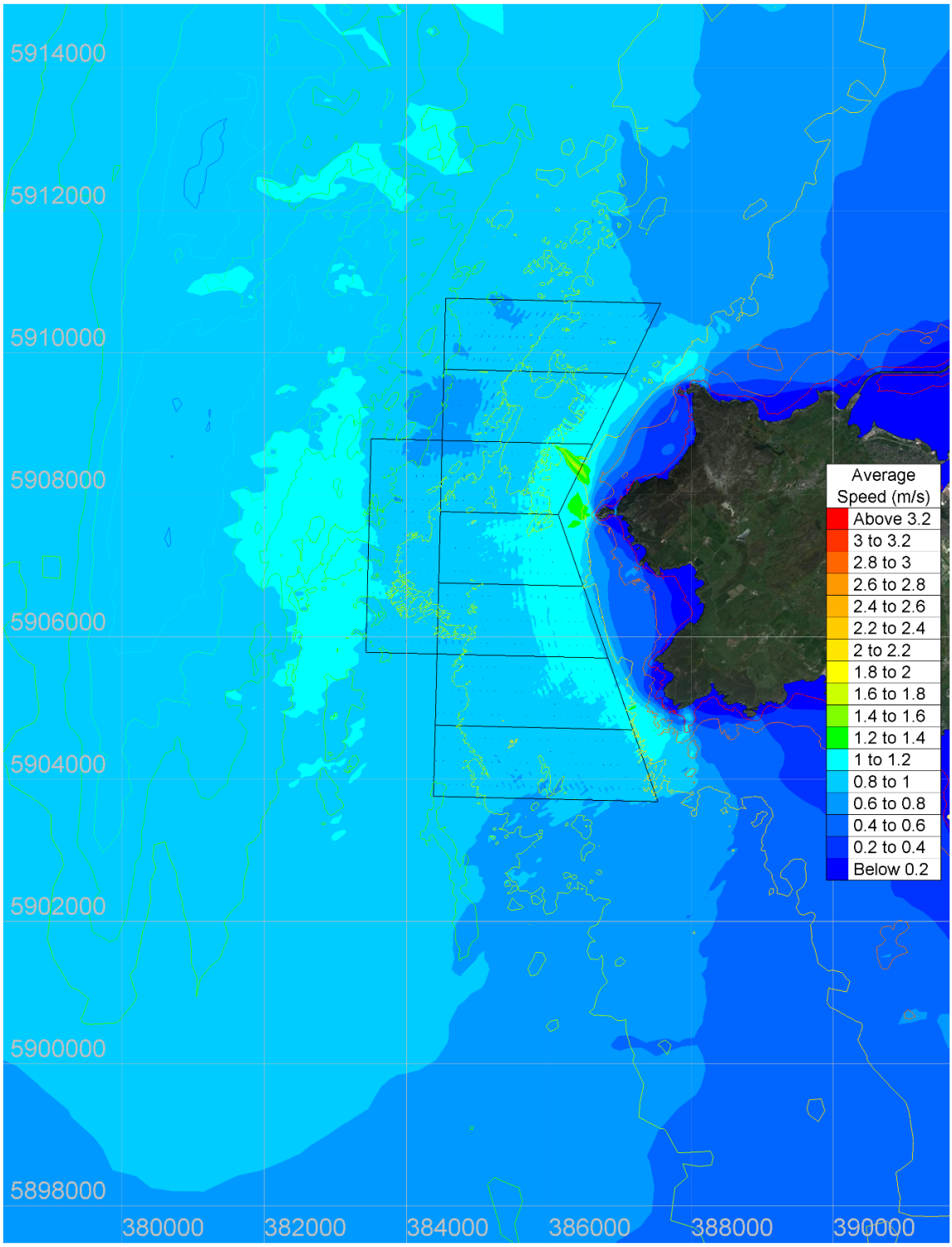

Figure 4.23: Scheme – Average flow speeds over 29.5 days

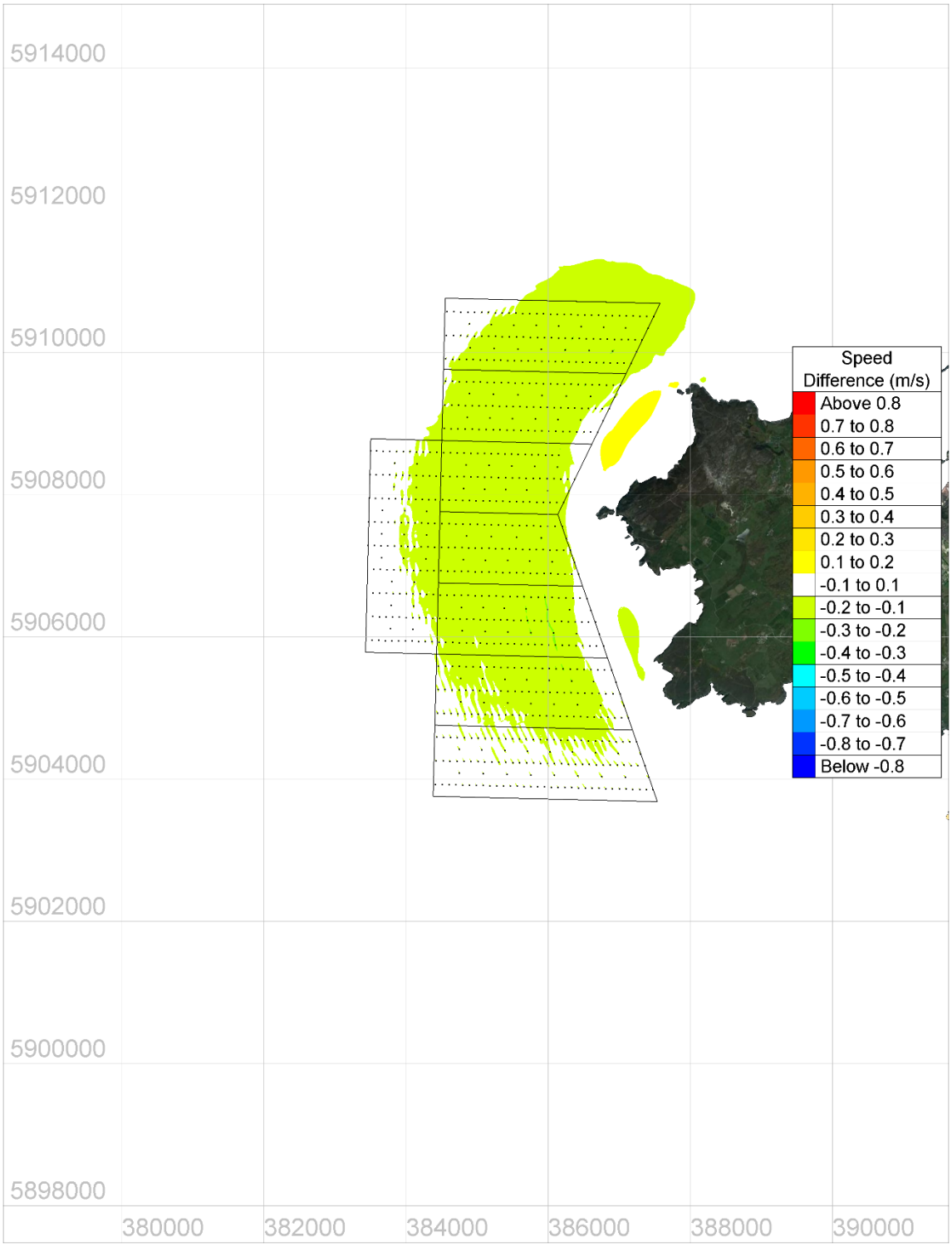

Figure 4.24: Scheme – Difference in average flow speeds over 29.5 days (scheme minus baseline)

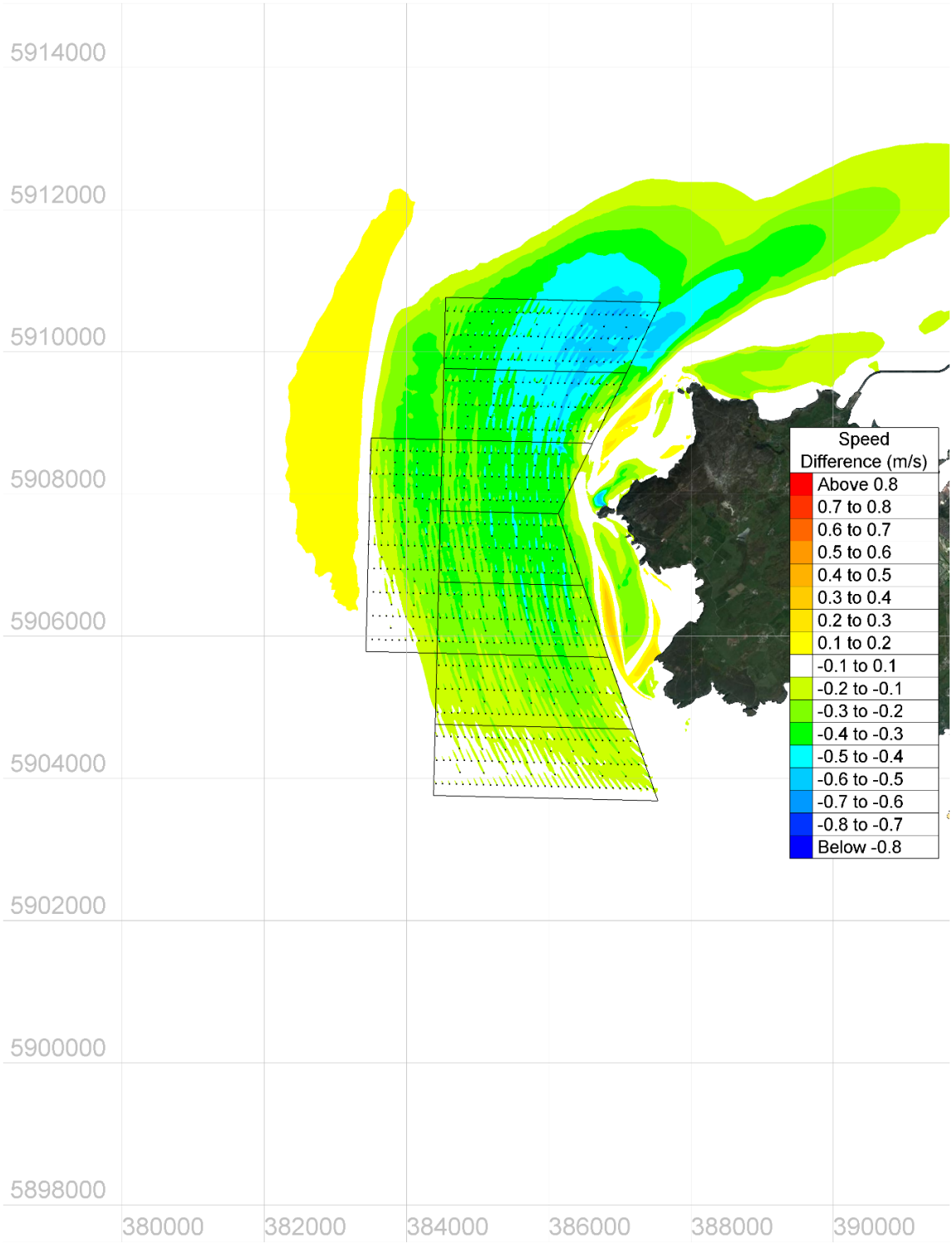

Figure 4.25: Change in mean spring tide peak speed (flood flow, scheme minus baseline)

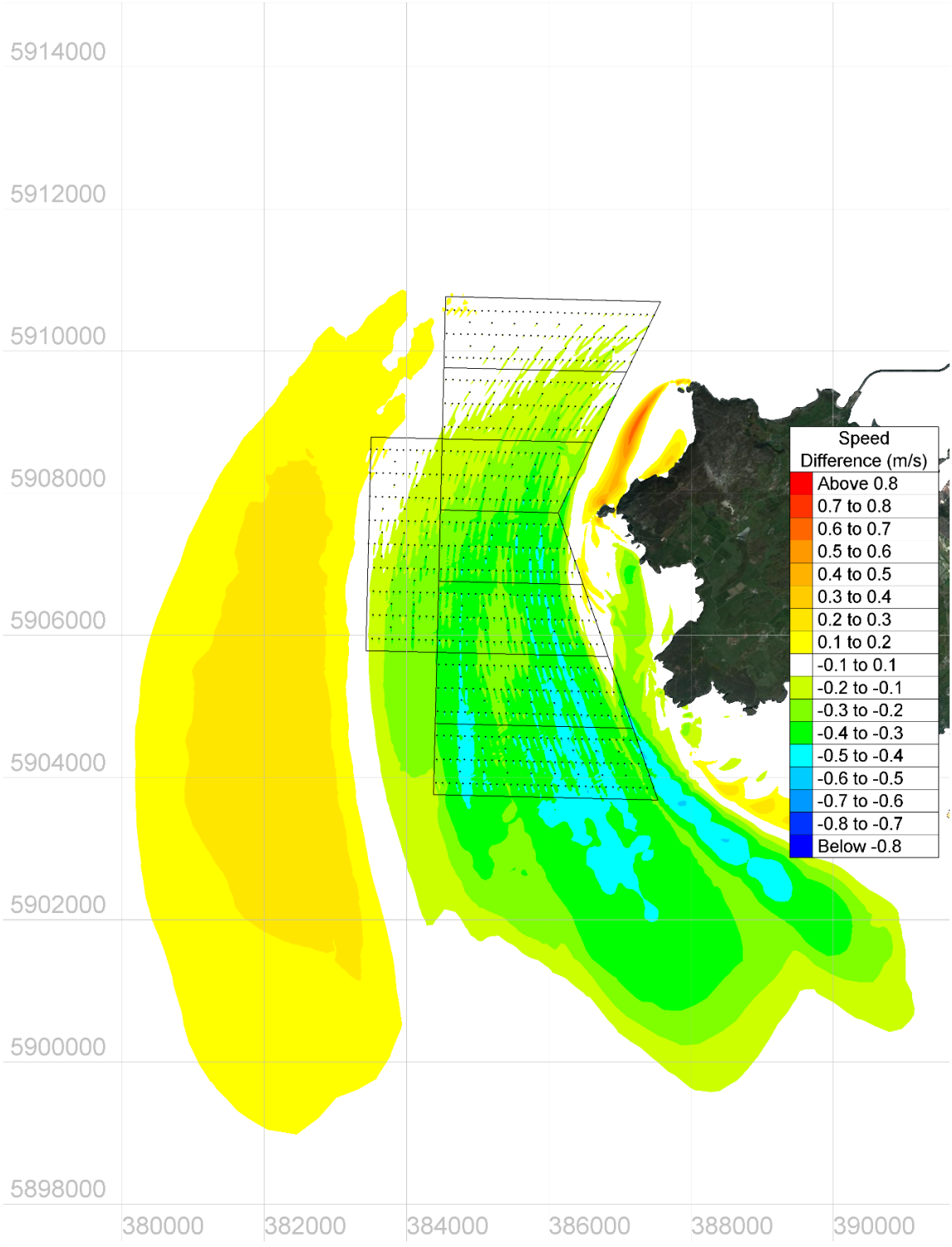

Figure 4.26: Change in mean spring tide peak speed (ebb flow, scheme minus baseline)

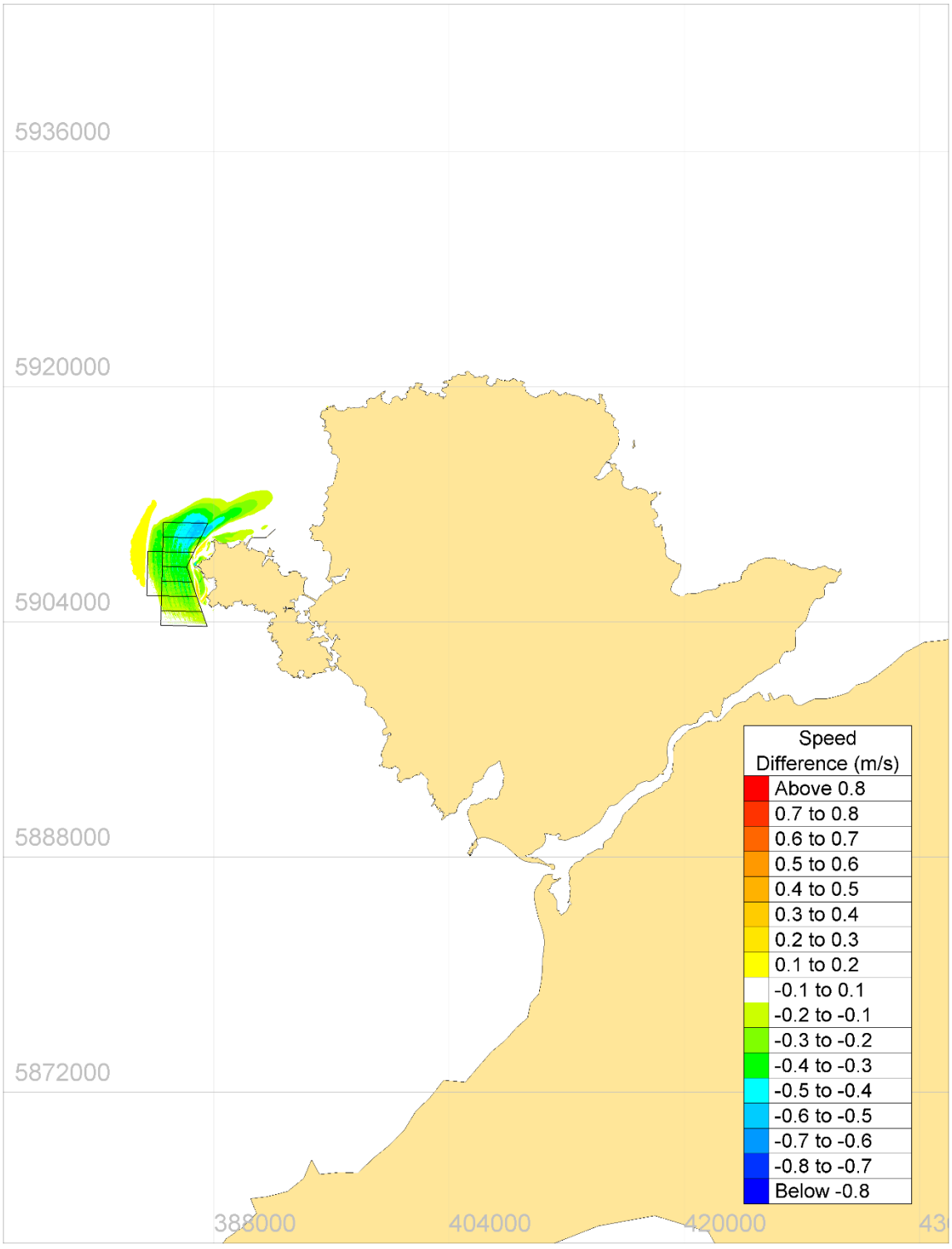

Figure 4.27: Change in mean spring tide peak speed (flood flow, scheme minus baseline) – Anglesey View

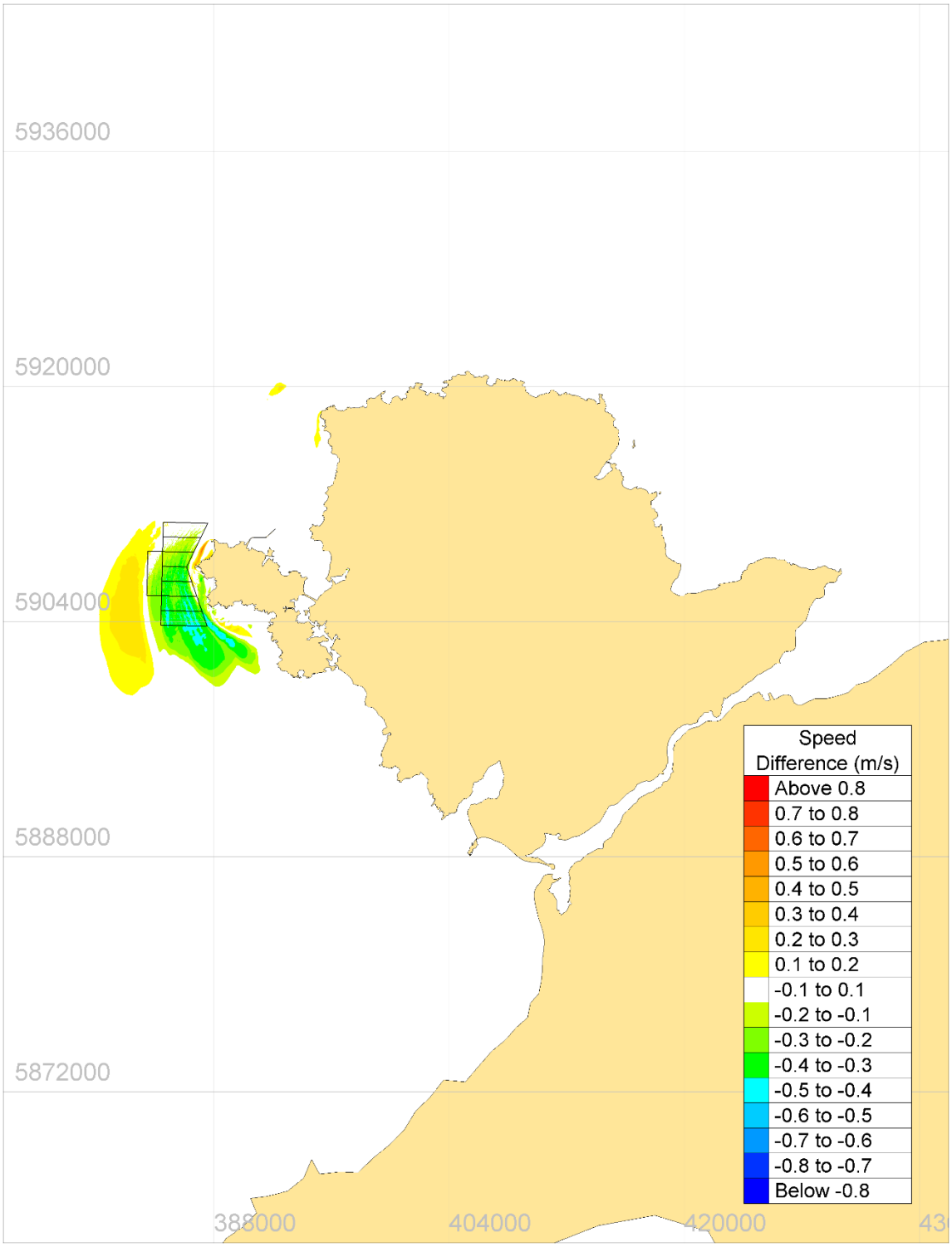

Figure 4.28: Change in mean spring tide peak speed (ebb flow, scheme minus baseline) – Anglesey View

4.4.4. Interactions between subzones

For each modelled scenario, outputs are provided for a complete lunar cycle (see separate spreadsheets) at a series of measurement points (100m intervals) along the boundaries of the buffer zones. Outputs include mean velocity, peak velocity, mean spring peak velocity, average power density.

These measurements allow a comparison of the scenarios to comply with the resource assessment standard IEC TS 62600-201:2015. The comparison is on the basis of theoretical extractable power and including a conversion factor to electrical power output provided by Menter Môn.

Measures include mean velocity, peak velocity, mean spring tide peak velocity, and average power density. Figure 4.29 shows the buffer zone line numbers for each of the subzones. Table 4.4 and Table 4.5 show the values of these measures as averaged from the outputs at 100m intervals along each of the buffer zone lines. The 29.5 day values relate to a modelled lunar month and the peak spring tide values are taken from a modelled tide later in the simulation. Section 4.4.1 describes the extrapolation to a longer term average lunar month.

The effect on these measures of energy extraction by multiple arrays in multiple subzones is clearly seen by comparing these tables.

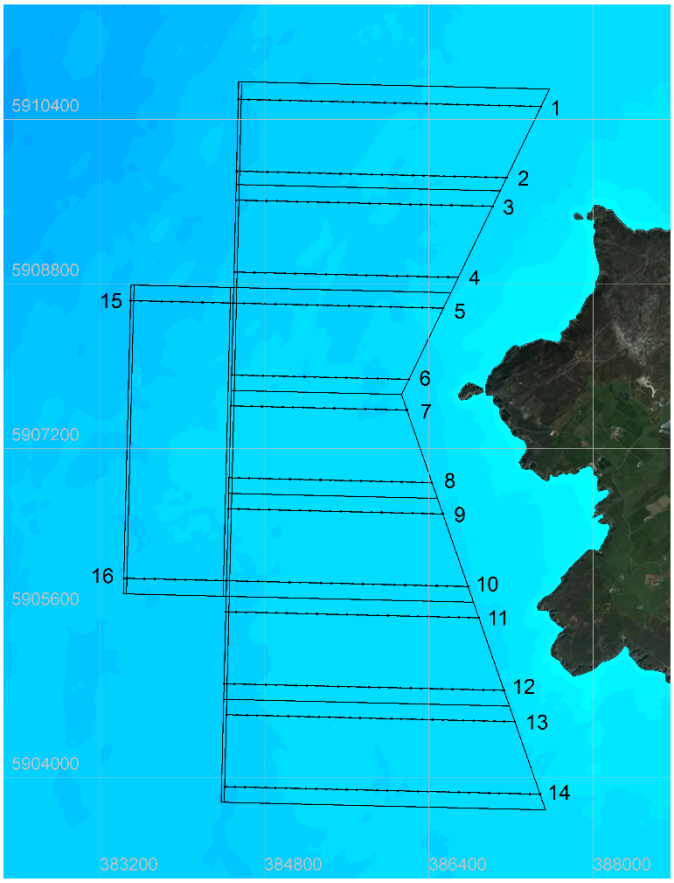

Figure 4.29: Buffer zone line numbers used for assessment of interaction between subzones

Table 4.4: Key modelled measures along buffer zone boundaries (Baseline – no turbines)

Buffer Zone Line No.	29.5 day mean speed (m/s)	29.5 day peak speed (m/s)	Mean spring tide peak speed (m/s)	29.5 day average power density (kW/m^2)
1	0.946	1.862	1.857	0.718
2	1.017	2.052	2.047	0.915
3	1.027	2.091	2.071	0.966
4	1.040	2.137	2.127	1.023
5	1.082	2.228	2.222	1.210
6	1.087	2.321	2.316	1.227
7	1.134	2.447	2.445	1.417
8	1.123	2.463	2.463	1.399
9	1.109	2.471	2.468	1.370
10	1.064	2.452	2.450	1.276

Buffer Zone Line No.	29.5 day mean speed (m/s)	29.5 day peak speed (m/s)	Mean spring tide peak speed (m/s)	29.5 day average power density (kW/m^2)
11	1.061	2.472	2.471	1.279
12	1.029	2.436	2.436	1.183
13	0.993	2.361	2.361	1.071
14	0.899	2.138	2.135	0.789
15	0.908	1.982	1.981	0.707
16	0.950	2.222	2.218	0.921

Source: Averaged values of model data extracted at 100m intervals along each buffer zone boundary line shown in Figure 5.8. HR Wallingford.

Table 4.5: Key modelled measures along buffer zone boundaries (Scheme)

Buffer Zone Line No.	29.5 day mean speed (m/s)	29.5 day peak speed (m/s)	Mean spring tide peak speed (m/s)	29.5 day average power density (kW/m^2)
1	0.828	1.716	1.770	0.507
2	0.868	1.716	1.780	0.573
3	0.881	1.742	1.817	0.606
4	0.902	1.794	1.889	0.634
5	0.958	1.898	1.996	0.810
6	0.952	1.990	2.098	0.777
7	0.992	2.103	2.221	0.886
8	0.974	2.153	2.264	0.864
9	0.966	2.151	2.264	0.852
10	0.943	2.208	2.314	0.860
11	0.922	2.207	2.315	0.803
12	0.924	2.283	2.382	0.884
13	0.897	2.221	2.318	0.812
14	0.834	2.076	2.159	0.670
15	0.830	1.724	1.812	0.531
16	0.910	2.197	2.283	0.828

Source: Averaged values of model data extracted at 100m intervals along each buffer zone boundary line shown in Figure 5.8. HR Wallingford.

5. Wave Modelling

5.1. Overview

Baseline wave climate conditions are required to provide the appropriate wave forces for input to the sediment transport study. In addition, it is also necessary to quantify the impacts the worst case scenario of the tidal turbine structures and associated infrastructure on the wave regime particularly at the coast and the on any subsea sandbanks.

The turbine structures will have a direct blocking effect on the waves, although since the structures are small in relation to the wavelength, this effect is likely to be small. In addition, waves around Anglesey are likely to experience refraction effects due to strong tidal currents as well as refraction due to the changing bathymetry. Previous modelling by HR Wallingford has shown that the array of tidal turbines will modify the tidal currents in the area, causing local effects around each turbine and wider area reductions in the current speeds. The changes in the tidal currents due to the turbines will result in changes to the refraction effects of the waves which will also need to be considered.

5.2. Offshore wave climate

The offshore wave climate was based on the UK Met Office Remap model data. A local SWAN (Simulating WAves Nearshore) wave model was set up to represent the wave transformation from the Met Office model point to the coast of Anglesey. Figure 5.1 shows an aerial image taken from Google Earth with the Met Office Remap data marked on. It shows that the Remap point is West of Anglesey 11.5km offshore. The Met Office point is placed on the western boundary of the model to allow direct forcing from the data. The Met Office data cover 40 years between 1980-2020. Between 1980-2000 the data is every three hours and from 2000-2020, the data is hourly.

Figure 5.1: Anglesey and the location of the Met Office Remap Data point

Source: Google Earth

5.2.1. Wave climate

As the Met Office Remap data point is located in the Irish Sea, only certain wave directions will not be fetch limited. A wave rose of wave directions against wave height shows that the most frequent waves approach from 210°N. Waves from this direction are able to travel from large distances across the North Atlantic to reach the point meaning that waves from this direction are not only the most frequent, but also have the potential to have the highest significant wave heights. Waves from 240°N may also have large wave heights as waves can also propagate from the North Atlantic while refracting into the Irish Sea. Waves from 270-330°N are fetch limited as waves are blocked by mainland Ireland. A wave climate table gives the breakdown of the wave height from each direction. This confirms that the most prominent waves approach from 210°N.

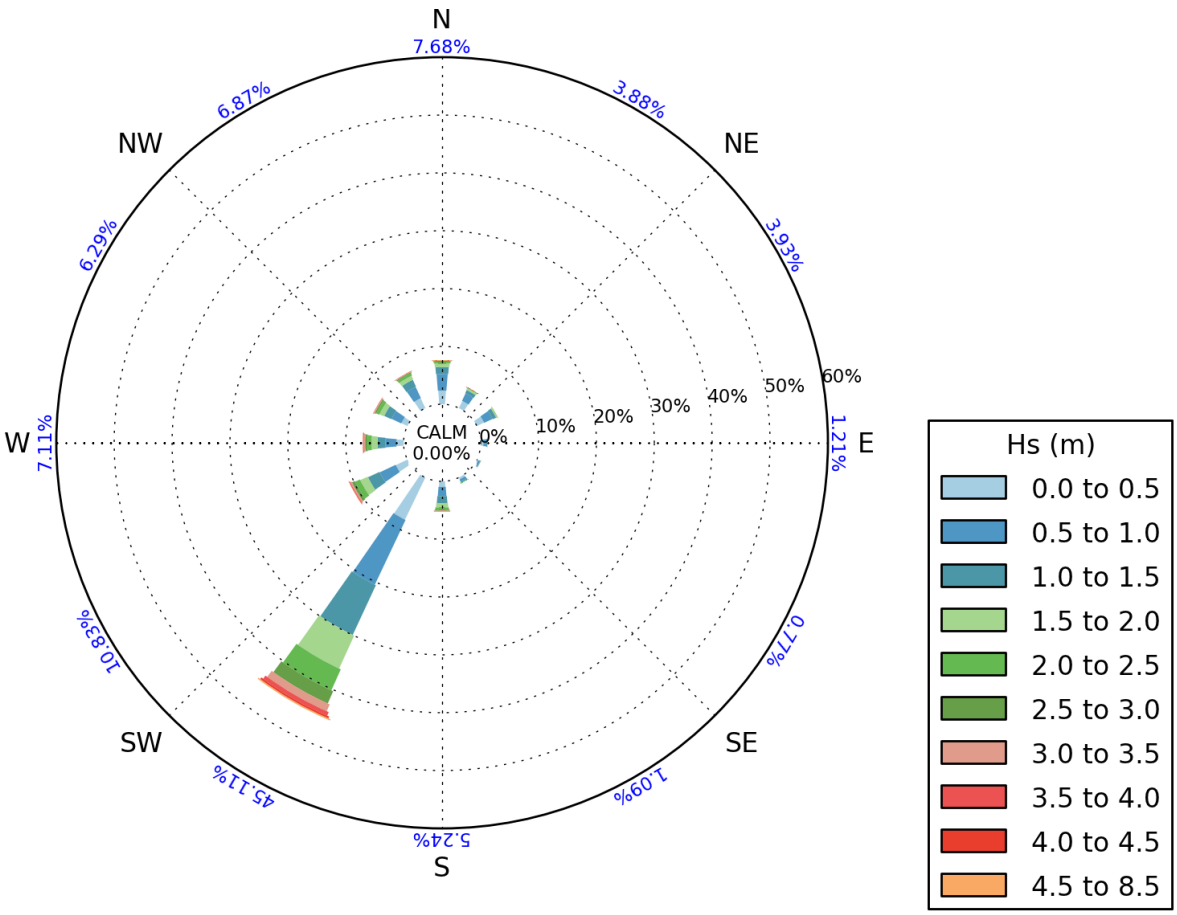

Figure 5.2: A wave rose of Met Office Remap data between 1980-2020 showing the directions of waves with corresponding significant wave height

Source: UK Met Office Remap data

Table 5.1: Offshore wave climate

Hs (m)		P(Hs>Hs1)	Mean direction (deg N)											
			-15.0	15.0	45.0	75.0	105.0	135.0	165.0	195.0	225.0	255.0	285.0	315.0
Hs1	Hs2		15.0	45.0	75.0	105.0	135.0	165.0	195.0	225.0	255.0	285.0	315.0	345.0
0.00	0.50	100.00%	2350	1361	1376	471	293	351	950	8082	2221	1222	1166	1903
0.50	1.00	78.25%	2820	1414	1610	506	319	455	1621	12386	3032	1909	1853	2166
1.00	1.50	48.16%	1253	620	653	167	105	221	1218	9460	2206	1401	1364	1339
1.50	2.00	28.16%	616	291	217	51	30	71	769	6257	1419	1027	867	710
2.00	2.50	15.83%	290	112	51	8	13	10	387	4008	933	716	549	414
2.50	3.00	8.34%	157	44	14	2	5	4	201	2330	515	422	281	208
3.00	3.50	4.16%	73	11	6	2	0	1	71	1293	254	243	153	96
3.50	4.00	1.95%	25	5	1	2	0	0	27	677	151	131	64	56
4.00	4.50	0.81%	14	2	0	0	0	0	3	352	53	47	14	24
4.50	5.00	0.30%	6	0	0	0	0	0	1	133	23	11	2	6
5.00	5.50	0.12%	0	0	0	0	0	0	0	62	6	4	0	2
5.50	6.00	0.05%	0	0	0	0	0	0	0	25	3	2	0	0
6.00	6.50	0.02%	0	0	0	0	0	0	0	8	2	1	0	0
6.50	7.00	0.01%	0	0	0	0	0	0	0	1	0	1	0	0
7.00	7.50	0.00%	0	0	0	0	0	0	0	2	0	0	0	0
7.50	8.00	0.00%	0	0	0	0	0	0	0	1	1	0	0	0
8.00	8.50	0.00%	0	0	0	0	0	0	0	1	0	0	0	0
Total for each mean direction			7.6%	3.9%	3.9%	1.2%	0.8%	1.1%	5.2%	45.1%	10.8%	7.1%	6.3%	6.9%

Source: Met Office Remap model. Data in parts per hundred thousand

Using the wave climate from the Met Office Remap data, both representative and extreme conditions were derived. It was decided to include waves from different direction bins to get an overview of the full range of waves which may interact with the tidal energy structures. Waves are broken down in to 5 directions: 210°N, 240°N, 270°N, 300°N and 330°N. The representative conditions have been chosen using a morphological average condition from each direction bin (See Section 6.2.2) (Table 5.2).

Table 5.2: Representative wave conditions

Wave Direction (deg N)	Sig Wave Height (m)	Peak Period (s)	Wind Speed (m/s)	Wind Direction (deg N)
210	2.16	6.9	13	210
240	2.06	6.8	13	240
270	2.14	6.9	13	270
300	1.92	6.7	13	300
330	1.81	6.6	13	330

Source: HR Wallingford

The extreme conditions are calculated by fitting a Weibull extreme value distribution. The full timeseries of waves was analysed to extract storm peak wave heights using a peaks over threshold method. Weibull probability distributions were fitted to the storm peaks from each direction sector to derive extreme waves for a range of return periods from each direction sector. Figure 5.3 to Figure 5.7 show the extreme value distributions. Table 5.3. shows the 1 in 200 year extreme conditions from each direction sector that were chosen to be run in the model. A 200 year return period event is a severe storm for which the impacts of the devices may be of interest. This is a typical return period used in the design of coastal protection. Appropriate wave periods corresponding to the extreme wave heights were derived using an average wave steepness from the storms data. Corresponding associated wind speeds were chosen based on the correlation between winds and waves observed in the Met Office model data for each direction.

Table 5.3: Extreme wave conditions

Wave Direction (deg N)	Sig Wave Height (m)	Peak Period (s)	Wind Speed (m/s)	Wind Direction (deg N)
210	8.50	12.3	27	210
240	8.30	11.4	27	240
270	7.60	10.4	26	270
300	6.30	9.4	24	300
330	6.30	9.8	24	330

Source: HR Wallingford

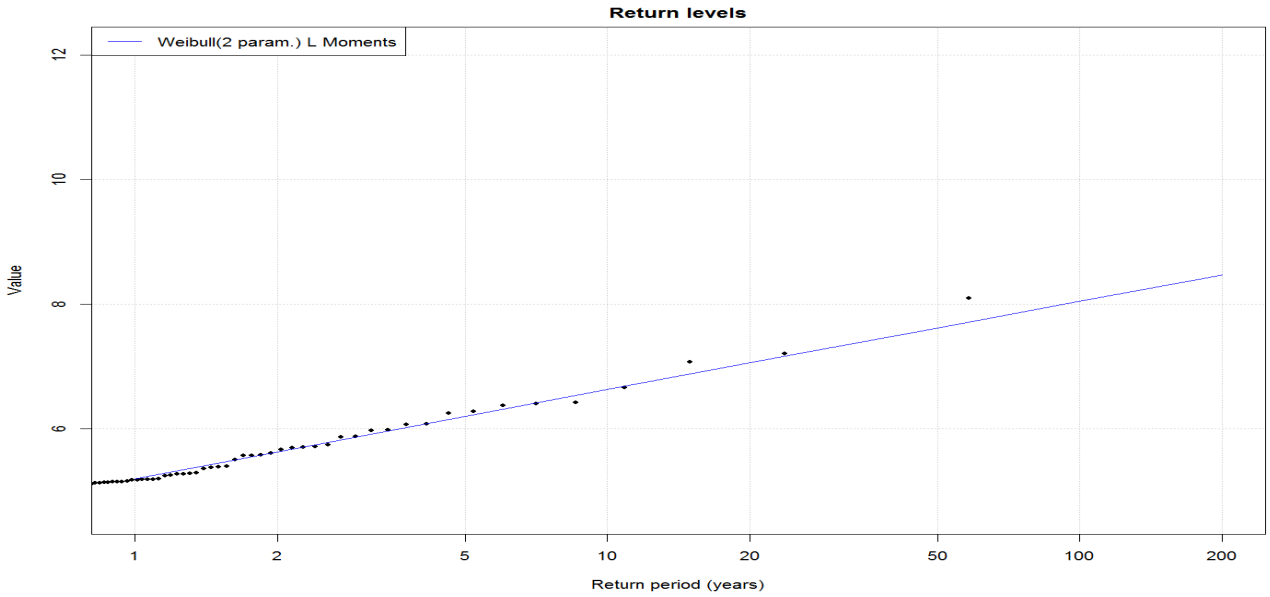

Figure 5.3: Return period plot for waves from 195 to 225 ºN for a return period of up to 1 in 200 years

Source: HR Wallingford

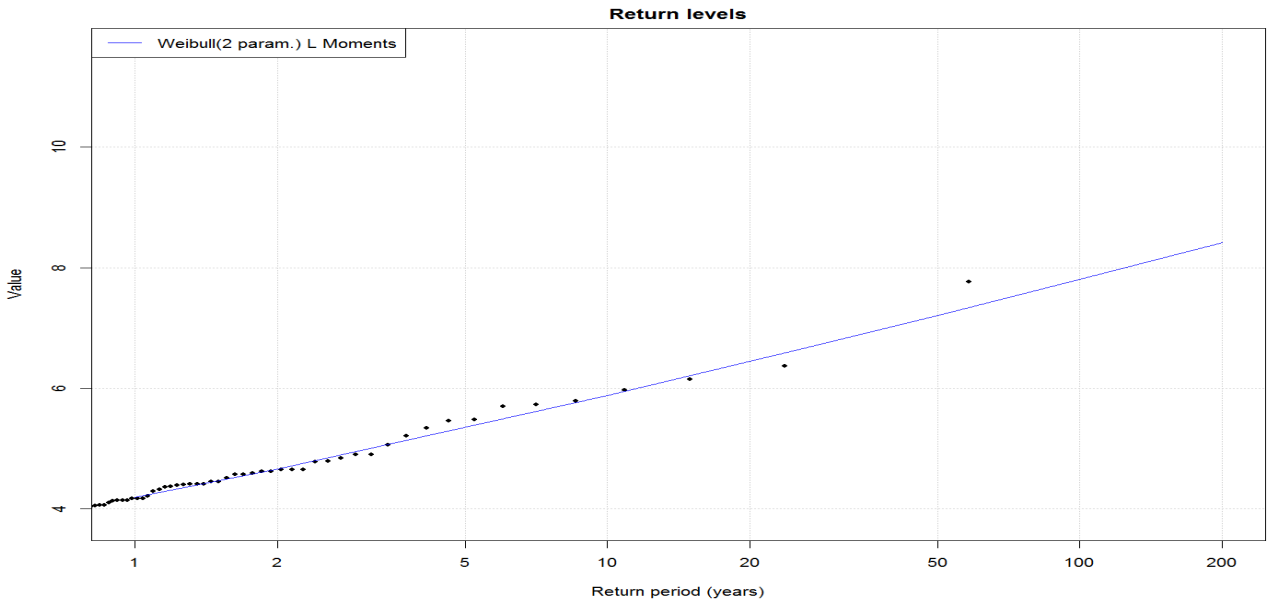

Figure 5.4: Return period plot for waves from 225 to 255 ºN for a return period of up to 1 in 200 years

Source: HR Wallingford0 years 0^syears

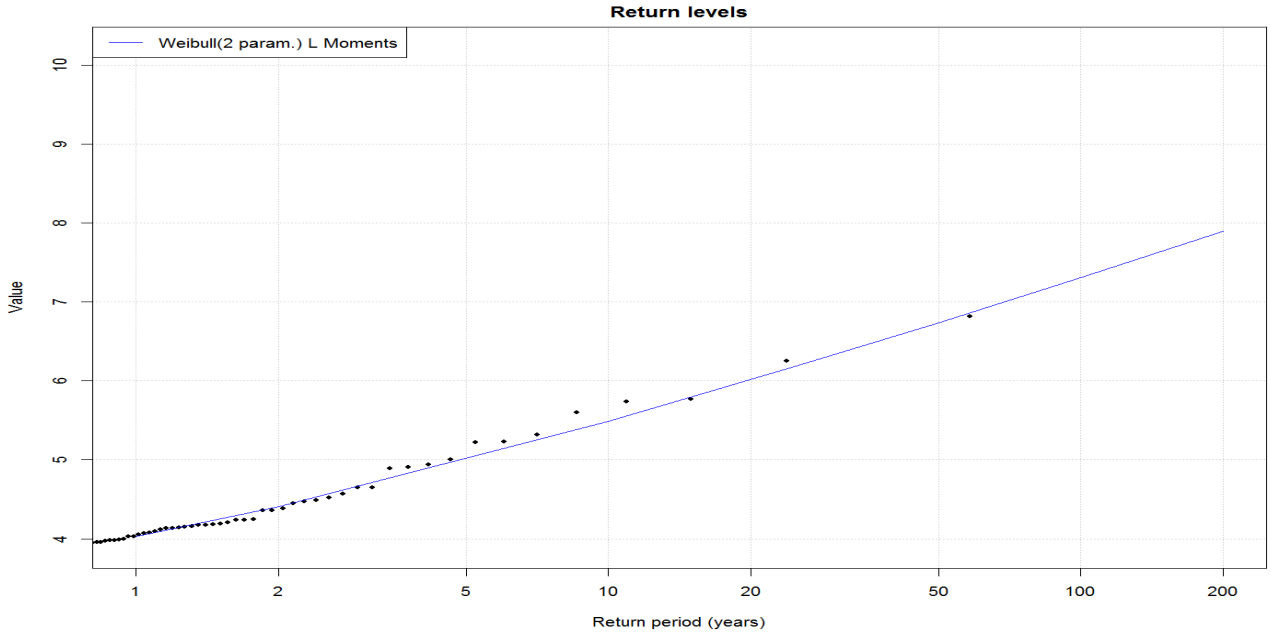

Figure 5.5: Return period plot for waves from 255 to 285 ºN for a return period of up to 1 in 200 years

Source: HR Wallingford

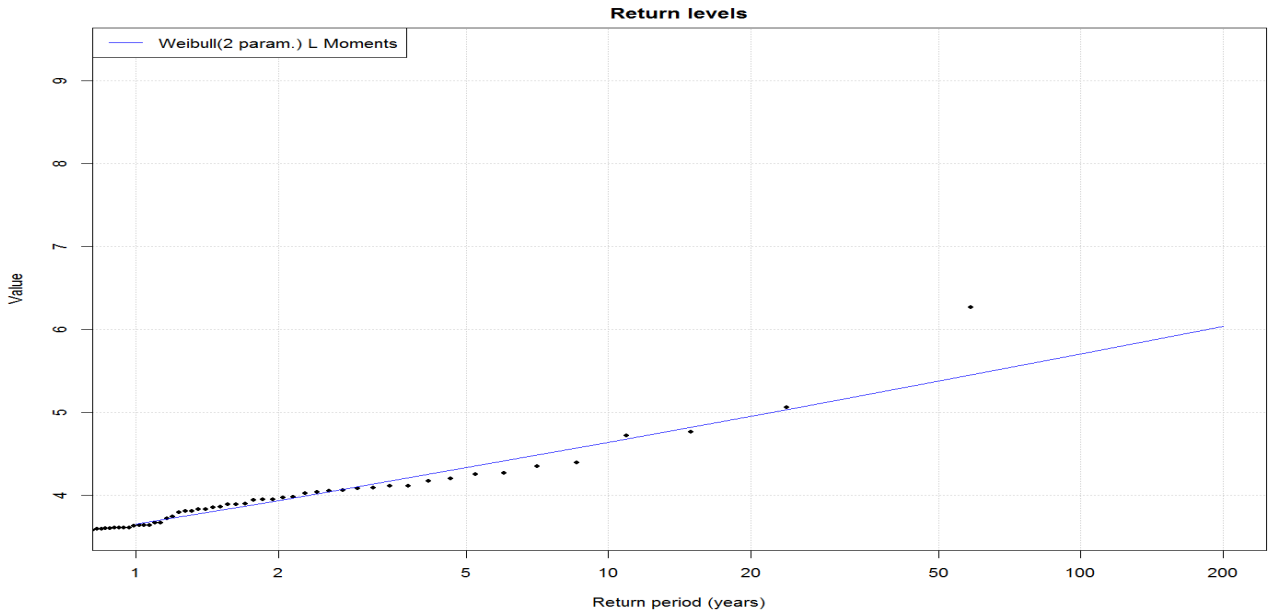

Figure 5.6: Return period plot for waves from 285 to 315 ºN for a return period of up to 1 in 200 years

Source: HR Wallingford

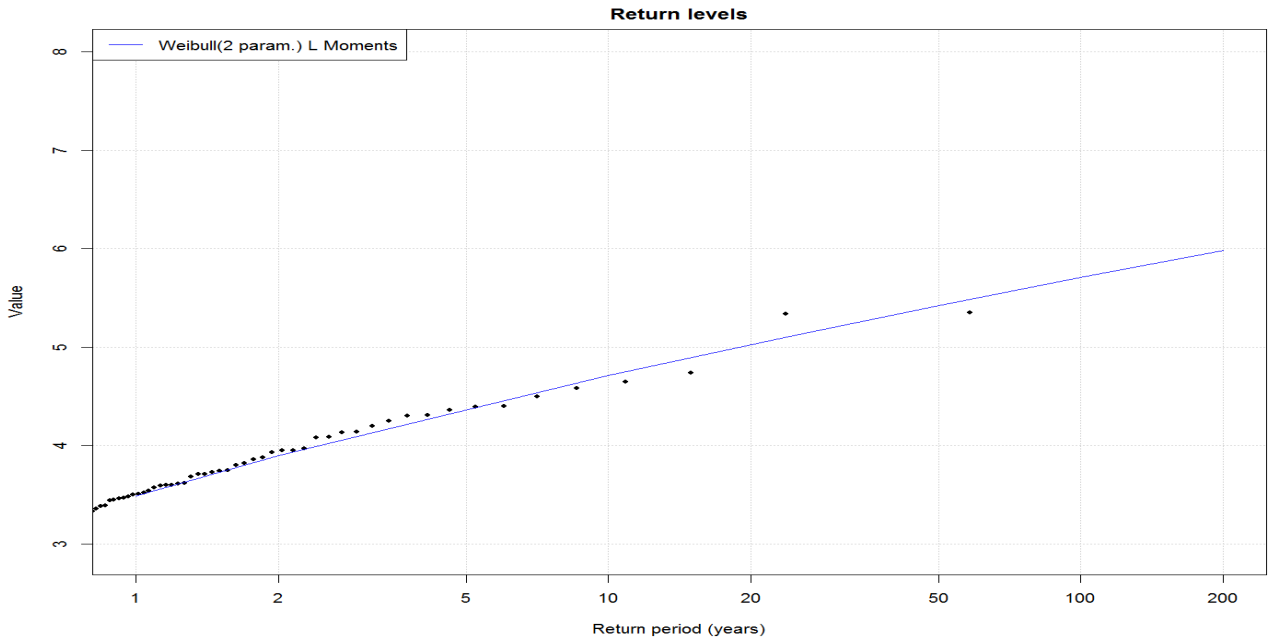

Figure 5.7: Return period plot for waves from 315 to 345 ºN for a return period of up to 1 in 200 years

Source: HR Wallingford

5.3. Wave model set-up

The SWAN wave model was set up to use the same bathymetry as the flow model as described below. The model mesh however is a smaller subset of the flow model itself (Figure 5.8). The reason that the wave model uses a subset of the flow model is to keep both the nodes and elements the same but to have an offshore boundary at the Met Office model point. In total, the wave model has 390905 nodes and 773270 elements. As the mesh is unstructured, around the boundary the mesh is coarser with node spacings of roughly 2km offshore with the finest mesh being located in the turbine development area and at the beaches of interest with a resolution of 10m. The offshore wave climate is based on the UK Met Office Remap data The wave model is driven by wave conditions from the open boundaries, with wind being applied across the full extent of the model. This allows any additional wave growth within the area of the model.

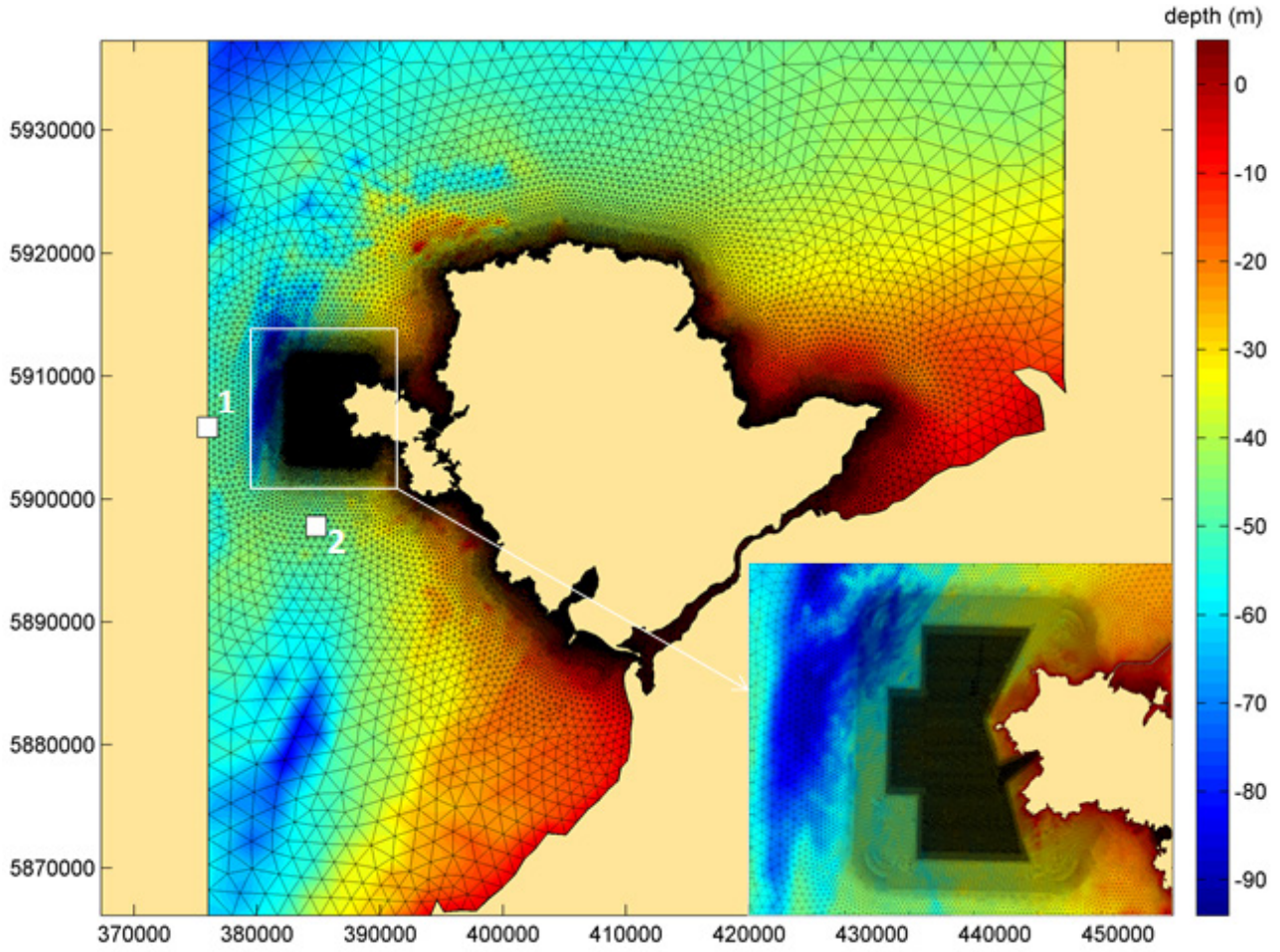

Figure 5.8: A bathymetry plot underlying the wave model mesh. Point 1 is the location of the Met Office Remap point and point 2 is the location of the SEACAMS wave buoy

Source: HR Wallingford SWAN model

5.3.1. The SWAN model

The widely used SWAN (Simulating WAves Nearshore model, Ref. 1) was used to represent the waves transferring from the boundary to the coast of Anglesey.

SWAN is a 3rd generation spectral wave model which simulates the transformation of random directional waves considering the following processes:

- Wave shoaling;
- Wave refraction by bathymetry and currents;
- Depth-induced breaking, bottom friction and whitecapping;
- Wave growth due to the wind;
- Wave reflections from structures or rocky shorelines;
- Far field diffraction.

The SWAN model has been extensively validated and is ideally suited to the transformation of wave energy spectra in relatively large coastal areas. This is particularly true where the features of the seabed, such as offshore banks and reefs, result in depth-induced wave breaking and wave–wave interactions. The model also includes wave generation by the wind within the model area and the influence of currents on the waves.

5.4. Wave model validation

The wave model has been extensively validated for extreme wave conditions which have been measured by the SEACAMS wave buoy. The SEACAMS wave buoy was deployed three times between 2014-2016 at a location approximately 8km west of Anglesey. Figure 5.8 shows the location of the SEACAMS buoy in relation to the model. An analysis of storm peaks was carried out on the wave data to find the most extreme conditions measured by the buoy from three directions during its deployment.

In total, four storms were chosen to validate the wave model. The most extreme storm measured by the SEACAMS buoy occurred on the 14th of January 2015. The predominant wave direction approached from 210°N which is expected as this direction has the largest fetch. The event which occurred on June 1st 2015 was also from the south west, but approached from 240°N. The event which occurred on the 21st of October 2014 approached from 300°N. Although the wave height is high, compared to the events which approach from the southwest, the peak period of this wave condition from the northwest is relatively low because the waves are more dominated by locally generated wind waves whereas waves from the southwest have the potential to be swell dominated.

Table 5.4: A list of the storm events captured by the SEACAMS wave buoy. The numbers stated occurred at the peak of the storm event

Date	Sig wave height	Wave period	Wave direction
January 14th 2015	6.61	11.11	216.6
June 1st 2015	4.66	9.52	237.7
October 21st 2014	4.50	8.00	303.8
October 16th 2016	3.29	11.76	201.1

Source: HR Wallingford analysis of SEACAMS data

To validate the model a non-stationary run was carried out using the Met Office Remap data to force the boundary for each storm. Each run extended over 2 days of build up before the peak of the storm. Figure 5.9 shows that the model accurately measures the peak wave height however there is some localised fluctuation which is not seen in the model run. This is the same for peak period and wave direction. All validation runs accurately model the peak of each event with Figure 5.10, Figure 5.11 and Figure 5.12 showing that the modelled data closely follows the SEACAMS measured data for significant wave height, peak period and wave direction. Near the beginning of the final storm record (Figure 5.12) the measured directions are rather variable but this is due to the fact that the wave height is very low so the wave buoy has trouble determining the wave direction.

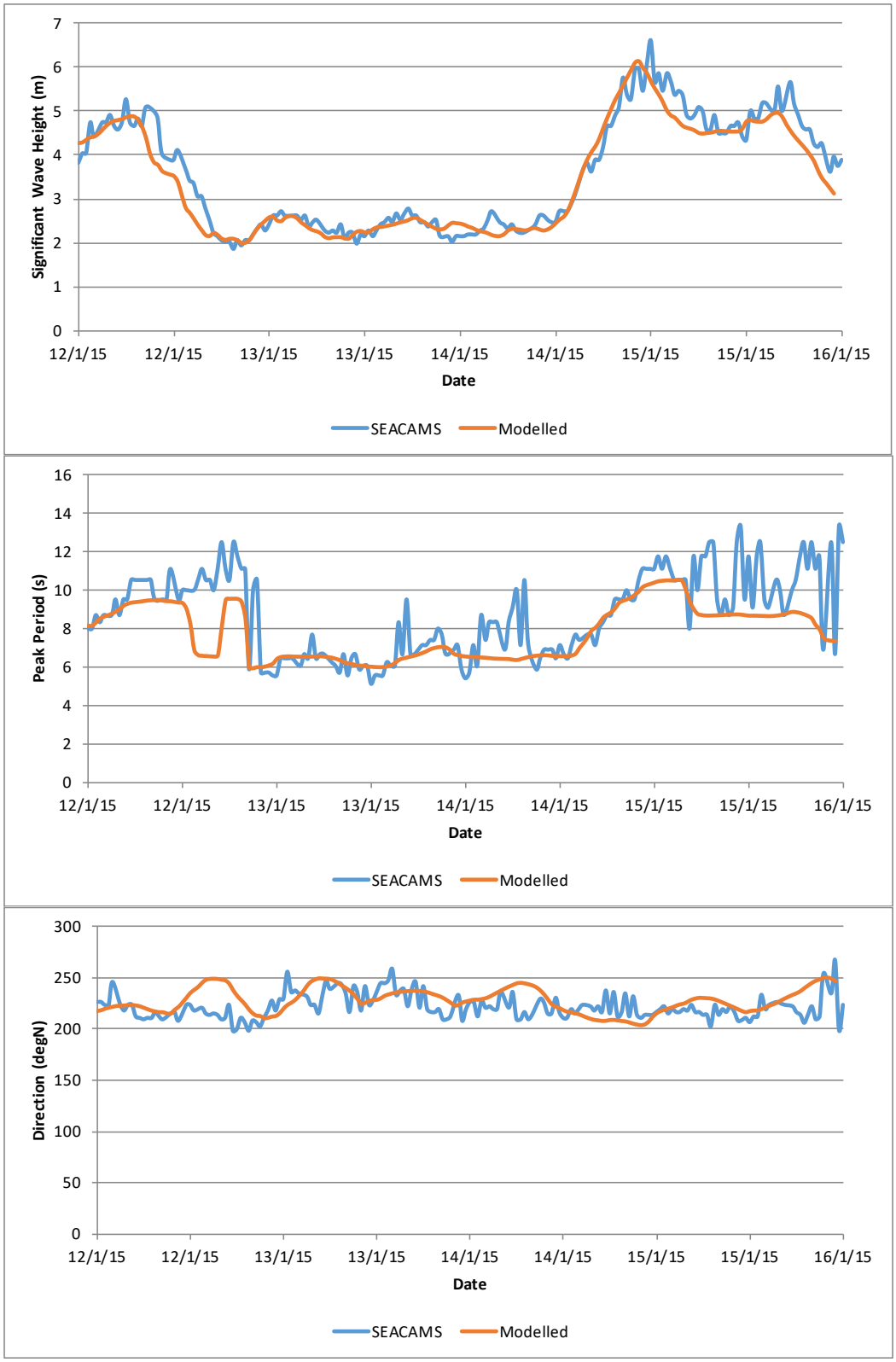

Figure 5.9: A comparison of modelled against measured wave conditions at the SEACAMS wave buoy during the 14/01/2015 storm: Top: Significant wave height, Middle: peak period, Bottom: Wave direction

Source: HR Wallingford SWAN model and SEACAMS data

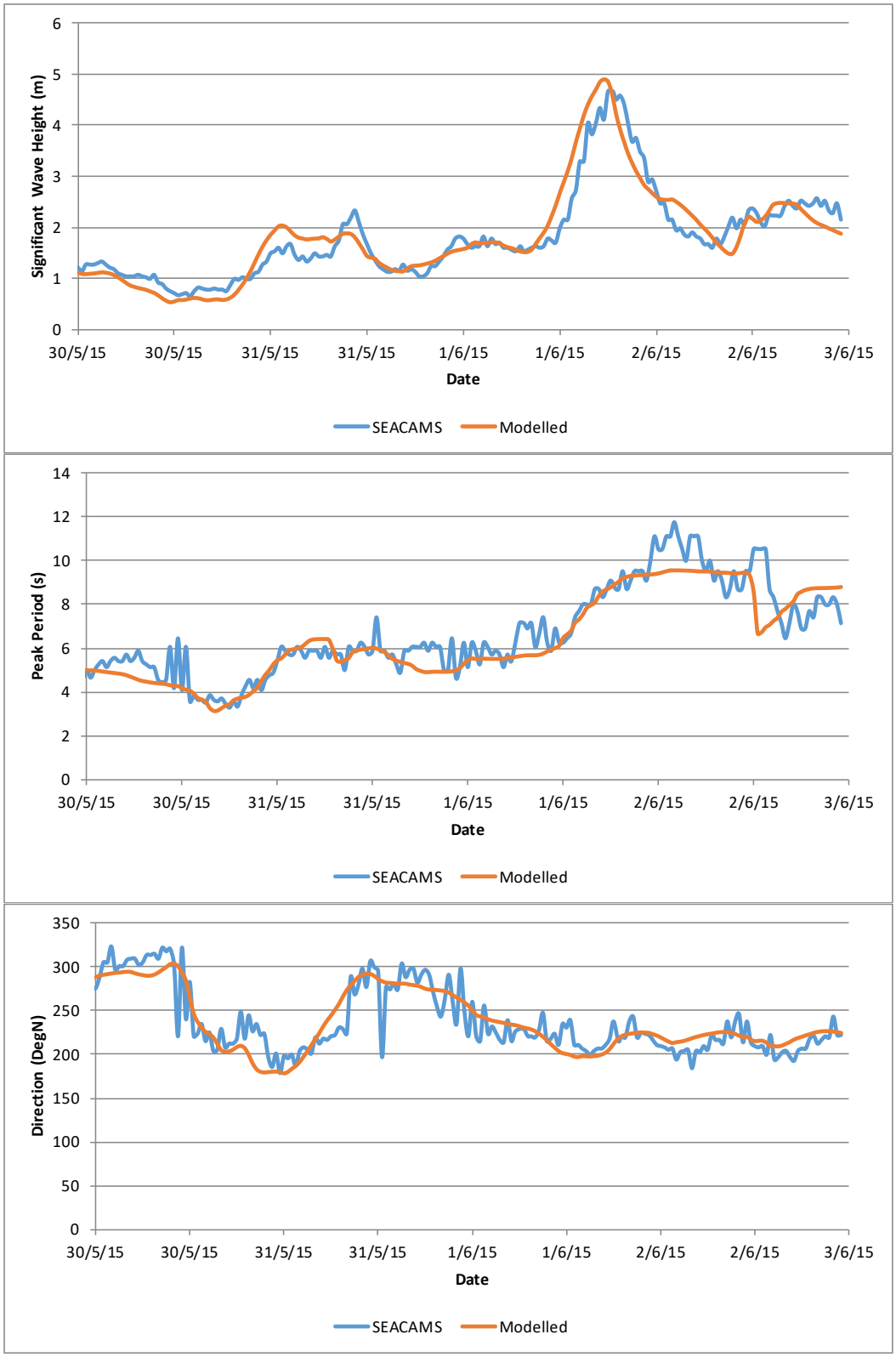

Figure 5.10: A comparison of modelled against measured wave conditions at the SEACAMS wave buoy during the 01/06/2015 storm: Top: Significant wave height, Middle: peak period, Bottom: Wave direction

Source: HR Wallingford SWAN model and SEACAMS data

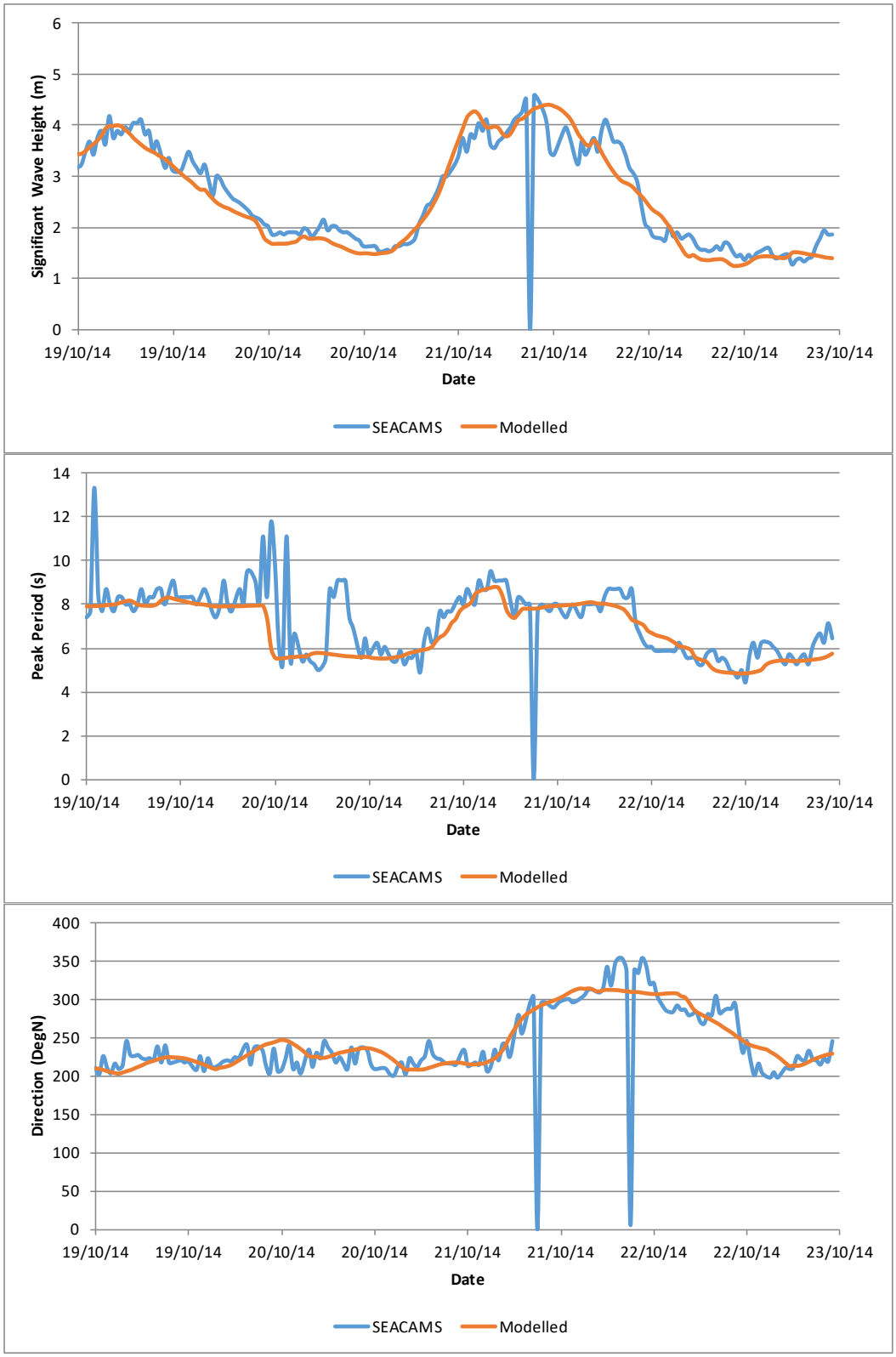

Figure 5.11: A comparison of modelled against measured wave conditions at the SEACAMS wave buoy during the 21/10/2014 storm: Top: Significant wave height, Middle: peak period, Bottom: Wave direction

Source: HR Wallingford SWAN model and SEACAMS data

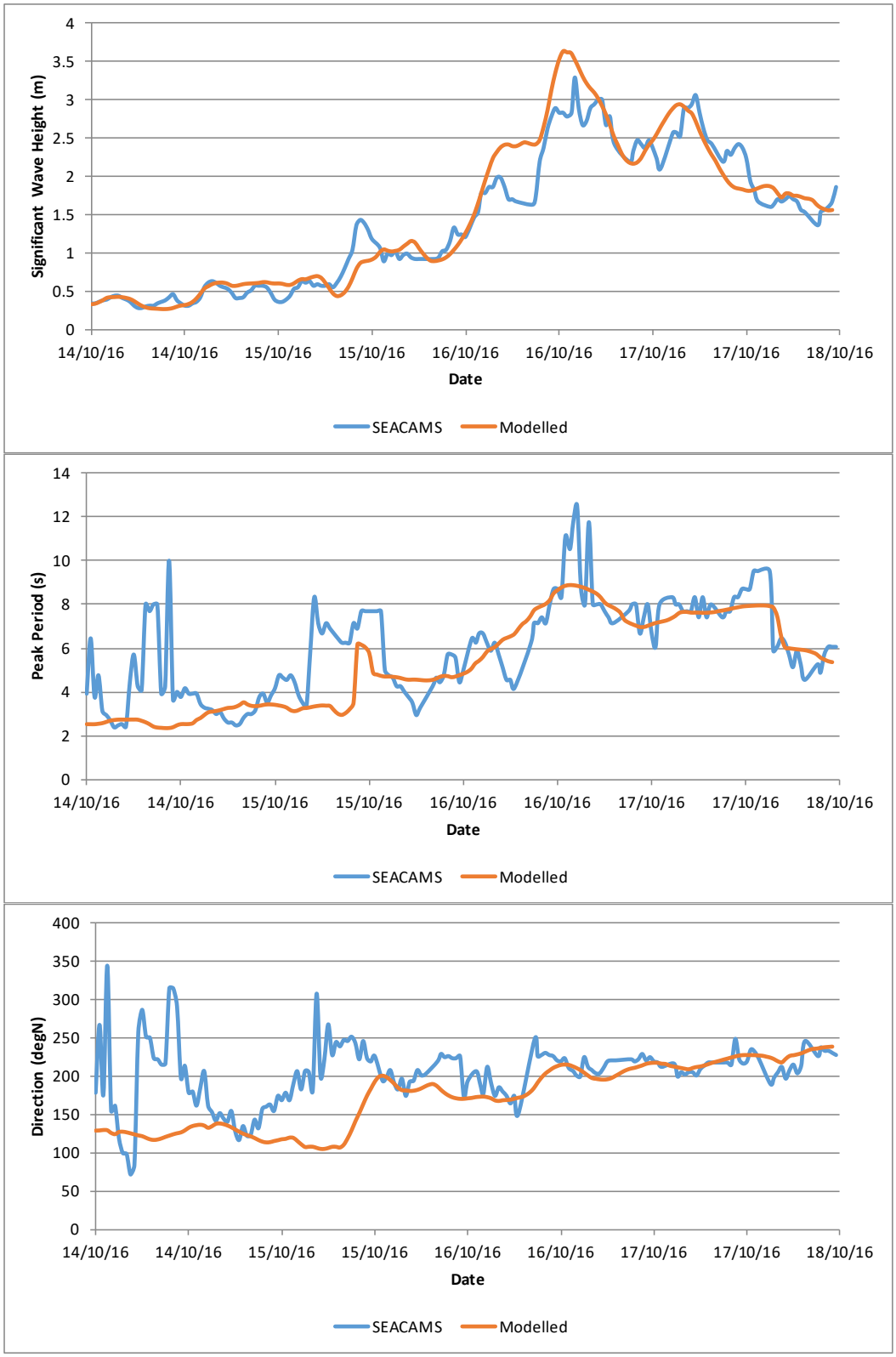

Figure 5.12: A comparison of modelled against measured wave conditions at the SEACAMS wave buoy during the 16/10/2016 storm: Top: Significant wave height, Middle: peak period, Bottom: Wave direction

Source: HR Wallingford SWAN model and SEACAMS data

The IEC TS 62600-201 report on tidal energy does not specify standards for wave model validation. The most relevant standards are from the Environment Agency (Ref. 5) report regarding validation of wave models for use in coastal flood forecasting. This report defines different standards of validation depending on the use of the model. The highest standard (Standard 1) is for models used in the design of coastal defences. This specifies that the predictions of Hs from the model should have a Relative Bias < 10% and a Scatter Index (SI) < 20%. Based on the wave validation presented above for all data throughout the 4 storms and for the storm peaks, the error statistics are as shown in Table 5.5 below. This shows that the model validation is very good and easily meets the targets from EA 2016 (Ref. 5).

Table 5.5: Error statistics from wave model validation

	Relative Bias	Scatter Index (SI)
All data throughout storm	-1.5%	13.7%
Storm peaks	-0.9%	14.3%
Target Standard 1 (EA 2016)	10%	20%

Source: SWAN model and EA(Ref. 5)

5.5. Wave model simulations (Direct effect)

After the validation was complete, the model was run for the baseline situation with both the representative and extreme conditions mentioned in section 5.2.1. The model was run for 2 tidal cycles with results from high water being plotted. The baseline runs from high water are most likely to have an effect on the coast as during extreme conditions, the greatest impact on the coastline occurs during high tide. Diffraction is not included in the model since the SWAN model can only represent far-field diffraction rather than the detailed near field interactions of diffracted waves around structures. Figure 5.17 shows an example of an extreme condition run from 210°N for the baseline scenario.

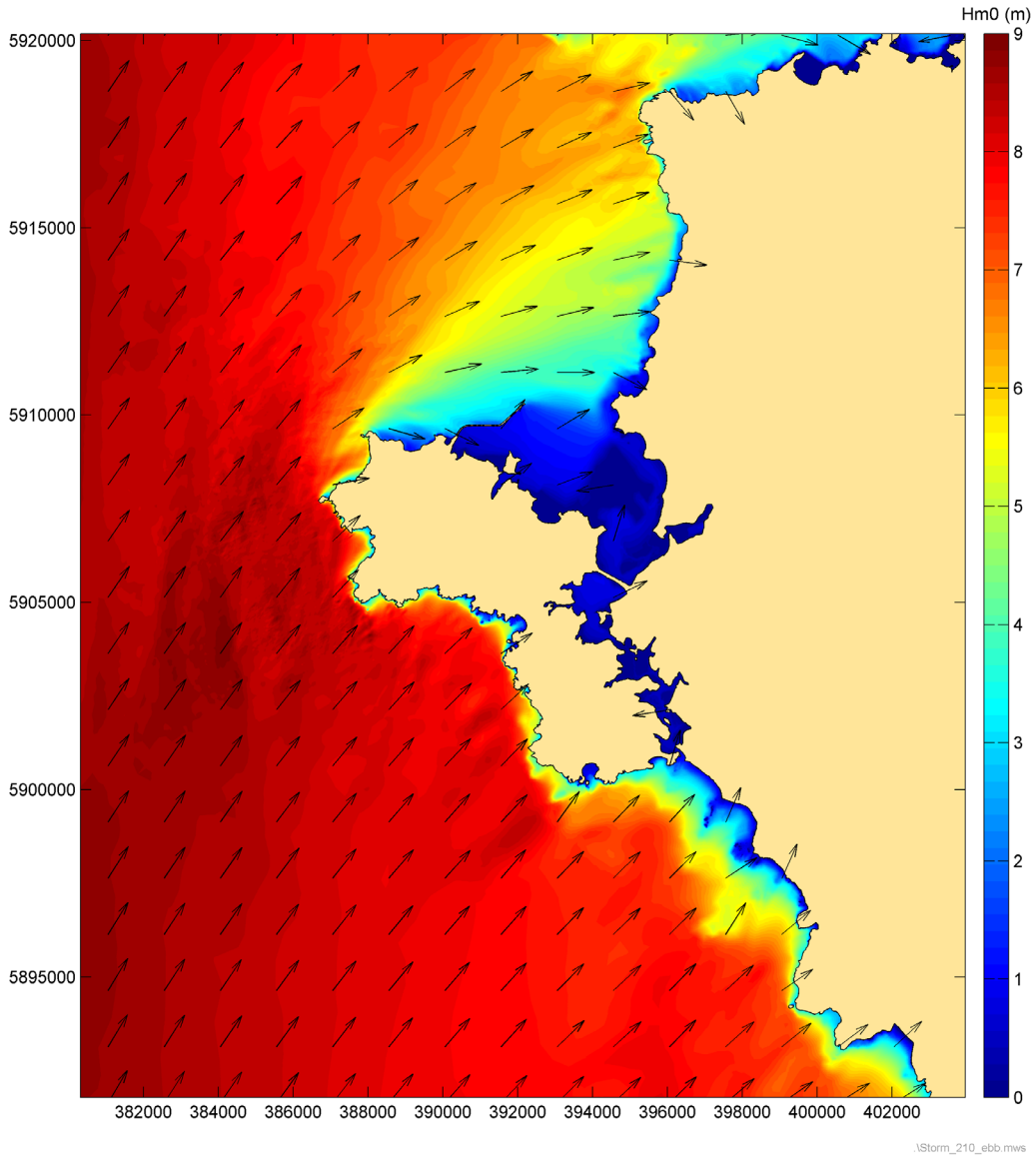

Figure 5.13: An extreme baseline condition model run for waves from 210°N at high water

Source: HR Wallingford's SWAN model

5.5.1. Structures

In order to model the impact of the tidal energy structures, a "worst case" scenario was considered which is likely to have the greatest effect on the waves (Figure 5.14). Floating devices will have a greater impact on the waves than seabed mounted structures as they can directly block the waves. As the seabed mounted structures are located in relatively deep water (around 30 to 40m depth) the effect of these structures on the waves is likely to be low. This is the same for the seabed mounted hubs, but as these are larger, they may have some effects as they can change the orbital velocity of the wave due to friction. The surface piercing hubs will have an effect on the waves as they extend over the whole water column. In total, the worst case scenario for wave impact had 60 2MW floating devices located in the southern area of the design zone as

these are not allowed to be located in the northern half, 310 seabed devices, 60 seabed hubs and 8 surface piercing hubs.

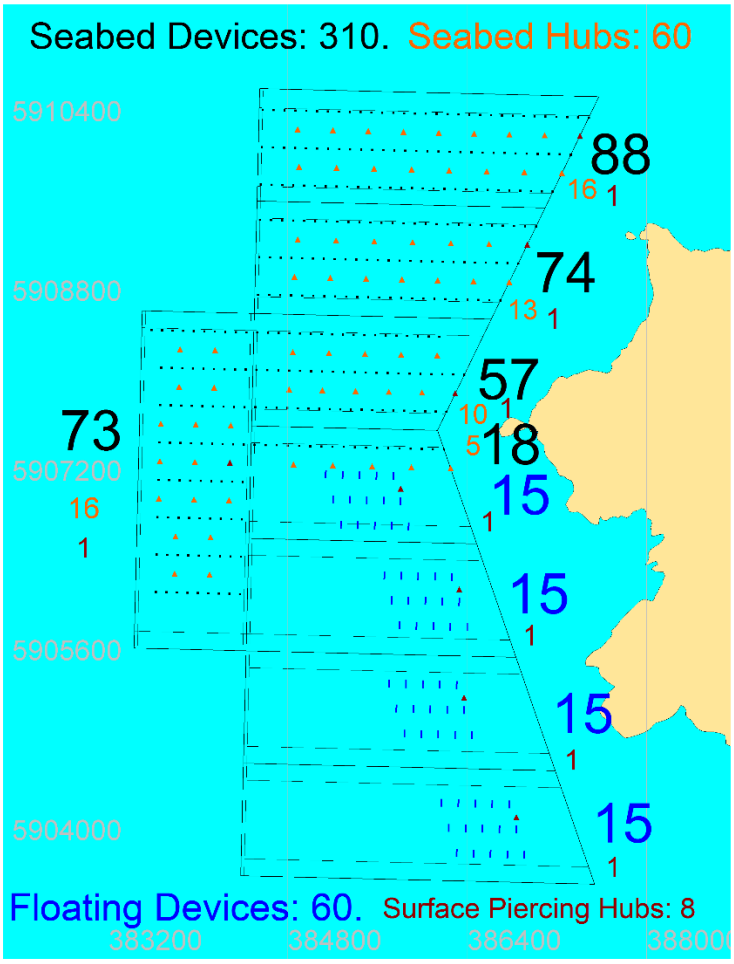

Figure 5.14: An overview of the worst case wave scenario for tidal turbines

Source: HR Wallingford

In order to model the devices in the wave model, different techniques were implemented depending on the type of the device. The seabed hubs have been modelled by raising the bathymetry at their location by 8m. this creates patches of shallower water, but as they are still located in deep water (30-40m), they were shown to have no real effect on the waves. Since the seabed devices are smaller and cause less of a blockage (Figure 4.17) and still located in deep water, they have been ignored in terms of the direct impact. The way the seabed devices are likely to change the waves is in the indirect effect of slowing the currents that then affects the wave transformation. This is modelled later in the report (Section 5.6).

Both the floating devices and surface piercing hubs were implemented as obstacles in the SWAN model. The surface piercing hubs were given a transmission coefficient of 0 and a reflection coefficient of 1. This is because the hubs occupy the full water column so no energy can be transferred through them and as they are vertical, there will be significant wave reflection.

5.5.2. Calculation of transmission and reflection coefficients

The largest floating turbine devices are the 73m long Orbital devices as shown in Figure 5.15. Drawings of the device show that the float extends to 2.5m below the waterline. In addition there is an additional blockage effect of the turbine supports. Calculating the cross-sectional area of the turbine support structure and redistributing it over the length of the float adds an extra 1m to the blockage. Therefore the effect of each of the floating turbine devices on waves has been represented by a 73m long floating breakwater with draught 3.5m. This is conservative since floating breakwaters are designed specifically to reduce wave energy transmission whereas the turbine float is more streamlined.

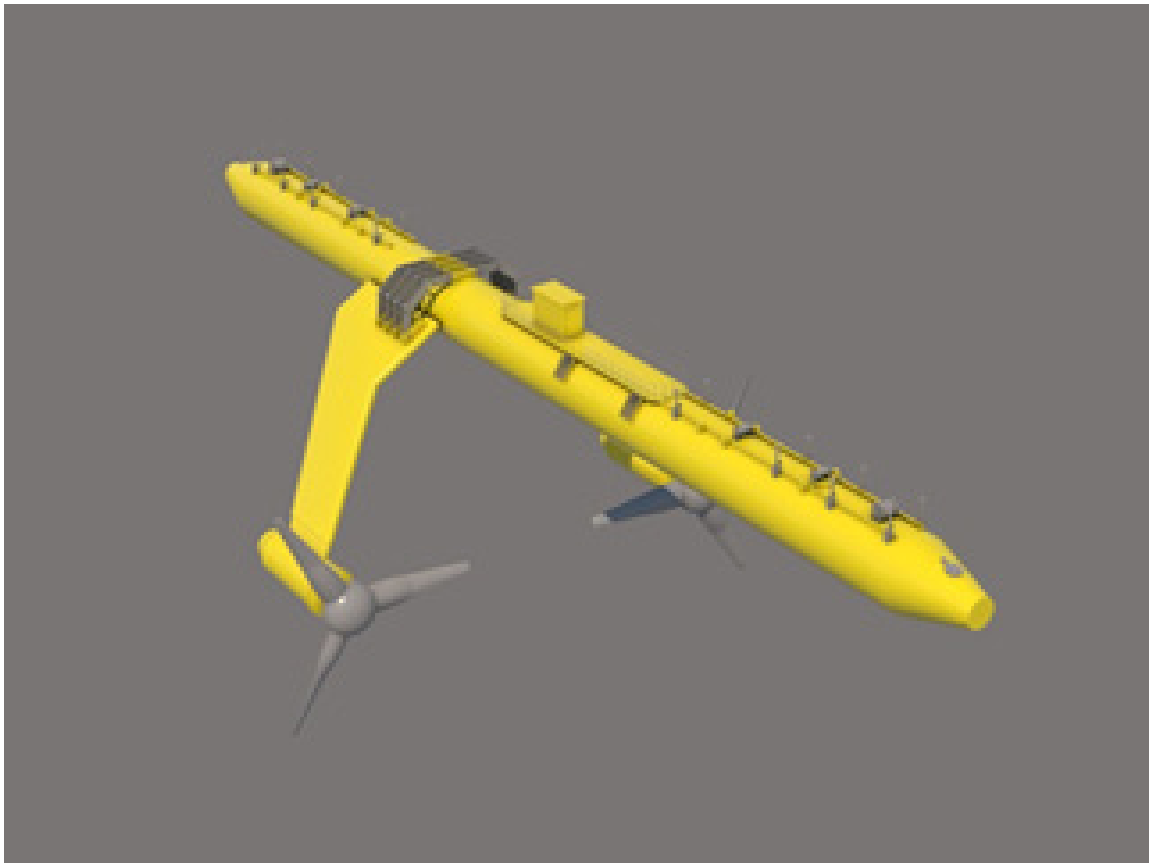

Figure 5.15: Orbital 2MW floating turbine

Source: Menter Môn

A literature review of methods to estimate the transmission coefficient of floating breakwaters was carried out. Figure 2.7 of PIANC(1994, Ref. 16) is reproduced below. This presents the transmission coefficient K_t (ratio of transmitted wave to incident wave) in terms of the relative depth z/d and the ratio d/L where:

- z is the draught of the floating breakwater (3.5m);
- d is the water depth (30m at the shallowest point);
- L is the wavelength.

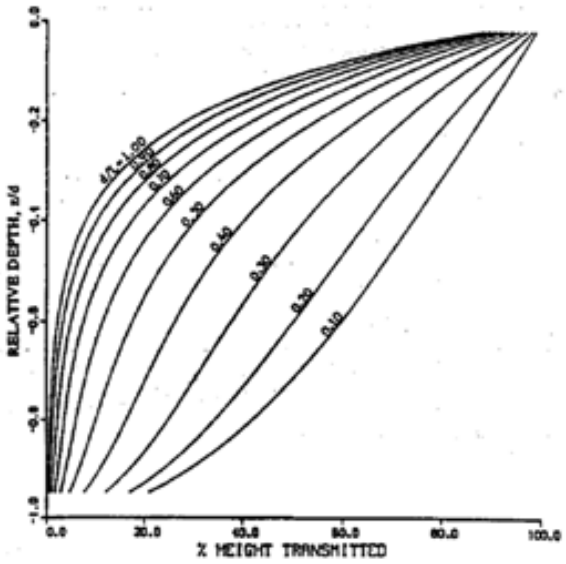

Figure 5.16: Transmission coefficient of floating breakwaters

Source: PIANC(1994)

For the representative waves, the peak wave periods were 6-7s and the extreme waves nearer 11s.

A transmission coefficient of 1 means that all the wave energy passes through or under the device whereas a coefficient of 0 would be for a solid wall blocking all wave energy. Longer period waves are affected less by the floating device since the device will just move up and down on the wave and a larger proportion of the wave energy passes underneath. The smaller the transmission coefficient, the more effect the floating structures will have on the coastline. Therefore to be conservative in representing their effects, lower estimates were made of the transmission coefficients, giving 0.7 for the shorter period representative waves and 0.85 for the longer period extreme waves. These values are also similar to what would be calculated from (Kriebel, 1996, Ref. 12) for waves passing under a rigid skirt breakwater barrier, indicating that the chosen transmission coefficients are conservatively low.

Wave reflection coefficients were also applied to the floating turbine structures. Koutandos (2004, Ref. 11) presents experimental results of both reflection and transmission coefficients for some floating breakwater structures. In these results the reflection coefficients (K_r) were generally approximately related to the transmission coefficients by $K_r = 1 - K_t$. Therefore reflection coefficients were calculated in this way for application to the structures represented as obstacles in the SWAN model.

5.5.3. Comparison of pre and post structure

The representative conditions are derived for use in the sediment model (Section 6.2.2). These conditions are typical “everyday” conditions which will be useful for assessing the effects on the long term sediment transport processes. Figure 5.17 and Figure 5.18 show the baseline and with structures runs from 210°N. the structures only have a local effect on the wave model. Figure 5.19 to Figure 5.26 present the representative waves from the other directions. Waves from 270°N approach perpendicular to the floats of the tidal turbines (which align approximately North-South with the flow. Although this means that there is greater blockage of the waves from 270°N, the representative waves from this direction are relatively small so there are still only

local effects to the wave heights. Waves from the northwest have similar effects to those from the southwest but on a smaller scale as the wave heights are lower. The arrows on the figures show the wave direction.

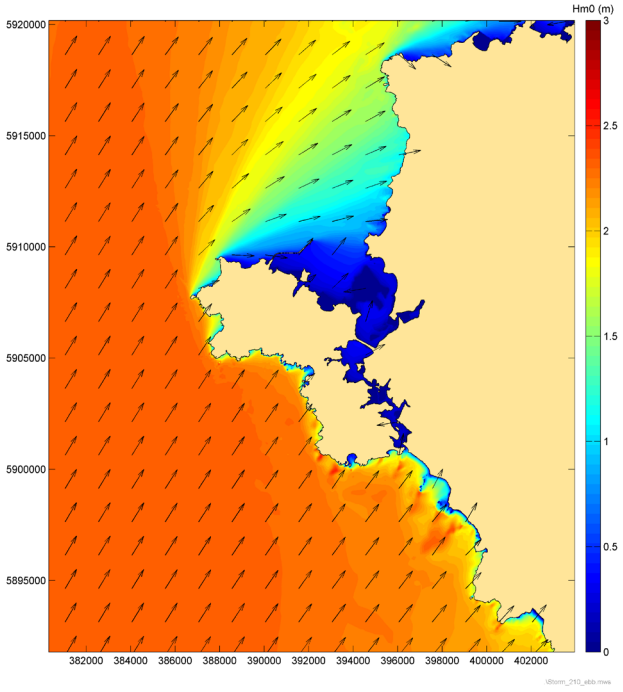

Figure 5.17: Baseline condition model run for Representative waves from 210°N at high water

Source: SWAN

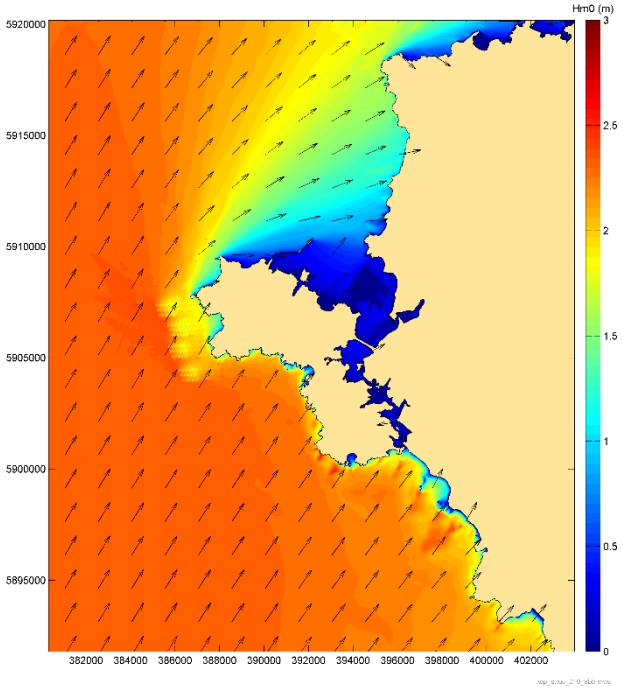

Figure 5.18: With structures condition model run for Representative waves from 210°N at high water

Source: SWAN

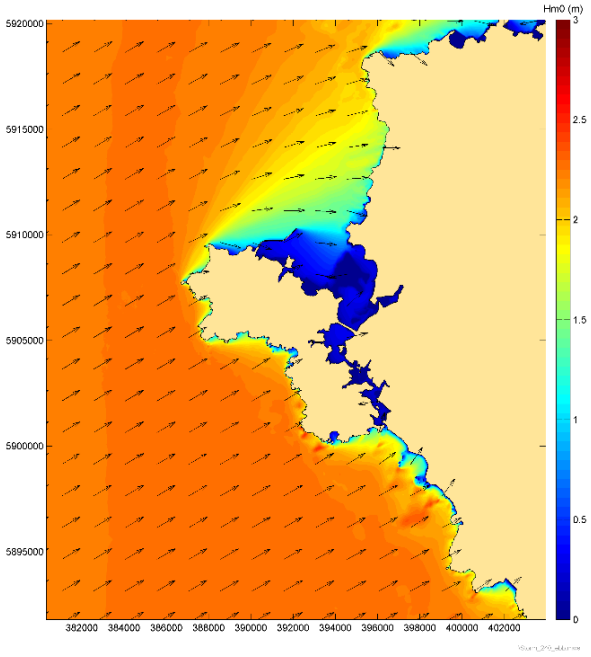

Figure 5.19: Baseline condition model run for Representative waves from 240°N at high water

Source: SWAN

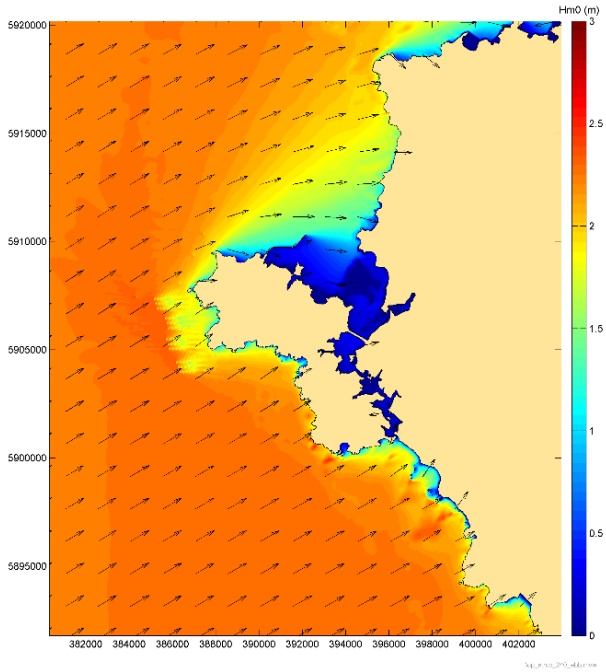

Figure 5.20: With structures condition model run for Representative waves from 240°N at high water

Source: SWAN

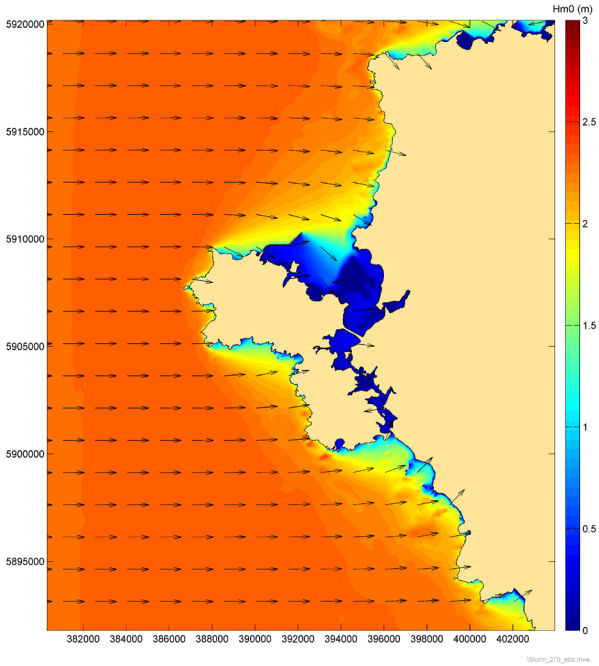

Figure 5.21: Baseline condition model run for Representative waves from 270°N at high water

Source: SWAN

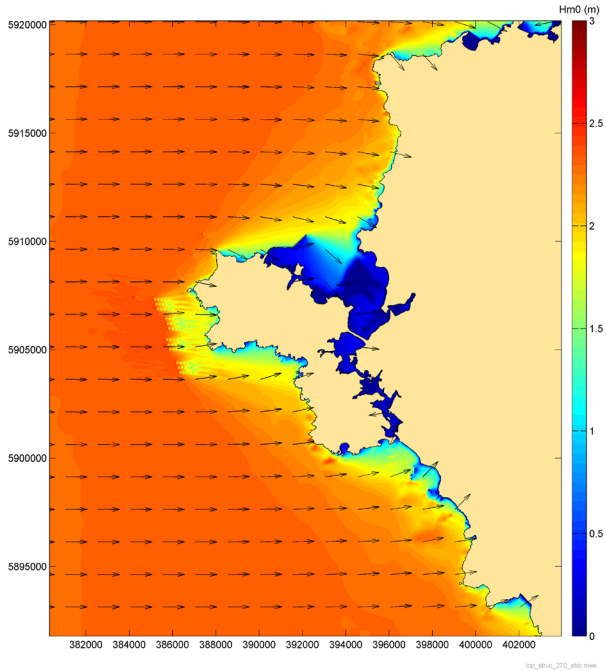

Figure 5.22: With structures condition model run for Representative waves from 270°N at high water

Source: SWAN

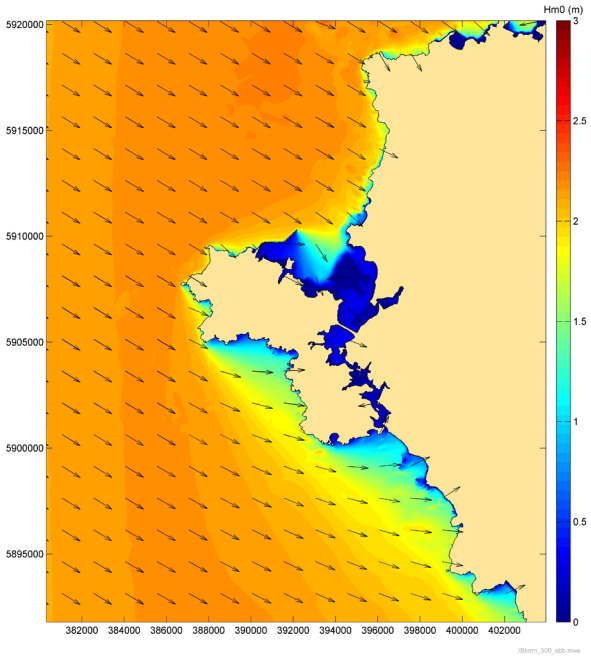

Figure 5.23: Baseline condition model run for Representative waves from 300°N at high water

Source: SWAN

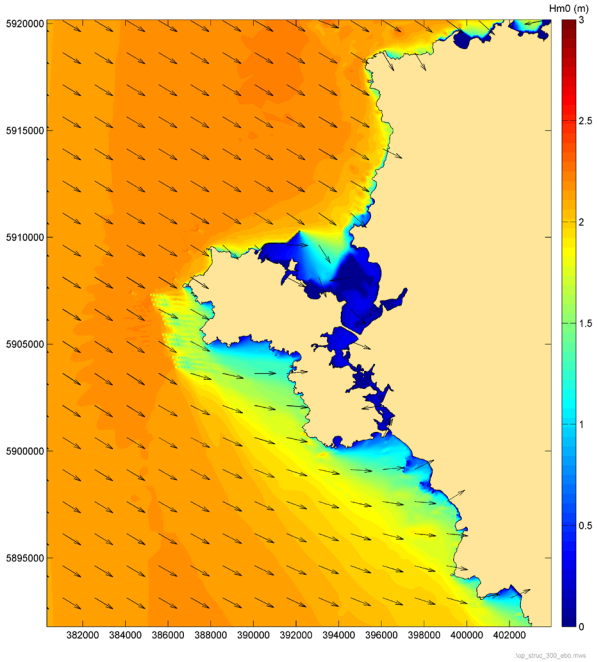

Figure 5.24: With structures condition model run for Representative waves from 300°N at high water

Source: SWAN

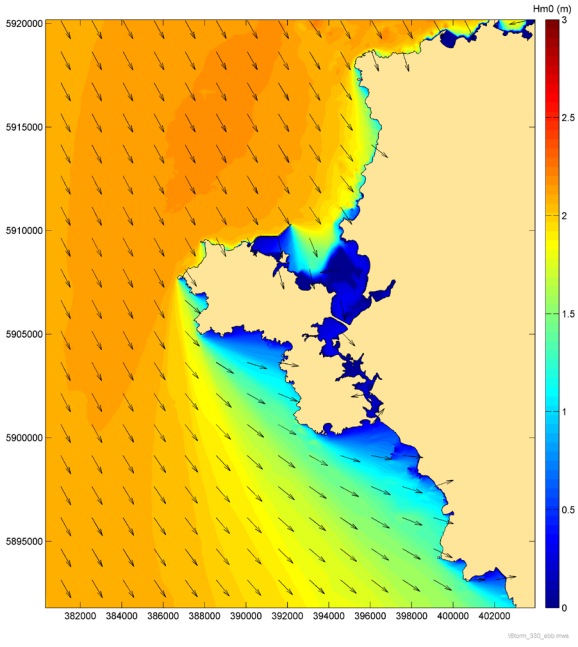

Figure 5.25: Baseline condition model run for Representative waves from 330°N at high water

Source: SWAN

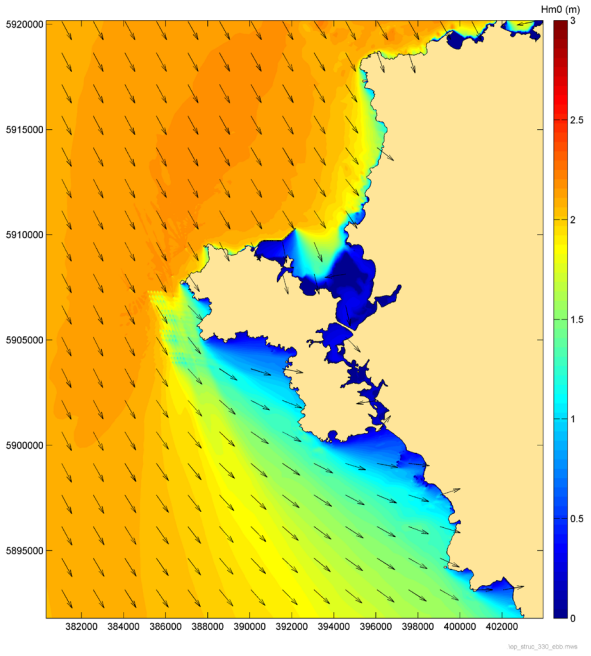

Figure 5.26: With structures condition model run for Representative waves from 330°N at high water

Source: SWAN

Extreme conditions will have a greater effect on the coastline. This is because large waves carry large amounts of energy which can result in coastal erosion, structural damage and even coastal flooding. The extreme waves are most dominant from 210°N as the wave is not fetch limited. Since the extreme waves have a larger period then the representative conditions, a higher transmission coefficient is used, which allows more wave energy to pass the devices. As more energy is passing the devices, it is expected that the structures will have proportionately less effect on the extreme conditions.

As seen in the representative conditions, the tidal devices also only have a local blocking effect on the extreme waves. The amount of blocking caused by the devices is likely to be conservative as diffraction is not switched on in the model. The floating devices also cause a slight change in the direction of the waves. The direction change, like the change in wave height is only localised. Although Figure 5.27 to Figure 5.36 indicate that there is only a small change in wave height, the devices may act to dampen the waves meaning that the risk of erosion and flooding from wave attack may be reduced.

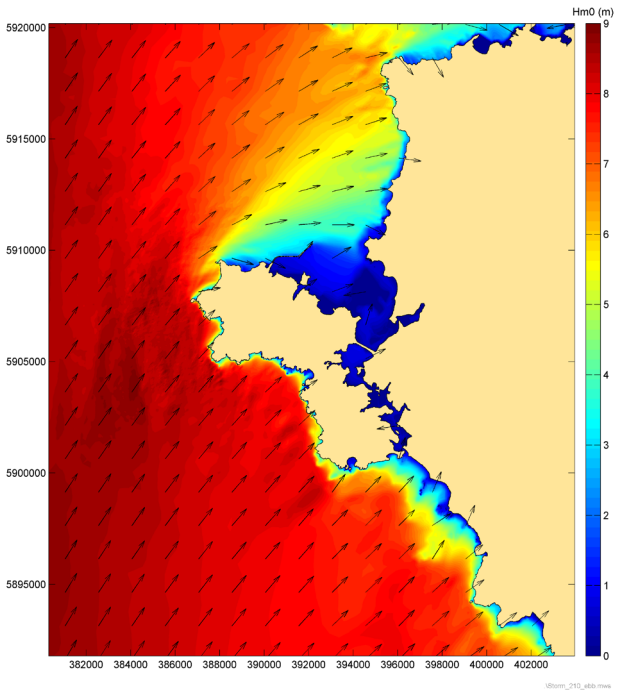

Figure 5.27: Baseline condition model run for Extreme waves from 210°N at high water

Source: SWAN

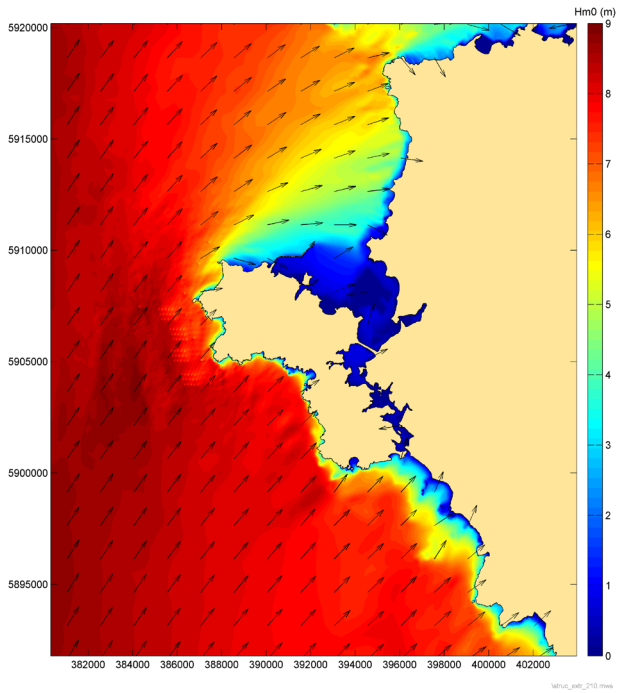

Figure 5.28: With structures condition model run for Extreme waves from 210°N at high water

Source: SWAN

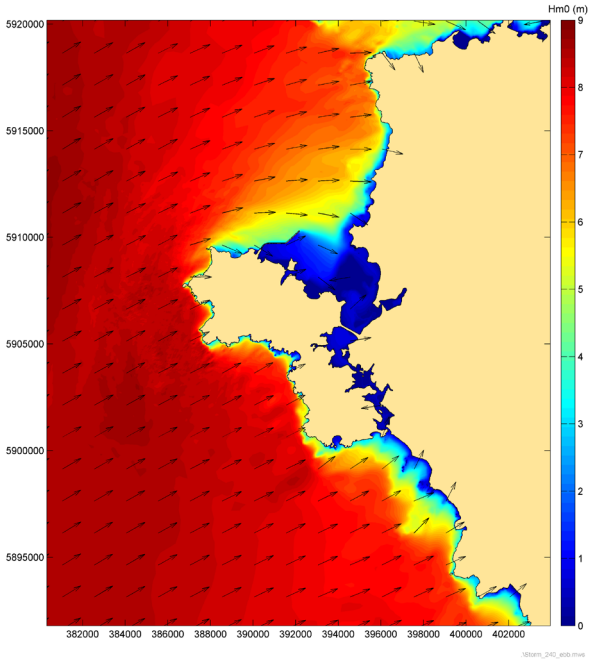

Figure 5.29: Baseline condition model run for Extreme waves from 240°N at high water

Source: SWAN

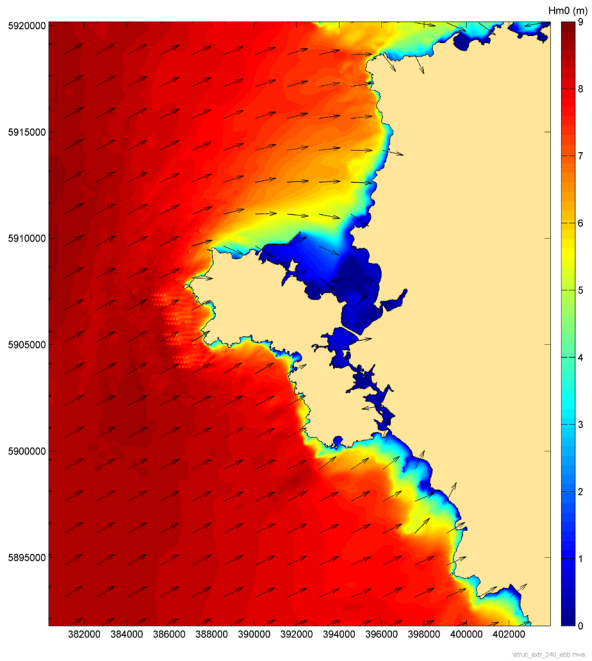

Figure 5.30: With structures condition model run for Extreme waves from 240°N at high water

Source: SWAN

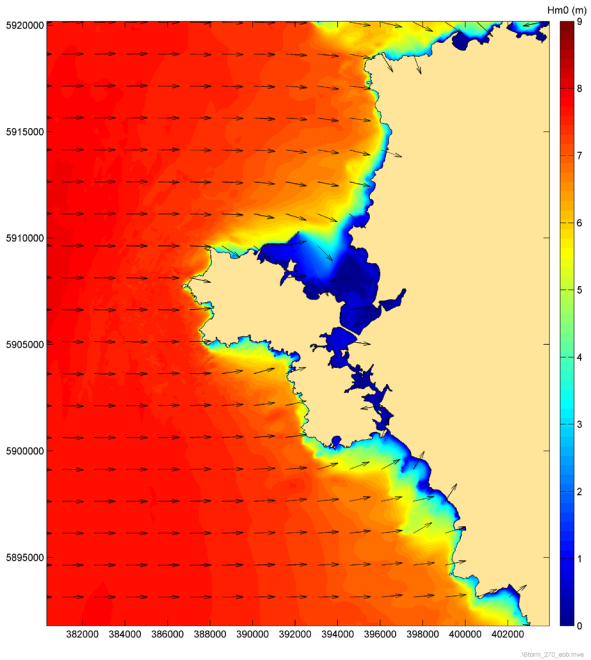

Figure 5.31: Baseline condition model run for Extreme waves from 270°N at high water

Source: SWAN

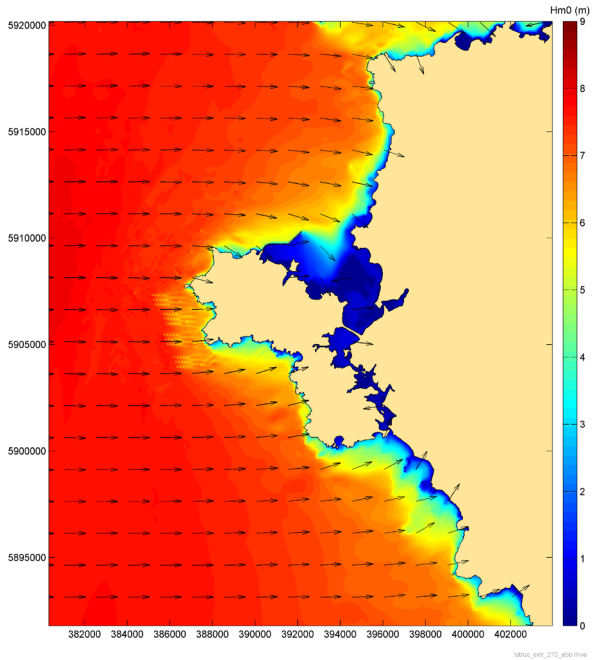

Figure 5.32: With structures condition model run for Extreme waves from 270°N at high water

Source: SWAN

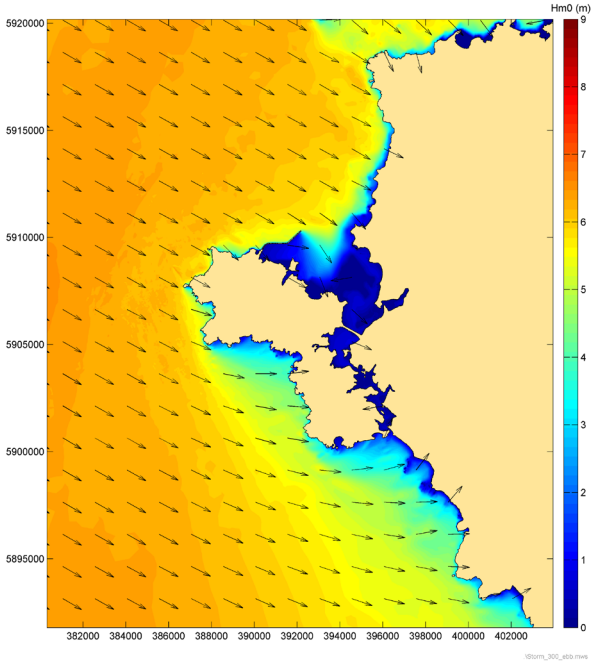

Figure 5.33: Baseline condition model run for Extreme waves from 300°N at high water

Source: SWAN

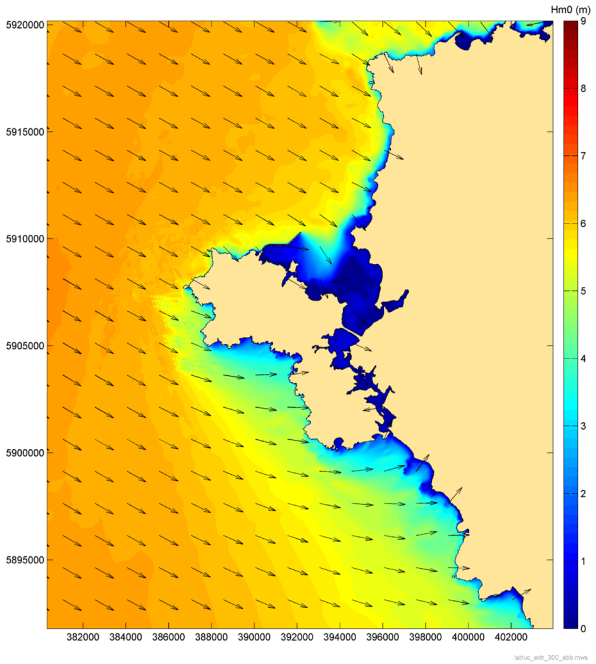

Figure 5.34: With structures condition model run for Extreme waves from 300°N at high water

Source: SWAN

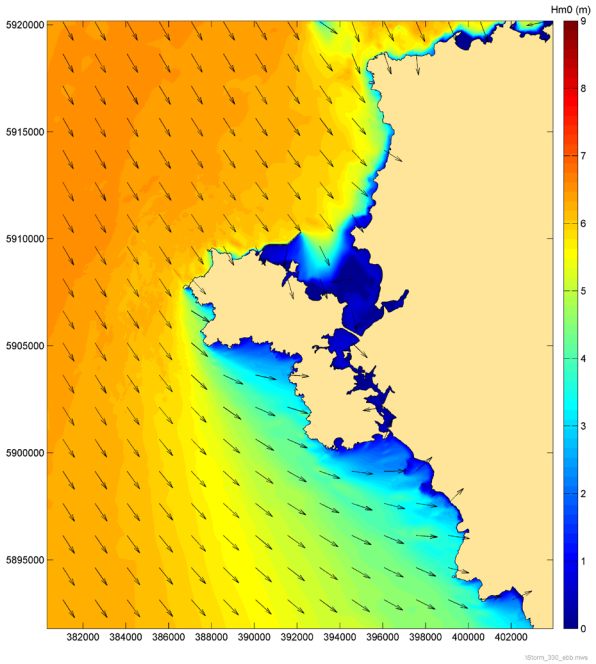

Figure 5.35: Baseline condition model run for Extreme waves from 330°N at high water

Source: SWAN

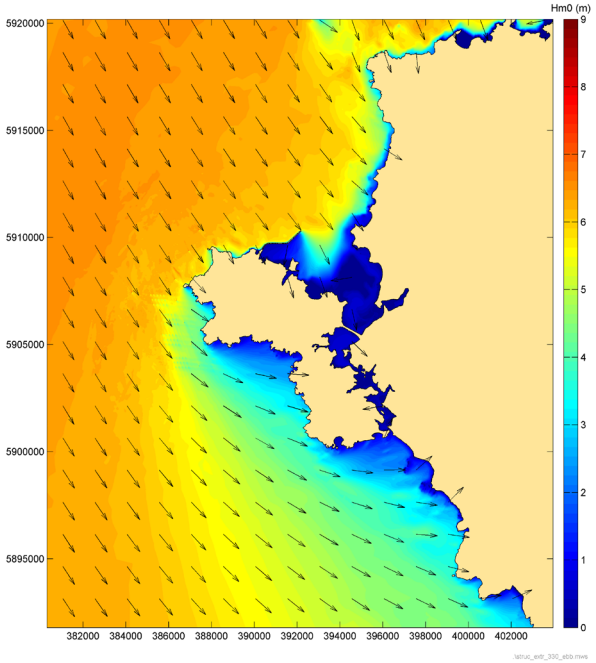

Figure 5.36: With structures condition model run for Extreme waves from 330°N at high water

Source: SWAN

To visually represent the direct effects of the tidal devices on the wave conditions, difference plots have been made for both the representative and extreme conditions (Figure 5.38 to Figure 5.47 and differences plots focused near Holy island are given in Appendix B.1). In order to understand the effects of the tidal devices, 7 key points have been selected based on areas of morphological interest. Point 2 is located on the northern point of Langdon ridge, point 3 is located at the South Stack banner bank and point 4 and 5 are located at the 'mouths' of Gogarth Bay and Abraham's Bosom just north and south of South Stack. Points 1, 6 and 7 are more distant pocket beaches (Cemlyn Bay, Rhosneigr,and Aberffraw). Details of the 7 points are given in Table 5.6 and shown in Figure 5.37. A change in the waves at these locations may have an effect on the sediment transport as well as on coastal erosion.

Table 5.6: Wave model – 7 key points of interest

Point	Location	Easting	Northing	Bathymetry (mOD)
1	Cemlyn Bay	400225	5919935	-16.3
2	Langdon ridge	394763	5916331	-16.9
3	South Stack banner bank	386236	5908594	-23.5
4	Gogarth Bay	387631	5908793	-16.8
5	Abraham's Bosom	387795	5906670	-11.3
6	Rhosneigr	398315	5896942	-11.9
7	Aberffraw	401792	5892784	-8.5

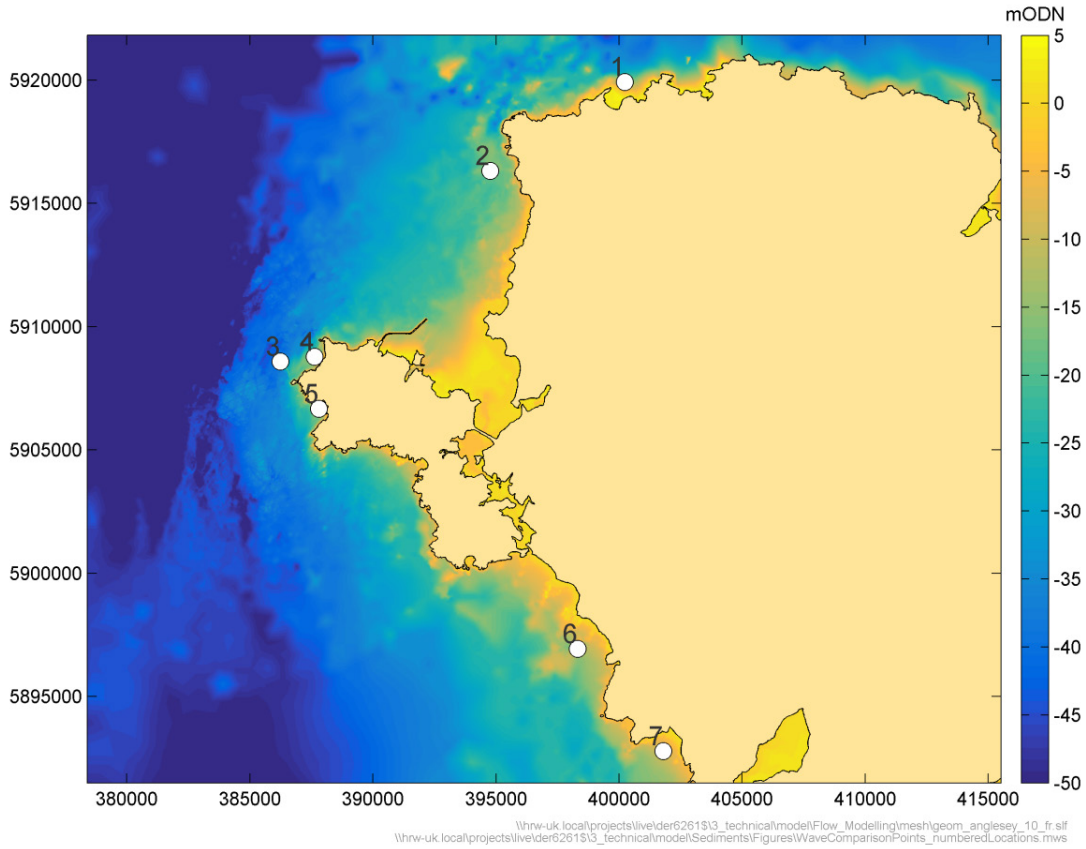

Figure 5.37: Wave model – 7 key points of interest

It is clear to see that the structures cause waves from all directions to reduce which is expected as the structures dissipate the wave energy. Points 3, 4 and 5 are most affected by waves from 210°N, 240°N and 270°N as the structures directly block the wave propagation (Figure 5.48). Waves from 300°N and 330°N have less of an effect on these points as the waves have not come into contact with the points before the structures. These waves however do have an effect on the waves heights on waves south west of Holy Island. This is the same whether it is a representative or extreme wave, but there is a greater proportional change in wave heights in the representative conditions. Points 1, 2, 6 and 7 are not in close proximity of the structures and are not affected by the structures reaffirming that the direct impact of the structures will only have a localised effect on the waves.

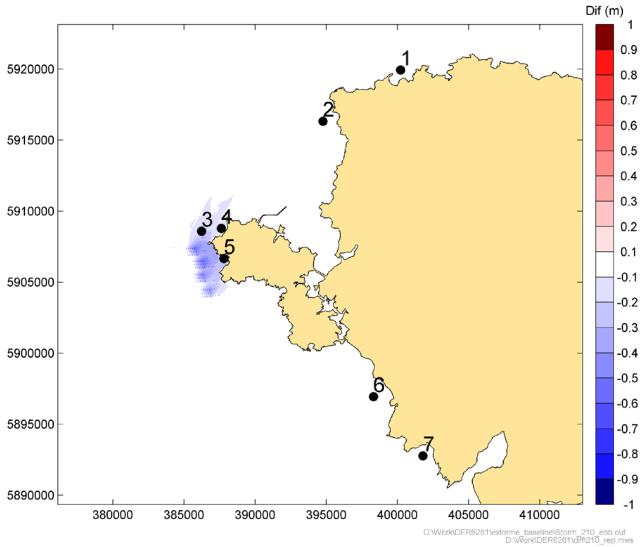

Figure 5.38: Difference in wave height from 210°N for a representative condition

Source: SWAN

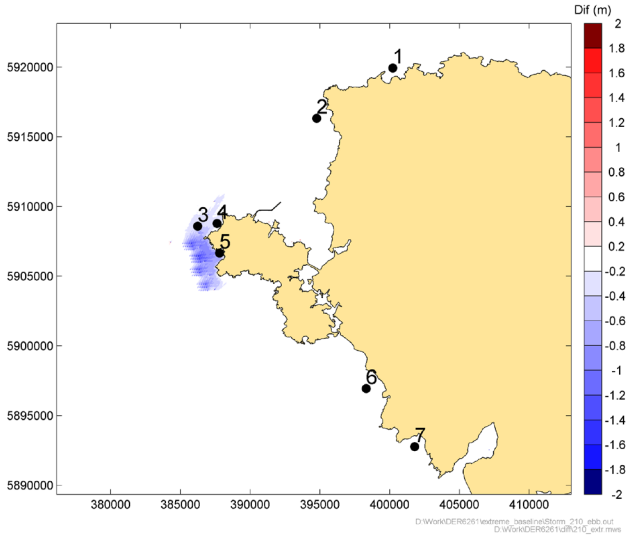

Figure 5.39: Difference in wave height from 210°N for an extreme condition

Source: SWAN

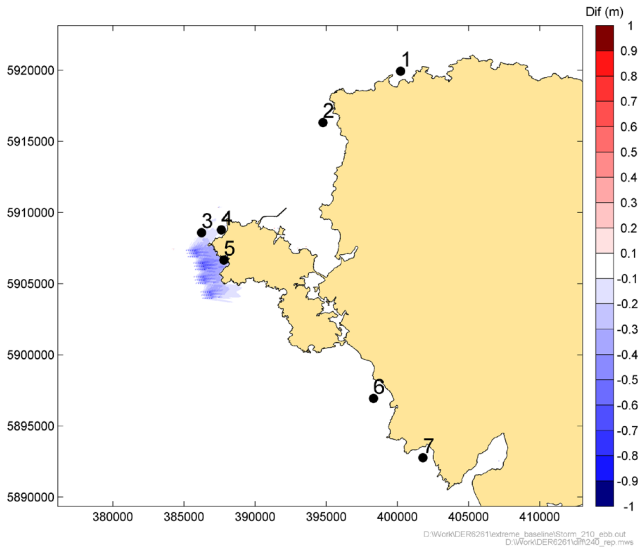

Figure 5.40: Difference in wave height from 240°N for a representative condition

Source: SWAN

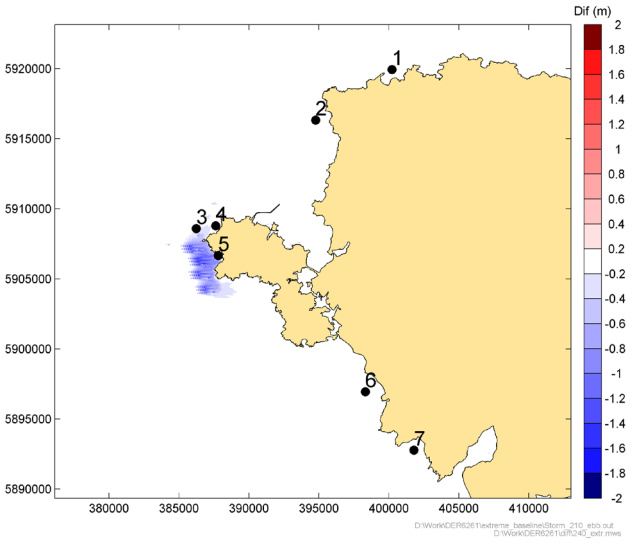

Figure 5.41: Difference in wave height from 240°N for an extreme condition

Source: SWAN

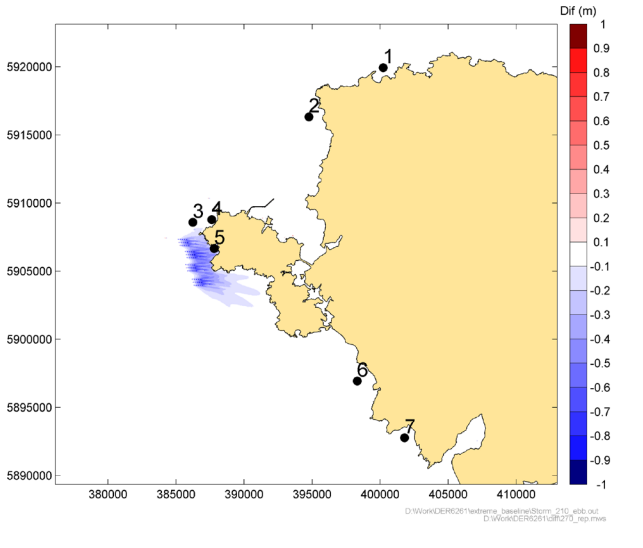

Figure 5.42: Difference in wave height from 270°N for a representative condition

Source: SWAN

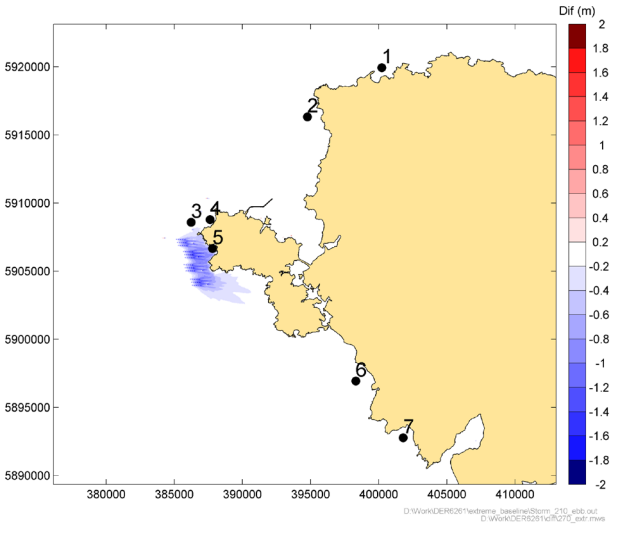

Figure 5.43: Difference in wave height from 270°N for an extreme condition

Source: SWAN

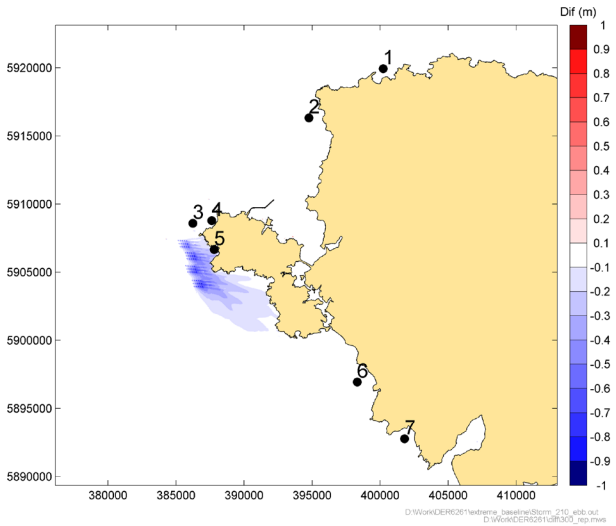

Figure 5.44: Difference in wave height from 300°N for a representative condition

Source: SWAN

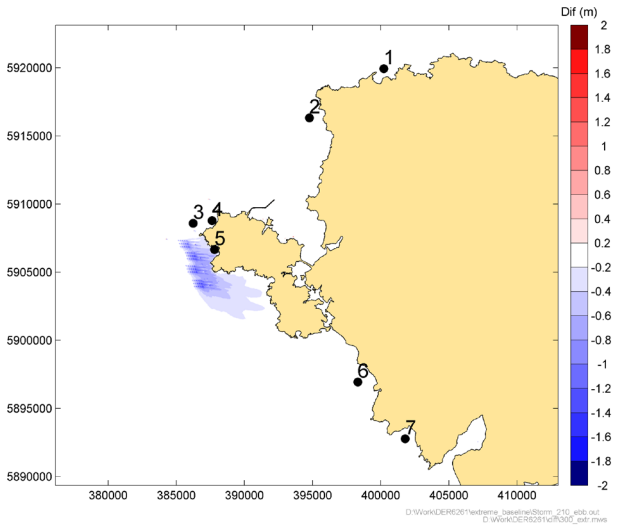

Figure 5.45: Difference in wave height from 300°N for an extreme condition

Source: SWAN

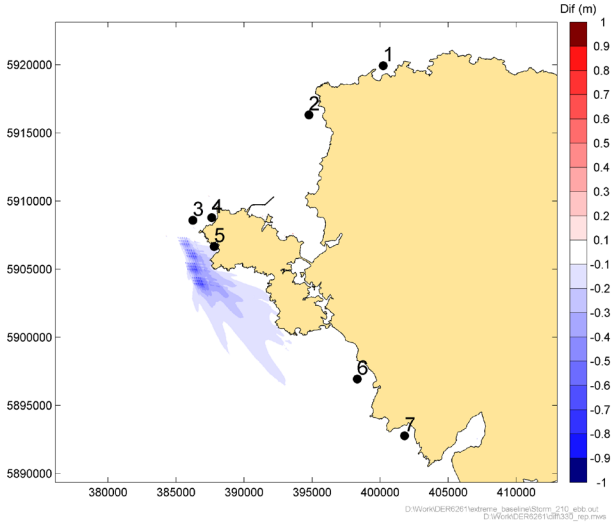

Figure 5.46: Difference in wave height from 330°N for a representative condition

Source: SWAN

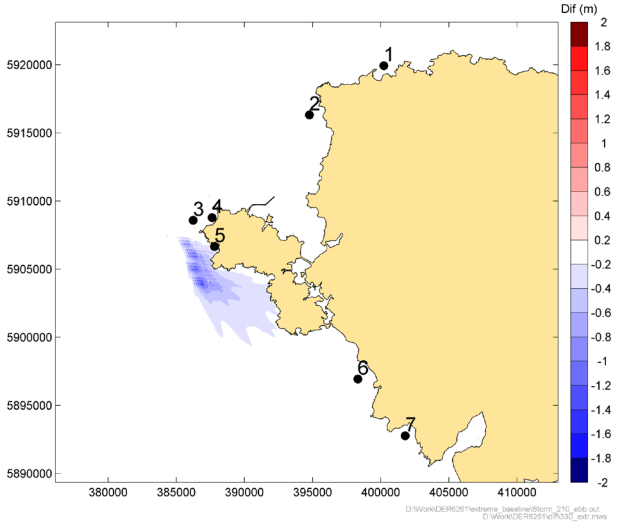

Figure 5.47: Difference in wave height from 330°N for an extreme condition

Source: SWAN

210°N

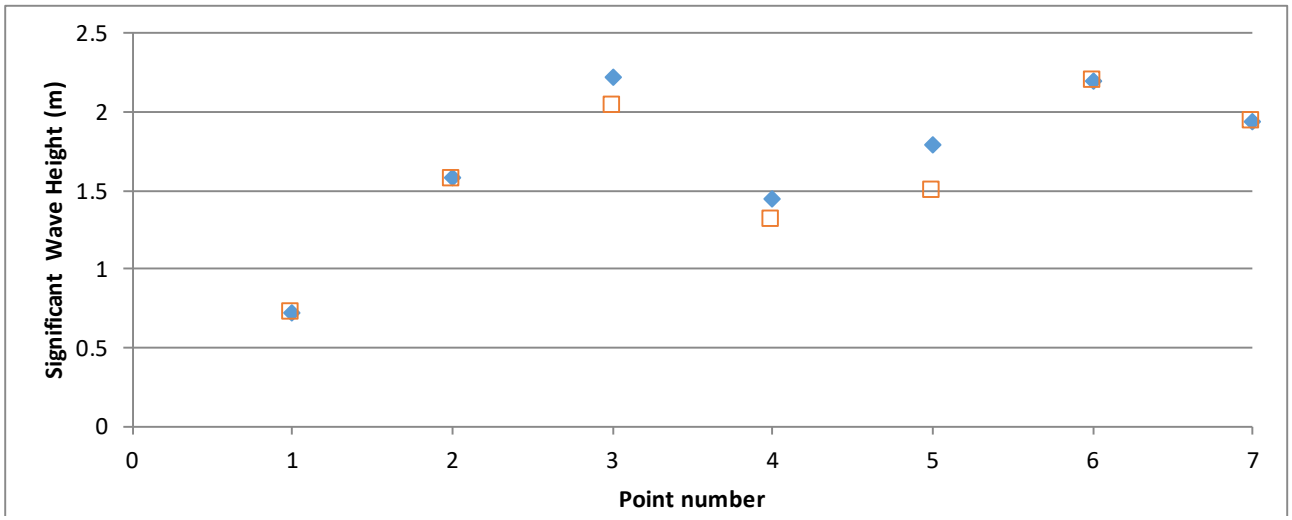

240°N

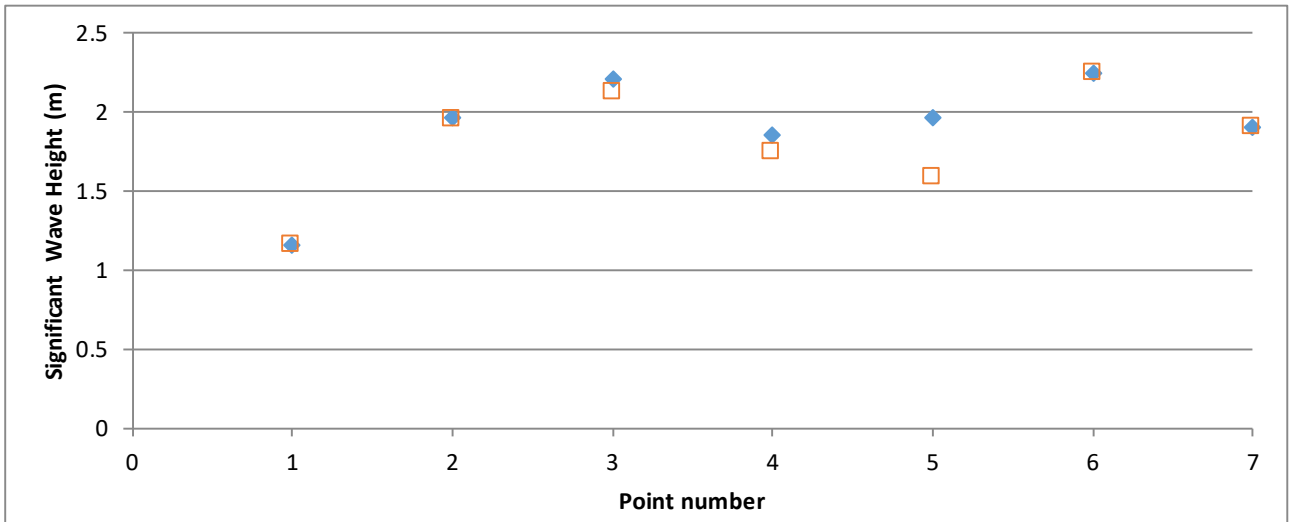

270°N

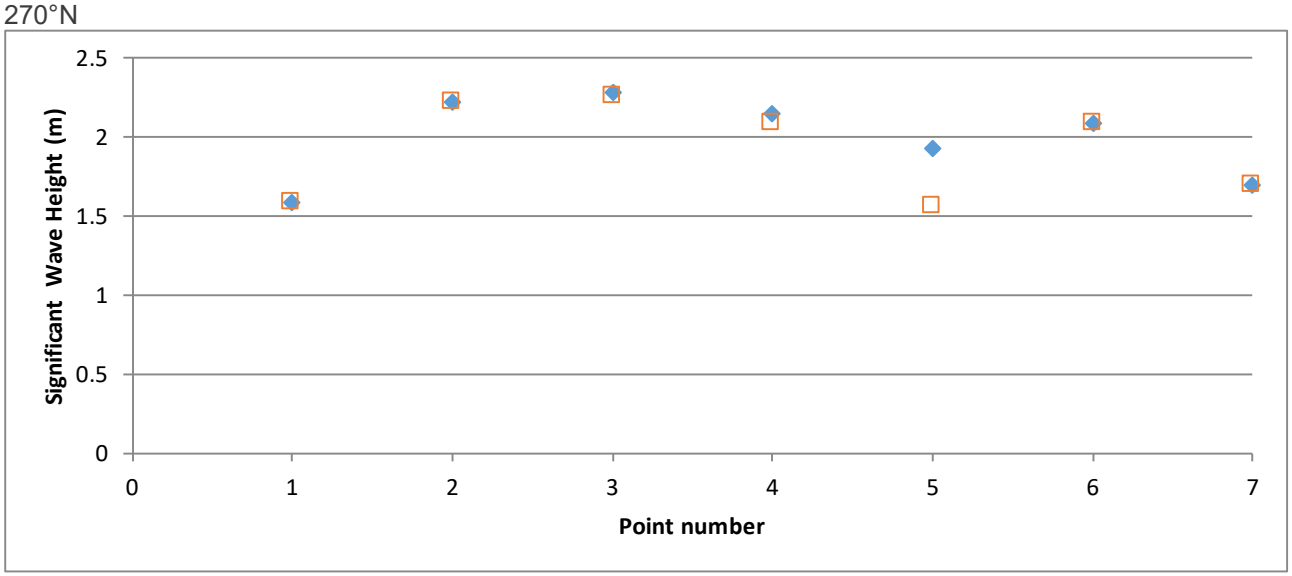

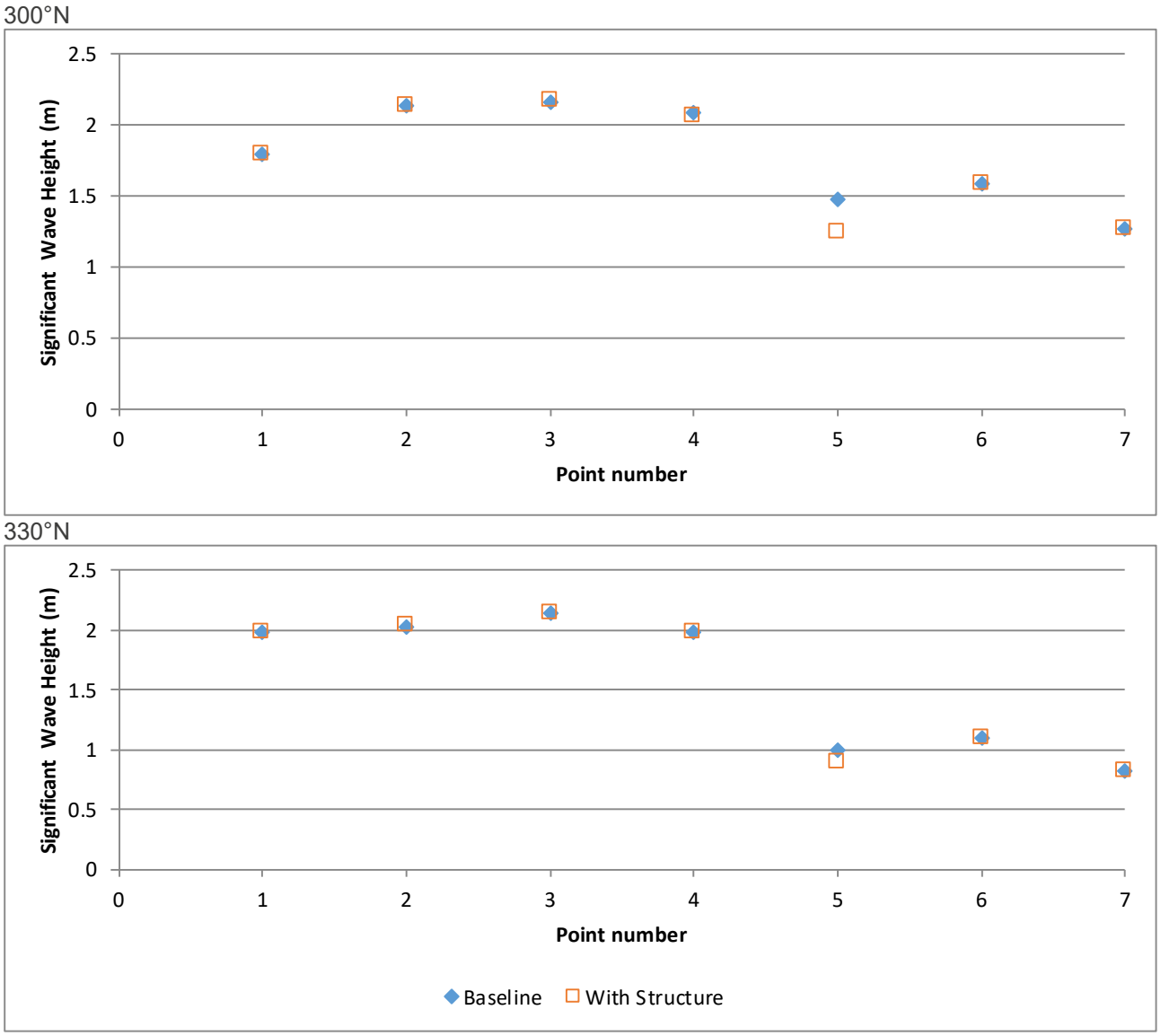

Figure 5.48: A comparison of wave heights from each point between Baseline and With Structures for Representative waves: Top to bottom: 210°N, 240°N, 270°N, 300°N, 330°N

Source: SWAN

210°N

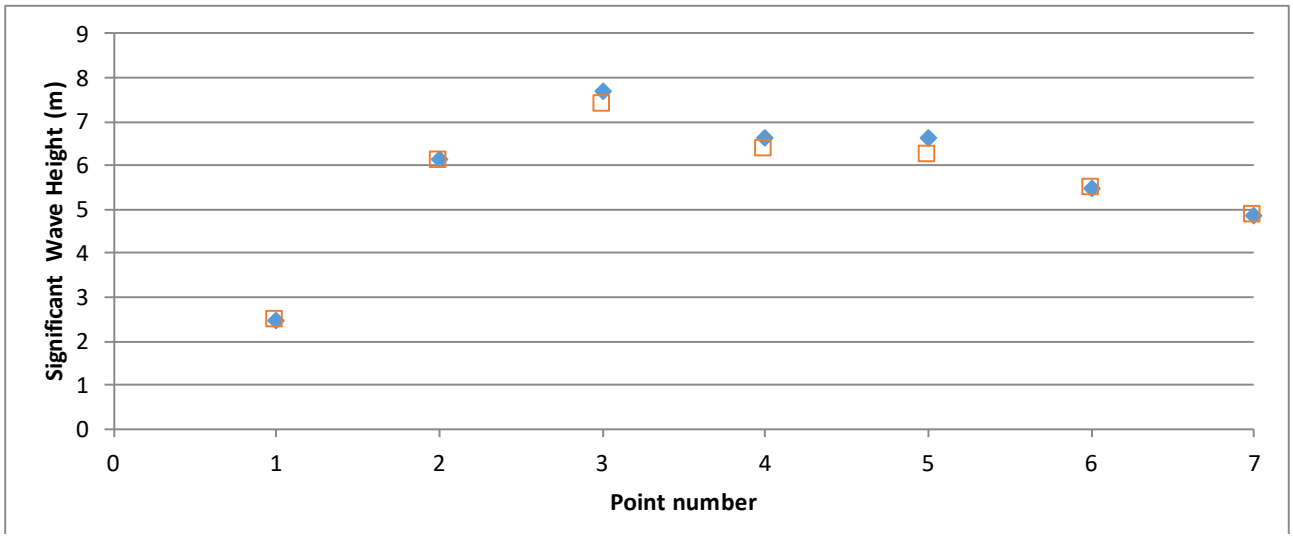

240°N

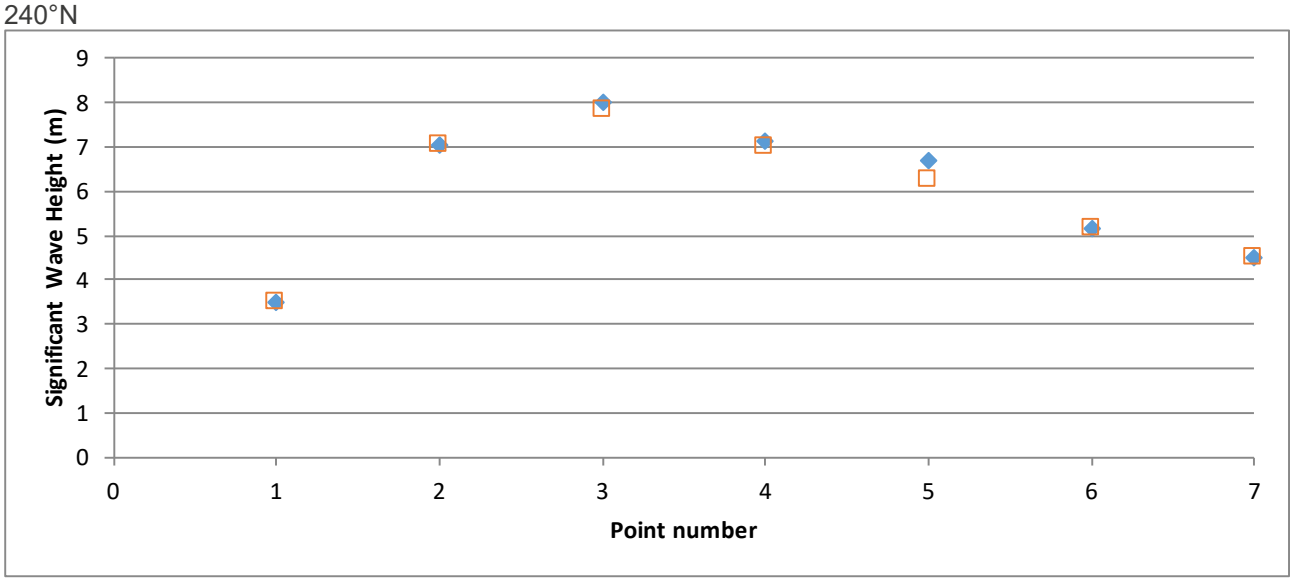

270°N

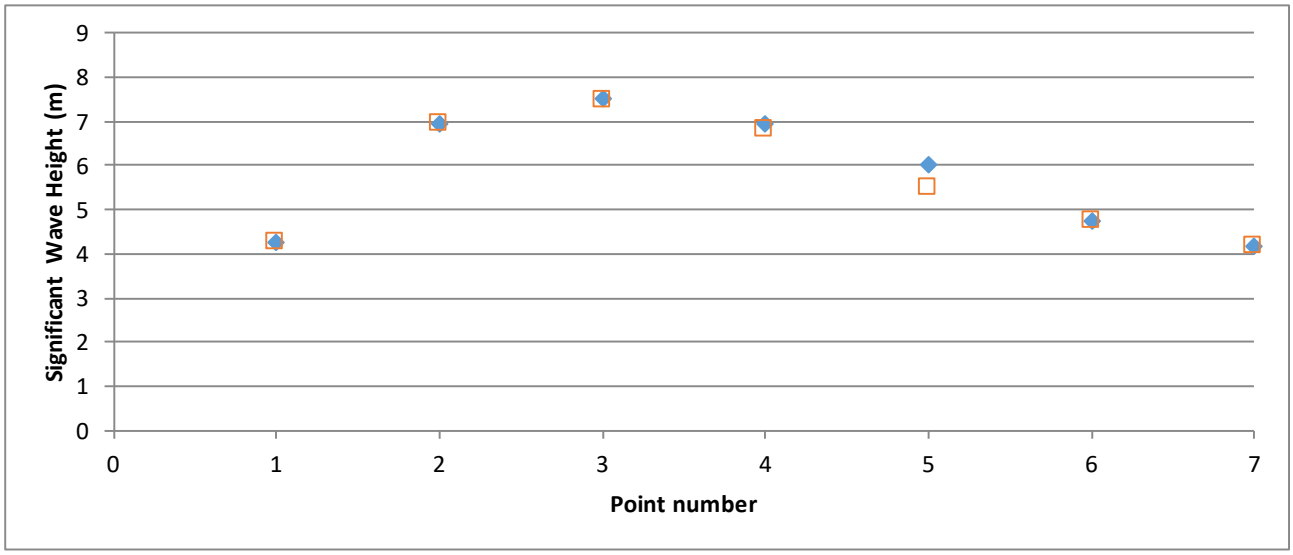

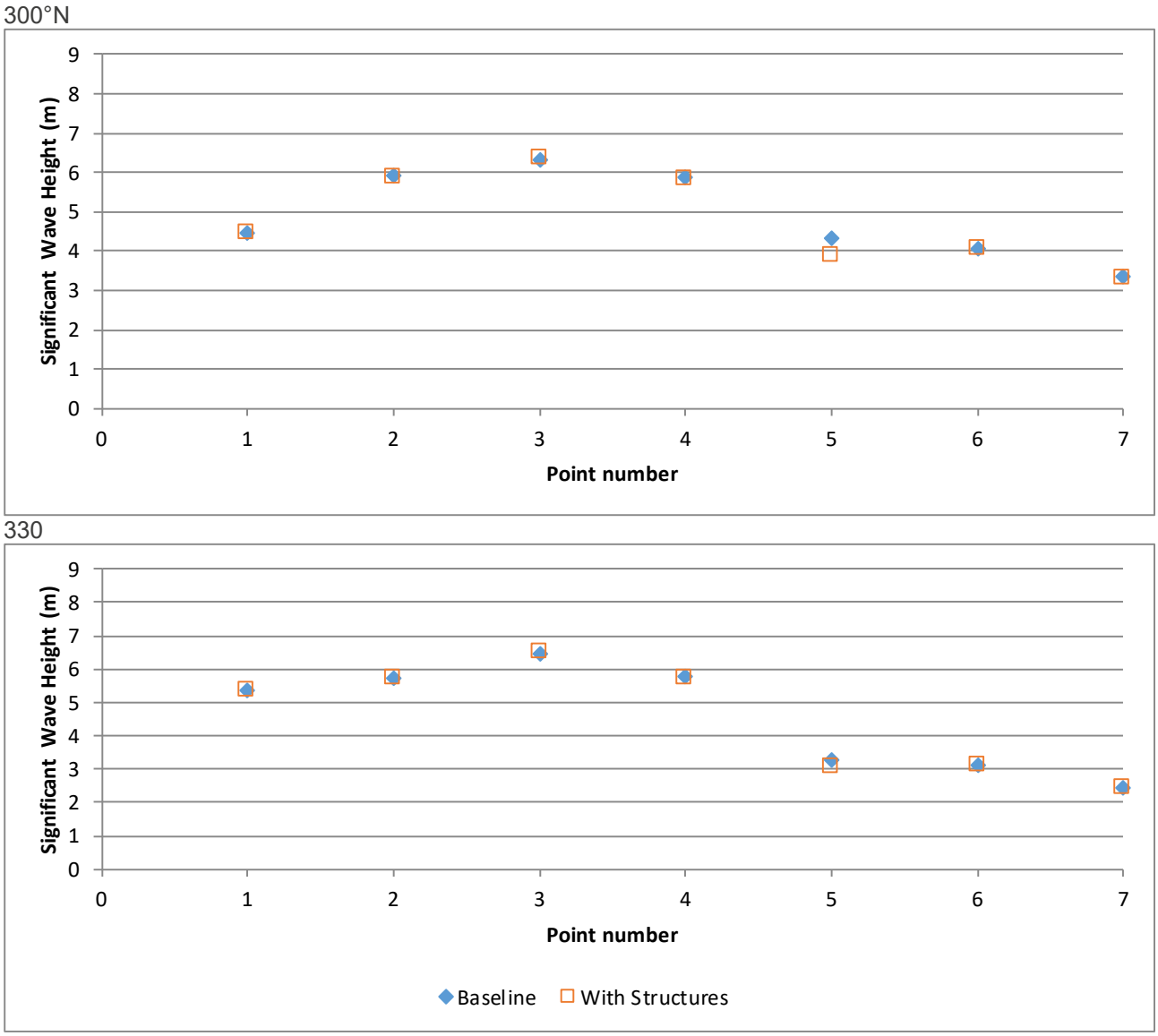

Figure 5.49: A comparison of wave heights from each point between Baseline and With Structures for Extreme waves: Top to bottom: 210°N, 240°N, 270°N, 300°N, 330°N

Source: SWAN

5.6. Wave model simulations (Currents)

Currents can have a large effect on the wave climate as they cause refraction effects and opposing currents cause shoaling of waves and potentially wave blocking. The wave climate therefore changes throughout the tidal cycle as currents change based on the state of the tide. Dependent on the wave direction, waves may shoal up during ebb or flood flows as the wave direction may be opposite to the tidal direction.

To model the effect that the changing currents caused by the structures have on the wave conditions, the worst case flow model was used instead of the worst case wave condition (See Section 5). The flow fields are affected by the structures over a wider extent than the footprint of the structures themselves. This means that the indirect effect of the changed currents on the waves may be a wider scale effect than the direct

blocking effect of the structures on the waves. A coarser (150m resolution) regular grid SWAN model was used to model the effects of the currents on the waves. Figure 5.50 shows the wave height with the current directions for times close to high tide, low tide, peak ebb and peak flood for waves from 210°N. During peak ebb, the wave direction and current directions are opposing causing the waves to shoal.

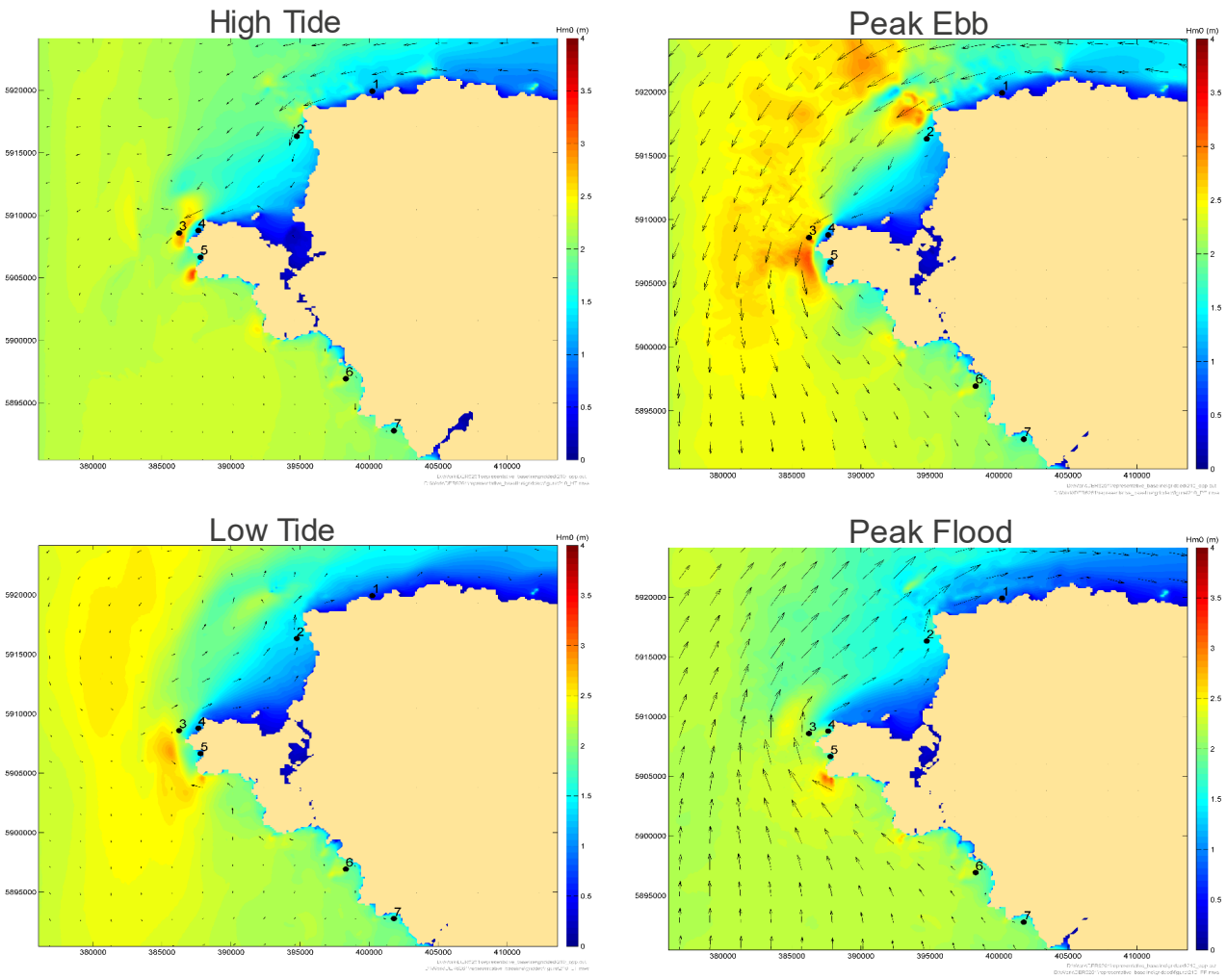

Figure 5.50: A colour contour of wave height overlaid with current directions for a representative baseline wave condition from 210°N, showing the wave conditions throughout a tidal cycle

Source: SWAN

In order to model the changes to wave height due to the influence of the structures on currents, the SWAN model was run throughout several tidal cycles using Spring tide currents for the baseline situation and also for the currents modified by the turbines. Figure 5.51 to Figure 5.55 show an analysis of the differences caused by the changes to the flows on the waves (difference plots focused near Holy island are given in Appendix B.2). The colour contour plots are produced by calculating the maximum wave height throughout the tidal cycle at each location for both the Baseline and With Structures flows and subtracting these. Only the representative conditions have been modelled as these are more important for the long term sediment transport processes. Also, during extreme events, the main threat to coastal protection occurs at high tide, which is when the current velocity is small.

Waves from 210°N and 240°N are most affected by the changing currents due to the devices. As the turbines reduce the current speed, there is less of a shoaling effect during peak ebb meaning the wave height reduces in this area. However, in areas either side of the development area where current velocities increase, the waves increase post construction of the devices due to shoaling of waves in opposing flows. These increases in wave heights are predominantly away from the coastline. Waves from 300°N and 330°N only see a reduction in the wave heights.

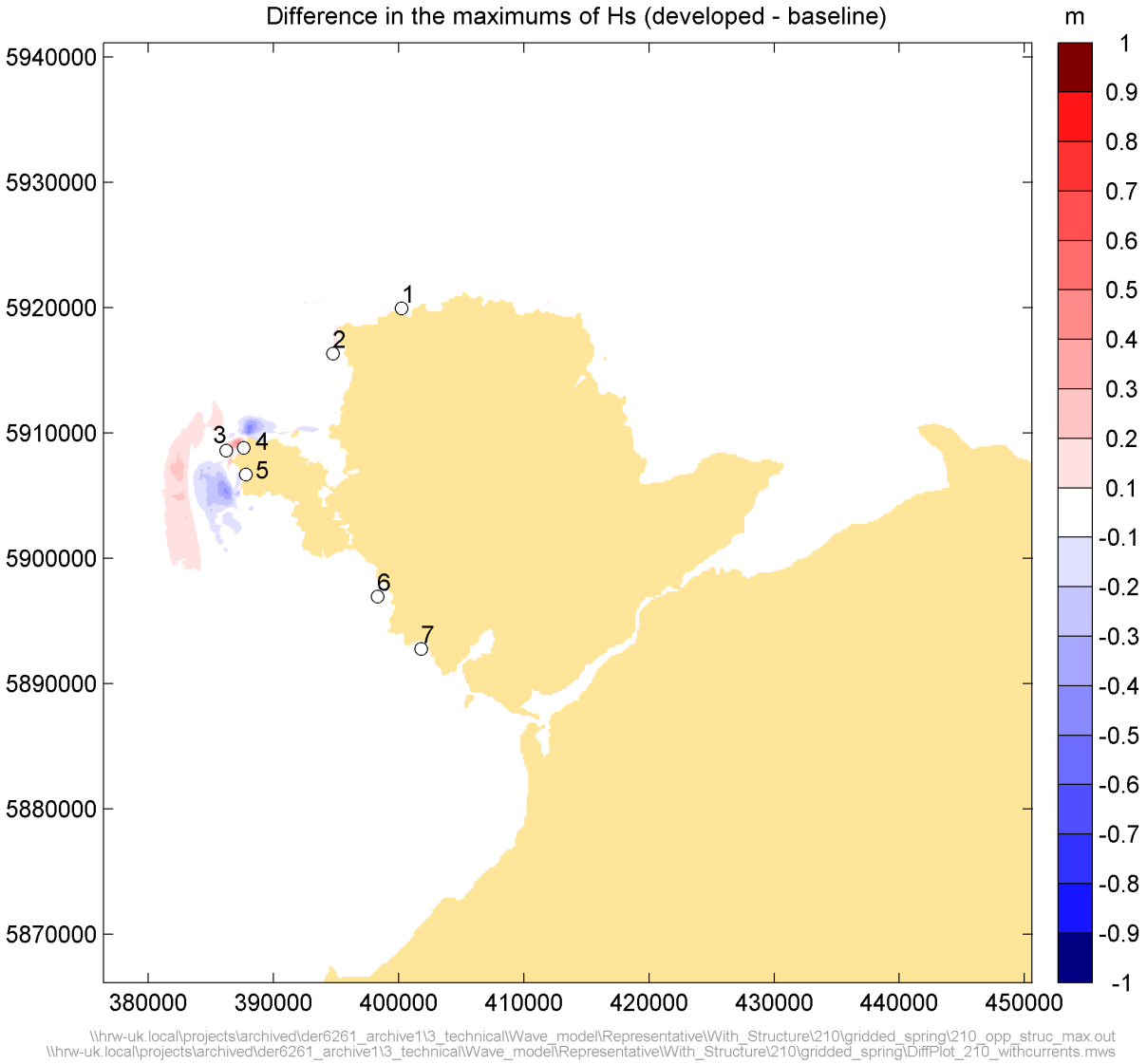

Figure 5.51: Difference in the maximum wave height throughout a tidal cycle at each node for a wave direction from 210°N

Source: SWAN with currents

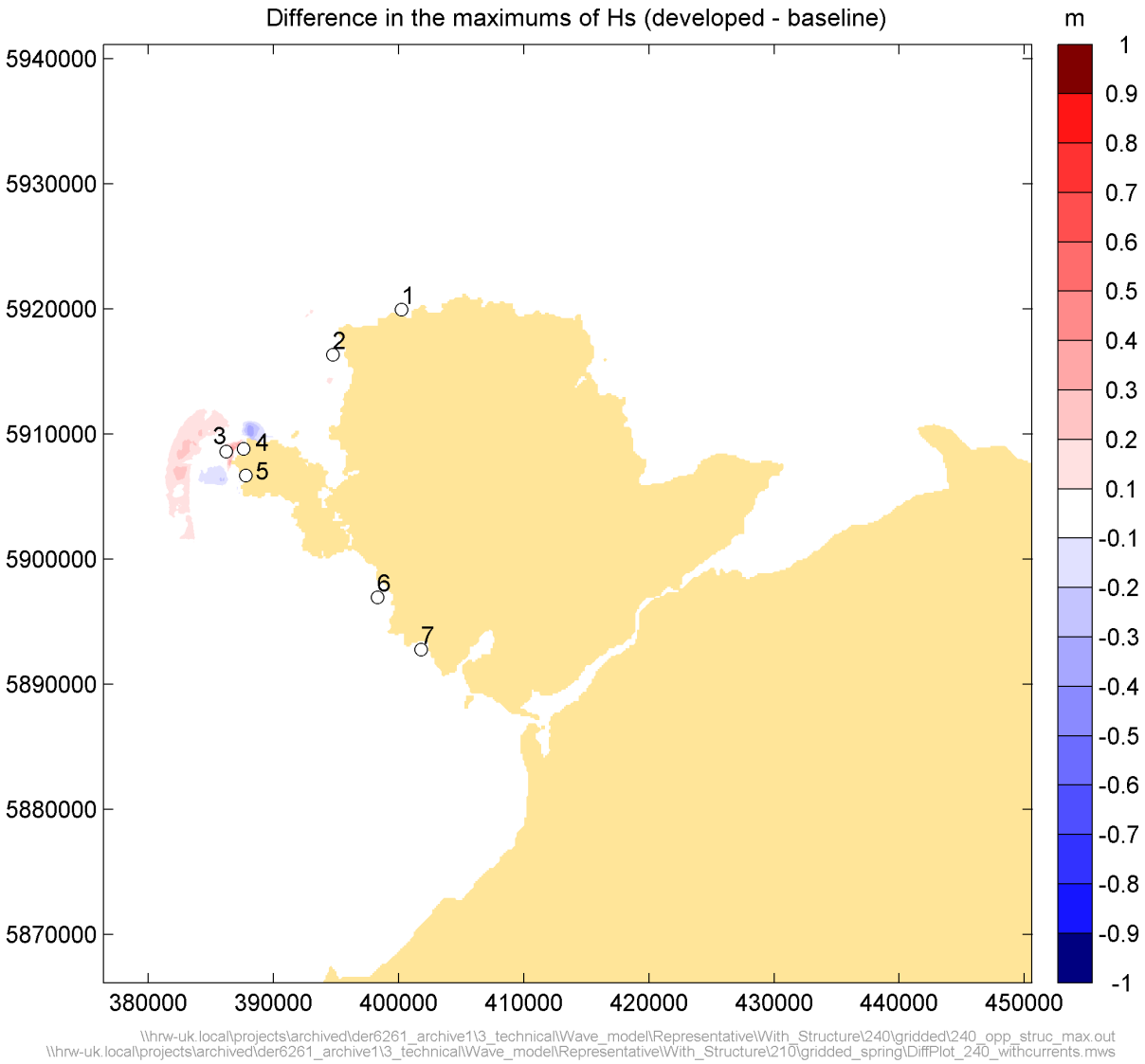

Figure 5.52:Difference in the maximum wave height throughout a tidal cycle at each node for a wave direction from 240°N

Source: SWAN with currents

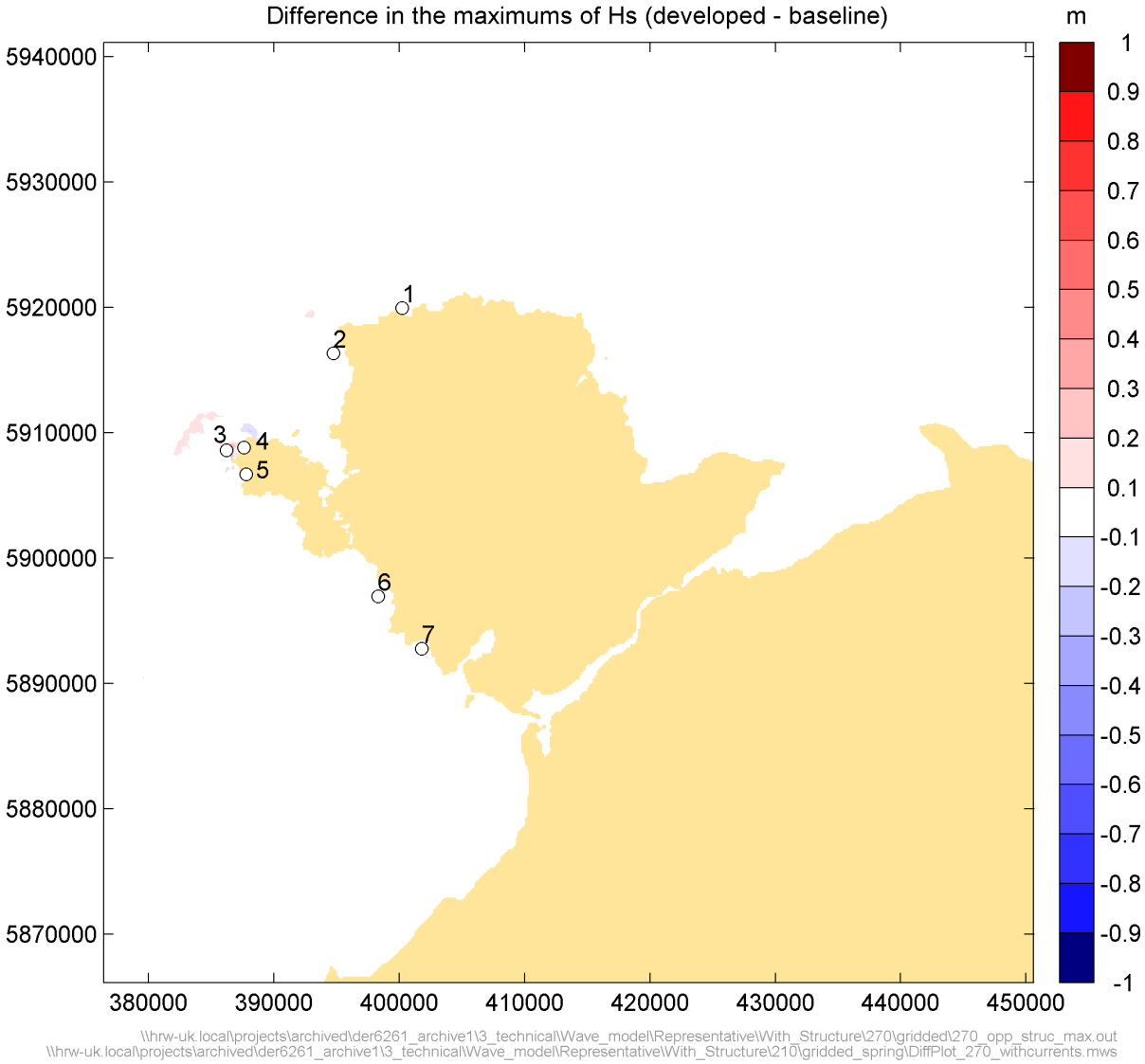

Figure 5.53: Difference in the maximum wave height throughout a tidal cycle at each node for a wave direction from 270°N

Source: SWAN with currents

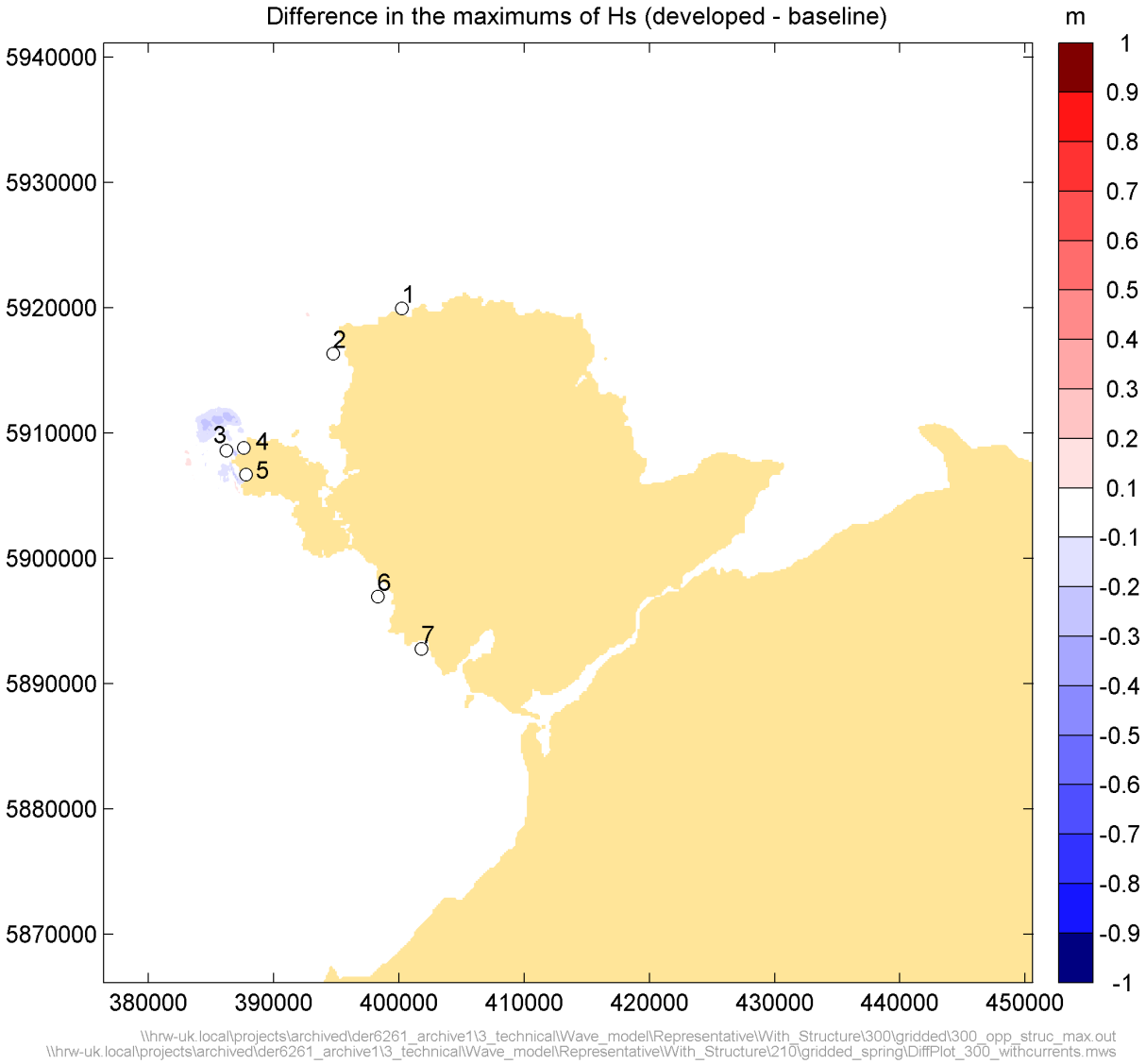

Figure 5.54: Difference in the maximum wave height throughout a tidal cycle at each node for a wave direction from 300°N

Source: SWAN with currents

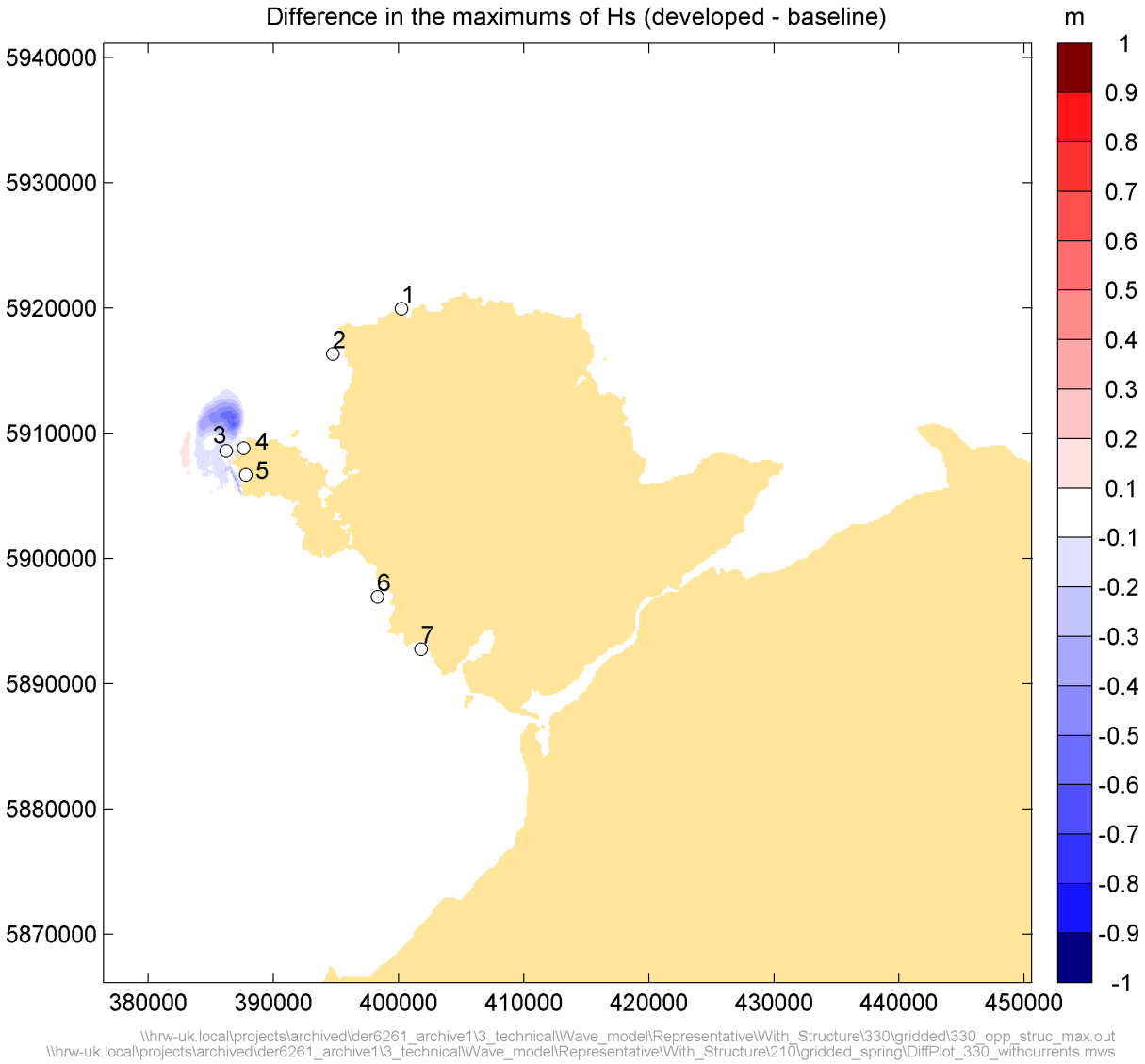

Figure 5.55: Difference in the maximum wave height throughout a tidal cycle at each node for a wave direction from 330°N

Source: SWAN with currents

The effect of the tidal devices on the current causes a shift in the time of maximum wave throughout the tidal cycle at some locations. Dependant on the direction of the waves, the timing of the peak wave height at each point varies. For waves from 210°N, the peak wave is during the ebb tide at points 3, 4 and 5 when the wave is shoaled up by an opposing current. However the modification in the flow field due to the turbines causes the peak in wave height to occur earlier in the ebb tide (Figure 5.56). At points 2 and 3, the waves have increased in wave height as seen in Figure 5.51 due to the localised area of increased ebb currents between the turbines and the coast causing increased shoaling for a short period of time during the tidal cycle. Figure 4.24 shows the area where ebb tidal currents are increased as some of the flow is diverted inshore of the tidal turbine area. Around HW and on the initial part of the ebb, the waves from 210°N are travelling against this area of increased current speed and are shoaled up slightly by the current, causing the slight increase in wave heights at points 2 and 3 at these times of the tide.

Point 1

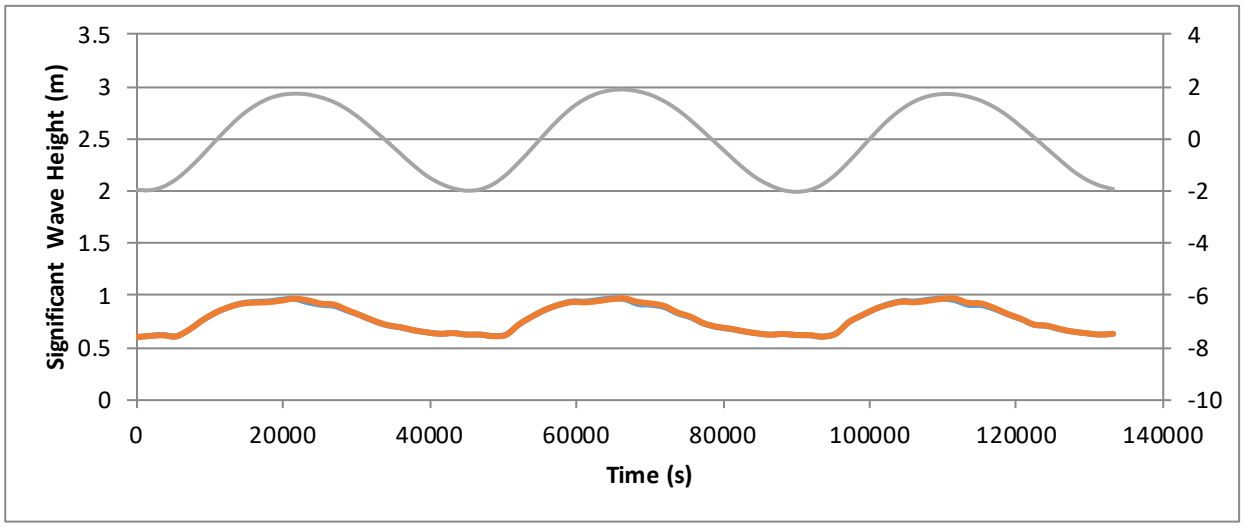

Point 2

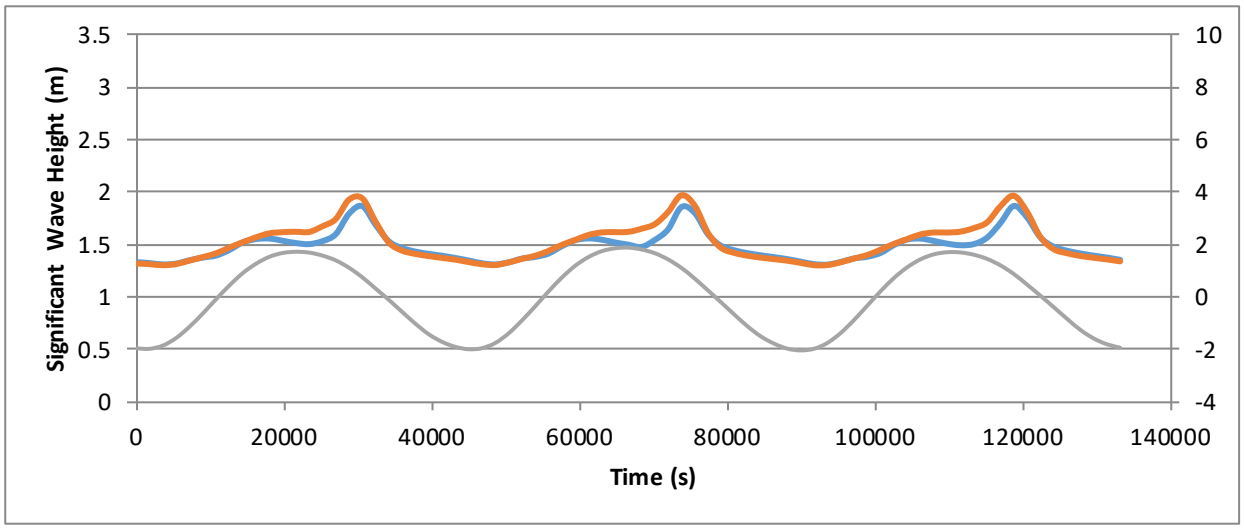

Point 3

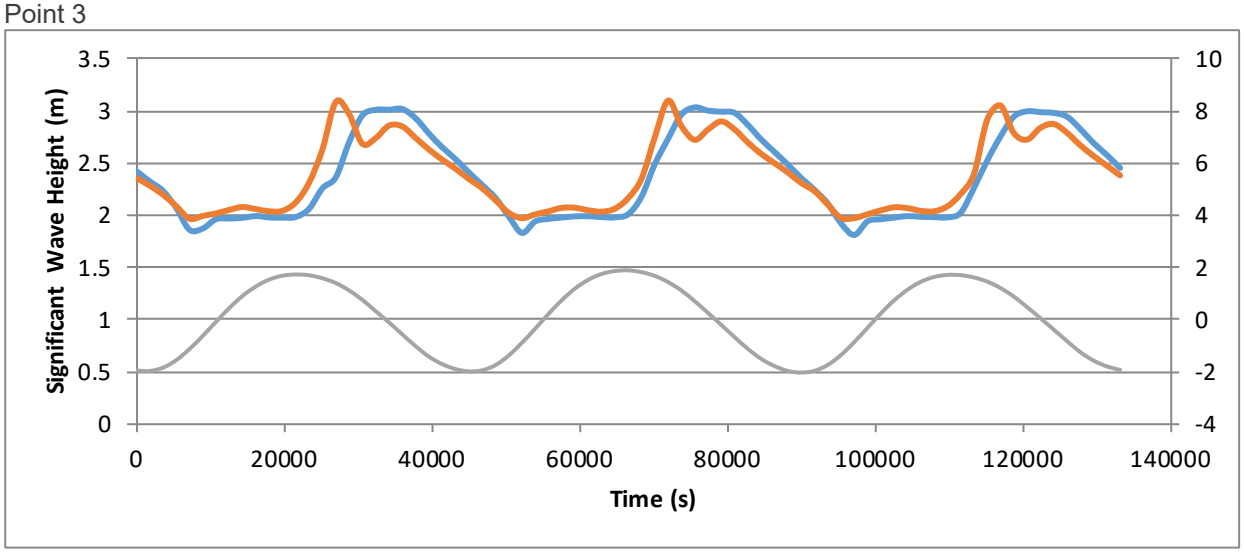

Point 4

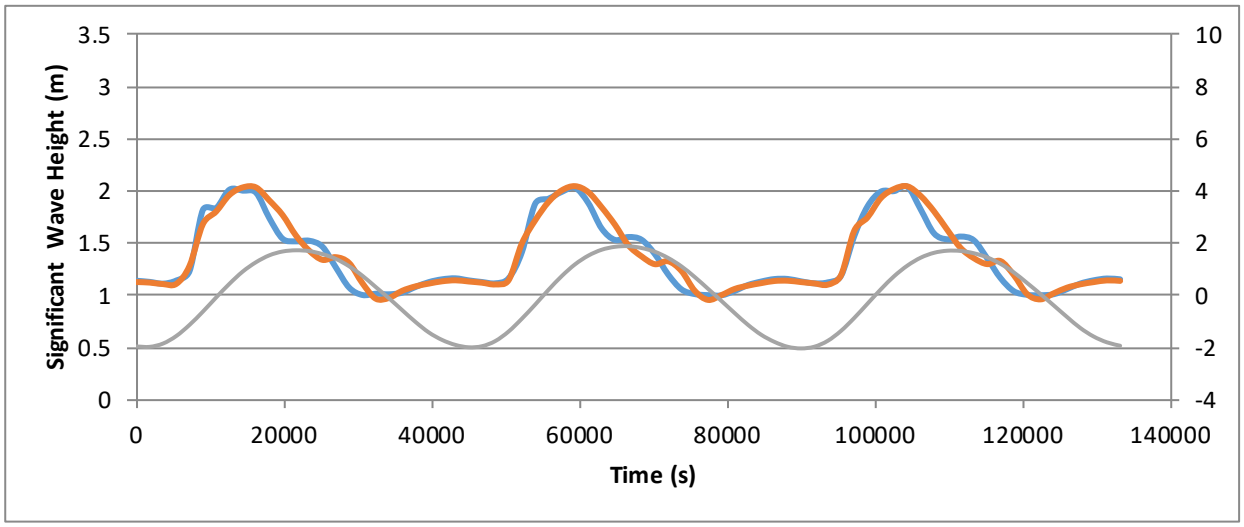

Point 5

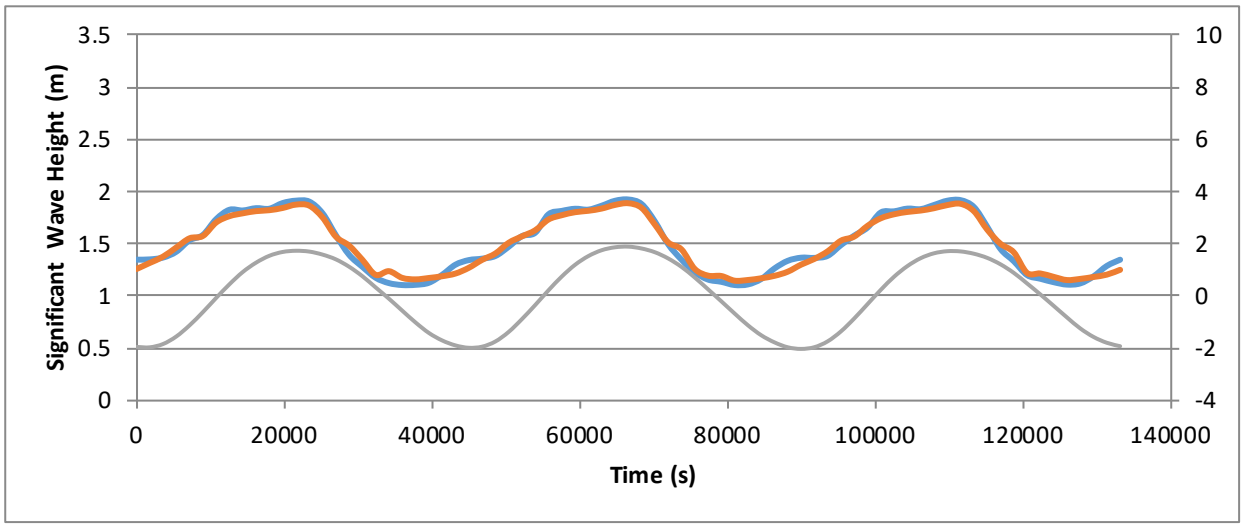

Point 6

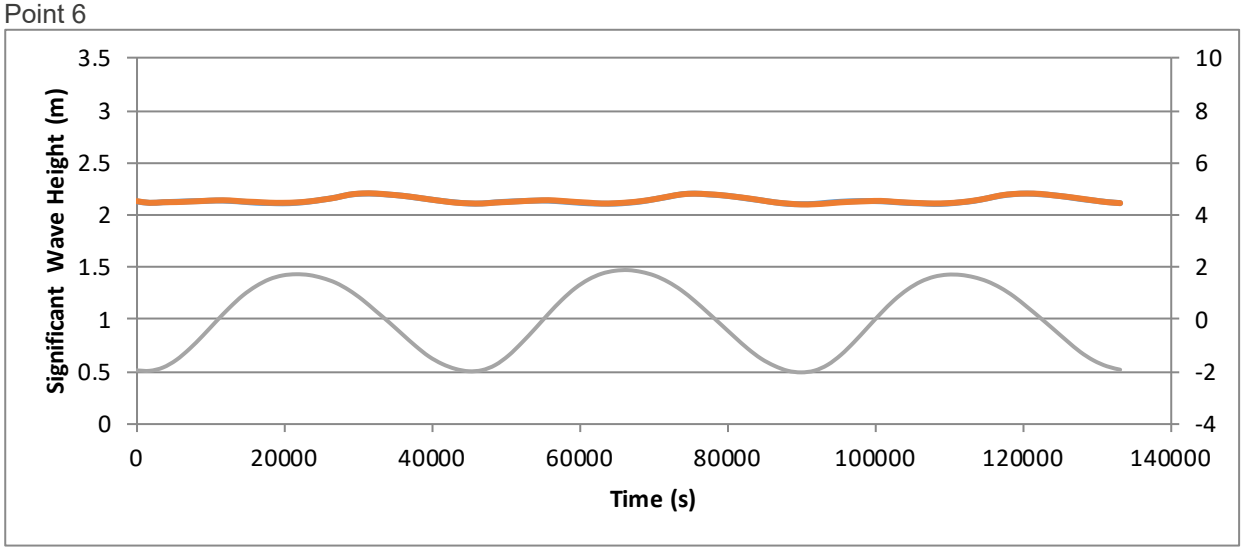

Point 7

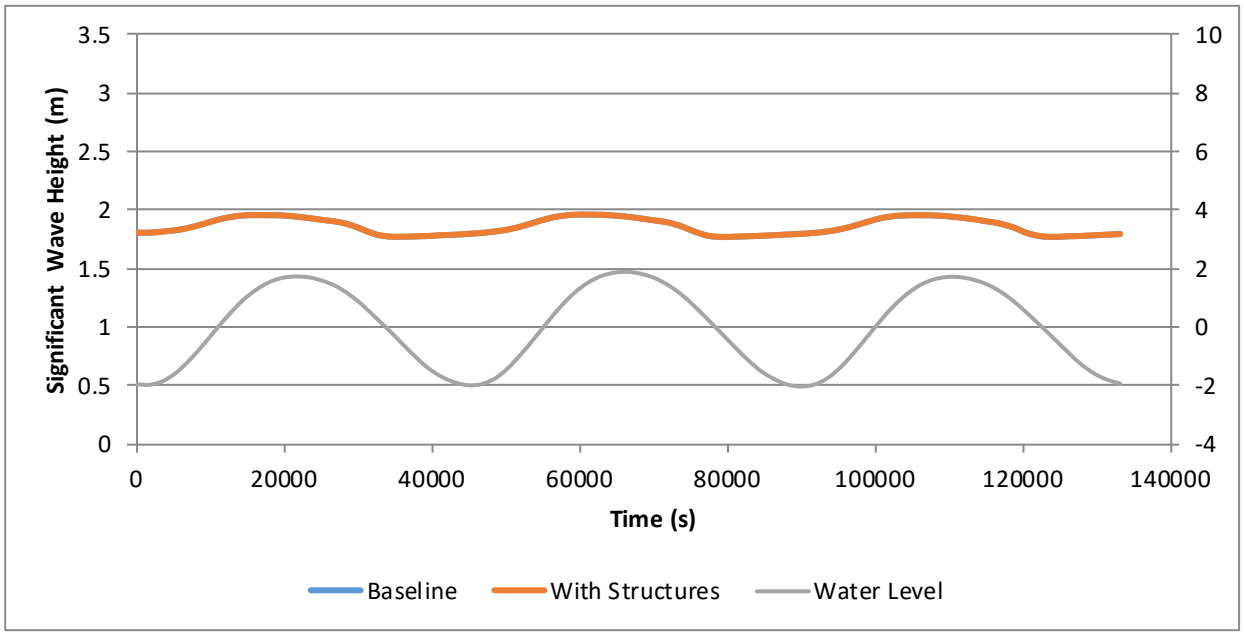

Figure 5.56: Time series of Hs throughout the tide for Representative waves from 210°N showing the Baseline and With Structure runs along with the tidal level for points 1-7 (top to bottom)

Source: SWAN with currents

In contrast, waves from 300°N peak during the peak flood as the wave direction opposes the current directions. As the waves are typically smaller from the North-west and due to the location of the turbines, waves from this direction had less of an effect on the points of interest than waves from the southwest. Wave heights at all points have reduced from baseline to post structures from 300°N (Figure 5.57).

For all wave directions, it is seen that the effects of changes in currents due to the turbines have a small impact over a wider area then the direct impact from the structures themselves. However, the direct impact of the structures are larger than the impact caused by a changing current. There will likely be a combined effect which is both caused by the currents and the direct impacts from the structures themselves. This has not been modelled explicitly as to model the worst case wave and current scenarios require a different implementation of tidal devices. This combined effect is still likely to be small and localised to points 3, 4 and 5. The combined effect has been considered in the sediment transport modelling.

Point 1

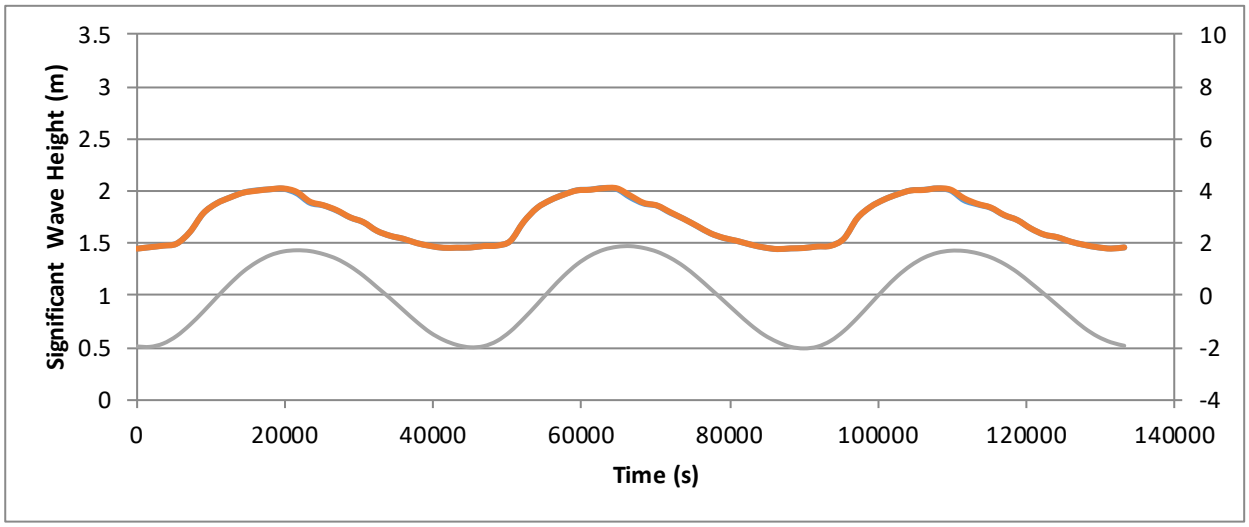

Point 2

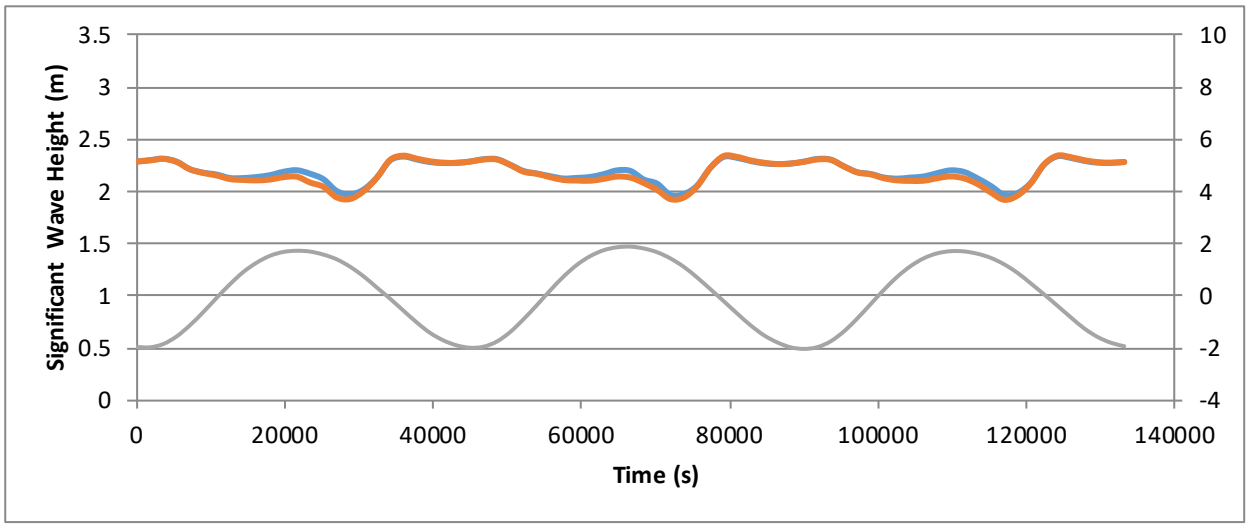

Point 3

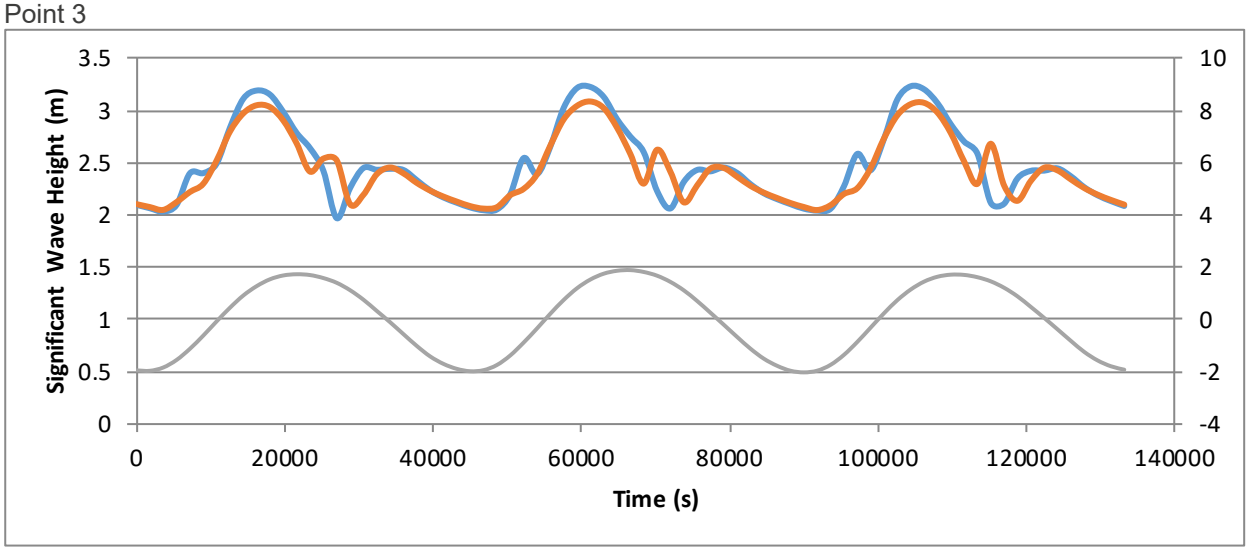

Point 4

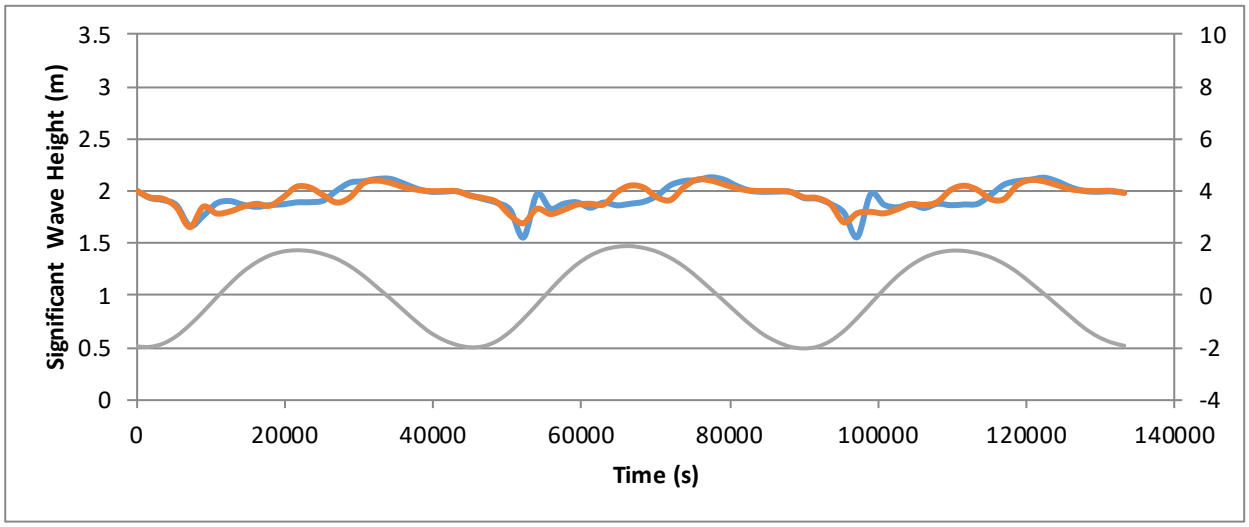

Point 5

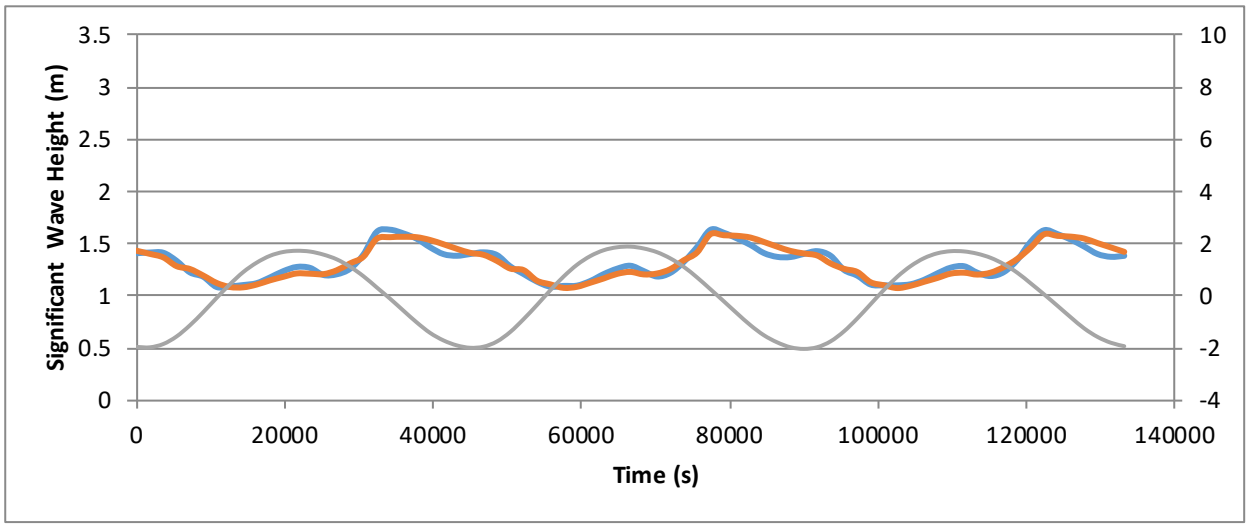

Point 6

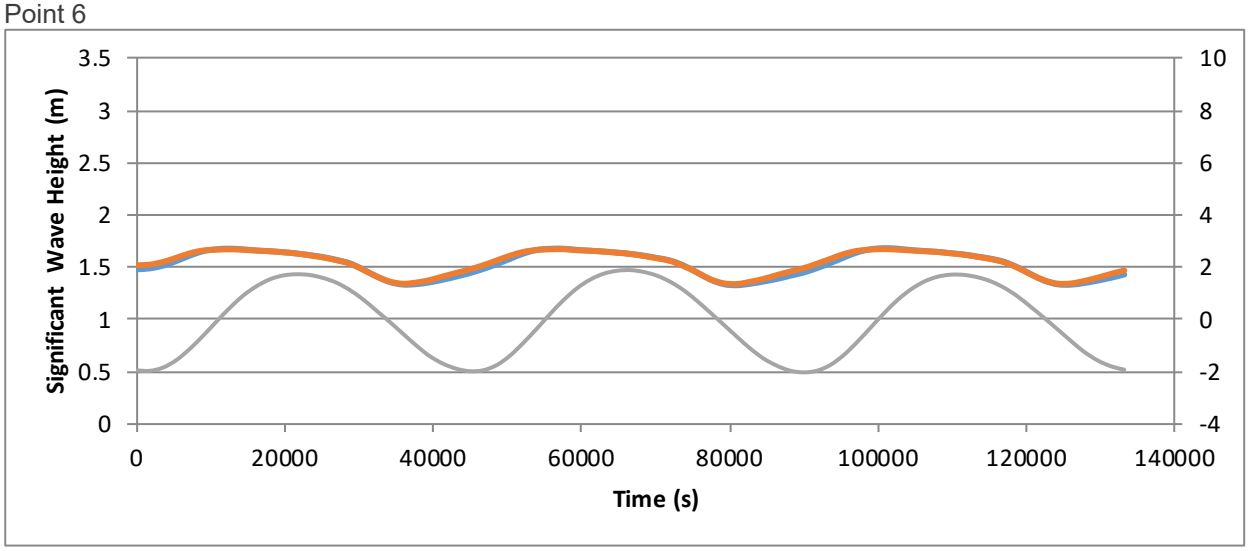

Point 7

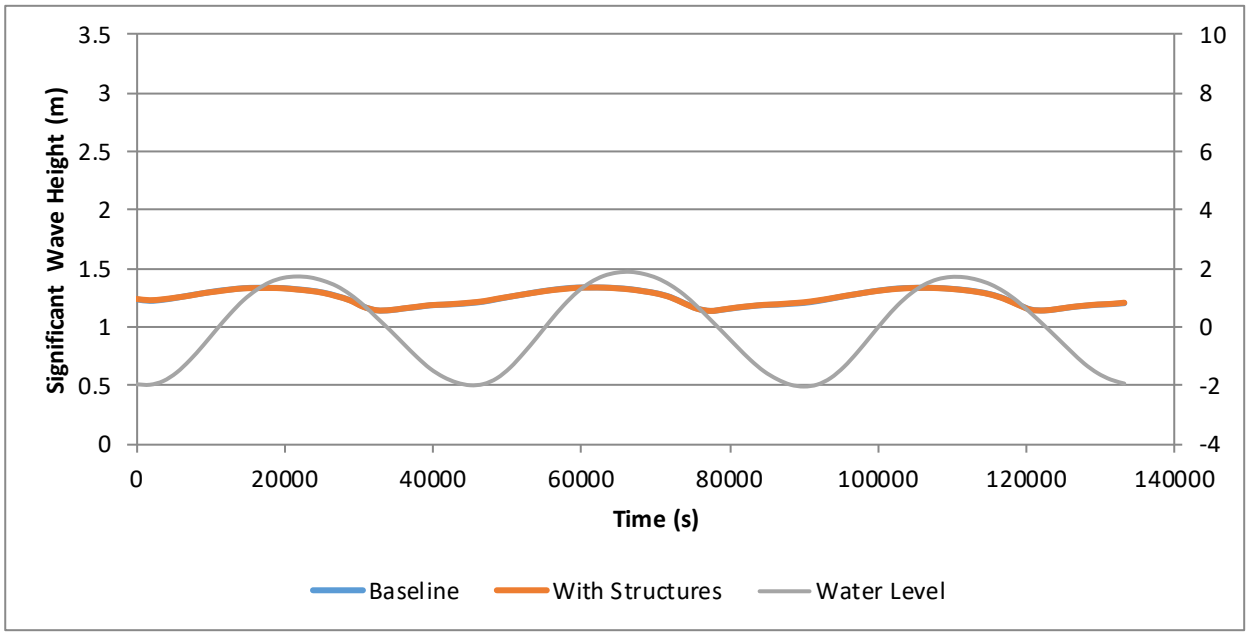

Figure 5.57: Time series of Hs throughout the tide for Representative waves from 300°N showing the Baseline and With structure runs along with the tidal level for points 1-7 (top to bottom)

Source: SWAN with currents

6. Sediment transport modelling

6.1. Morphological baseline

To understand the importance of the potential impact of the MDZ on local sediment dynamics, a baseline state needs to be defined, describing the present sediment deposits and their variability / dynamics. A brief data and literature review has been undertaken focussing on the historical changes of the sediment deposits in the west of Anglesey area, giving emphasis to the Gogarth Bay and Abraham's Bosom sediment deposit zones; the South Stack banner bank and Langdon Ridge to the north (Figure 6.1).

The following section aims to estimate and, where data allows, quantify any discernible historical trends and variation in the sediment deposits in and around the MDZ.

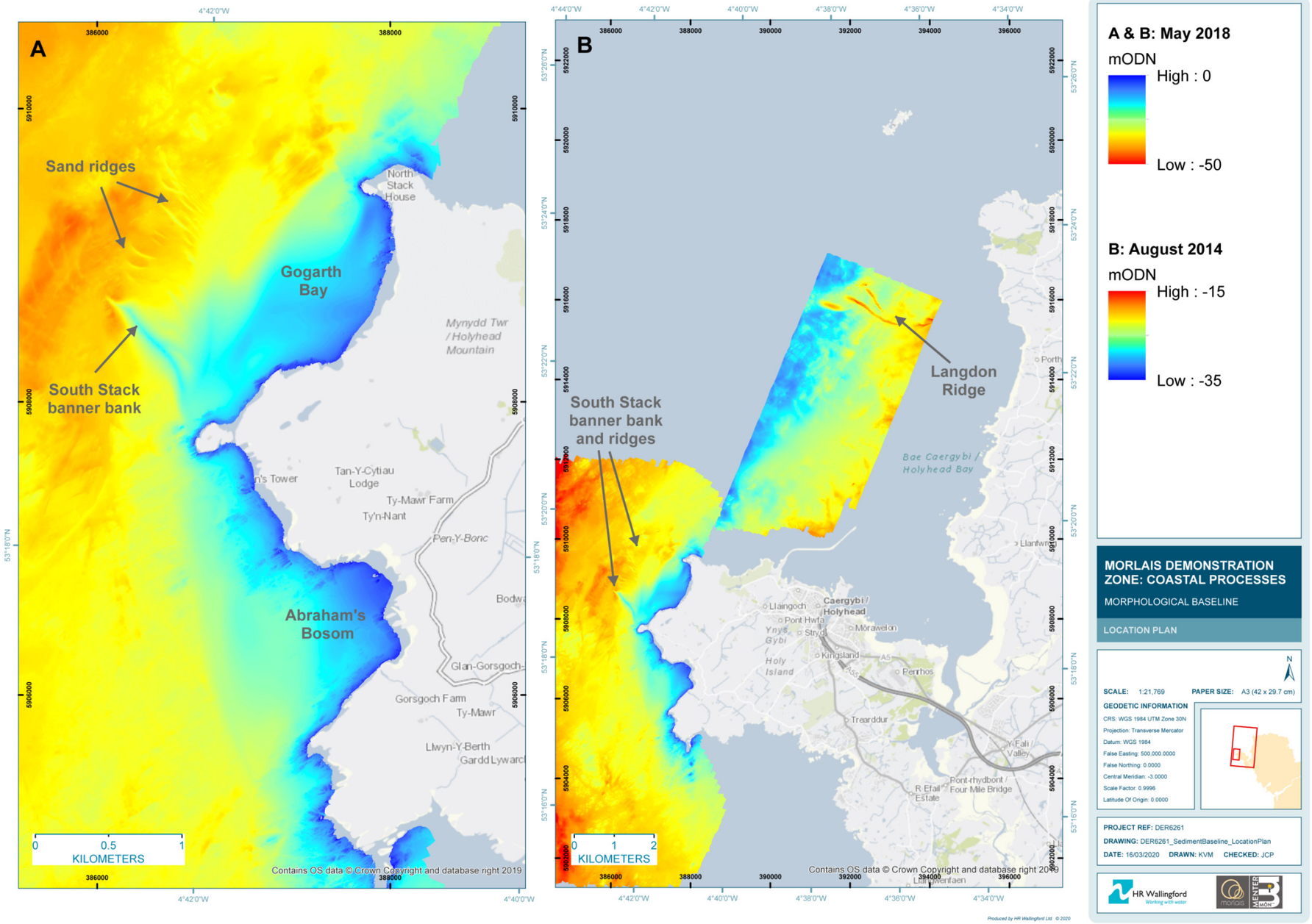

Figure 6.1: Location plan for morphological baseline

Source: HR Wallingford

6.1.1. Data availability and assessment

Particle size information

The collation of particle size information to form a sediment map is described in Section 6.2.1, with the final map using the Folk classification system shown for the MDZ area in Figure 6.15. The data show how offshore of Holy Island the seabed is composed of coarse gravel and exposed bedrock, as would be expected for areas subject to high energy tidal flows.

The generation of large-scale eddies due to tidal flow around the headlands limits the offshore extent of the sandy deposits, with sand and sandy gravel tending to remain in the embayments either side of South Stack headland. Headland dynamics are also responsible for the formation of the South Stack banner bank and further north Langdon Ridge, which can also be considered as a banner bank. These features, along with the sandwaves north of the South Stack banner bank in the mouth of Gogarth Bay, are composed of gravel and coarse sand, and represent the most significant morphological features within the vicinity of the MDZ.

Admiralty Chart editions

Often the main sources of historical (decadal scale) data for seabed change are the various updates made for each new edition of an Admiralty navigational chart. There are two charts that cover the MDZ, and the HR Wallingford archive holds various issues and editions as described in Table 6.1.

The data used to make up these editions is shown as area polygons, and the only change in the locality of west Holy Island off of South Stack occurred in 1985, with the difference in contours between the 1985 and 1990 editions illustrated in Figure 6.2.

Table 6.1: Historical chart availability in the HR Wallingford archive

Chart Number	Chart Title	Issue	Edition	Scale
1413	Approaches to Holyhead	1976	1989	25,000
1413	Approaches to Holyhead	1976	1984	25,000
1977	Holyhead to Great Ormes Head	1977	1990	75,000
1977	Holyhead to Great Ormes Head	1977	1985	75,000
1977	Holyhead to Great Ormes Head	1977	1981	75,000
1977	Holyhead to Great Ormes Head	1961	1973	75,000
1977	Holyhead to Great Ormes Head	1961	1972	75,000

Source: HR Wallingford using information from UKHO

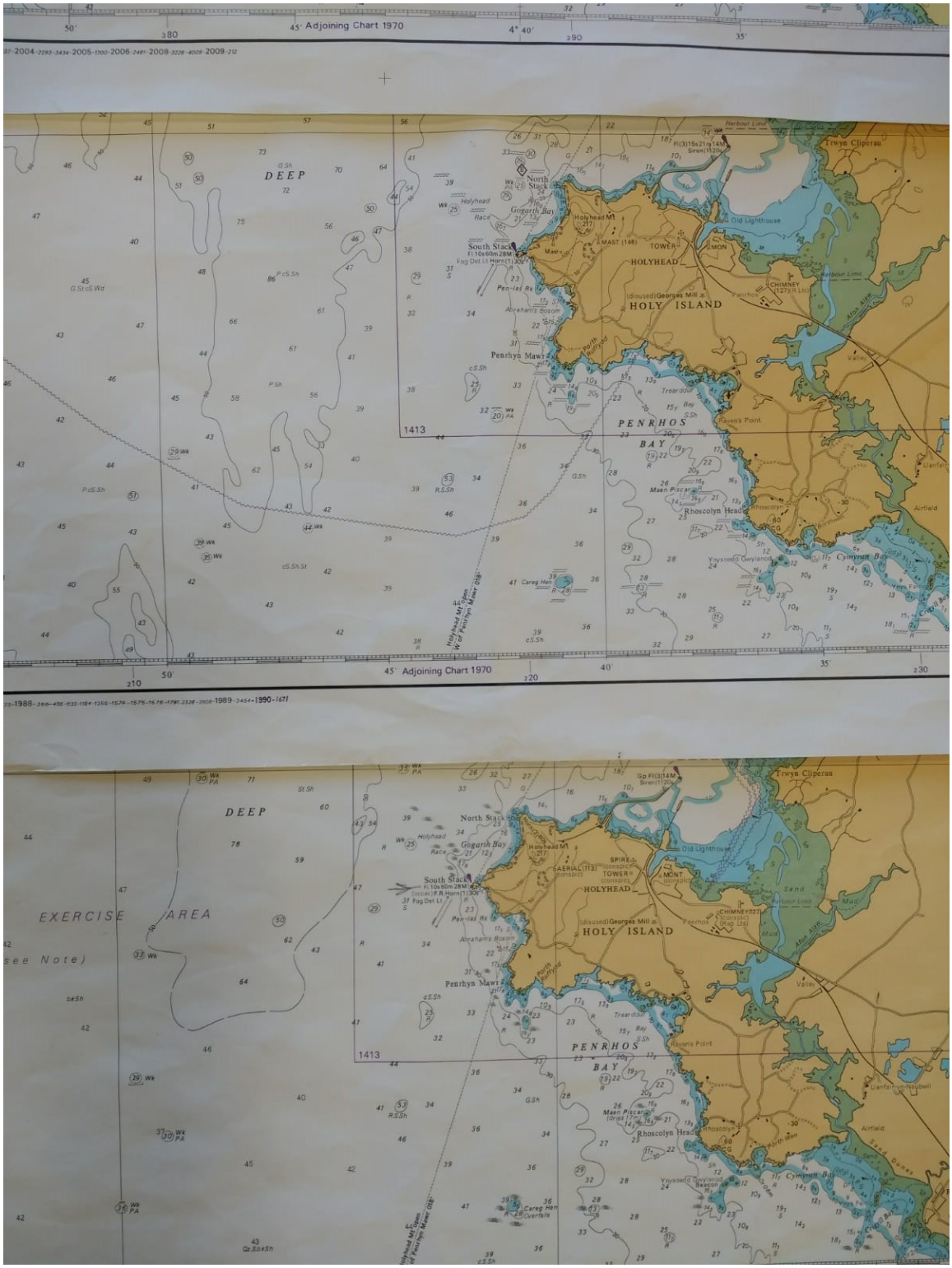

Figure 6.2: Contours and spot depths off South Stack in the Admiralty Chart No. 1977, Issue 1961, Edition 1985

Source: HR Wallingford

Bathymetry data

Local bathymetry survey data provided by Menter Môn (2015) and Partrac (2018) were included as part of this baseline assessment, with the latter representing the most recent bathymetric survey data available in the MDZ and local area.

Dated bathymetric survey data for Wales is available through the IMARDIS portal as part of the SEACAMS2 project. Multiple overlapping surveys were available for download in the study area (screenshot of available surveys shown in Figure 6.3). Surveys of appropriate coverage and quality were downloaded (see Table 6.2), and those surveys that were sufficiently close in time (e.g. within the same month) were combined. These surveys form the basis of the difference analysis presented in Section 6.1.2. All of the surveys that were included in the difference analysis are shown in Figure 6.4 and Figure 6.5).

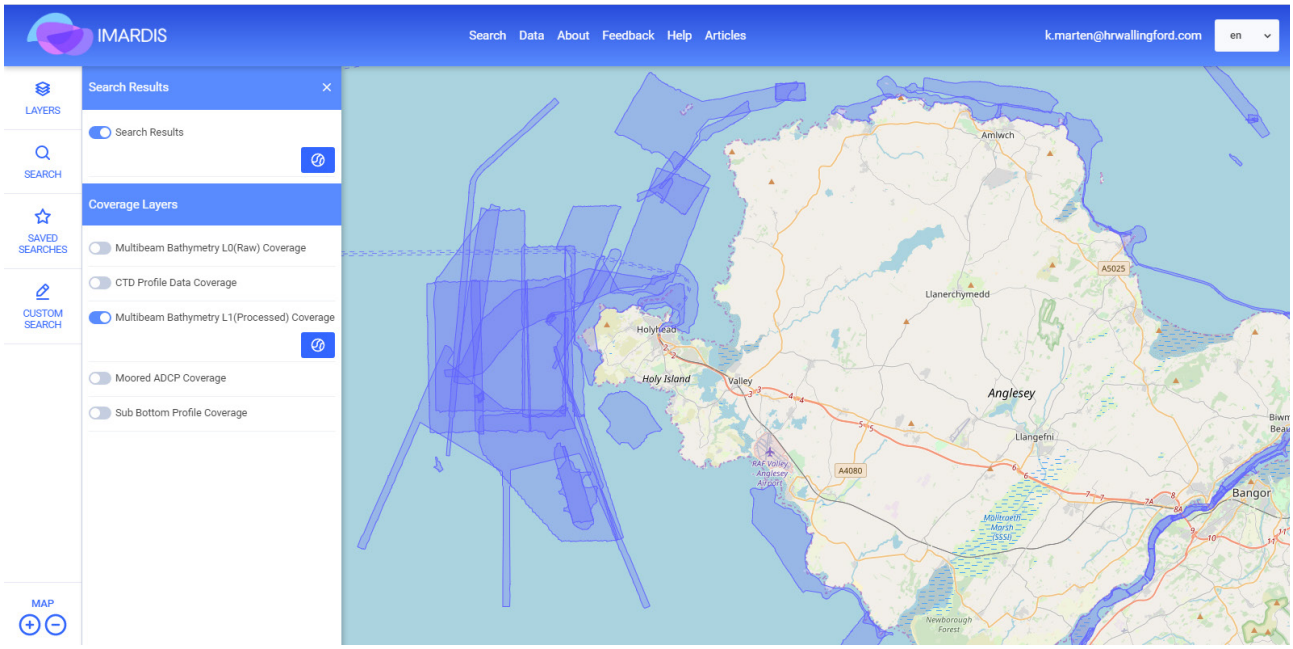

Figure 6.3: Screenshot of the IMARDIS portal showing availability of processed Multibeam bathymetry data

Source: https://portal.imardis.org/

Table 6.2: Processed MBES surveys downloaded from the IMARDIS portal

Survey name	Survey date/s
Langdon Ridge	September 2012
Penrhos Bay	May 2012
Holyhead Deep	March 2013
West Anglesey Demo Zone	June 2014
West Anglesey Demo Zone	July 2017
Holy Island	June 2015
South Stack	March 2015

Source: HR Wallingford based on metadata available on the IMARDIS portal (https://portal.imardis.org/),

Note: All processed data were available at 1 m grid size, reduced to OD(Newlyn) and in co-ordinate system WGS84 UTM Zone 30N

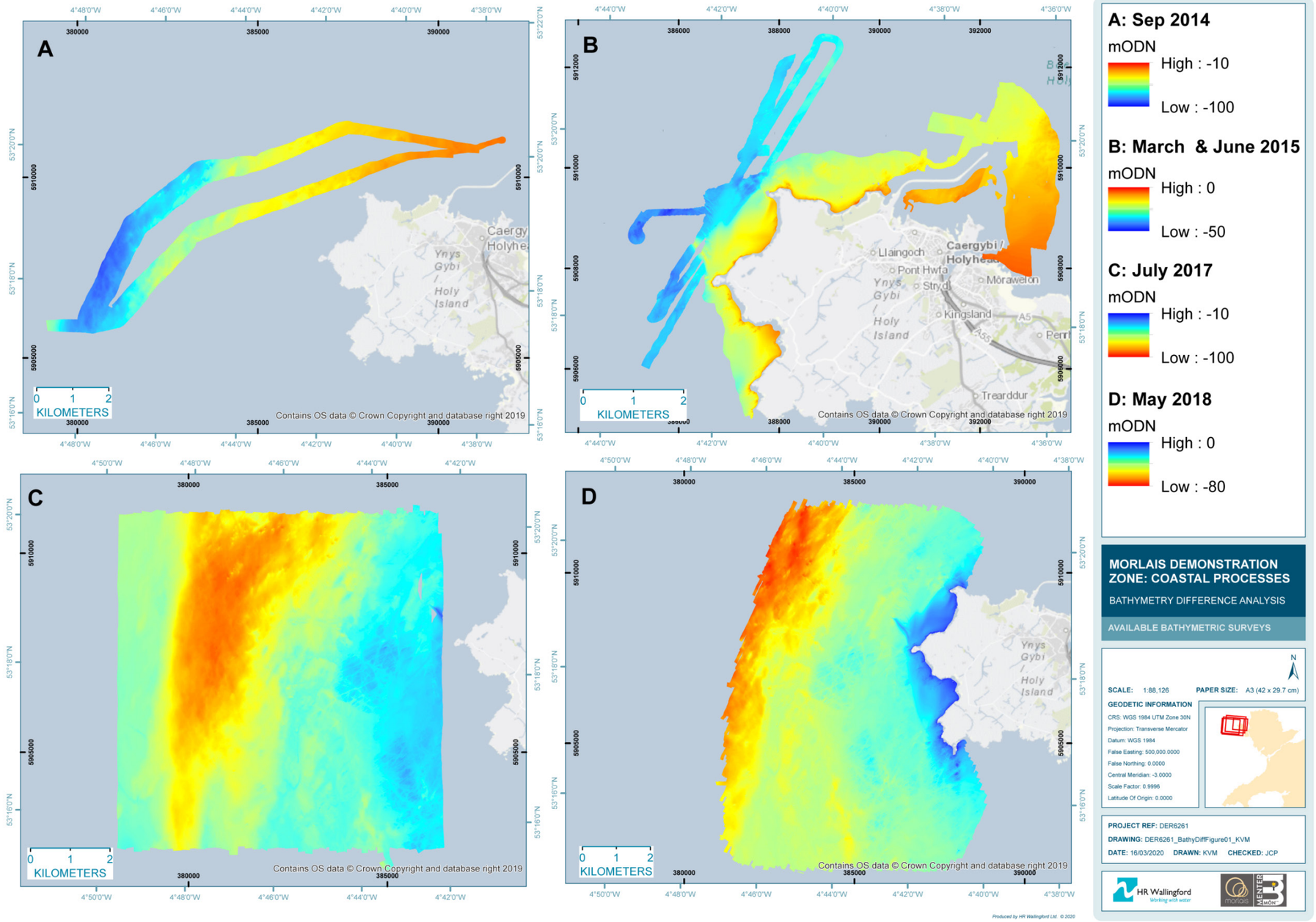

Figure 6.4: Bathymetric surveys available with mainly inshore coverage

Source: HR Wallingford using data downloaded from IMARDIS

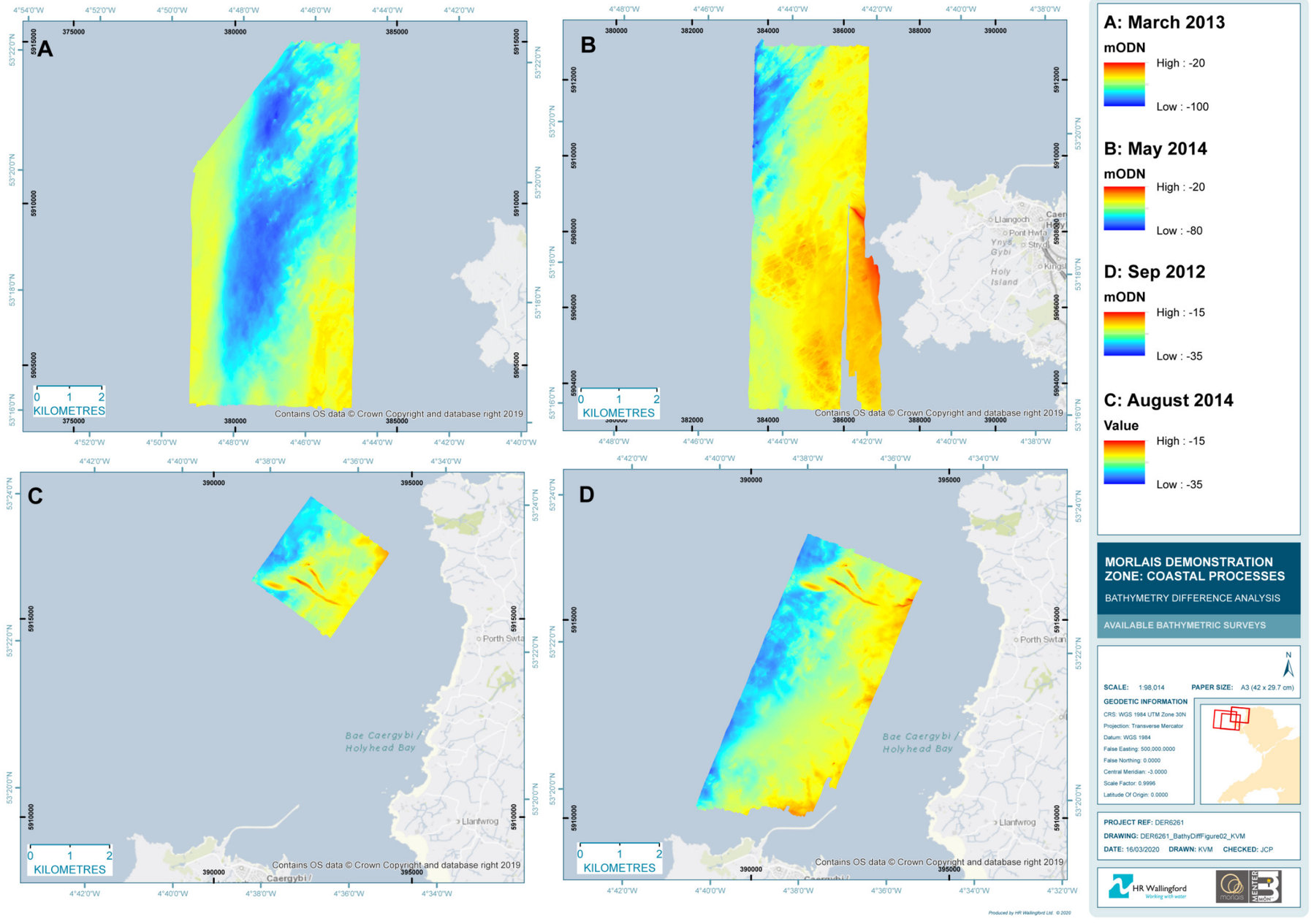

Figure 6.5: Bathymetric surveys available with mainly offshore coverage

Source: HR Wallingford using data downloaded from IMARDIS

Historical LiDAR

While there are a number of bathymetric surveys available for the project area offshore, these surveys do not include detail of the seabed closer to the shore in the target areas of Gogarth Bay and Abraham's Bosom.

A portal exists, hosted by NRW, for review and download of historical LiDAR surveys across Wales. A comparison of LiDAR surveys taken at different times would provide a useful tool for assessing area-wide mobility within these embayments. However, though the appropriate tile states there is one LiDAR survey in 2010, upon inspection the survey covers inland areas of Holy Islands, with no coverage in the Gogarth Bay or Abraham's Bosom.

Beach profiles

The established method for assessing variation in beach levels is via monitoring programs that include beach profiles at constant positions surveyed on at least an annual basis. Enquiry was made to Anglesey Council, Gwynedd Council and the Wales Coastal Monitoring Centre (WCMC) for access to beach profiles. The Gwynedd Council coastal monitoring team provided data and summary reports for biannual surveys for dating back to 1996, however WCMC confirmed that Anglesey Council did not have a monitoring program in place.

The two closest Gwynedd beaches to the MDZ are south of the mouth of the Menai Strait at Pontllyfni and Aberdesach. These beaches are outside the region of interest.

Literature

Three key papers reporting research into the impact of tidal arrays on headland sandbank dynamics are available, these being Neill et al. (2009), Neill et al. (2012) and Robbins et al. (2014), with the latter focussing on the impact of tidal arrays on the natural variability of sedimentary processes, and including a test case just to the north of the proposed MDZ, including detail on Langdon Ridge.

More general papers relating to relevant sand bank formations include Dyer and Huntley (1999) describing the origin, classification and modelling of sand bank ridges; Bastos et al. (2003) and Schmitt and Mitchell (2014) dealing with the formation and dynamics of headland related sandbanks; and Margalit (2018) investigating the effects of marine renewable energy on natural seabed forms.

6.1.2. Difference analysis

The available bathymetric surveys were compared to provide maximum spatial and temporal coverage for those surveys that fully or partially overlap. The earlier survey depths were subtracted from the later survey depths such that positive values indicate an increase in bed level over time and vice versa. Changes within ±0.35 m are not shown due to uncertainty in the accuracy of older survey data. The results were grouped to show change for three main areas, as described below.

Change to the South Stack banner bank and sandwaves at the mouth of Gogarth Bay

Changes in this area are shown in Figure 6.6 for various observation periods. Note that there is a survey artefact present in the June 2014 survey data which causes the 'stripes' either side of the banner bank in panel C. Away from this survey artefact, the changes can be summarised as:

- bed level changes over South Stack banner bank are up to ±5 m on either side of the crests position (decreasing to around ±1 m on the flanks) for the various observation periods, demonstrating both intra and inter-annual variability in the crest position.

- the tip of the bank shows evidence of moving in both a north-westerly and south-easterly direction in panels C and D. The north-westerly movement occurs over a one year period, while the south-easterly migration over a four year period indicates that this is the long-term migration direction of the South Stack banner bank feature.
- the sandwaves off the mouth of Gogarth Bay occur in 40 m of water though still show evidence of systematic migration, with associated bed level change of around ±5 m. This value is equivalent to the sandwave height with the features moving by a wavelength or more within the various observation periods.

Changes in bed level further offshore

Changes in this area are shown in Figure 6.7 for various observation periods. Note that there is evidence of survey artefacts indicated by the systematic stripes in all panels to differing degrees, as well as an increasing offset relative to Chart Datum moving offshore in panel A. Aside from the effects of survey artefacts, the changes offshore can be summarised as:

- largely within the bounds of survey accuracy (i.e. within ±0.35 m), which would be expected given the limitation on mobile material due to the large current speeds;
- the only significant change is at the South Stack banner bank, which is viewable in more detail in panel D of Figure 6.6.

Changes to the three key locations (Gogarth Bay, Abraham's Bosom and Langdon Ridge)

Changes in these areas are shown in Figure 6.8. Note that there is an area of lowering in panel B that is too rectangular to be natural – this may be related to survey artefacts, or may be a test pit of some kind. Away from this anomaly, the changes can be summarised as:

- in panel A, change over the almost three year observation period is widely within the bounds of survey accuracy;
- where change is outside of this envelope of uncertainty, there is a tendency towards an increase in bed level within Gogarth Bay, and a tendency towards a decrease in bed level in Abraham's Bosom. Both of these observed changes occur close to the shore and likely to be driven by the waves and wave driven currents;
- the sandwaves at the mouth of Gogarth Bay are shown to be around 5 m high and actively migrating, up to 60 m in the three year comparison period;
- in panel B, the bed changes at Langdon Ridge are restricted to the tops of the bank features, without the banding along the whole feature that would indicate wholesale migration;
- the Langdon Ridge feature remains static in position over the two year observation period, with small changes to bed level (on the whole within ± 1 m) being related to the migration of smaller scale bedforms (ripples and mega-ripples) that are superimposed onto the feature.

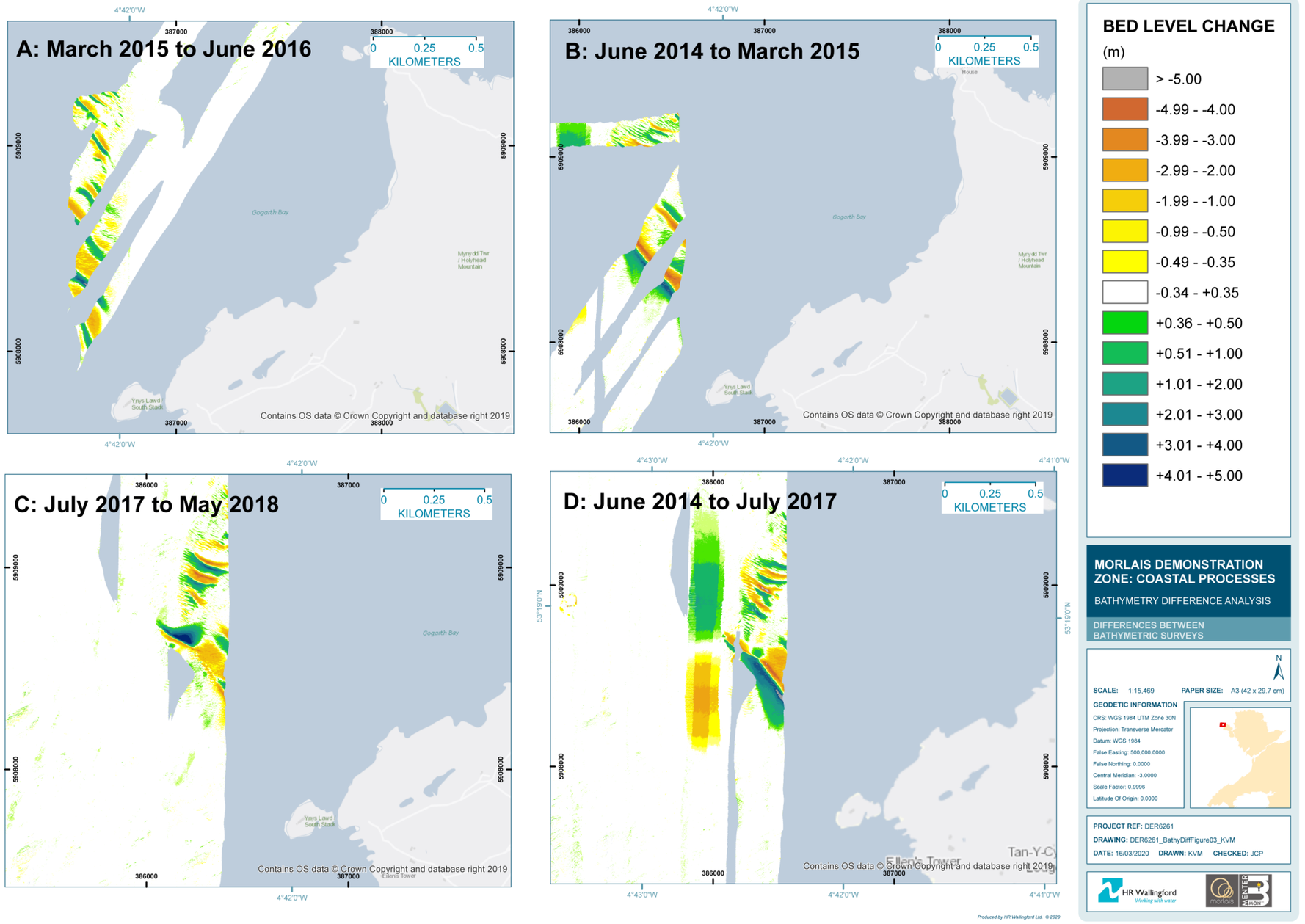

Figure 6.6: Bathymetric differences for the South Stack banner area and sandwaves in the mouth of Gogarth Bay

Source: HR Wallingford using data downloaded from IMARDIS

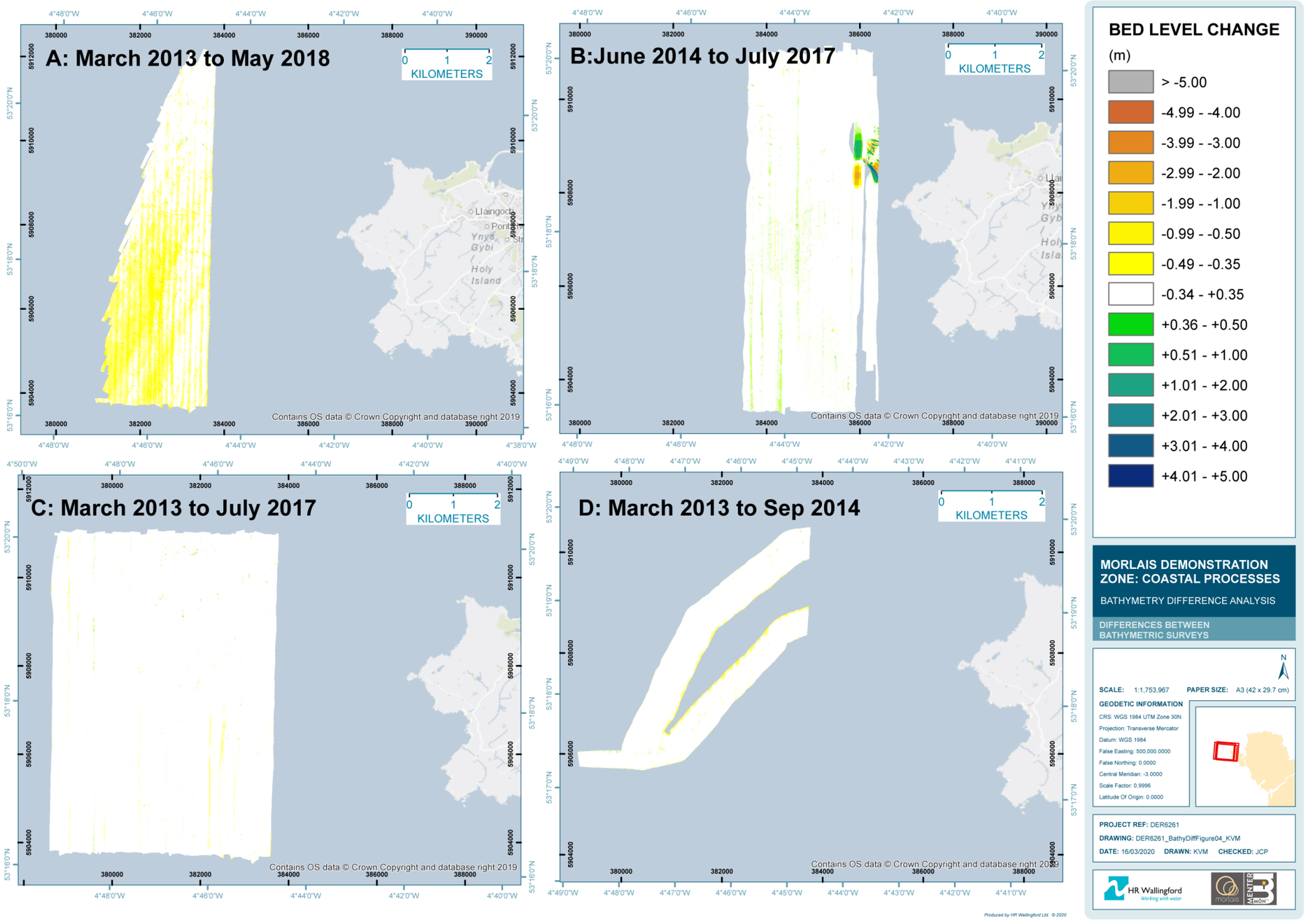

Figure 6.7: Bathymetric differences over the MDZ and further offshore

Source: HR Wallingford using data downloaded from IMARDIS

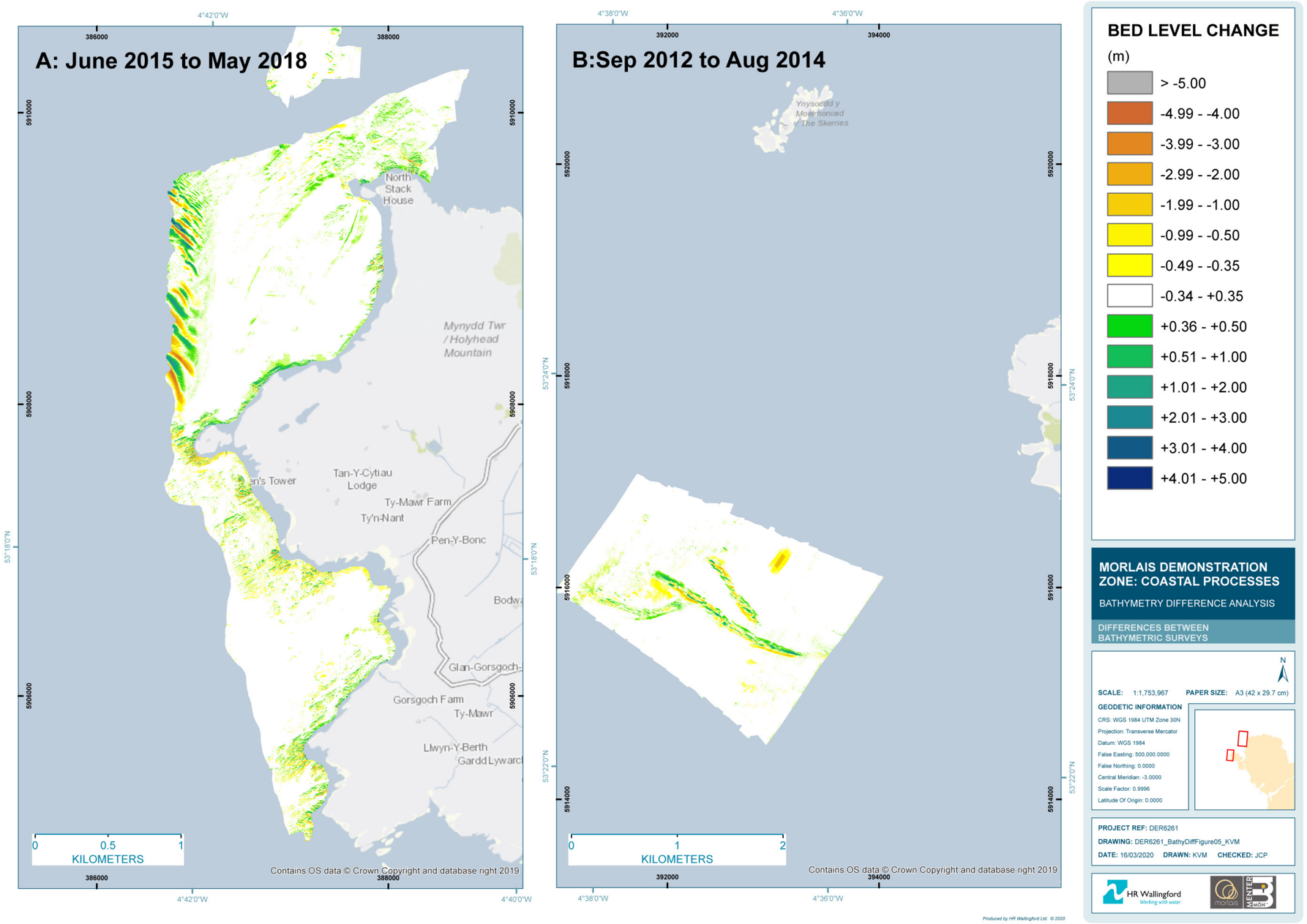

Figure 6.8: Bathymetric differences for Gogarth Bay, Abaraham's Bosom and Langdon Ridge

Source: HR Wallingford using data downloaded from IMARDIS

6.1.3. Summary and discussion

The seabed in the area of Holy Island and west Anglesey can be characterised as a high energy environment, with corresponding areas of exposed bedrock and coarse gravel due to finer material being unable to settle. Seabed change of any significance is isolated to the mobile ridge features and banner banks offshore of the South and North Stack headlands, and the Penbrynyreglwys headland to the north. The sediment deposits within the two embayments either side of South Stack comprise coarse sand and sandy gravel and the available data indicate that variability in seabed levels in these areas is low.

Large eddies generated by strong tidal flows past the headlands are the mechanism for the existence of the South Stack and Langdon Ridge banner banks. These formations have an important role in the local coastal processes, causing waves to refract and form localised areas of increased/decreased wave energy, affecting longshore drift volumes, as well as being important ecological habitats. Wave breaking in the shallower depths over the banks causes an overall decrease in wave energy reaching the shore which is an important component of coastal defence.

The available data show that the South Stack banner bank maintains overall position across the four year (2014 to 2018) observation period, but with seasonal and inter-annual variability in levels. The general and maximum level changes observed on the flanks of the South Stack banner bank over the past few years are generally within ±5 m, while the lateral position of the banner bank crest has remained constant, with a maximum change of 30 m. The Langdon Ridge feature remains static in position over the two year observation period (2012 to 2014), with small changes to bed level (on the whole within ± 1 m) being related to the migration of smaller scale bedforms (ripples and mega-ripples) that are superimposed onto the feature.

The same headland-generated tidal eddies mean that the sandy gravel known to be present in this area (see Figure 6.15) within Gogarth Bay and Abraham's Bosom tend to remain within the embayments. Seabed change in these areas is generally within ±0.3 m. Where change is outside of the this envelope of uncertainty, bed levels in Gogarth Bay tended to increase by up to 0.8 m between 2015 and 2018, while bed levels in Abraham's Bosom have tended to decrease by up to 0.5 m over the same period.

Robins et al (2014) used area modelling to investigate the impact of TEC arrays on natural variability of morphodynamics, with a case study on the west coast of Anglesey which included the Langdon Ridge feature. They demonstrated that with a TEC array situated 10 km up or downstream of the Langdon Ridge, the impact of extracting 100 MW of energy is an order of magnitude less than that caused by the natural variability of the feature.

Neill et al (2012) states that a TEC array need to be at least 800 m offshore to reduce any impacts on banner banks formed due to headland dynamics. The MDZ array design maintains this distance as a minimum to the Holy Island coastline across the array, except for the device closest to the South Stack headland which is approximately 500 m from the South Stack island.

In summary, the mobile bed features within the vicinity of the MDZ have been shown to experience natural variability that is likely to exceed the impacts of the proposed TEC array.

6.2. Sediment transport model set-up

The SISYPHE model (Villaret et al, 2013, Ref. 19) was employed to predict the sediment transport rates and resulting bed evolution. Full details of the model are provided in Appendix A.

SISYPHE is the sediment transport and bed evolution module of the TELEMAC modelling system. It can be coupled to either the 2D or the 3D flow modules of the TELEMAC system, as well as to wave models. It models complex morphodynamic processes in diverse environments, including river, estuarine and coastal applications.

In SISYPHE, sediment transport processes are grouped as bed-load, suspended-load or total-load, with an extensive library of transport relations. A subset of these relations accounts for the combined effects of waves and currents on sediment transport. In this study, the Soulsby-van Rijn formula was used (Soulsby, 1997), which has been widely applied to a wide range of coastal environments.

SISYPHE is applicable to non-cohesive sediments (single-sized or multi-sized sediments), cohesive sediments, as well as sand-mud-gravel mixtures. A number of additional physically-based sediment transport processes are incorporated into SISYPHE, such as the influence of secondary flow, the effect of bed slopes, variation in bed roughness and the presence of areas of non-erodible bed, among others.

6.2.1. Sediment size and distribution

To ensure representation of the sediment environment in the model, it is necessary to build a map of sediment distribution. The following section described the available data and subsequent processing to generate this map.

Ocean Ecology (2018) acquired four grab samples as part of their benthic ecology characterisation survey. One of these samples was taken in the demonstration zone, two within the buffer area and one within the south cable corridor. The positions of these grab samples are shown in Figure 6.10. These samples were analysed for gravel, sand and mud content and their representative median grain size (d50) found (Table 6.3). The samples were also sieved and their particle size distributions (PSD) determined (Figure 6.9).

Table 6.3: Sediment grain analysis of grab samples

Station	Gravel (%)	Sand (%)	Mud (%)	d50 (mm)	Description
41	73	27	0	3.80	Sandy GRAVEL
15	9	89	2	0.63	Gravelly SAND
20	7	93	0	0.75	Gravelly SAND
42	0	96	4	0.41	SAND

Source: Ocean Ecology (2018)

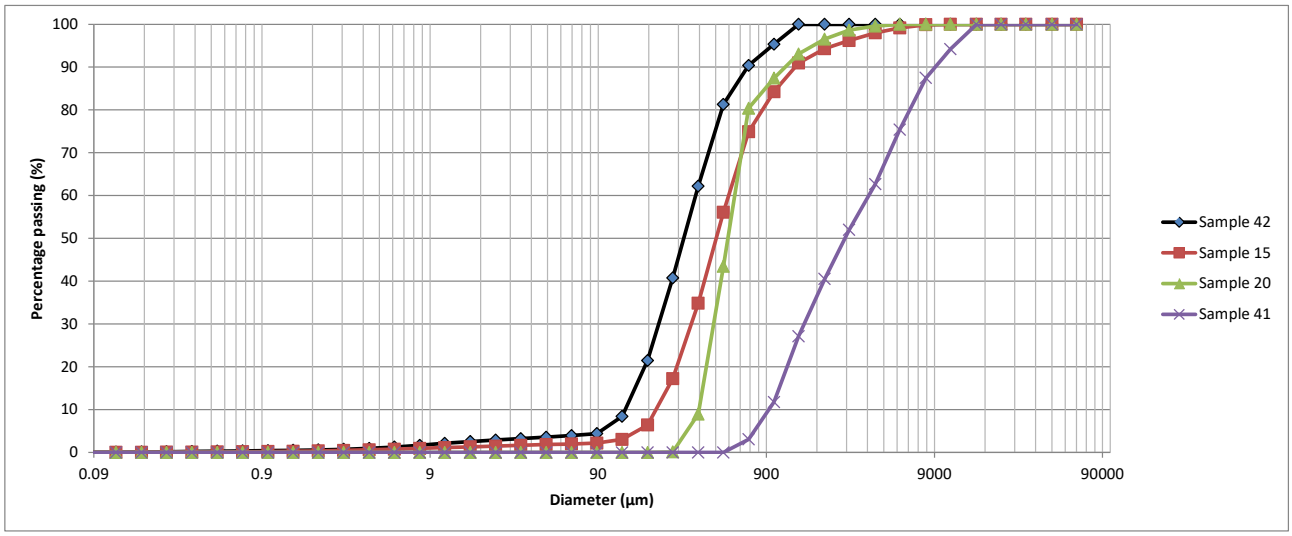

Figure 6.9: Particle Size Distribution from Ocean Ecology (2018) grab samples

Source: Using data from Ocean Ecology (2018)

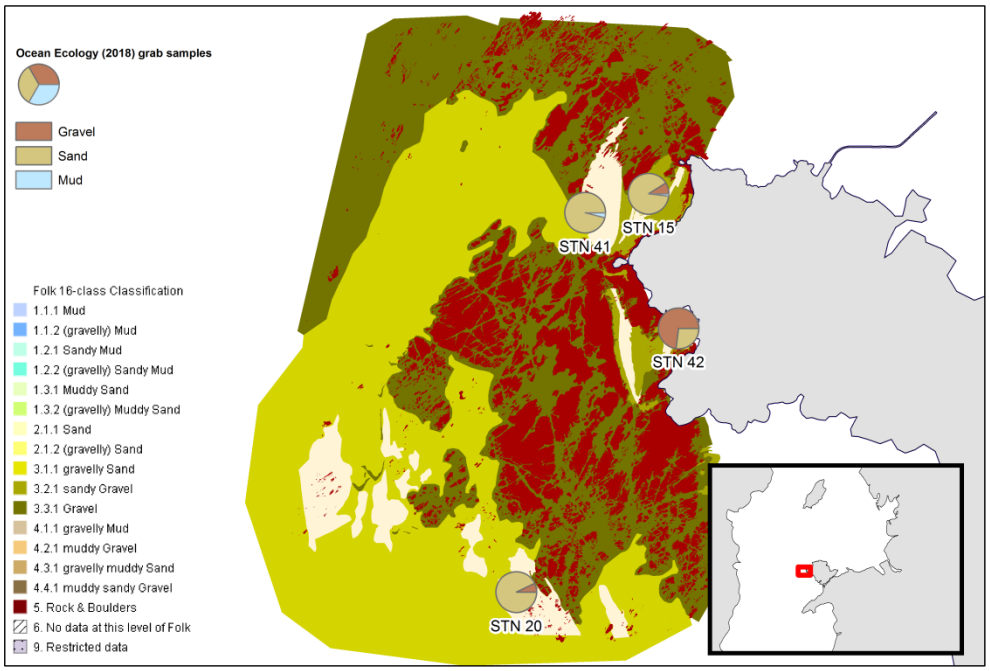

Figure 6.10: Folk-16 class classification using Partrac (2018) seabed features with Ocean Ecology (2018) grab samples overlain

Source: Using data from Partrac (2018) and Ocean Ecology (2018)

In 2018 Partrac conducted a site-wide geophysical investigation (Partrac, 2018). One of the outputs of this investigation was a seabed features map (Figure 6.10). The composition of the surficial sediment was determined using the strength of the backscatter return from the sidescan sonar survey. The Partrac (2018) sediment classification is, therefore, restricted to the area covered by the 2018 sidescan survey. Partrac used ten different classes to describe both the sediment type and the features (ridges, megaripples and outcrops). In Figure 6.10 these classes have been simplified and described using the Folk-16 scale (Folk, 1954).

To determine the surficial sediment properties of the seafloor outside of this area additional sources of information were referred to. The BGS sea-bed sediment (250k scale) map was used to provide information on the classification of the seabed types for the wider Irish Sea area (Figure 6.11). To create this map BGS used a range of remotely sensed and physical ground-truthing data. For each area the sediment is classified using the Folk-16 scale (Folk, 1954).

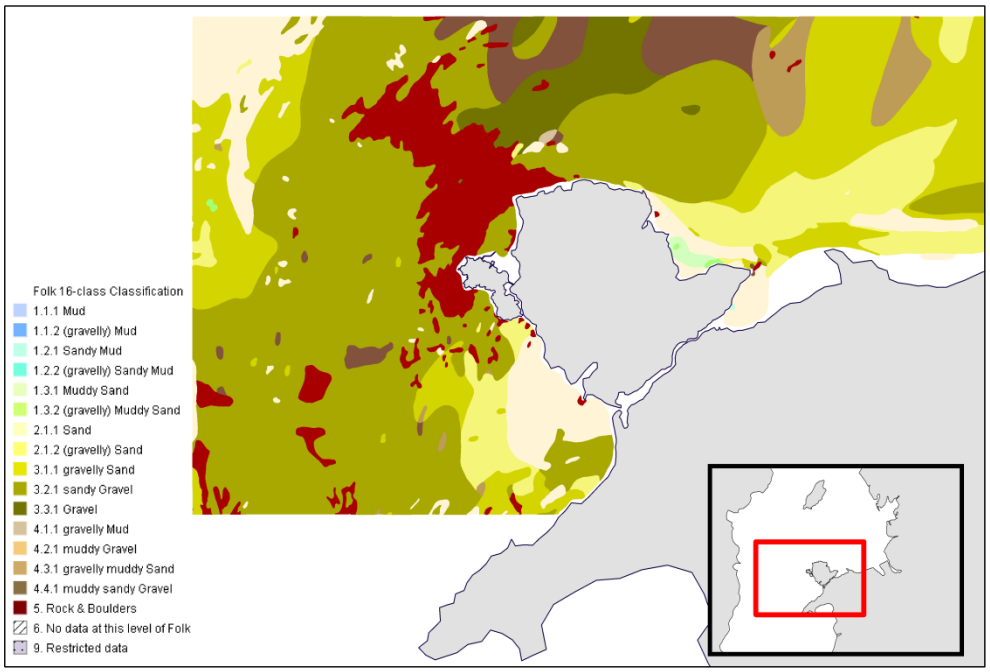

Figure 6.11: Folk-16 class classification using BGS sea-bed 250k

Source: Using data from BGS

The BGS sea-bed 250k data does not extend all the way to the model boundary, large areas of the nearshore are not covered and the Menai Straits have no information on their sediment composition. To fill in these gaps grab samples taken by the UKHO (UKHO, 2018) were used (Figure 6.12). The composition of these grab samples were described in terms of mud, sand, gravel, shell, pebble and rock contribution. From these grab samples HR Wallingford created polygons of the coastal areas and the Menai Strait using the Folk16 classification (Figure 6.13).

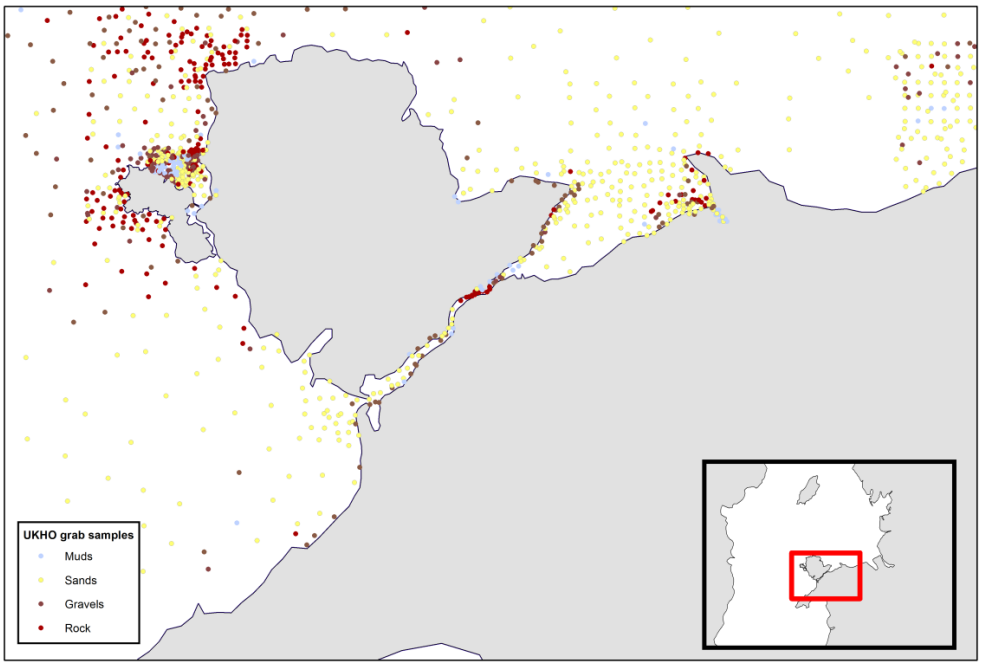

Figure 6.12: UKHO (2020) predominant sediment composition of grab samples

Source: Using data from UKHO (2020)

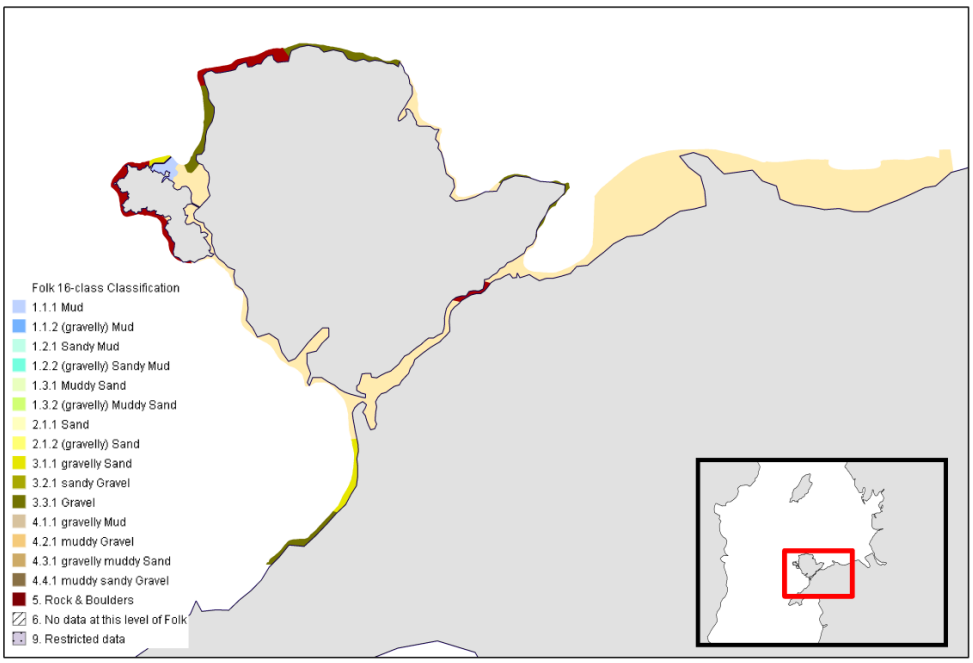

Figure 6.13: Folk-16 class classification of nearshore area

Source: HR Wallingford

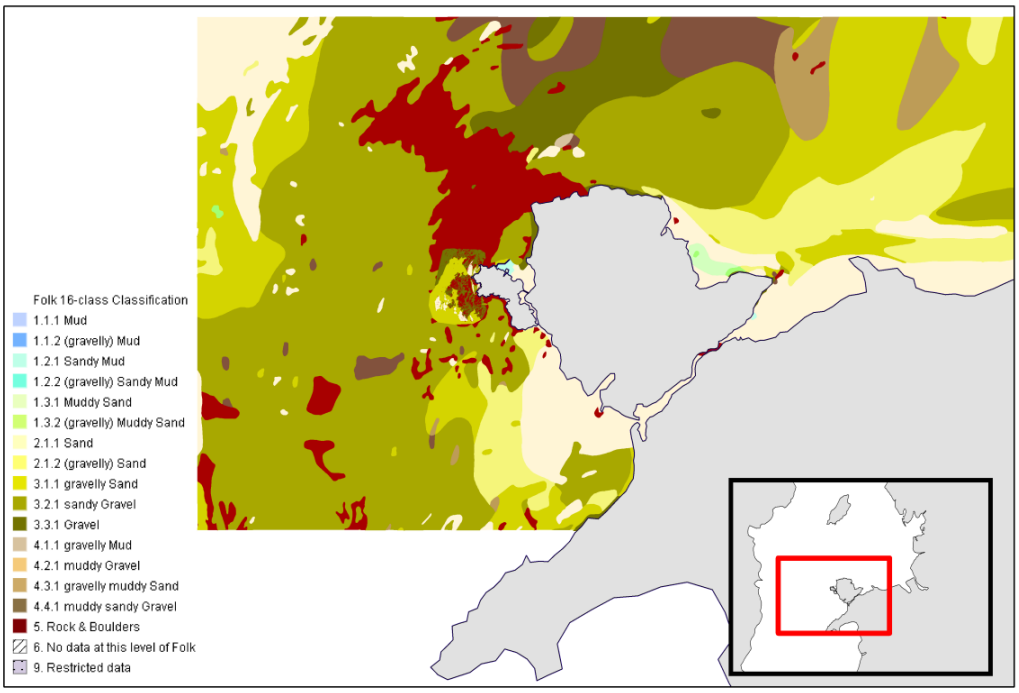

Figure 6.14: Combined (Partrac, BGS, UKHO) Folk-16 classification

Source: HR Wallingford

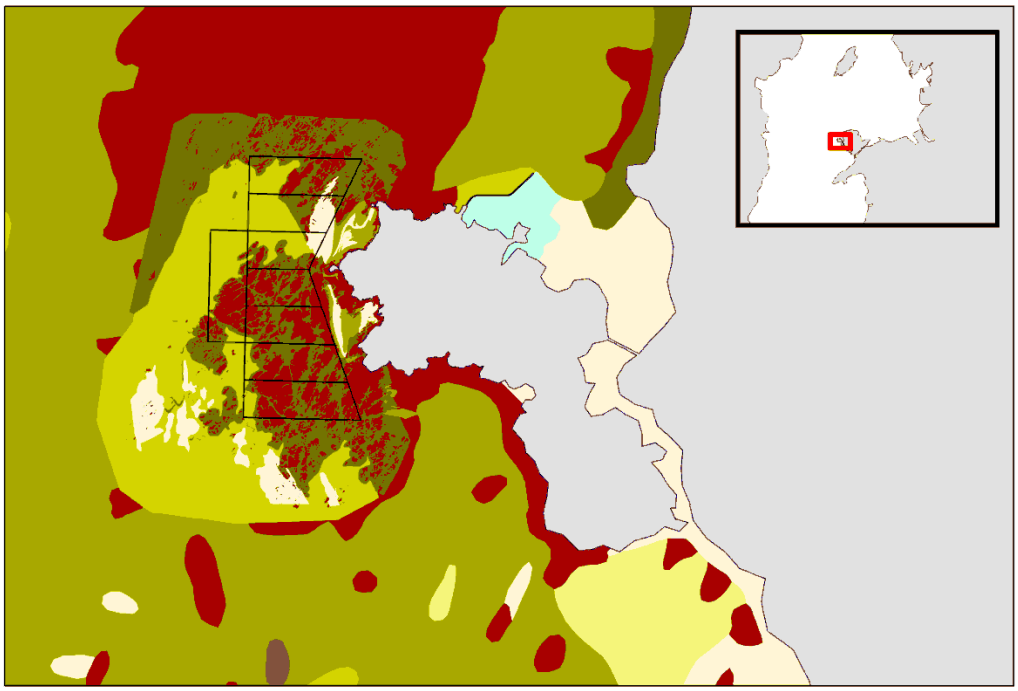

Figure 6.15: Combined (Partrac, BGS, UKHO) Folk-16 classification shown in more detail for the MDZ area. For legend, see Figure 6.14

Source: HR Wallingford

Using the Partrac (2018), BGS and UKHO derived polygons (in this order of preference) each area of the seafloor is described in terms of a Folk-16 class (Figure 6.14). This gives information on the contribution of each sediment class, but does not give information on the median grain sized (required as an input to the TELEMAC model). Using the four Ocean Ecology (2018) grab samples and information from the sediment map data of Wilson et al., (2018) a lookup table was developed to give each Folk-16 classification a value of d_{50} (Table 6.4). Wilson combines a large public data set of sediment grain size information with the BGS sediment classification data, where all the gaps are filled with theoretical relationships and accepted correlations between wave and current energy water depth and grain sizes.

The number of sediment classes were simplified to reduce the model complexity.

The information in Table 6.4 in conjunction with the Folk-16 classification map was used to generate maps of percentage fractions of cobbles, gravel and sand which were in turn direct inputs into the model.

Table 6.4: Lookup table for conversion from Folk16 to d_{50} and percentage gravel, sand and mud

Folk-16 Description	Partrac (2018) description	Source of PSD information	d_{50} (mm)	Gravel (%)	Sand (%)	Mud (%)
1.2.1 (gravelly) MUD 1.3.2 (gravelly) sandy MUD		Wilson et al., (2018)	0.15	0	10	90
1.3.1 Muddy SAND 2.1.1 SAND	Coarse sand, Fine sand	Ocean Ecology STN_42	0.4	1	99	0
2.1.2 (gravelly) SAND 3.1.1 Gravelly SAND 4.3.1 Gravelly muddy SAND	Gravelly Sand with occasional rock outcrop	Ocean Ecology STN_15 and 20	2.1	30	70	0
3.2.1 Sandy GRAVEL 4.4.1 Muddy sandy GRAVEL	Sandy Gravel	Ocean Ecology STN_41	3.80	70	30	0
3.3.1 GRAVEL 4.2.1 Muddy GRAVEL	Gravel with intermittent rock outcrop, Gravel ridge features, Gravel exhibit irregular topography, Rock outcrop with intermittent Gravel areas	Wilson et al., (2018)	6.0	100	0	0
5 Rock and boulders	Exposed Rock, Rock outcrop and high density of Boulders	Rock made artificially large so as to be non-erodible	1000	0	0	0

Source: HR Wallingford

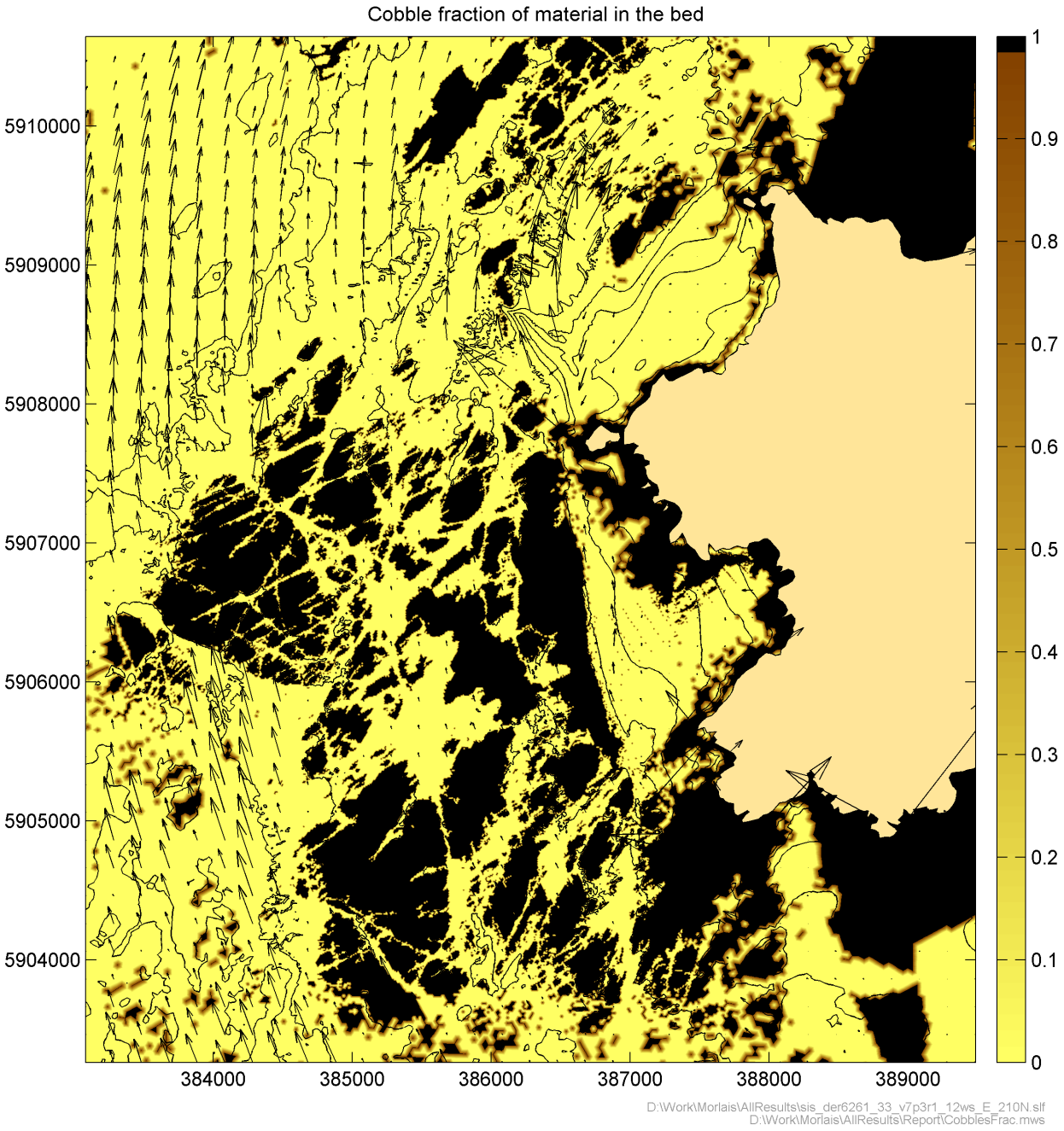

Figure 6.16: Cobbles fraction of material on the bed for model input

Source: HR Wallingford

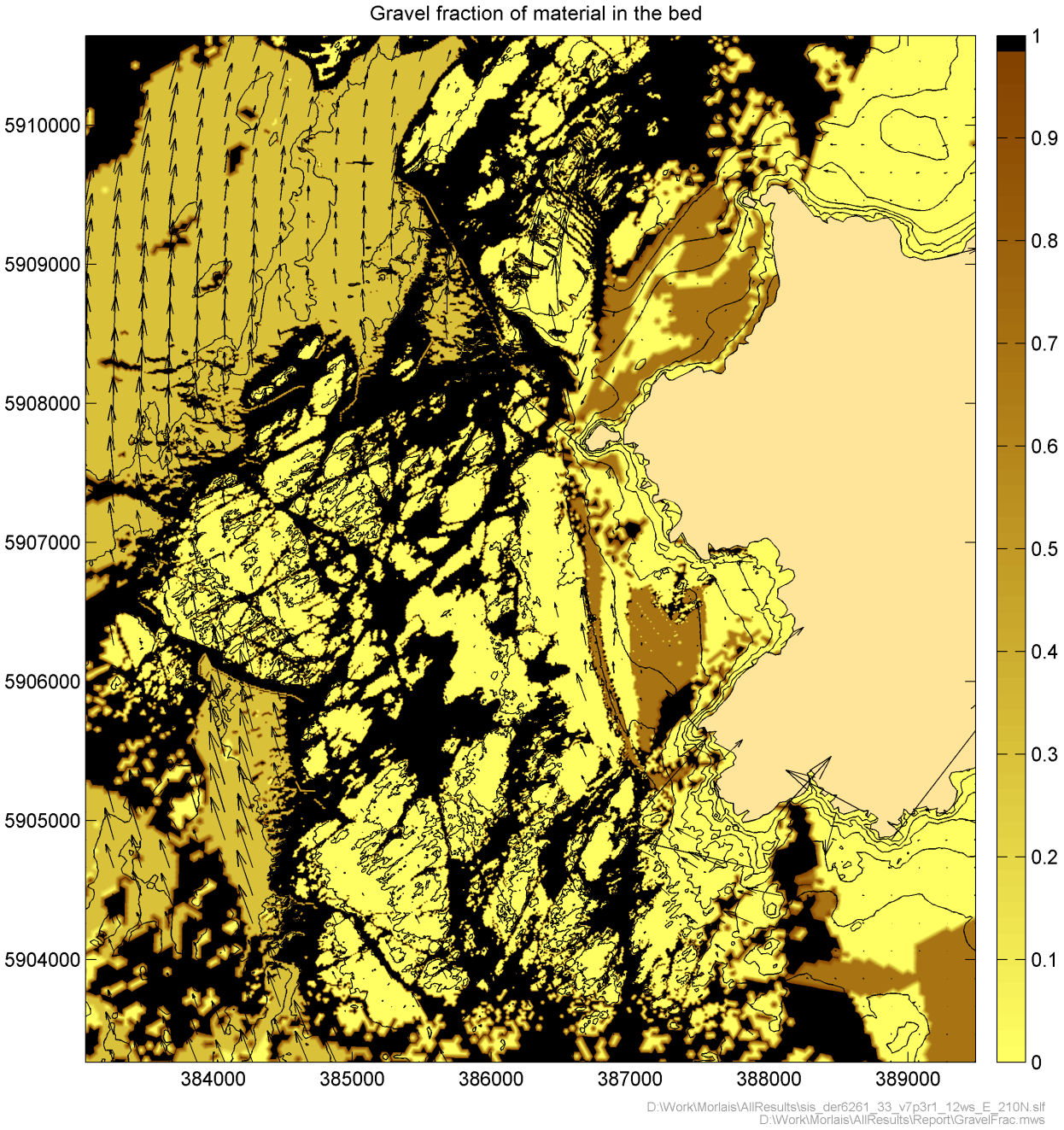

Figure 6.17: Gravel fraction of material on the bed for model input

Source: HR Wallingford

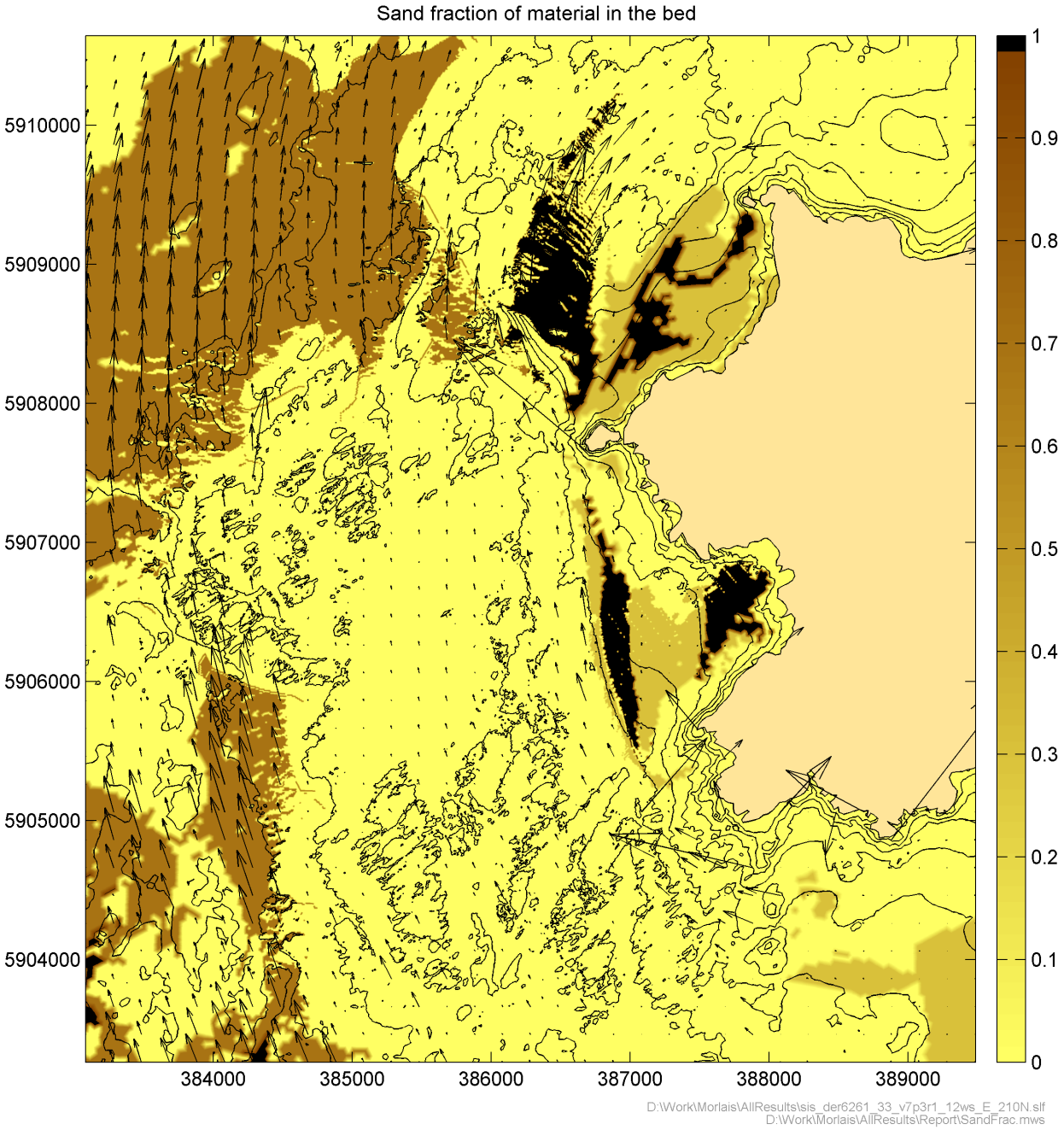

Figure 6.18: Sand fraction of material on the bed for model input

Source: HR Wallingford

6.2.2. Choice of wave conditions

Specific wave conditions were selected on the basis of being representative of the effects of waves including wave driven currents on sediment transport. The approach used was based on research carried out by HR Wallingford (reported in Chesher and Miles, 1992). From this research, a procedure has been devised that filters the full wave climate into a reduced set of representative conditions that give rise to equivalent sediment transport rates to that which would be predicted using the full wave climate. In the case of wave driven currents, the transport rates are proportional to the significant wave height to the power 4.3. In this way, the annual sediment transport regime can be predicted using a limited number of wave conditions.

Using this approach, the waves required for the sediment transport modelling were filtered down to the five representative conditions summarised in Table 6.5, based on the Met Office Remap wave climate derived at the point shown in Figure 5.1 from 40 years of data via the process described in Section 5.2.1. By far the most wave energy (54%) is predicted to be incident from the thirty degree sector centred on 210 degrees. In total about two-thirds of the wave energy comes from the south west (210 and 240 sectors).

Table 6.5: Representative wave conditions

Direction	210	240	270	300	330
Hs (m)	2.16	2.06	2.14	1.92	1.81
Tp (s)	6.90	6.80	6.90	6.70	6.60
Percentage occurrence	45.1	10.8	7.1	6.34	6.9

6.2.3. Application of SISYPHE to the sediment modelling study

Sisyphe was run in uncoupled mode for tidal flows over a 15 day spring-neap period with spatially varying roughness and grain sizes. The roughness height for the sediment transport was based on the sediment fraction maps in Figure 6.16 to Figure 6.18, with the mean diameter of each fraction assigned the representative grain sizes shown in Table 6.6.

To incorporate the effect of waves, the five wave cases were run as in Section 5.5 using water levels from the flow model over a spring tide period, with waves forces imposed on the flow in order to calculate wave driven currents. The tidal flows, wave driven currents and wave orbital velocity field were used in the Soulsby van Rijn formulation to calculate total load transport for representative tidal periods.

For each scenario (15 day tide only, five wave cases for spring tide period), the model was run with and without the operating turbines, and the results compared to discern impacts.

Table 6.6: Representative grain sizes used in the model

Sediment type	Representative grain size (mm)
Boulders	100
Gravel	6
Sand	0.35
Silt	0.06

6.3. Sediment transport model simulations and results

The sediment transport model was applied to both the baseline and the developed situation. For each, a full spring neap cycle was simulated. In addition, five representative wave conditions (explained in 6.2.2) were simulated during three consecutive spring tides.

The results show the residual transport, i.e. the average of all the transport over the time of the simulation, to provide information on the long term movement of the sediment. In addition, erosion and deposition plots provide insight into the bed level changes. All results are scaled up to provide annual amounts. As this scaling up ignores relaxation of the erosion and deposition rates over time, it does lead to some overestimates in the predicted bed level changes.

6.3.1. Tide only

Baseline

Figure 2.1 shows the resulting residual sediment transport rates and directions around Anglesey. The general pattern is in line with expectations, based on the data analysis and literature review (Section 6.1).

There is a northward residual transport of bed material west of Anglesey (Figure 6.20). The area directly west of Holy Island, where the turbines are proposed to be located, has the highest residual transport rates. This implies that this area is likely to be sediment starved. Any mobile material here is likely to be moved over this area more quickly than it can be supplied from the south. This is in agreement with the information on the bed composition, which shows that there are patches of exposed bed rock in the area.

Just north of Anglesey, there is an area shown in Figure 6.19, where the residual transport rates are high. It contains a convergence point on the north-western point of the island, where the north-easterly directed sediment transport to the west of Anglesey meets the westerly sediment transport along the northern shores of the island. This convergence is combined with the easterly directed transport slightly further north (approximately 5km north of the island). This transport pattern forms a trap for the mobile sediments. This effect is reported in literature by Ellis et al (2008), who describe it as an area of high suspended sediment concentrations.

In the Menai Strait, a southward residual sediment transport is predicted. This residual transport varies over the length of the Strait, explaining the existence of sand bars in the southern half of the Strait.

Figure 6.21 shows the yearly averaged sediment transport around the banner bank connected to South Stack. It shows a residual transport from the south feeding the bank, and a circulation pattern to the north, with the sediment taken away from the bank at the offshore tip of the bank and returned (at a lower rate) on the landward side. This mechanism maintains the bank.

North of the bank, where the bathymetry shows sandwaves in the bed, the residual sand transport is predicted to be northwards. Note, that the predicted sediment transport rate in this area is probably too high. Based on available bed information, the model assumes a full sand cover, but the shape of the bedforms suggests that these are isolated sandwaves on a harder substrate. If this is the case, the actual transport rates will likely reduce to levels similar to those east and west of the area.

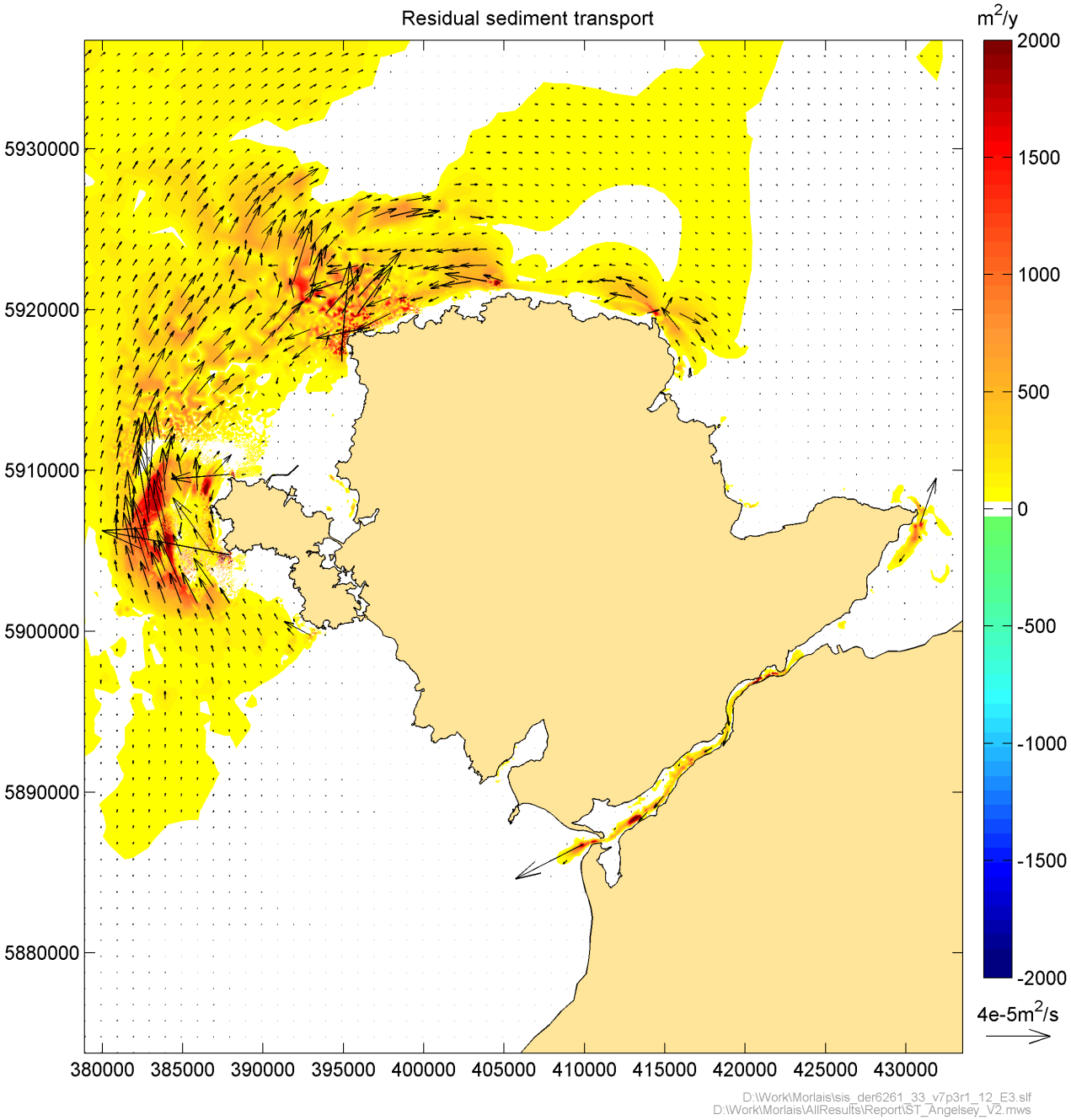

Figure 6.19:Yearly averaged residual sediment transport around Anglesey

Source: HR Wallingford

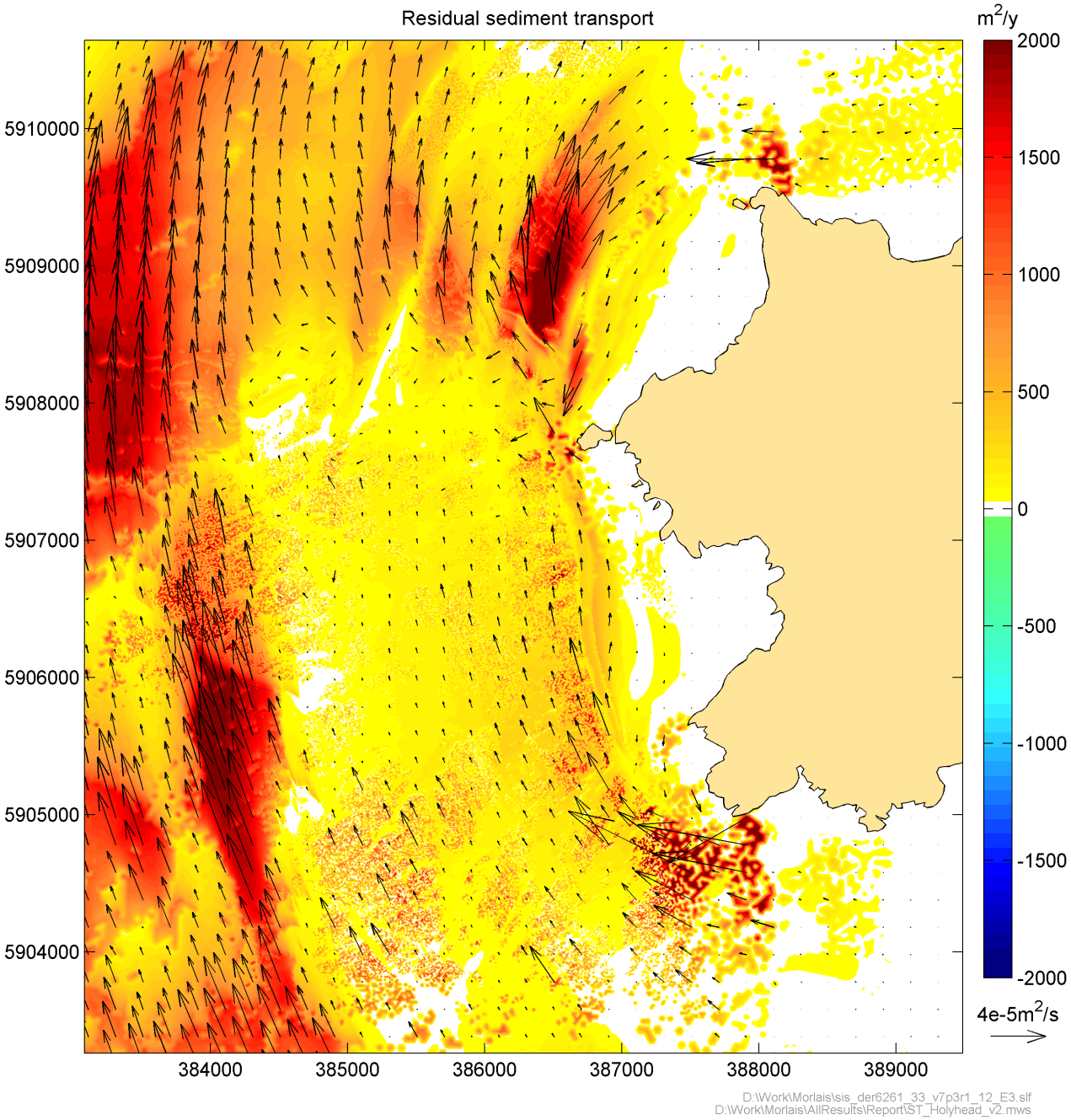

Figure 6.20: Yearly averaged residual sediment transport off Holy Island

Source: HR Wallingford

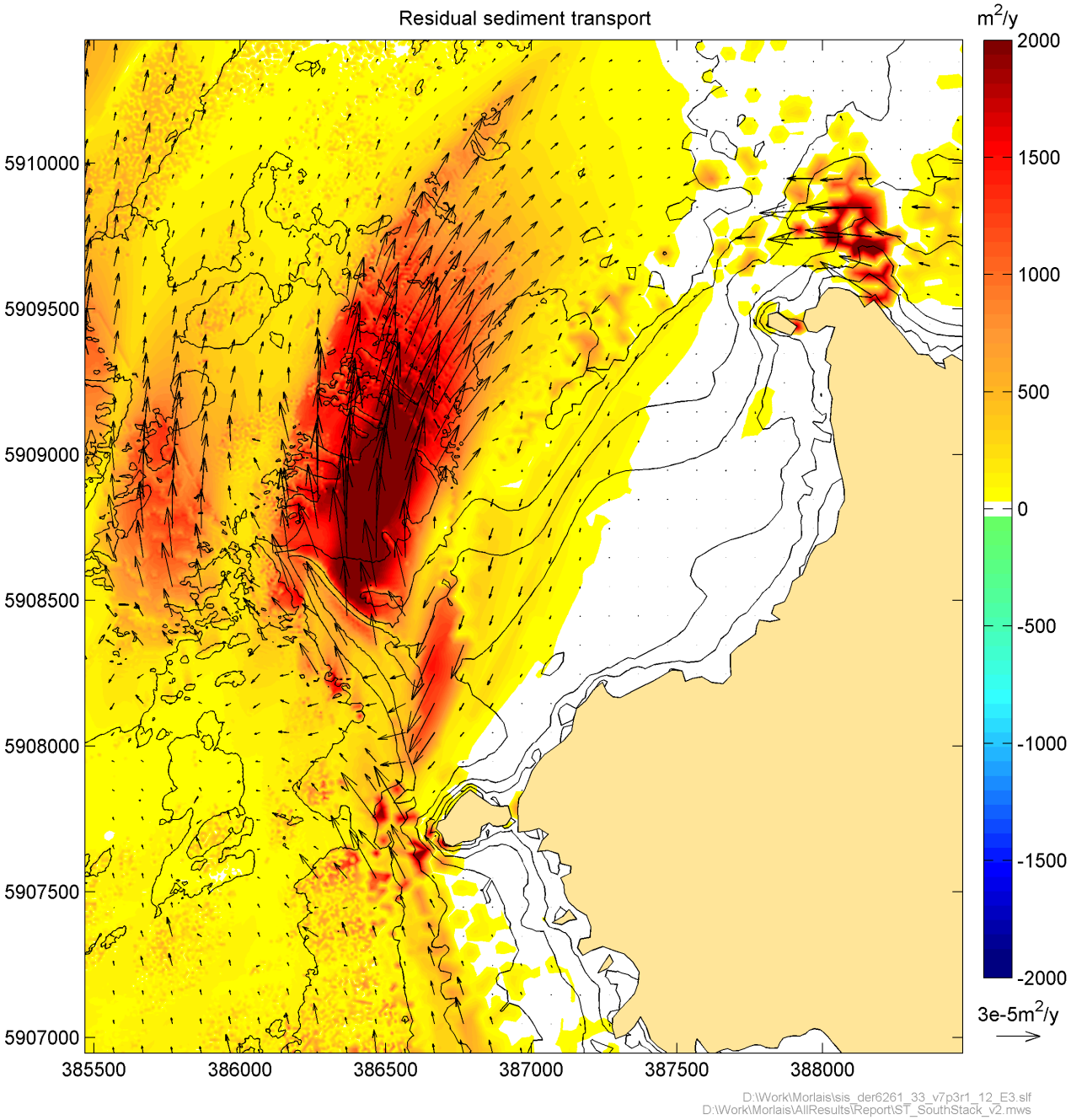

Figure 6.21: Yearly averaged residual sediment transport around the South-Stack banner bank

Source: HR Wallingford

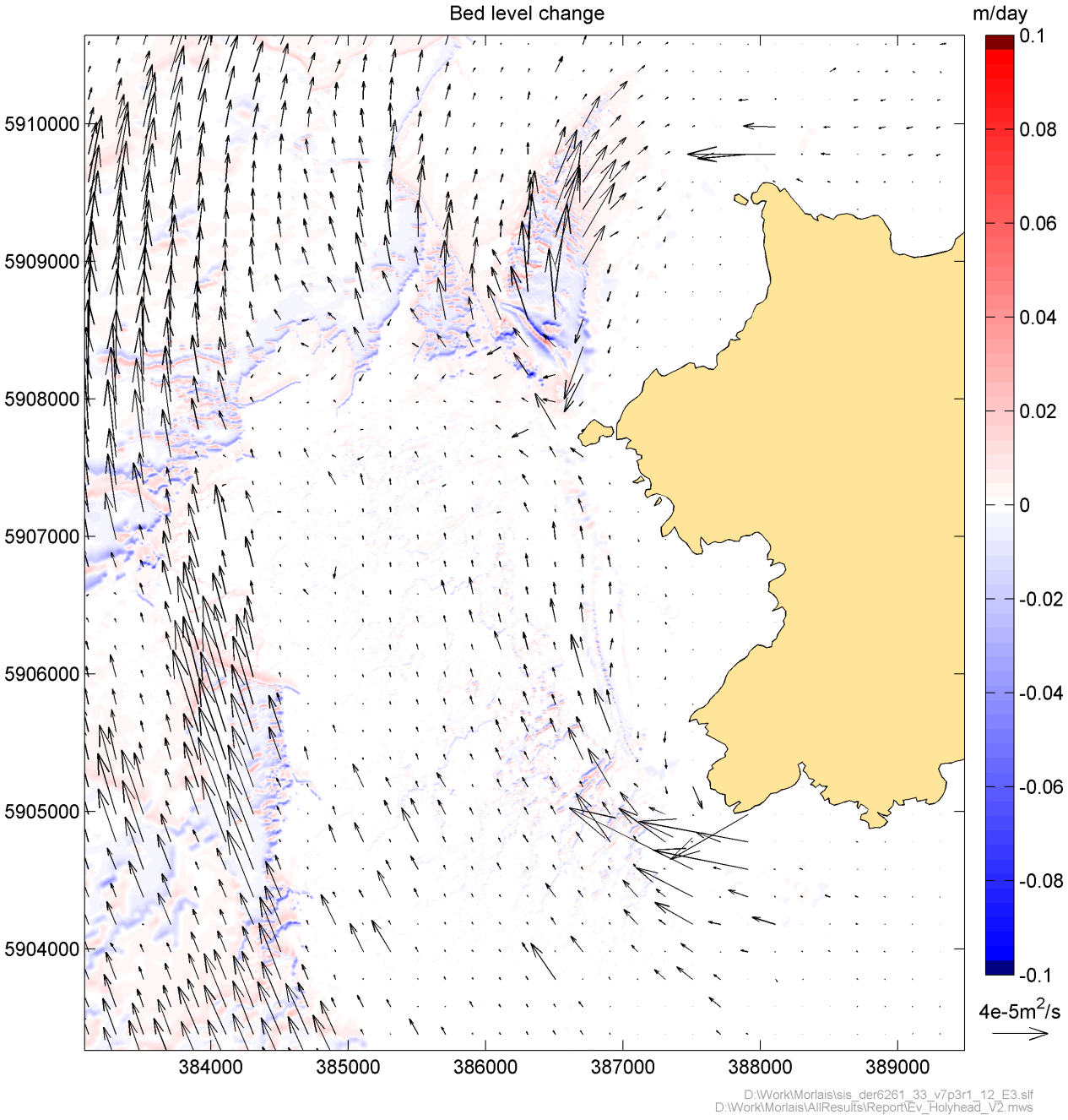

Figure 6.22: Predicted bed level changes west of Holy island

Source: HR Wallingford

The predicted bed level changes (Figure 6.22) are concentrated at the edges of the bed rock layers and areas where sandwaves appear to be moving. For practical purposes, the area just North of South Stack is the only location where much bed change is predicted. It shows a reshaping of the South Stack banner bank, where the model is trying to adapt the bank shape from the actual observed morphology to a form that would be in equilibrium with the slightly different model conditions. Although this is unlikely to be a real effect, the order of magnitude of change is similar to the observed changes in repeat surveys of the area. To the north, the seabed is predicted to lower. In this area, the sandy bed material has sandwaves on the surface. The overall lowering is an indication that the bed contains a mixture of coarser material with sandwaves travelling over it, rather than the full sand cover derived from the available bed composition data that has been implemented in the model.

Impact

The overall impact of the tidal turbine scheme on the residual sediment transport and the related bed level changes are typically less than 10% of the residual sediment transport, which in turn is less than 5 to 10% of the gross sediment transport.

Figure 6.23 shows the change in the residual transport due to the tidal turbines. Changes occur west of Holy Island, directly around the turbine area. No changes are predicted in the wider area. The same holds for the bed level changes which are limited to the area just west of Holy Island (Figure 6.24).

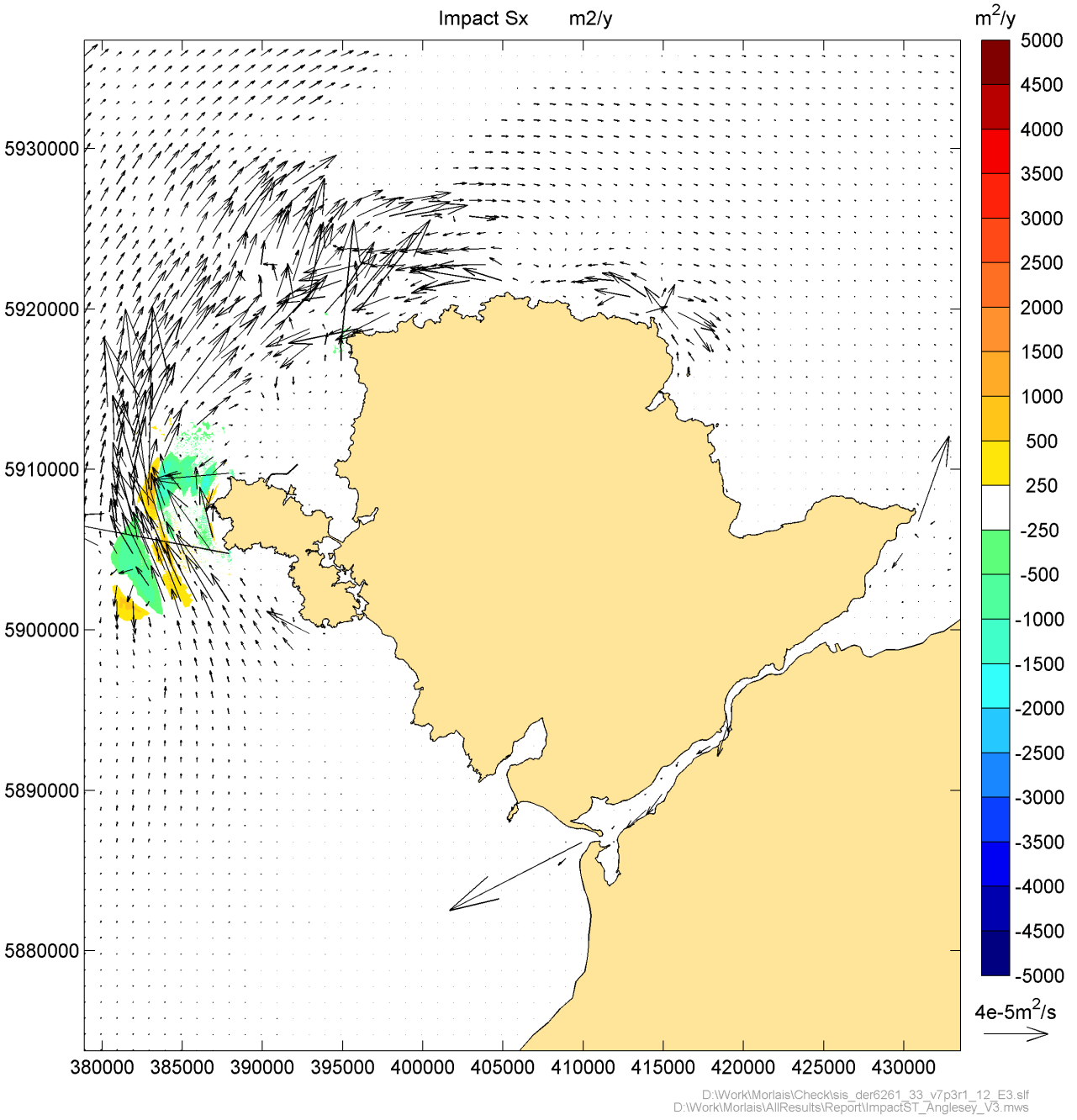

Figure 6.23: Impact of the tidal turbine array on the residual sediment transport around Anglesey

Source: HR Wallingford

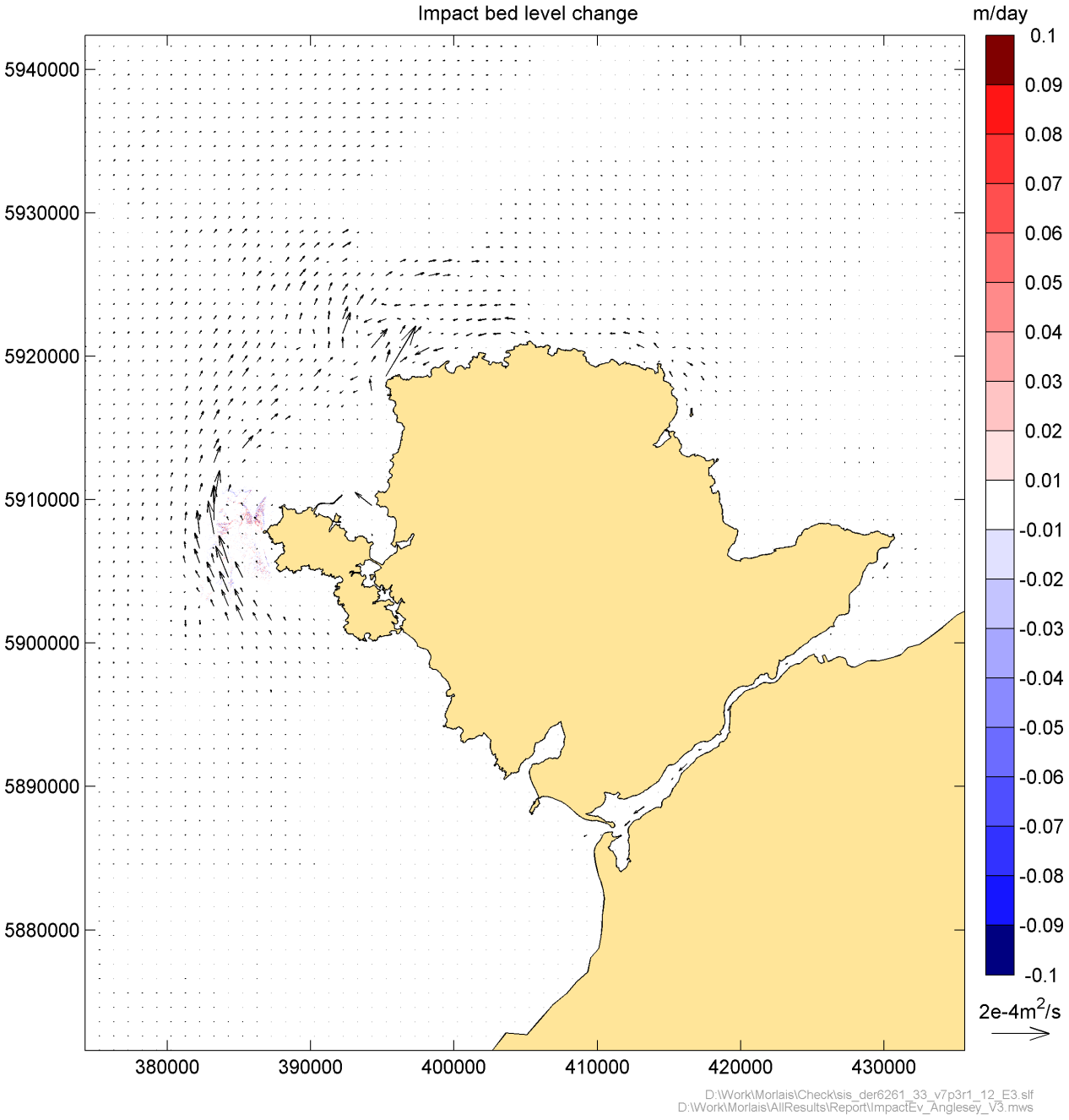

Figure 6.24: Impact of the tidal turbine array on the bed levels around Anglesey

Source: HR Wallingford

Figure 6.25, shows the predicted changes in the residual sediment transport around the area just west of the turbine array. Even there, the magnitude of the changes is less than 5 to 10% of the residual sediment transport. The slower currents due to the drag of the turbines, lead to a reduction of the sediment transport rates in the zones of the turbines. Offshore of the array, the flow velocities are higher, leading to an increase

in the residual transport. The same increase occurs in a narrow strip between the shore and the turbines, where the residual transport towards South Stack increases.

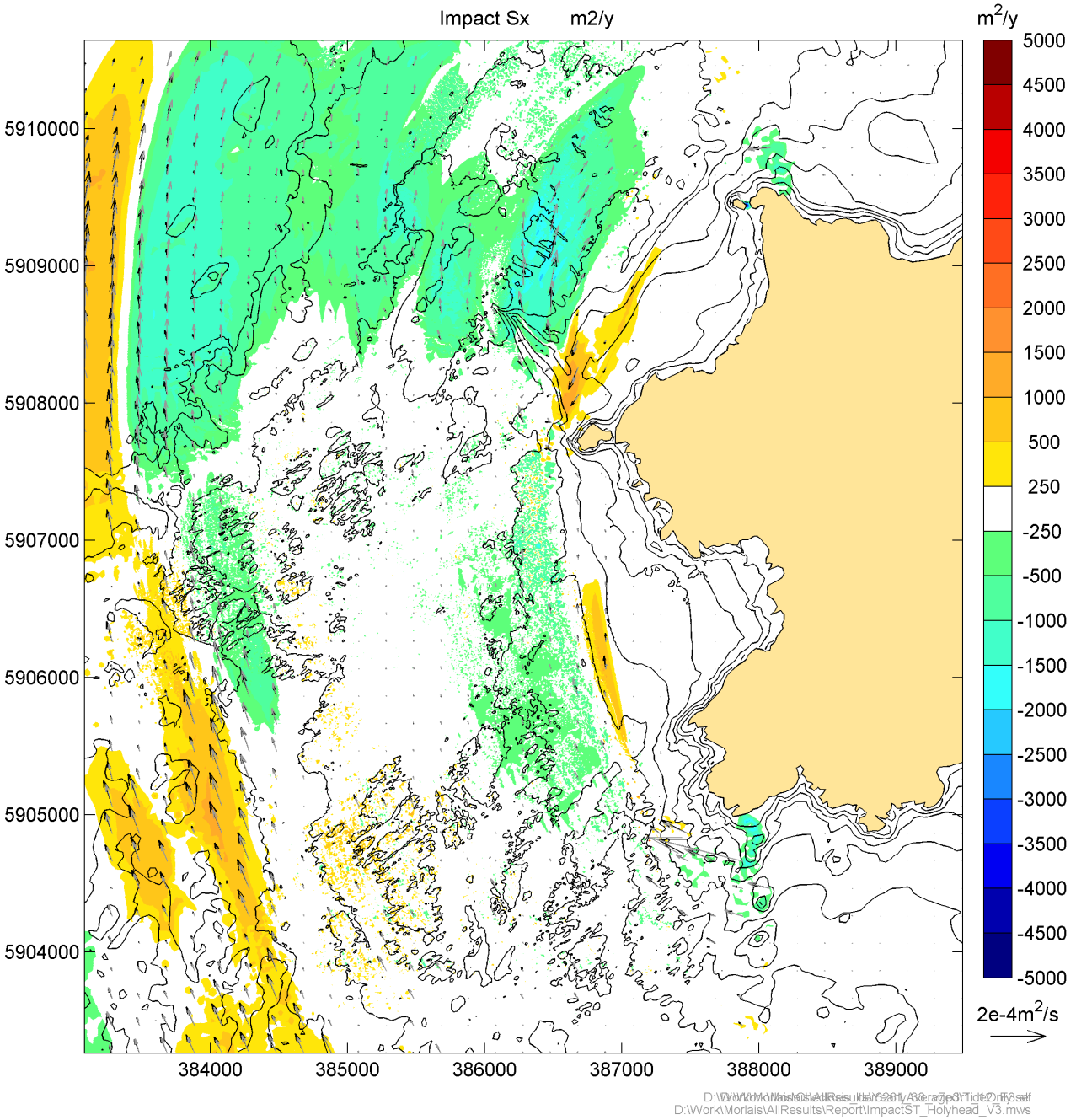

Figure 6.25: Changes in the yearly averaged residual sediment transport off Holyhead Island due to the tidal turbines

Source: Grey vectors show the baseline residual transport, while black arrows show the residual sediment transport for the developed situation.

The circulation cell in the residual sediment transport north of the South Stack banner bank is predicted to change. The northward transport north of the seaward tip reduces, while the residual transport towards the southern end of the bank increases. There is little change in the southward transport on the shoreside.

These changes may lead to some reconfiguration of the bank, leading to a more northward position of the bank and possibly some modifications to the height and length of the bar. The predicted volume changes in the model suggest that the bank initially gains 2,000m^3 per spring-neap cycle (on a bank volume of approximately 850,000m^3), with tthis material being supplied by erosion from the sand deposits in front of Gogarth Bay. However, the recirculation cell is not interrupted and on its northern end the changes have disappeared. This suggests that the size of the bank will not be affected significantly by these changes in the longer term.

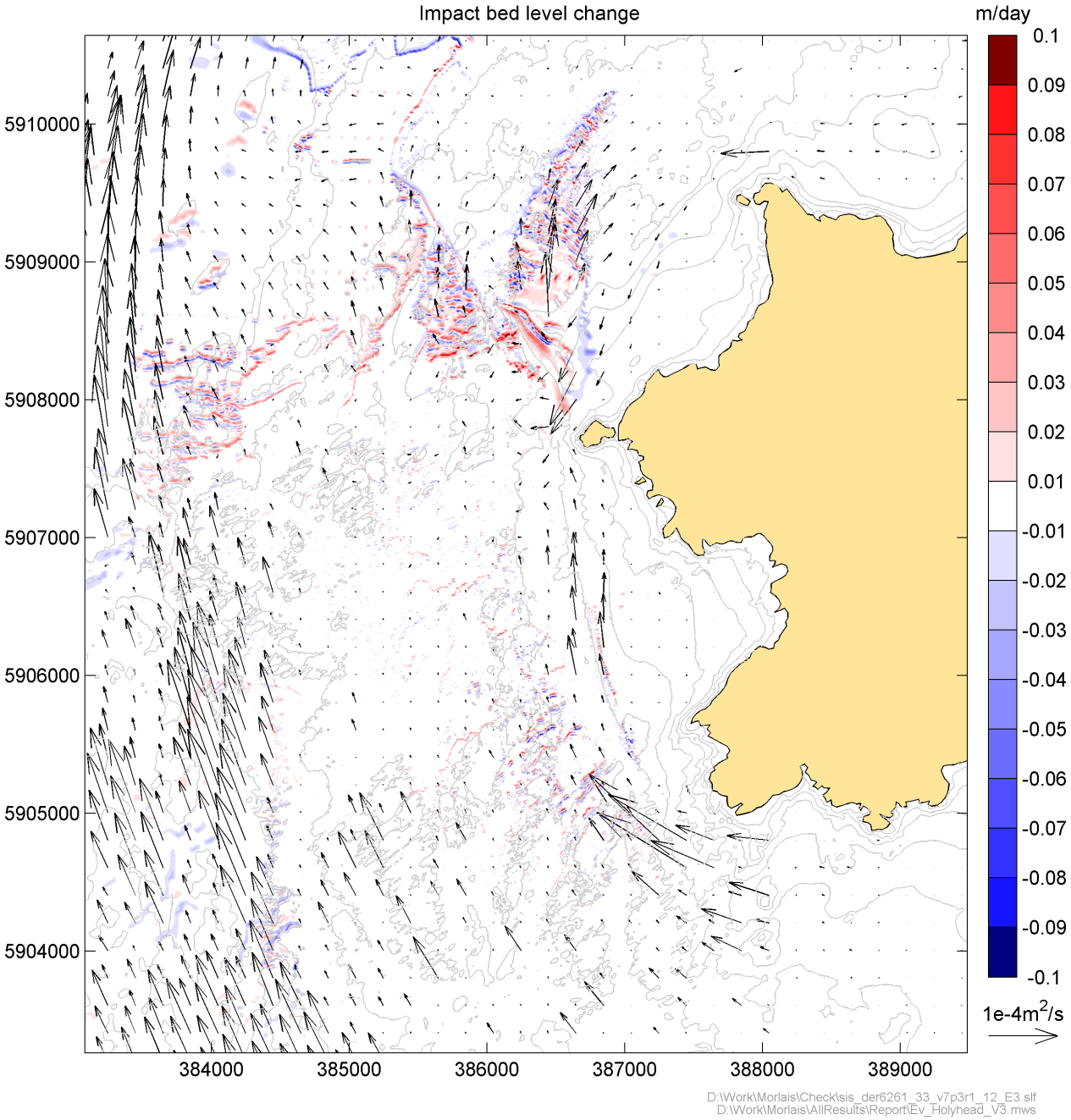

Figure 6.19: Impact of the turbines on the bed level changes in the area

Source: HR Wallingford

6.3.2. Wave driven currents

Yearly averaged Baseline

While for the tidal turbine location and the immediate surroundings, the tide is the dominating force driving the sediment, closer to the coast, the tide alone is not moving much sediment. Therefore, the sediment transport is also modelled with wave stirring and wave driven currents. This increases the hydrodynamic energy and the sediment transport intensity. Figure 6.20 shows the resulting residual sediment transport west of Holy Island. While the offshore patterns are similar for the flow only results, although at an increased magnitude, additional transport is happening along the shores, in particular in the bays.

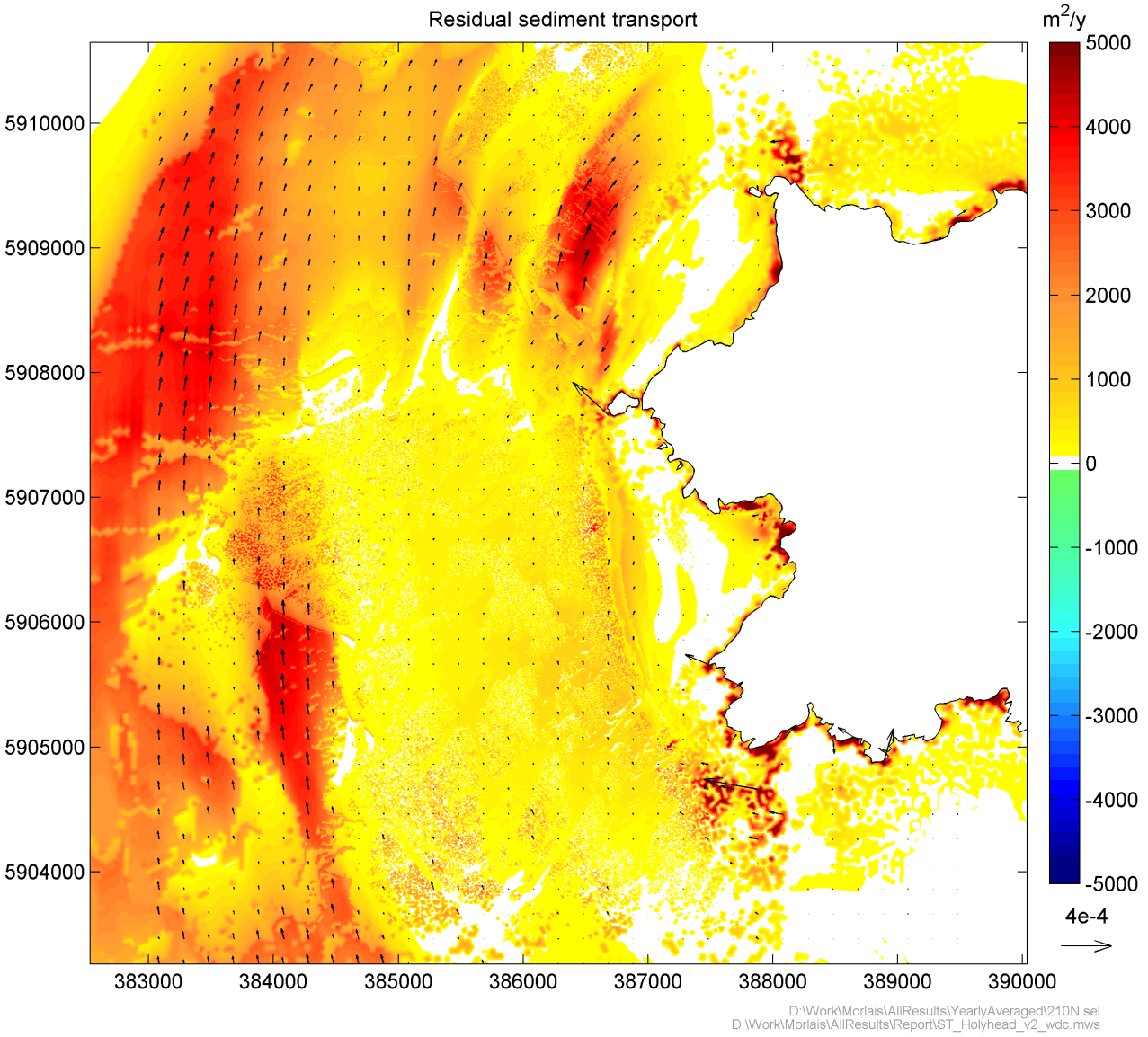

Figure 6.20: Annual residual sediment transport including wave stirring and wave driven currents

Source: HR Wallingford

In Gogarth Bay (Figure 6.21), there is a significant residual transport northward, driven by the waves arriving from the south-west. This residual transport is the cause for the absence of mobile material, which is swept out by the wave driven currents.

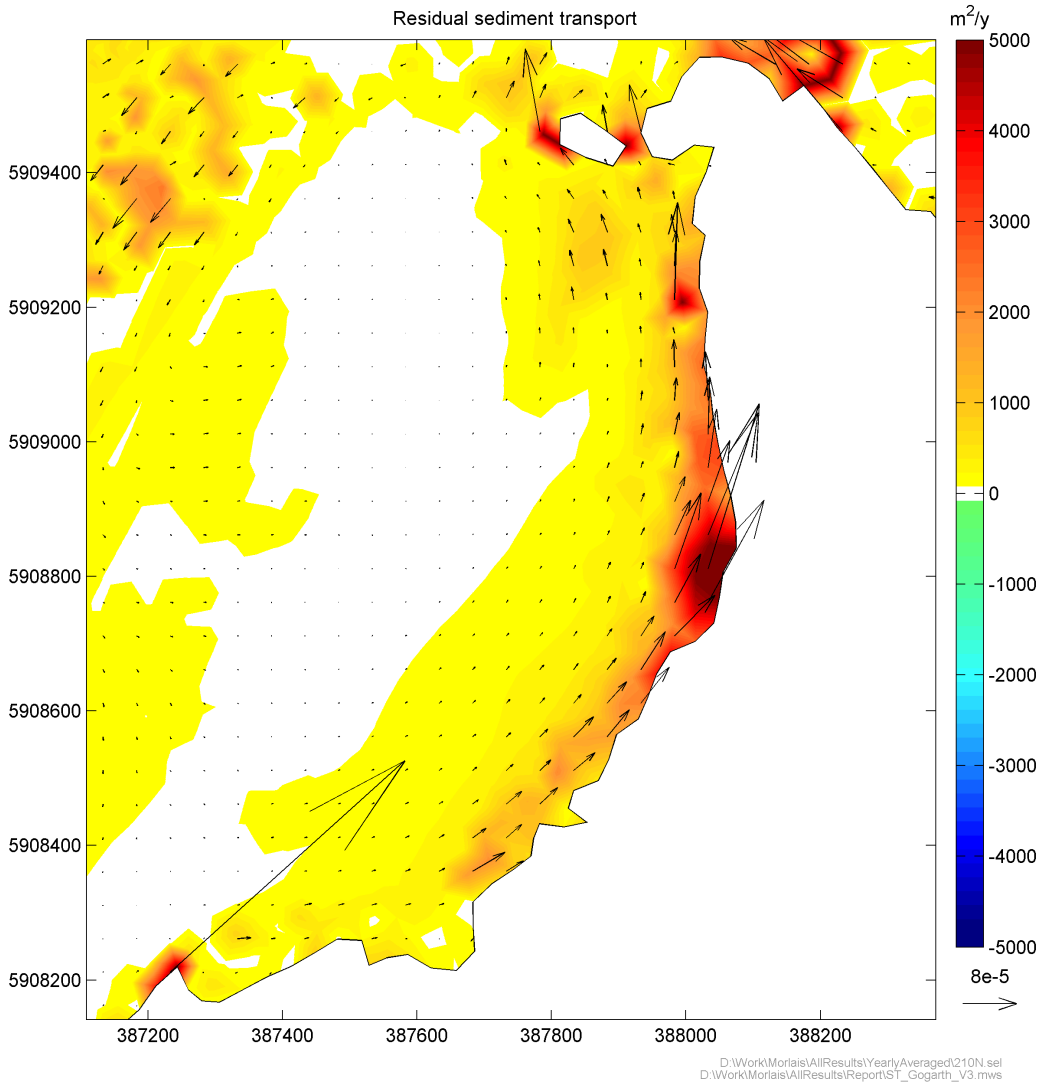

Figure 6.21: Annual residual sediment transport including wave stirring and wave driven currents in Gogarth Bay

Source: HR Wallingford

Abraham's Bosom (Figure 6.22) is much deeper and is flanked by protruding rocky headlands on both sides. As a result the residual sediment transport is less coherent, and the patterns allow for some mobile sediment to stay at the little beach at the landward end. Note that the predicted strong sediment transport on both sides of the bay are caused by incomplete bed composition in the model. These areas are assigned a mobile bed in the model, whereas an inspection of Google Earth shows rock stacks in this area.

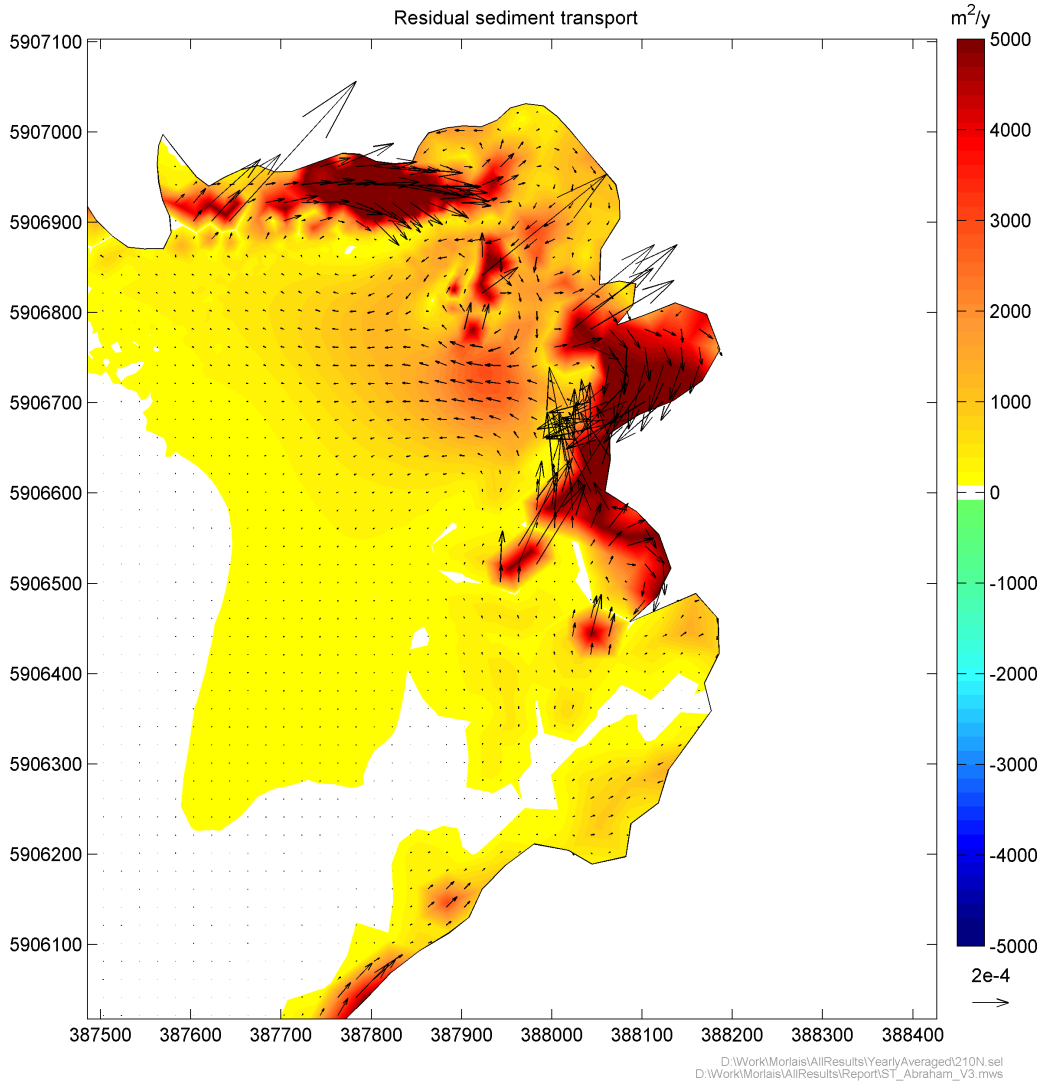

Figure 6.22: Annual residual sediment transport including wave stirring and wave driven currents in Abraham's Bosom

Source: HR Wallingford

Impact

The impact of the tidal turbines array on the residual sediment transport with waves and wave driven currents on the coastal morphology is small.

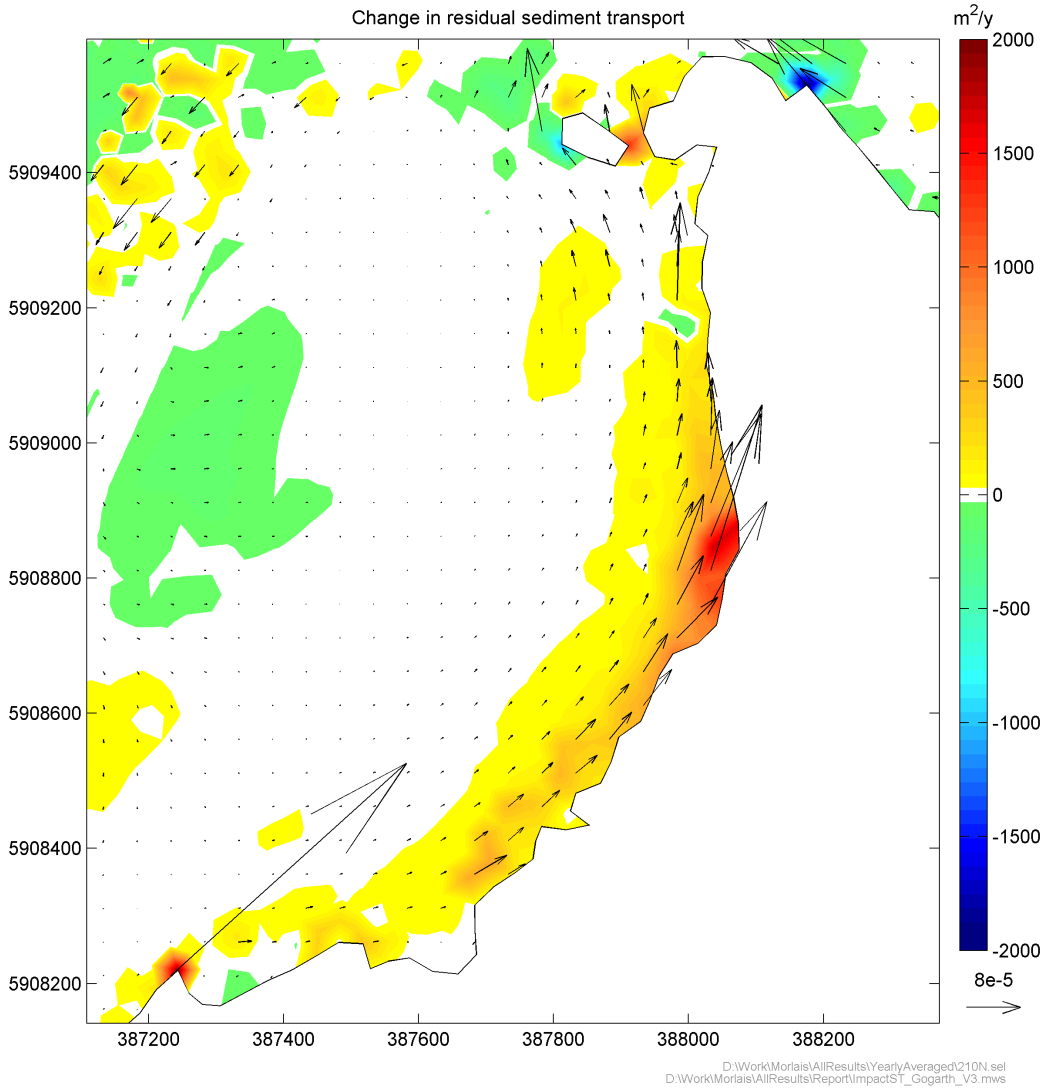

Figure 6.23: Impact of the tidal turbines array on the residual transport for wave driven currents west of Holyhead Island

Source: HR Wallingford

The changes in the residual transport along the shore in Gogarth Bay are shown in Figure 6.23. There is an increase of 10% to 20% in the residual transport along the shoreline in the bay. However, as there is no mobile beach in this area, this will have no impact on the coast. The increased rates of residual transport will maintain the rocky bed in the bay.

The changes in residual transport in Abraham's Bosom (Figure 6.24) is almost completely negative, indicating that the reduced wave height arriving at the entrance to the bay leads to less sediment transport. However, there is a small area at the toe of the mobile beach, indicating that the west to east residual transport slightly increases. This may lead to a small change in the orientation of the beach, which may become slightly more aligned north to south. However, this change is not expected to be larger than the annual variation in the beach orientation due to the natural fluctuation in the wave climates.

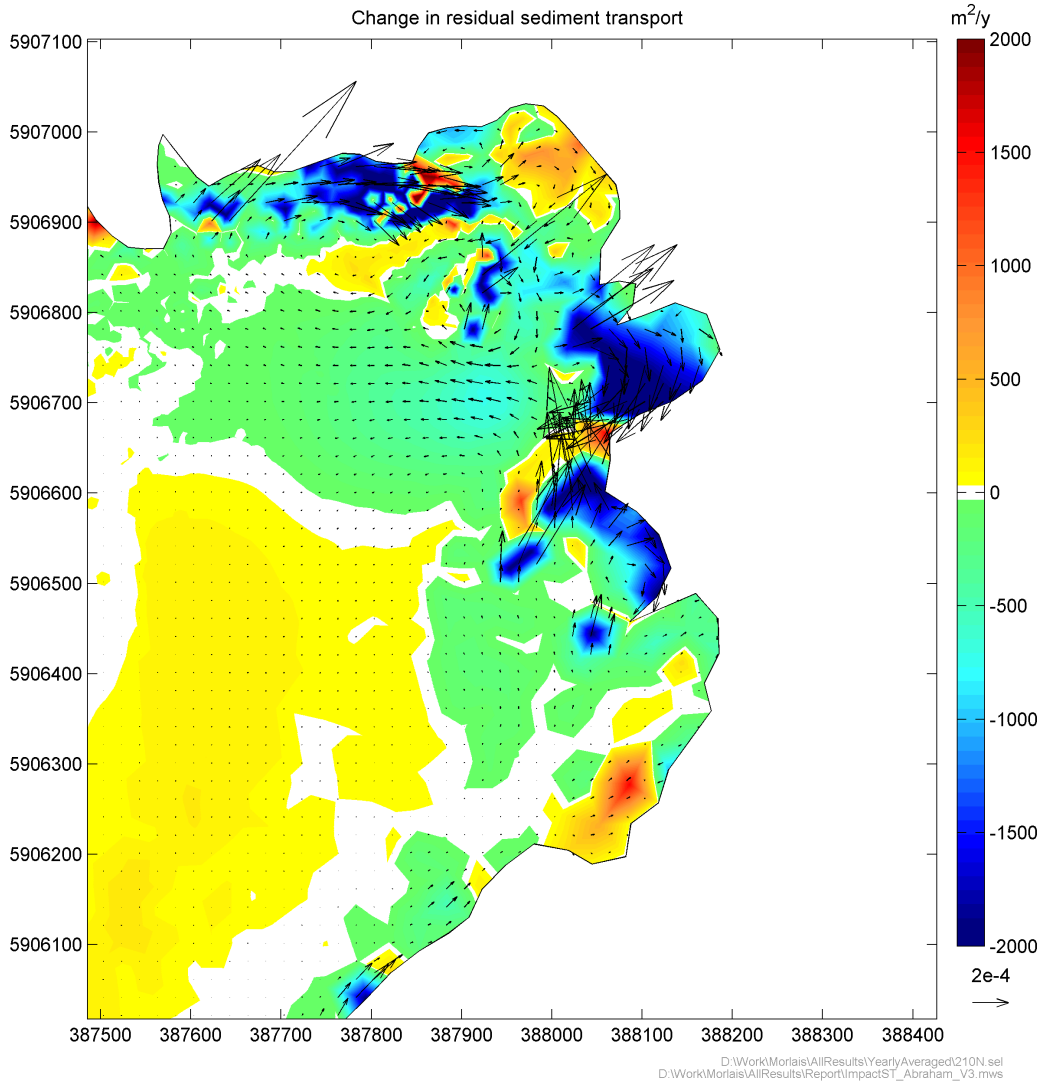

Figure 6.24: The relative impact of the tidal turbines on the residual sediment transport in Abraham's Bosom

Source: HR Wallingford

Dominant direction

Although the wave effects do not significantly alter the residual sediment transport offshore after averaging over all wave conditions, during some events some alterations to the sediment transport patterns occur. For the dominant wave direction (210N) the changes due to the tidal turbines are shown in Figure 6.24. In Figure 6.25 the black vectors show residual transport for the baseline case and the pink vectors the residual transport with the tidal turbines installed. The colour contours show the changes in the residual transport. The changes are very similar to those in Figure 6.20, but the reduction in the transport rates in the turbines area is enhanced, while the increase in transport rates in front of Gogarth bay is confined to a narrower strip. The enhanced transport in front of Abraham's Bosom occurs further northward. For the other wave sectors, which have less impact on the transport because the waves are typically smaller and occur less often, the changes will be slightly different to those presented for the 210N sector.

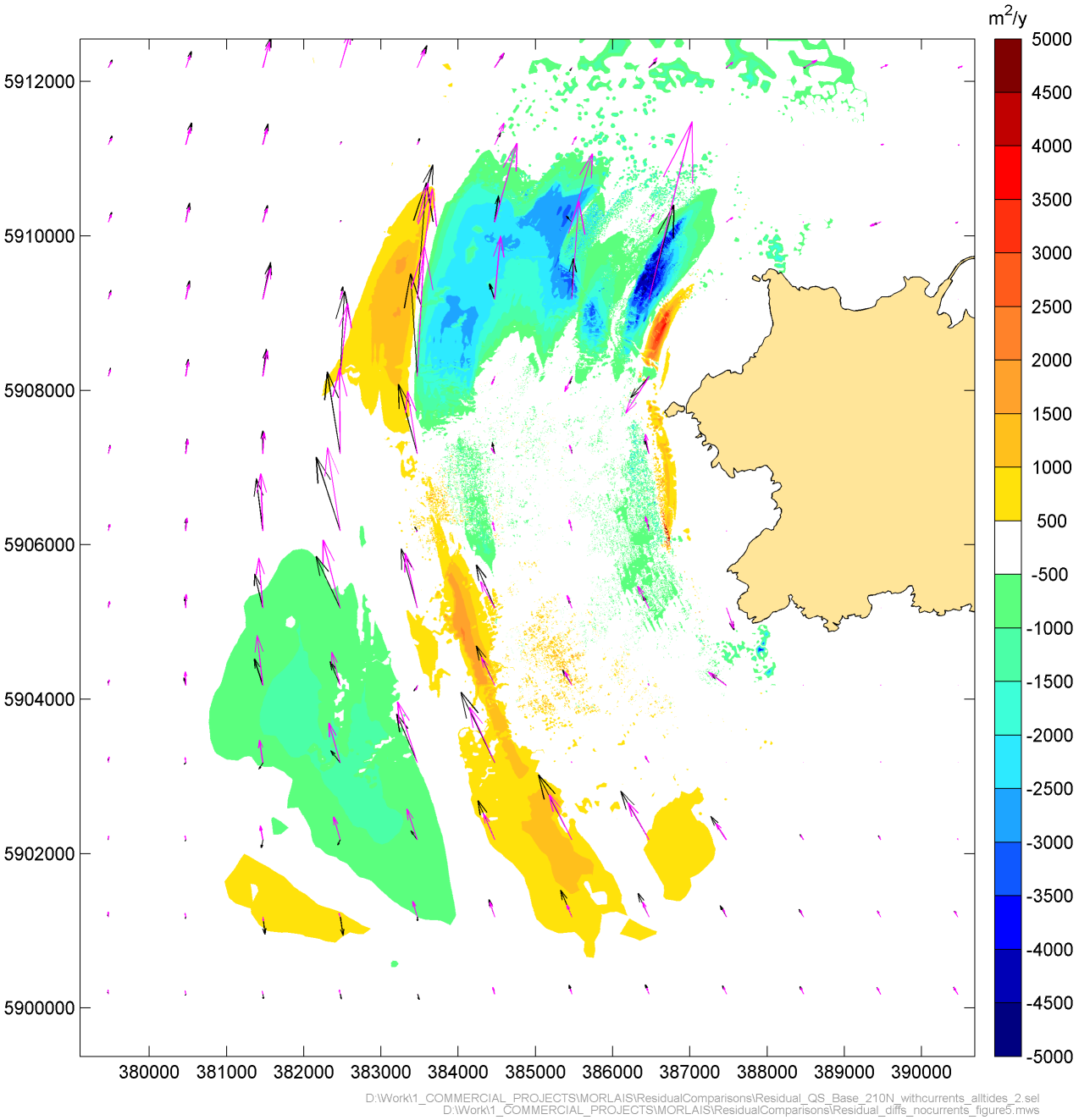

Figure 6.25: Changes in the residual sediment transport during a storm from the south-southwest

Source: HR Wallingford

6.4. Sediment transport model discussion and conclusions

The MDZ is located in an area where large parts of the coastline and seabed comprise exposed bedrock. The sediment modelling suggests that there is a northward potential residual transport to the west of Holy

Island. Mobile areas of seabed include the “South Stack Banner Bank” and areas of sand waves to the north of this location.

The MDZ is predicted to have little impact on this residual sediment transport. There is some reduction of the residual transport over the sand waves, which will move slightly slower as a result. Present day rates of movement of the sand waves are about 30m per year (m/y), so a predicted 10 to 20% reduction in transport rate suggests a reduction of about 5m/y. This difference will not be discernible from the natural variation due to climatological variations. In addition this decrease may lead to a slightly different orientation of the South Stack banner bank. The offshore end may move slightly northward, but again, this is likely to be within the natural variation of this morphological feature, which is observed to move between consecutive surveys. In addition there may also be a small increase in the sediment volume of the bank, originating from sand deposits in front of Gogarth bay.

The changes in the wave height due to the MDZ lead to small changes in the littoral drift, the longshore residual sediment transport in Abraham’s Bosom and Gogarth Bay. In Gogarth bay, the residual drift northwards is predicted to increase under predominant conditions, which implies that the rocky nature of the bay will be maintained with the devices in place.

In Abraham’s Bosom, the wave driven sediment transport reduces, leading to a potentially more stable small pocket beach in this bay. There may be changes in the beach orientation, but these will be small compared to the natural changes due to climatological variations.

Individual wave events can cause variations in the impact both nearshore and offshore. No changes in the sediment transport nearshore were predicted by the model beyond the direct neighbourhood of the MDZ.

6.4.1. Further SEACAMS data on seabed composition

During the latter stages of study, additional sediment samples from the SEACAMS database, collected in 2013/14 were made available. The locations of these data points are shown in Figure 6.26 below.

Where these data overlap with the more recently collected (2018) sediment data, the more recent data has been used for the modelling assessment. Towards the west and south of the MDZ these data provide additional new information on the 2013/14 seabed sediment composition in these areas.

This new information would indicate that potentially more sediment transport would occur through these areas south and west than predicted by the model.

Overall, however, the conclusions of this assessment as stated above and below are unchanged.

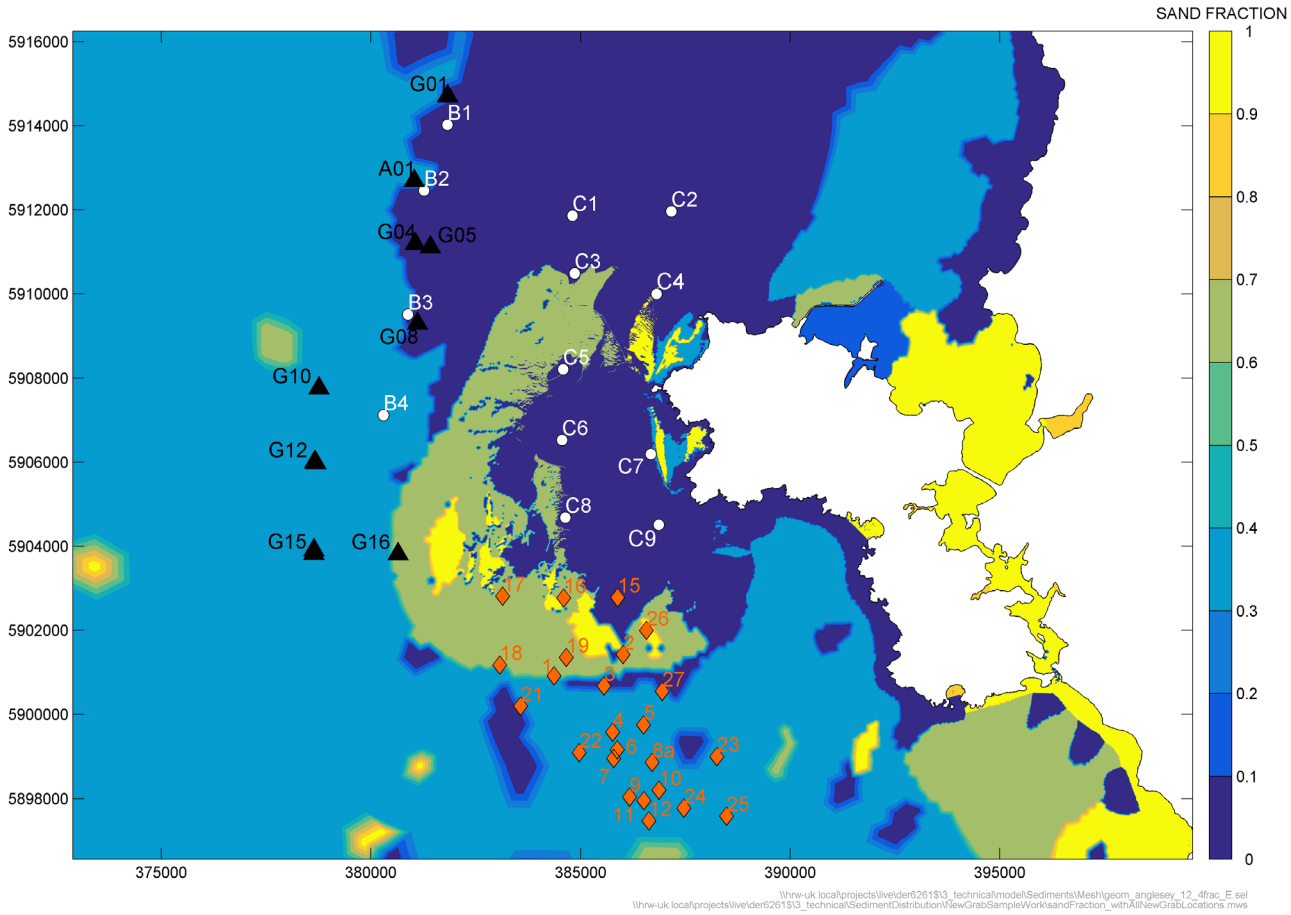

Figure 6.26: Locations of the additional sediment samples, super imposed on a map showing the fraction of sand in the bed

Note: White markers and labels show the '2014 Holyhead Deep' grab sample data; black markers and labels show the 'March 2013 HDD' grab sample data; red markers and labels show the '2014 DZ' grab sample data

7. Conclusions

The present study assessed the impact of the MDZ on coastal processes, including tidal currents, waves, and sediments.

HR Wallingford's existing high resolution 2D (depth averaged) finite element model has been extensively validated in accordance with IEC TS 62600-201:2015. In particular the flow model is validated against 6 tide gauges (Gladstone Dock, Port St Mary, Workington, Barmouth, Holyhead and Trearddur Bay) and 4 ADCP datasets: location 1, location 2, location NE and location NW. All Mean Absolute Errors are between 4.5% and 6% of the peak currents measured, meeting the approximately 5% ("c. 5%") recommended by the IEC TS 62600-201 guidelines.

The validated flow model was used to assess the direct impact of the worst case scenario (620 devices and the corresponding structures) on flow speeds. The difference in maximum speeds varies between a decrease of 0.7 m/s within the MDZ sub-zones and an increase of 0.3 m/s between the MDZ and the shore. The difference in average speeds is mostly a decrease up to 0.2 m/s within the MDZ sub-zones.

In order to assess the direct impact of the MDZ on the waves, a highly resolved SWAN wave model has been established. The wave model has been extensively validated for extreme wave conditions which have been measured by the SEACAMS wave buoy. In total, four storms were chosen to validate the wave model and predictions of Hs from the model have a Relative Bias (RB) of 0.9% to 1.5% and a Scatter Index (SI) of 13.7% to 14.3%. The wave model statistics meet the recommended RB up to 10% and a SI up to 20%, given by the Environment Agency guidelines.

The validated wave model was used to assess the direct impact of the worst case scenario (60 floating devices, 310 seabed-mounted devices and the corresponding structures) on wave heights. The differences in maximum Hs are mainly located within the MDZ and vary between a decrease of 0.4 m and an increase of 0.2 m.

The predicted changes to waves and flows are then used in a sediment transport model to assess the impact of the proposed development on sediment transport and in particular on key features such as the Gogarth Bay and Abraham's Bosom sediment deposit zones; the South Stack Banner Bank and the pocket beaches on Holy Island. First, literature and data review were undertaken to assess the existing conditions.

The MDZ is located in an area where large parts of the coastline and seabed comprise exposed bedrock. The sediment modelling suggests that there is a northward potential residual transport to the west of Holy Island. Mobile areas of seabed include the "South Stack Banner Bank" and areas of sand waves to the north of this location.

The MDZ is predicted to have little impact on this residual sediment transport. There is some reduction of the residual transport over the sand waves, which will move slightly slower as a result. Present day rates of movement of the sand waves are about 30m per year (m/y), so a predicted 10 to 20% reduction in transport rate suggests a reduction of about 5m/y. This difference will not be discernible from the natural variation due to climatological variations. In addition this decrease may lead to a slightly different orientation of the South Stack banner bank. The offshore end may move slightly northward, but again, this is likely to be within the natural variation of this morphological feature, which is observed to move between consecutive surveys. In addition there may also be a small increase to the sediment volume of the bank, originating from sand deposits in front of Gogarth Bay.

The changes in the wave height due to the MDZ lead to small changes in the littoral drift, the longshore residual sediment transport in Abraham's Bosom and Gogarth Bay. In Gogarth bay, the residual drift northwards is predicted to increase under predominant conditions, which implies that the rocky nature of the bay will be maintained with the devices in place.

In Abraham's Bosom, the wave driven sediment transport reduces, leading to a potentially more stable small pocket beach in this bay. There may be changes in the beach orientation, but these will be small compared to the natural changes due to climatological variations.

Individual wave events can cause variations in the impact both nearshore and offshore. No changes in the sediment transport nearshore were predicted by the model beyond the direct neighbourhood of the MDZ.

8. References

1. Booij, N., Ris, R, C., and Holthuijsen, L, H., (1999) A third-generation wave model for coastal regions, Part I: Model description and validation, *J.Geoph.Research,* 104, C4, 7649-7666.
2. Chesher T. J. and Miles G.V., 1992. The concept of a single representative wave. In: R.A. Falconer, S.N.
3. BSI Standards Publication (2015). Marine energy – Wave, tidal and other water current converters, IEC TS 62600-201.
4. Ellis K.M, Binding C.E, Bowers D.G, Jones S.E. and Simpson J.H. (2008) A model of turbidity maximum maintenance in the Irish Sea. Estuarine, Coastal and Shelf Science, 76, pp765-774.
5. Environment Agency(2016) Investigating coastal flood forecasting, Good practice framework. Report SC140007.
6. Folk, R.L., (1954). The distinction between grain size and mineral composition in sedimentary-rock nomenclature. The Journal of Geology, 62(4), pp.344-359.
7. Hersbach, H., “The ERA5 Atmospheric Reanalysis.” In AGU Fall Meeting Abstracts February, 2016.
8. Hersbach, H., Dee,D. “ERA5 reanalysis is in production.” ECMWF Newsletter No. 147 – Spring 2016.
9. Holthuijsen, L.H., Booij, N., Ris, R, C., Andorka Gal, J,H., and de Jong, J, C, M., (1997) A verification of the third-generation wave model "SWAN" along the southern North Sea coast, Proceedings 3rd International Symposium on Ocean Wave Measurement and Analysis, WAVES'97, ASCE, 49-63.
10. HR Wallingford (2019). Tidal Resource Modelling, Morlais Demonstration Zone, DEM8387-RT001 R01-00. Report produced for Menter Môn Morlais Limited.
11. Koutandos E.V, Karambas Th.V., Koutitas C.G.(2004) Floating breakwater response to waves action using a Boussinesq model coupled with a 2DV elliptic solver. J. Waterway, Port, Coastal and Ocean Eng. Vol 130 No 5 ASCE Sept 2004.
12. Kriebel D.L., Bollmann (1996) C.A. Wave transmission past vertical wave barriers. Chapter 191, Coastal Engineering 1996.
13. Ocean Ecology Limited (2018). Morlais Demonstration Zone (MDZ) Benthic Ecology Characterisation Survey 2018 – Technical Report. Report No. OEL_MMNMOR0518_TCR, 21 pp.
14. OSU (2008), OSU Tidal Data Inversion Software and Atlas, Oregon State University, Arabian Gulf (http://volkov.oce.orst.edu/tides/PerS.html).
15. Partrac (2018). Morlais Demo Zone (MDZ) Hydrographic & Geophysical Survey P1830.
16. PIANC (1994) Floating breakwaters, a practical guide for design and construction. Report of PIANC Working Group no 13.
17. Ris, R, C., Booij, N., and Holthuijsen, L, H., (1999) A third-generation wave model for coastal regions, Part II: Verification, *J.Geoph.Research,* 104, C4, 7667-7681.
18. UKHO (2020). Admiralty Marine Data Portal: Charted Bottom Qualities. Accessed from: https://data.admiralty.co.uk/server/rest/services/Hosted/Seabed/FeatureServer [05 February 2020].
19. Villaret, Catherine & Hervouet, Jean-Michel & Kopmann, Rebekka & Merkel, Uwe & Davies, Alan. (2013). Morphodynamic modeling using the Telemac finite-element system. Computers & Geosciences - COMPUT GEOSCI. 53. 10.1016/j.cageo.2011.10.004.
20. Wilson, R.J., Speirs, D.C., Sabatino, A. and Heath, M.R., (2018). A synthetic map of the northwest European Shelf sedimentary environment for applications in marine science. Earth System Science Data, 10, pp.109-130.

Appendices

A. SISYPHE Sediment Transport Model Description

SISYPHE Sediment Transport Model Description

SISYPHE is the state-of-the-art sediment transport model used at HR Wallingford. It combines the best of the SISYPHE sediment transport model, publicly available as part of the open source TELEMAC model suite (originally developed by the National Hydraulics Laboratory of the French Electricity Board – EDF-LNH), with additional formulations to incorporate HR Wallingford's extensive knowledge and experience of simulating sediment transport and bed evolution previously included in HR Wallingford's sediment transport model SANDFLOW-2D.

SISYPHE can be applied as a stand-alone post-processor model, using input from flow (e.g. TELEMAC) and wave (e.g. TOMAWAC or SWAN) models. Alternatively, SISYPHE can be run coupled to a TELEMAC flow model, whilst exchanging information on a time step level.

1.1. THEORETICAL BACKGROUND

SISYPHE can model sedimentary systems containing very fine and fine sands (with median grain diameters d_{50} between 0.06 and 0.25 mm) which mainly move in suspension. The model can also be used to identify trends in the case of medium sand (d_{50} between 0.25 and 0.5 mm). If the sediment contains a high proportion of clay or silt particle sizes less than 0.06 mm, it would be more appropriate to use models capable of simulating mud transport, e.g. the DELWAQ mud transport model used at HR Wallingford.

The main factors controlling sand transport are:

- advection by currents;
- settlement under gravity;
- turbulent diffusion in all directions (but only the vertical component is of significance under most circumstances);
- exchange of sediment between the flow and the bed.

The study of sand transport generally is very complex but more so in the case of estuaries or coastal areas. This is because the water movements are continually changing, with the rise and fall of the tide, and there is usually a wide range of sediments on the bed and possibly areas without mobile sediment, leading to unsaturated and oversaturated loads in the water.

1.1.1. Sediment transport formulations

The evaluation of bed exchanges requires a formulation for the sediment transport rate. SISYPHE offers the choice between a total load transport formula and a combination of a concentration equation with a bedload transport formula.

Within SISYPHE, the preferred option is the SANDFLOW-2D approach for suspended load transport, which determines the concentration based on the suspended load formula of Soulsby-van Rijn combined with the bedload predictor of Soulsby-Van Rijn. Other available bedload transport predictors are the Meyer Peter-Muller and the Einstein Brown formula. Three alternative equations are available to prescribe the reference concentration: Zyserman and Fredsoe, Bijker, and Van Rijn. Alternatively, one can use one of the total load formulae: Soulsby-Van Rijn, Bijker, Bailard and Dibanjnia and Watanabe, Engelund-Hansen.

The choice of sand transport relation requires a careful consideration of the site conditions and the limitations of the transport formulae. It should be borne in mind that most

relationships found in the literature are based on river or channel data where sediments are more narrowly graded than in estuaries. Usually, there is cohesive material present in estuary sediments and this may alter the transport properties. SISYPHE has the capability to model such mixed sediment systems, however it is noted that the behaviour of mixed sediments is not well understood.

1.1.2. Vertical Sediment Concentration Profile

Although sand transport in estuaries is really an unsteady, three-dimensional (3D) problem, it has been shown by HR Wallingford that it can be dealt with using a two-dimensional, depth-averaged (2Dh) model, provided special provision is made to account for the vertical profile effects of the sediment concentration. Under these circumstances the depth-averaged, suspended solids concentration c(x, y, t) satisfies the conservation of mass equation:

$$\frac{\partial \overline{C}}{\partial t} + u_{conv}\frac{\partial \overline{C}}{\partial x} + v_{conv}\frac{\partial \overline{C}}{\partial y} = \frac{1}{h}\left[\frac{\partial}{\partial x}\left(h\varepsilon\frac{\partial \overline{C}}{\partial x}\right) + \frac{\partial}{\partial y}\left(h\varepsilon\frac{\partial \overline{C}}{\partial y}\right)\right] + S \qquad (1)$$

where:

(u_{conv}, v_{conv})	depth-averaged convective components of the flow velocity (m/s)
ε	longitudinal (shear flow) dispersion coefficient (m^2/s)
(x,y)	Cartesian co-ordinates in horizontal plane (m)
t	time (s)
h	water depth (m)
S	entrainment from or deposition onto the bed ($kg/m^2/s$)

1.1.3. Bed exchange relations

The simplest formulation of the bed exchange relation is:

$$S = ß_s\, \omega_s\, (c_s - c) \qquad (2)$$

where:

c_s	depth-averaged concentration when the flow is saturated with sediment (kg/m^3)
c	instantaneous depth-averaged concentration (kg/m^3)
ω_s	representative settling velocity (m/s)
$ß_s$	profile factor to compensate for integrating out the vertical profile of suspended sediment ie to correct for higher sediment concentrations near the bed

Deposition or erosion takes place depending on whether the instantaneous sediment load (c) exceeds or is less than the saturated value (c_s). Pick up of sediment from the bed is prevented if there is no sediment available on the bed. A shortage of material on the bed is reflected in a low concentration of suspended solids being advected away by the flow.

Typical values of $ß_s$ could be obtained from actual observations of sediment profiles or from theoretical considerations. However, HR Wallingford has derived an analytical expression for this so that bed exchanges are performed automatically.

1.2. MODEL VALIDATION

Calibration of sediment models is complex because *in situ* sediment transport rate measurements are subject to large uncertainties and bed changes are usually too slow or too variable to measure anything significant for comparison. Sometimes historical charts or dredging records may be available but even then it is unlikely that the sources of suspended sediment can be quantified for the relevant period. Sometimes it is possible to get scaling factors for model results in cases where information is available and use these to estimate siltation in the new situation, but in many cases one is forced to use the best available values for the parameters and to demonstrate that the siltation and erosion patterns produced by the model agree with the observed state of the estuary or coastal region being studied.

Some evidence to support the physical realism of the model is given by the following results of simulation of sand transport in a flume and of observations from the Thames Estuary.

1.2.1. Foulness Experiment – Thames Estuary

The computer model results were compared with the results of a laboratory experiment performed in a flume with a length of 30 m, a width of 0.5 m and a depth of 0.7 m. The discharge was measured by a circular weir. The mean flow depth was 0.25 m and the mean flow velocity was 0.67 m/s. The bed material had a d_{50} = 230 μm and a d_{90} = 320 μm. The median diameter of the particles in suspension was estimated to be about 200 μm, resulting in a representative fall velocity of 0.022 m/s (water temperatures 9°C). The stream bed was covered with bed forms having a length of about 0.1 m and a height of about 0.015 m. Small Pitot tubes were used to determine the vertical distribution of flow velocity. Water samples were collected simultaneously by means of a siphon method at four locations to determine the spatial distribution of the sand concentrations. At each location (profile) five samples were collected at a height of about 0.015, 0.025, 0.05 and 0.22 m above the average bed level and these were integrated to give the suspended load transport.

The basic physics of SISYPHE have been tested using real field data from Foulness in the Thames Estuary. The measured sediment sizes showed a wide distribution. To reflect this spread, SISYPHE was run in mixed sediment mode using four fractions with median grain sizes of 75 μm, 100 μm and 150 μm and 200 μm, as well as in single fraction mode for each of the four fractions. The saturation concentrations in the model were calculated using the SANDFLOW-2D model based on the Soulsby-Van Rijn formula for suspended sediment transport.

The SANDFLOW-2D model, the predecessor of SISYPHE, was run for the same conditions assuming the overall shear velocity was 0.0477 m/s and the results in Figure 1 shows that the model can be calibrated using the available data.

The suspended sediment fluxes resulting from the four fractions simulation and from the 75 μm simulation are shown in Figures 2 and 3, plotted at half hourly intervals showing the progression through the tide. The model has a similar hysteresis effect to the observations on both stages of the tide. The systematic underestimation of the sediment flux during the ebb in the mixed sediment case (Figure 2) is caused by the higher availability of fines from further up the estuary, which has not been included in the simplified model. This is confirmed when modelling the fine sediments only (Figure 3), where the ebb sediment flux is reproduced, but the flood sediments highly over-predicted.

Therefore, this Foulness test demonstrates the general validity and accuracy of SISYPHE in a natural situation.

1.2.2. Flume Morphodynamics

The morphodynamic predictive capabilities of SISYPHE was evaluated using data from a flume experiment carried out at Delft Hydraulics (Van Rijn, 1986; Delft Hydraulics, 1985). The experiment was performed in a small flume with a length of 17 m, a width of 0.3 m and a depth of 0.5 m. Sediment was used with d_{50} = 0.1 mm and d_{90} = 0.13 mm. Sand was supplied at constant rate at upstream section of flume to maintain equilibrium conditions. The channel had side slopes of 1 to 12 and a depth of 0.125 m.

Regular waves with a period of 1.5 s and height of 0.08 m were generated and a steady current following the waves was imposed. The water depth was 0.255 m and the current velocity was 0.18 m/s. The mobile bed consisted of well sorted sediment with 0.1 mm median diameter (d_{90} = 0.13 mm) and density 2650 kg/m^3.

As SISYPHE is invalid for the experimental dimensions (Soulsby-Van Rijn requires at least a 1 m water depth), the model is scaled up to field dimensions, multiplying the domain lengths by 10 and the time by $\sqrt{10}$. Assuming the morphology is bedload dominated, the sediment grain size is left untouched. After the simulation, the time and spatial dimensions are rescaled back to the scales of the flume experiment.

Figure 4 shows that the SISYPHE accurately computes the shape and position of the trench after 10 hours.

1.3. MODEL APPLICATION

The application of the model and interpretation of the results requires a good understanding of sand physics. Firstly it is important to choose representative values for the main parameters. Ideally these should be based on laboratory tests of actual sediment samples from the site.

This may be done using measured suspended sediment concentrations and/or measured transport rates. However, these concentrations and transport rates usually cover short periods and are prone to measurement uncertainty and randomness in the forcing conditions. Ideally, observed bathymetric changes are used as well, as these give a better indication of the long-term processes.

In addition, it should be appreciated that sand transport is not an exact science. Accordingly, whatever model is used, and whatever parameter values are chosen it is essential that results required an expert assessment. Provided this is done SISYPHE provides a valuable engineering tool.

As with all models, it is preferable to calibrate and validate a model build with SISYPHE. Even though SISYPHE has been tested and validated against observations, each specific model application requires adaptation to the local conditions, by determining relevant sediment characteristics, choosing the best transport predictor and incorporating relevant hydrodynamics.

1.4. MODEL INPUTS

SISYPHE requires free surface elevation and flow velocities from a TELEMAC-2D flow model simulation (or depth-averaged values of from a TELEMAC-3D simulation), together with information describing the initial distribution of sand on the bed. If wave stirring is considered important, wave orbital velocities from an area wave model such as TOMAWAC or SWAN are required.

If available, a boundary data file specifying time-varying or constant sediment concentrations at the model open boundaries can be used, but often the preferred option is to use equilibrium conditions at the boundary whilst locating these boundaries sufficiently far away from the area of investigation. Other parameters required include the typical sediment grain size distribution, or a single median grain size. If available, other basic sediment properties, such as settling velocity and threshold shear stress for initiation of motion, can be used or alternatively these can be estimated using formulations included in the model.

Data is input to SISYPHE using ASCII data and steering files, and unformatted direct access results files from TELEMAC equivalent. The steering files are set up using the context sensitive editor included in the user interface. SISYPHE can be applied as a stand-alone post-processor model, using input from flow (e.g. TELEMAC) and wave (e.g. TOMAWAC or SWAN) models. Alternatively, SISYPHE can be run coupled to a TELEMAC flow model, whilst exchanging information on a time step level, including bed updating.

SISYPHE is controlled using HR Wallingford's user interface PYXIS, which includes an extensive model logging system with error checking, version control and run description. This interface enhances quality control of the model set-up and simulations and guarantees that simulations can be reproduces in the future.

1.5. MODEL OUTPUTS

SISYPHE produces a single binary output file containing relevant flow information, suspended concentrations for all grain size classes, the resulting bedload and suspended load transport rates, and the erosion-deposition patterns and instantaneous bed levels resulting from these transport rates at user selected intervals during the simulation.

The SISYPHE model results can be presented graphically and where required analysed further using various plotting and post-processing tools available at HR Wallingford

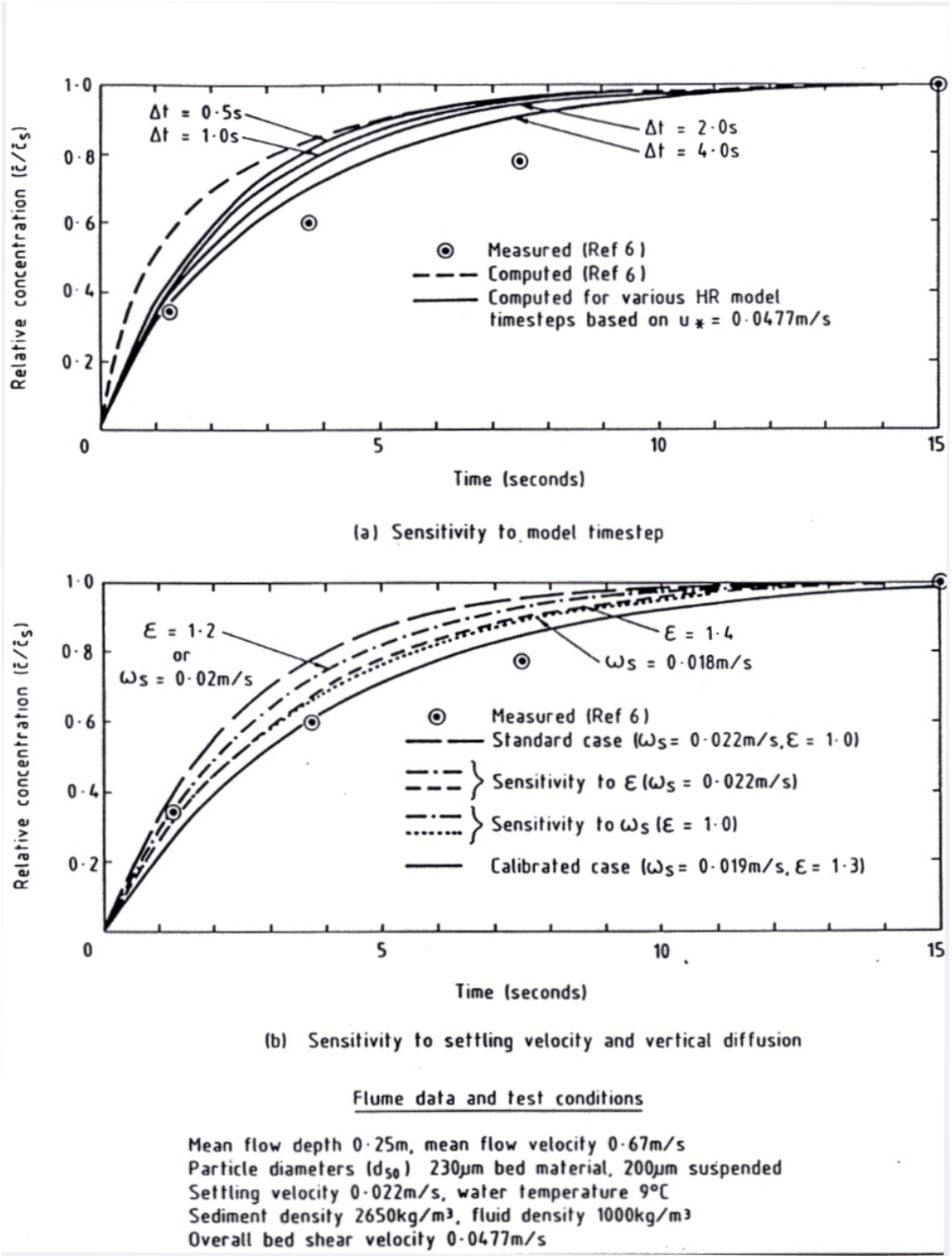

Figure 1 Computed and measured evolutions of sediment load

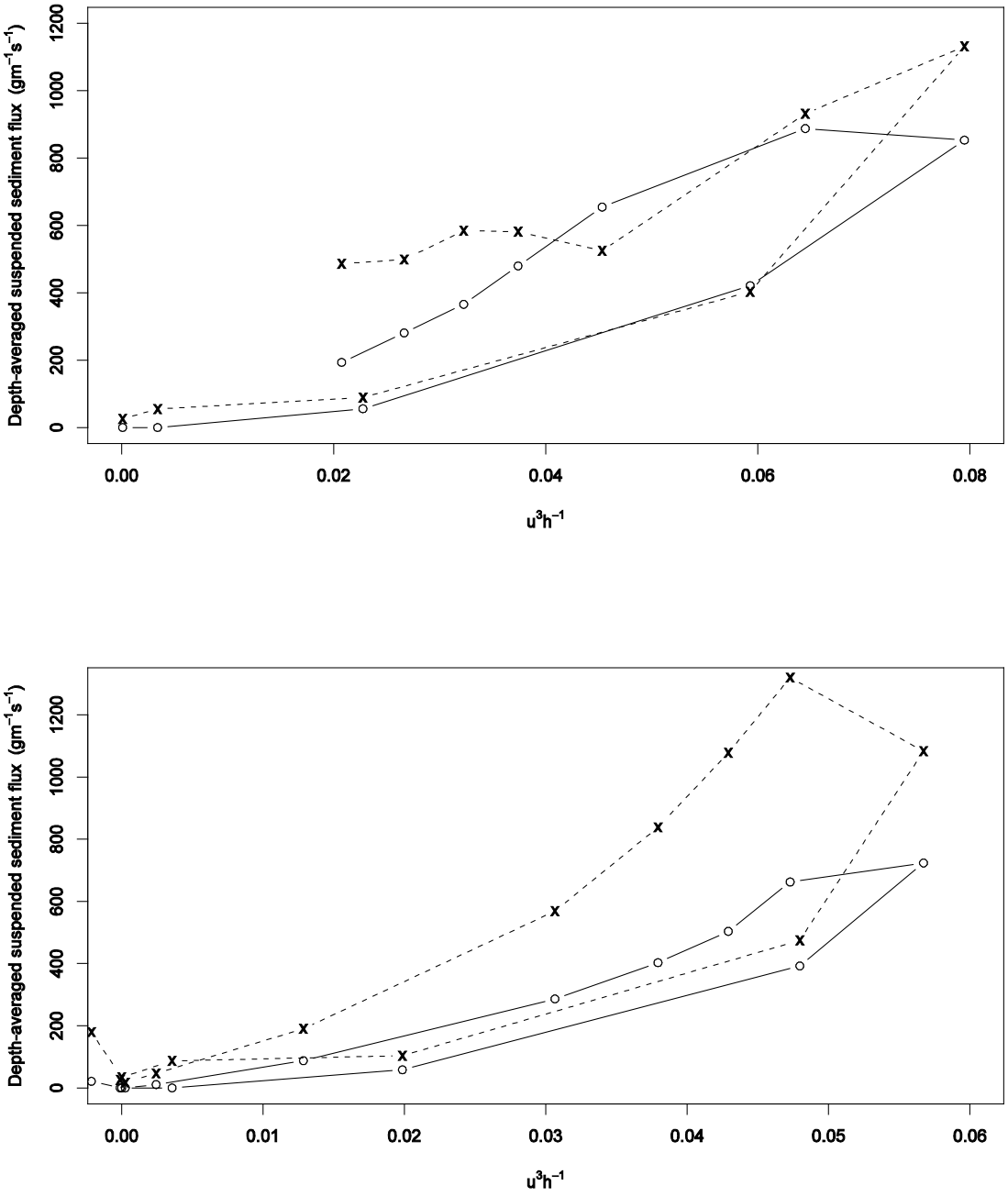

Figure 2 **Measured (dashed) and computed (solid) , with mixed sediments, depth-averaged sediment fluxes at half-hourly intervals for Foulness FM1 for flood (top) and ebb (bottom)**

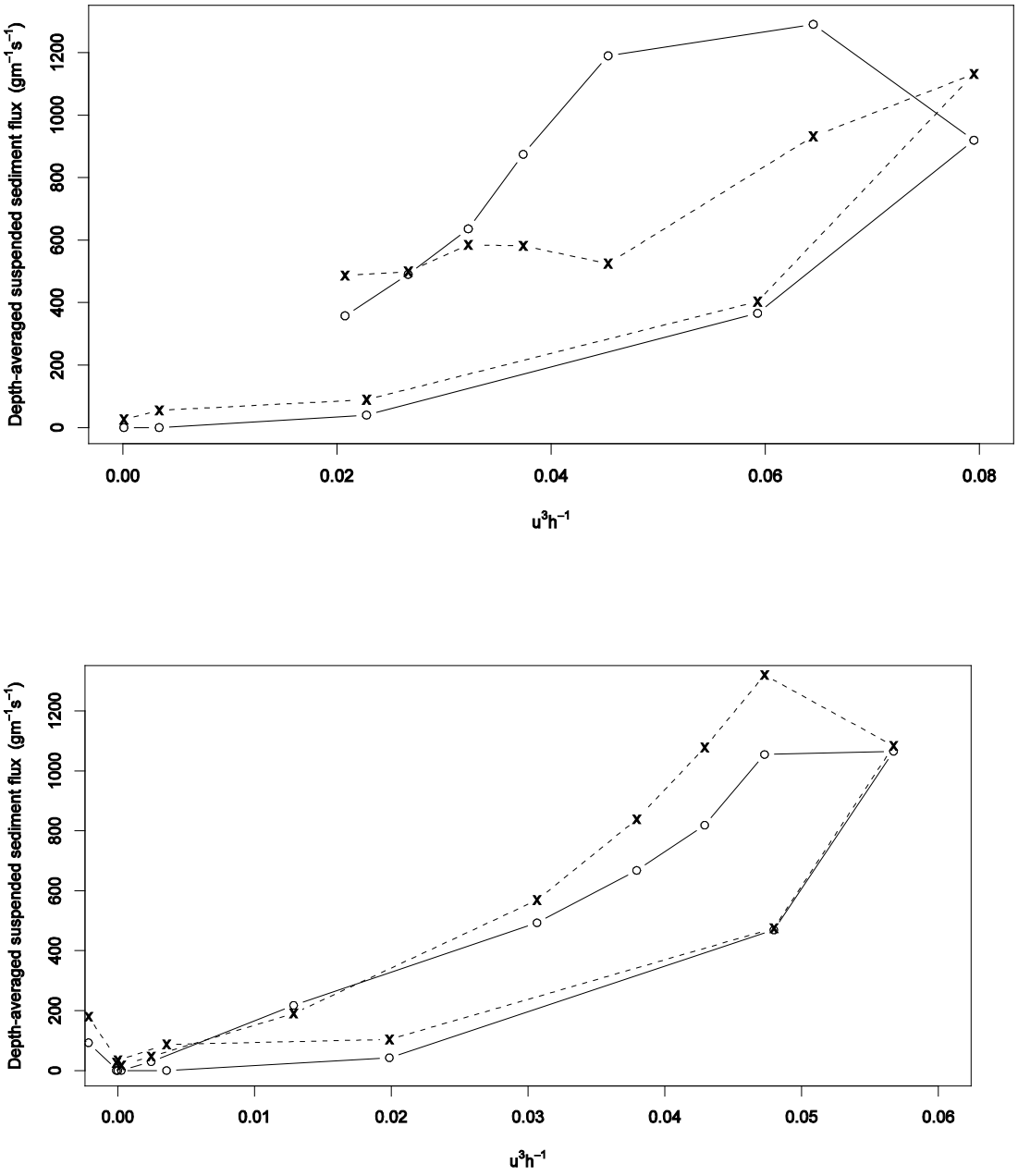

Figure 3 **Measured (dashed) and computed (solid), with D_{50}=75µm, depth-averaged sediment fluxes at half-hourly intervals for Foulness FM1 for flood (top) and ebb (bottom)**

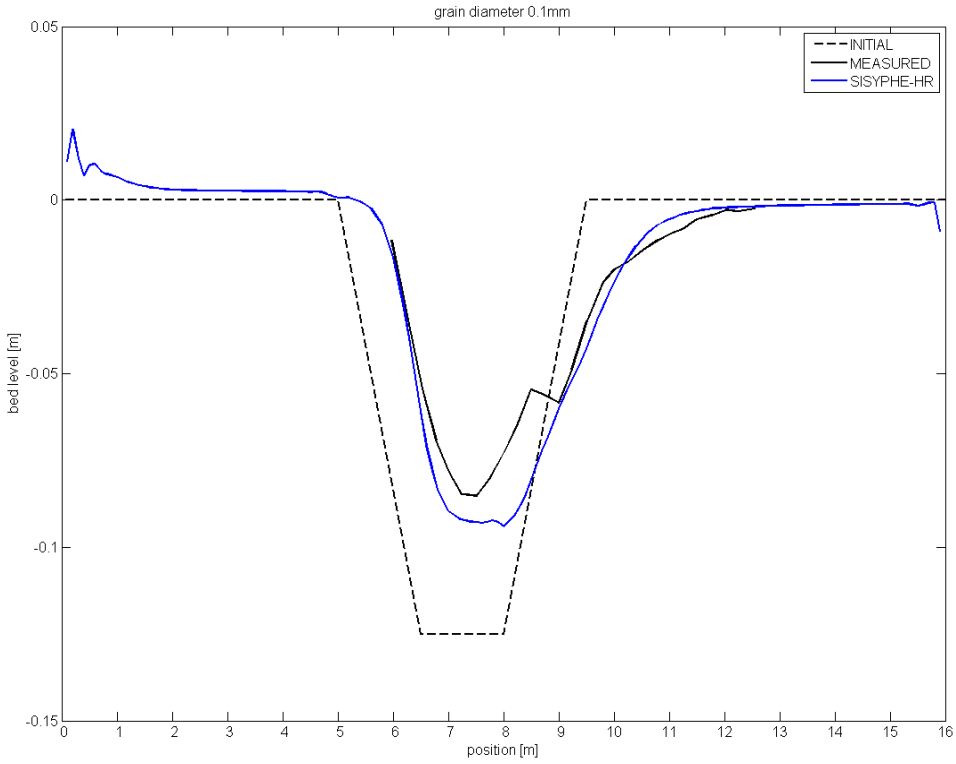

Figure 4 **Morphological development of a trench as measured (black) and modelled (blue) 10 hours after the initial situation (dashed)**

B. Wave model results

B.1. Waves only

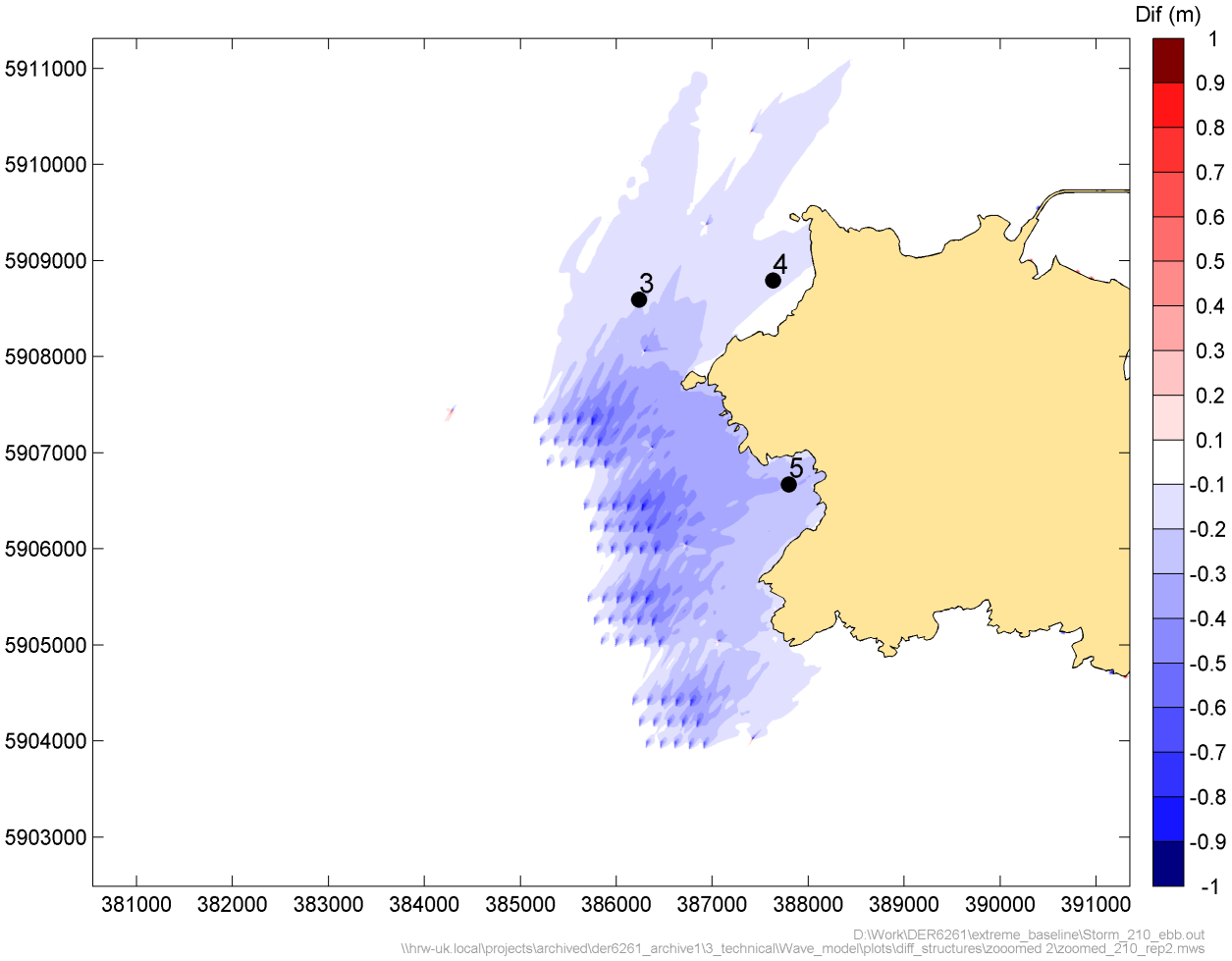

Figure B.1: Difference in wave height from 210°N for a representative condition

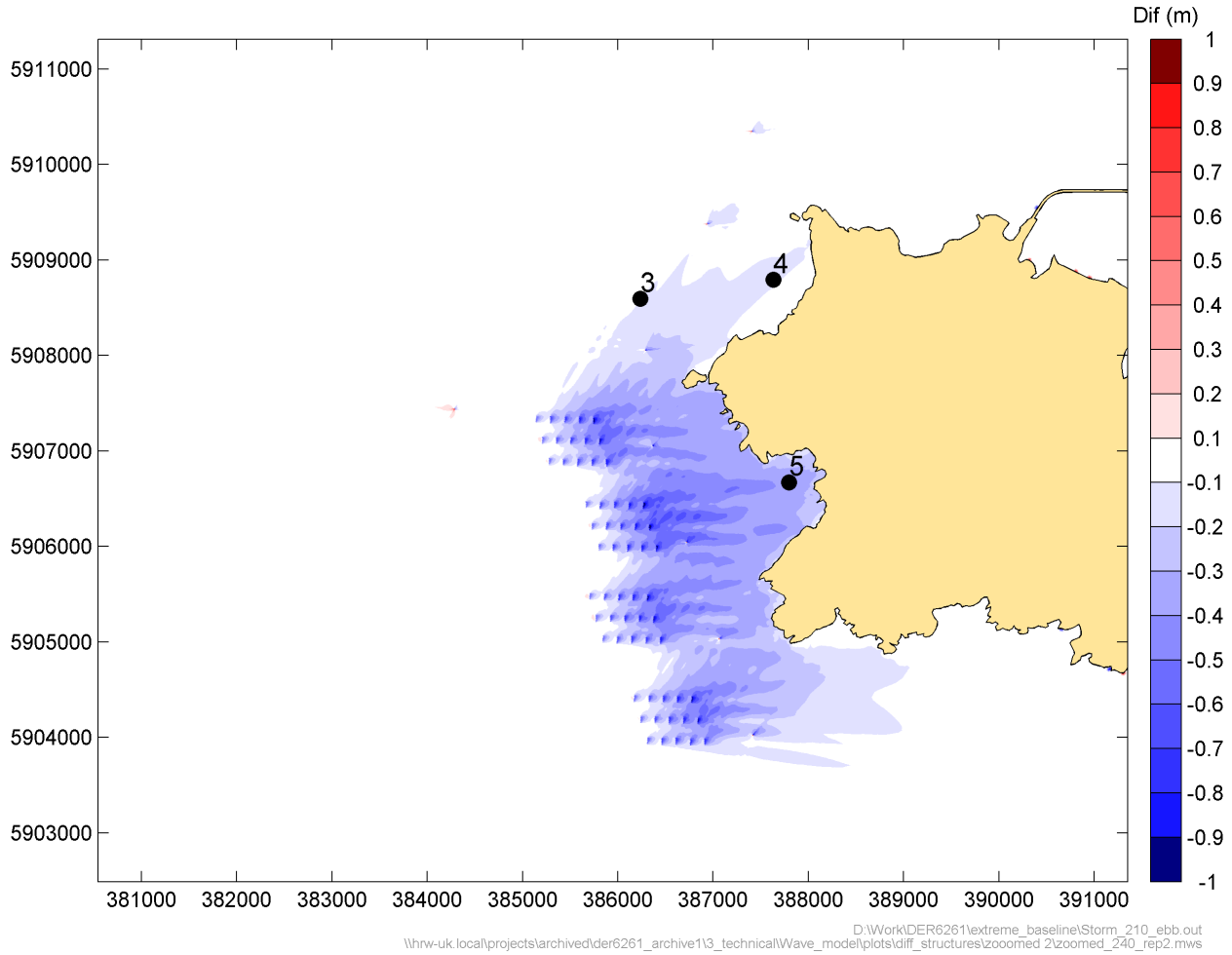

Figure B.2: Difference in wave height from 240°N for a representative condition

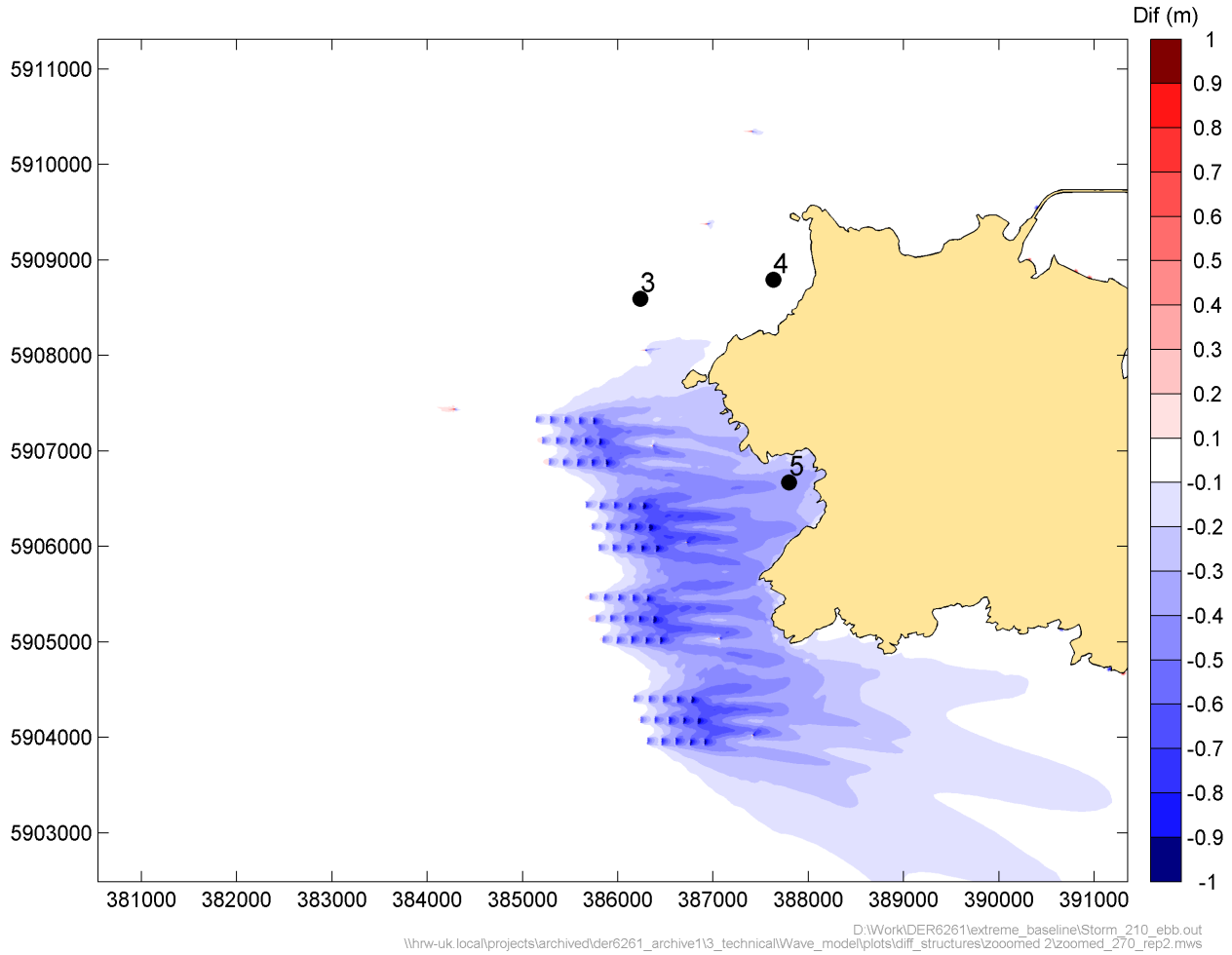

Figure B.3: Difference in wave height from 270°N for a representative condition

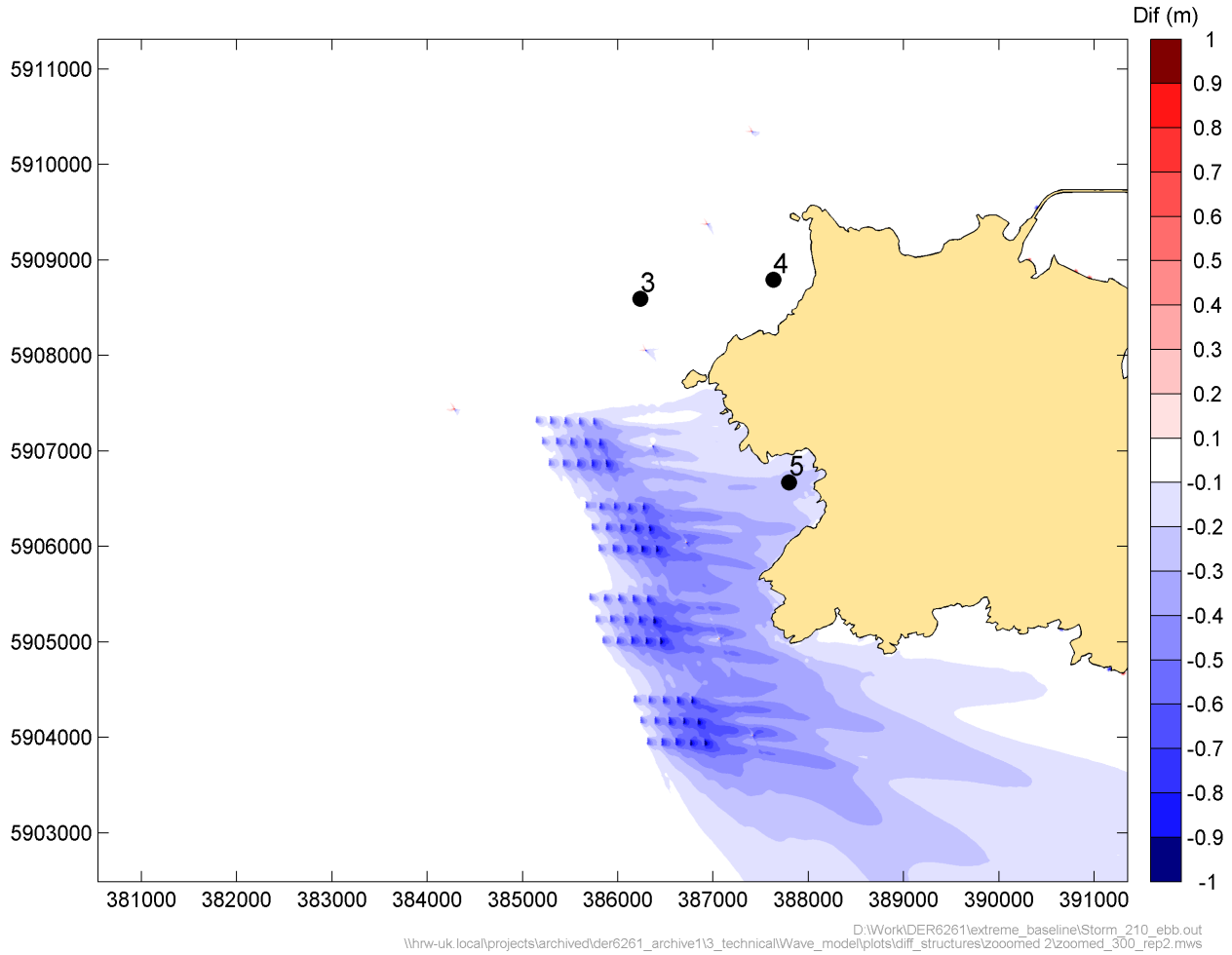

Figure B.4: Difference in wave height from 300°N for a representative condition

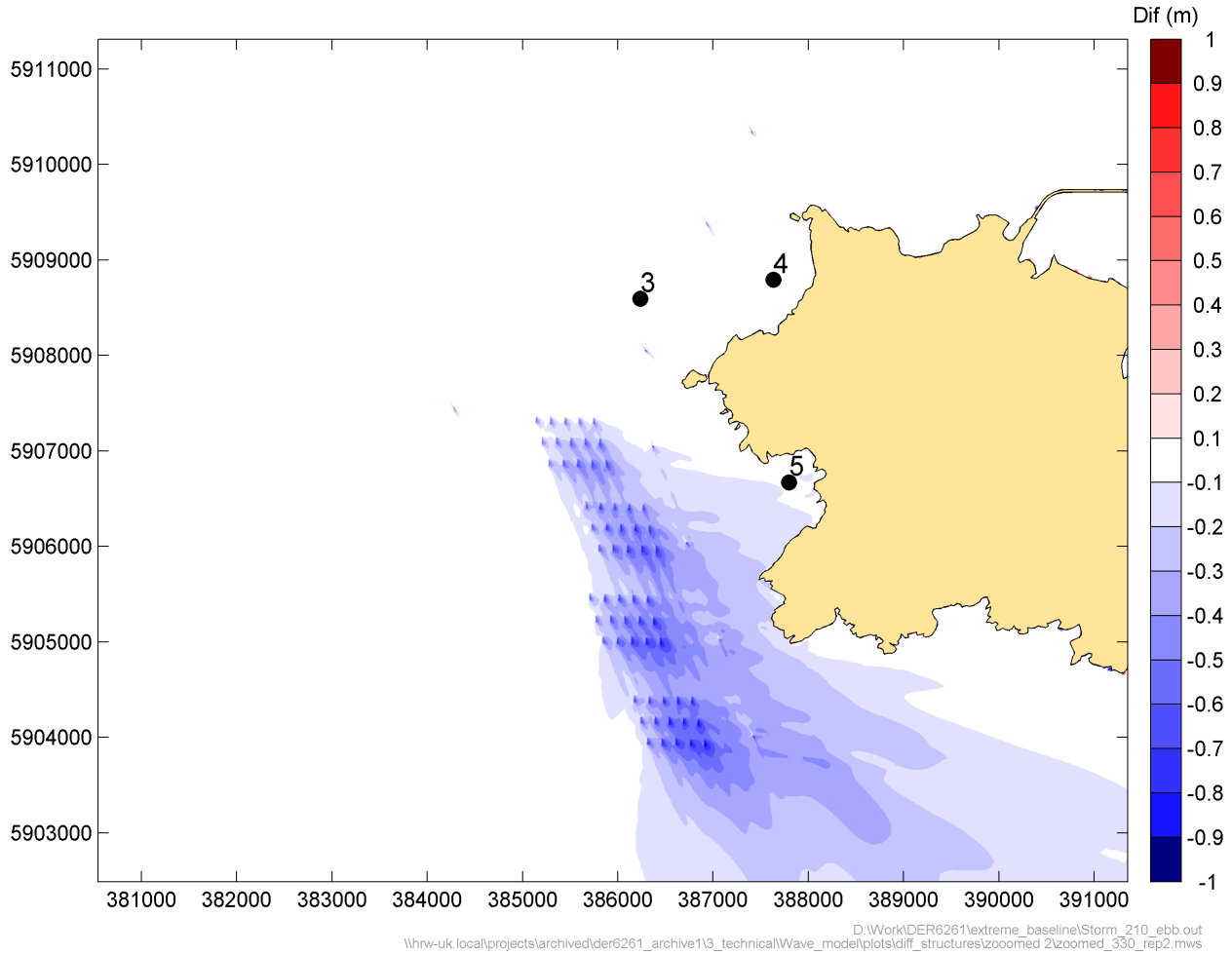

Figure B.5: Difference in wave height from 330°N for a representative condition

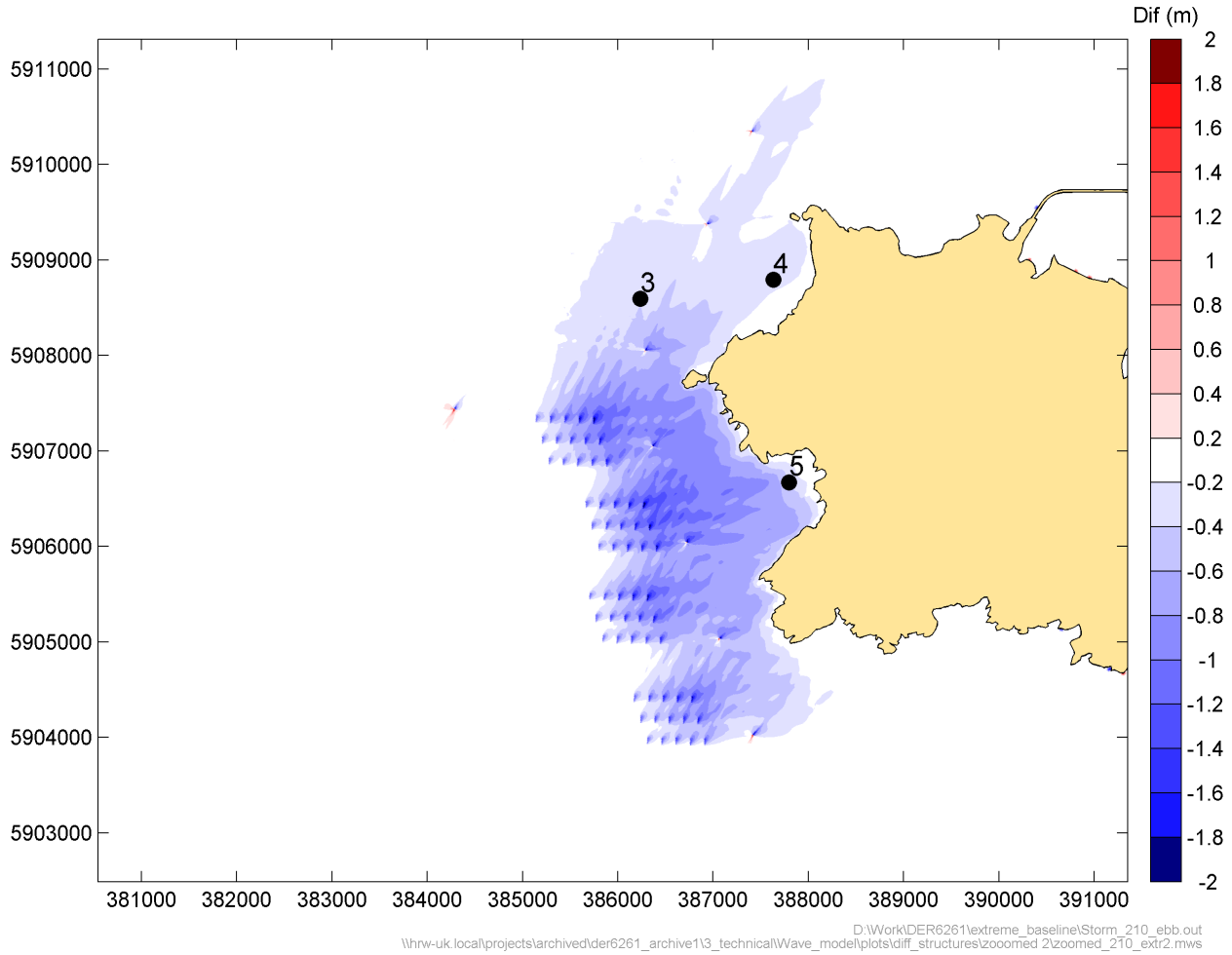

Figure B.6: Difference in wave height from 210°N for an extreme condition

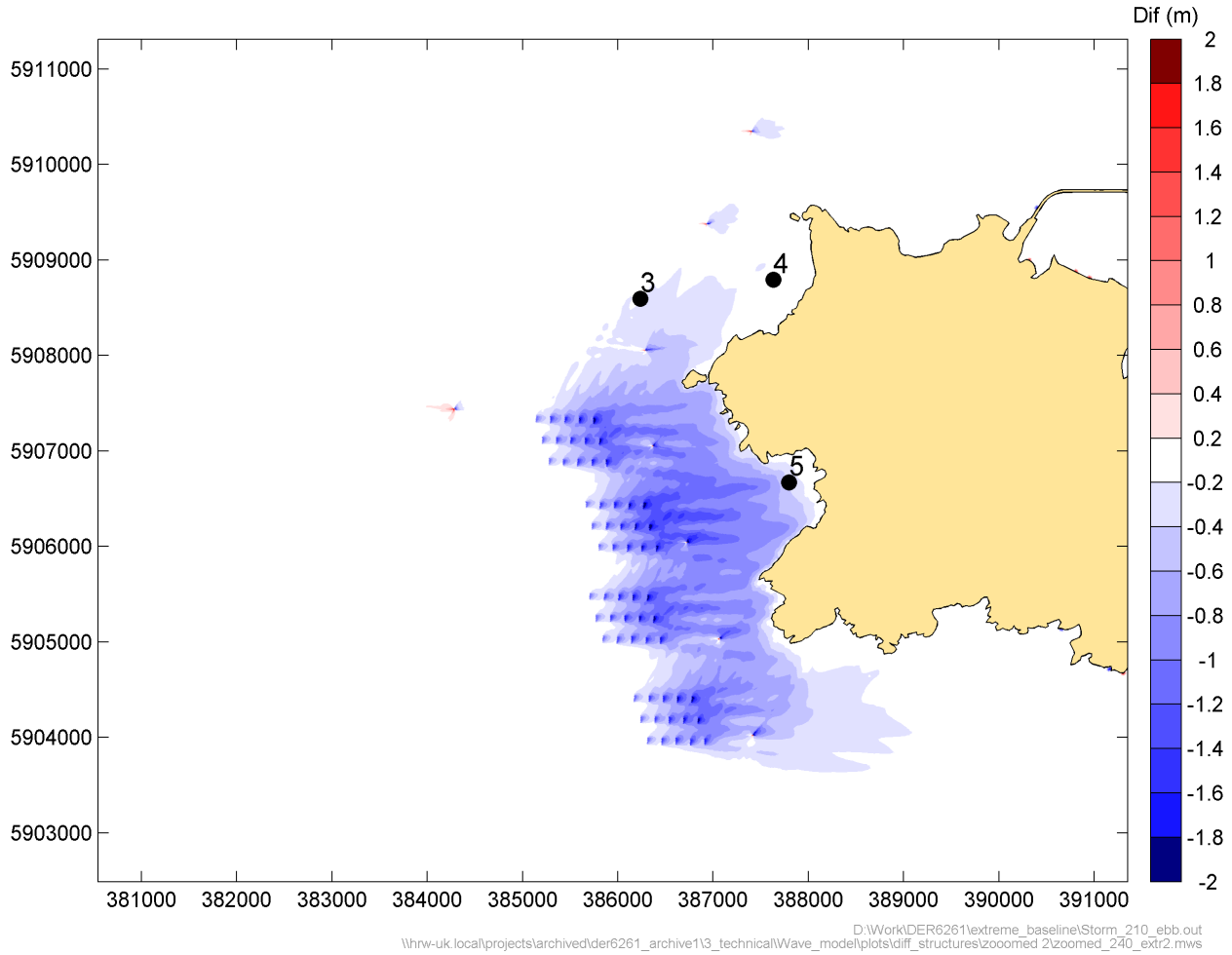

Figure B.7: Difference in wave height from 240°N for an extreme condition

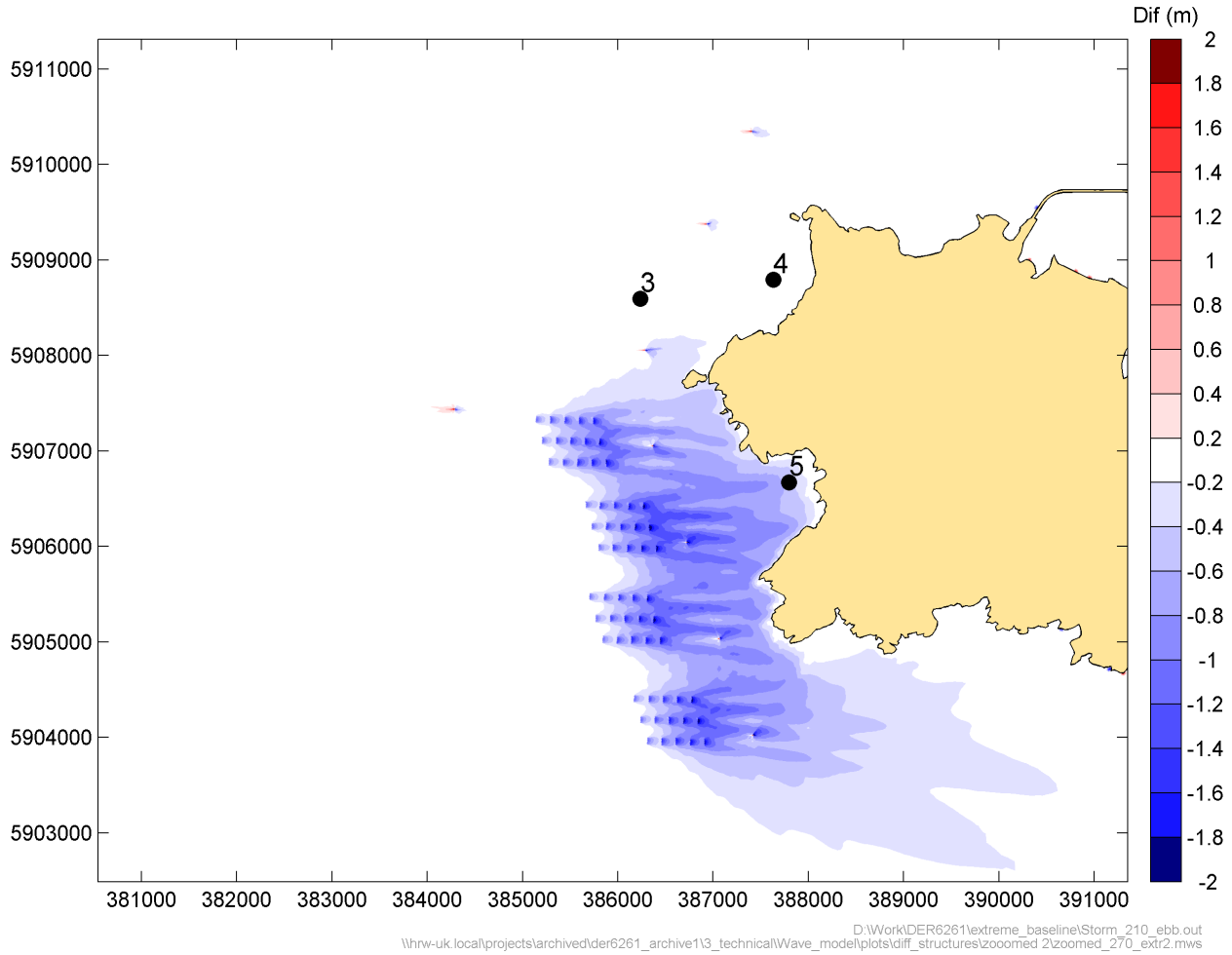

Figure B.8: Difference in wave height from 270°N for an extreme condition

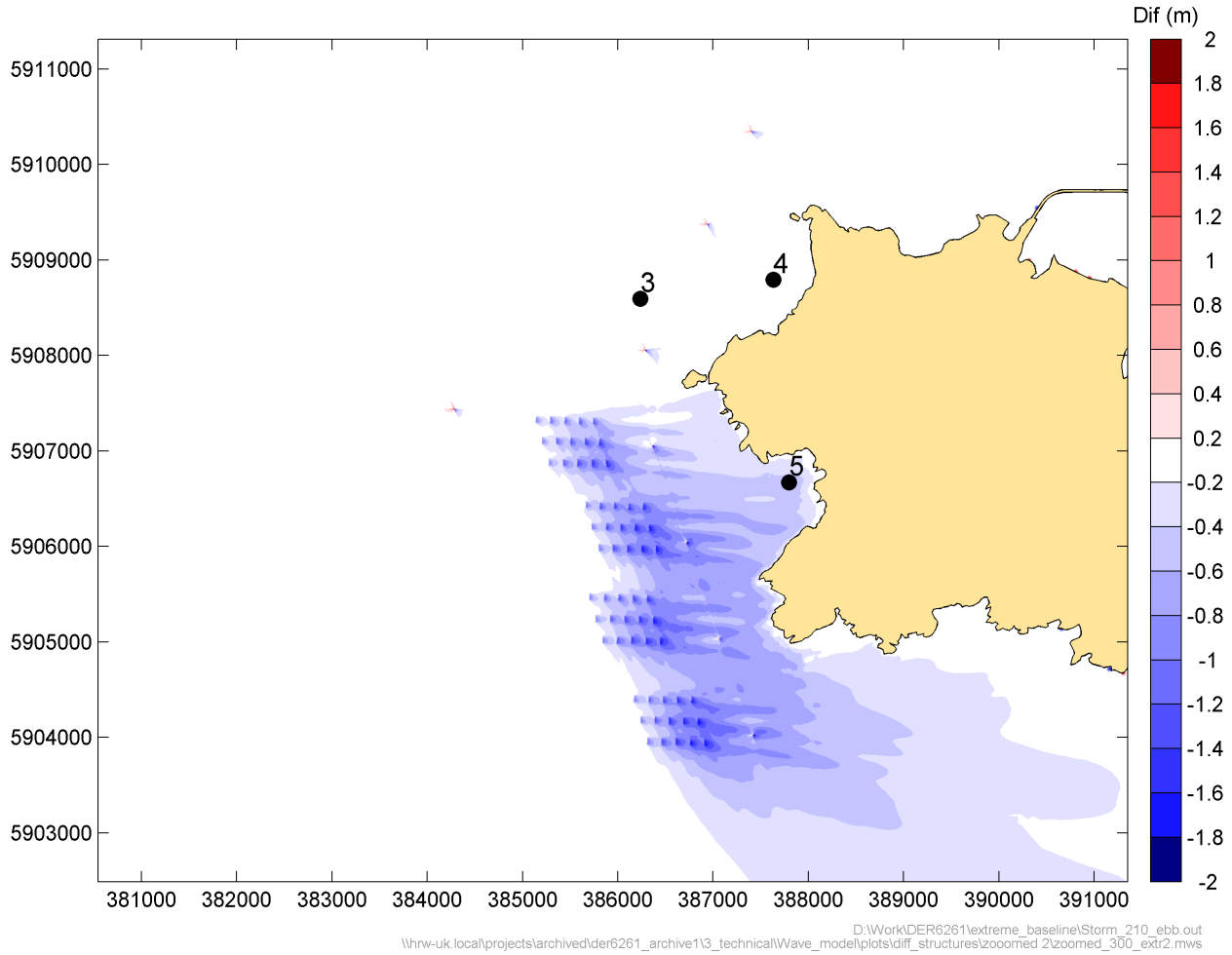

Figure B.9: Difference in wave height from 300°N for an extreme condition

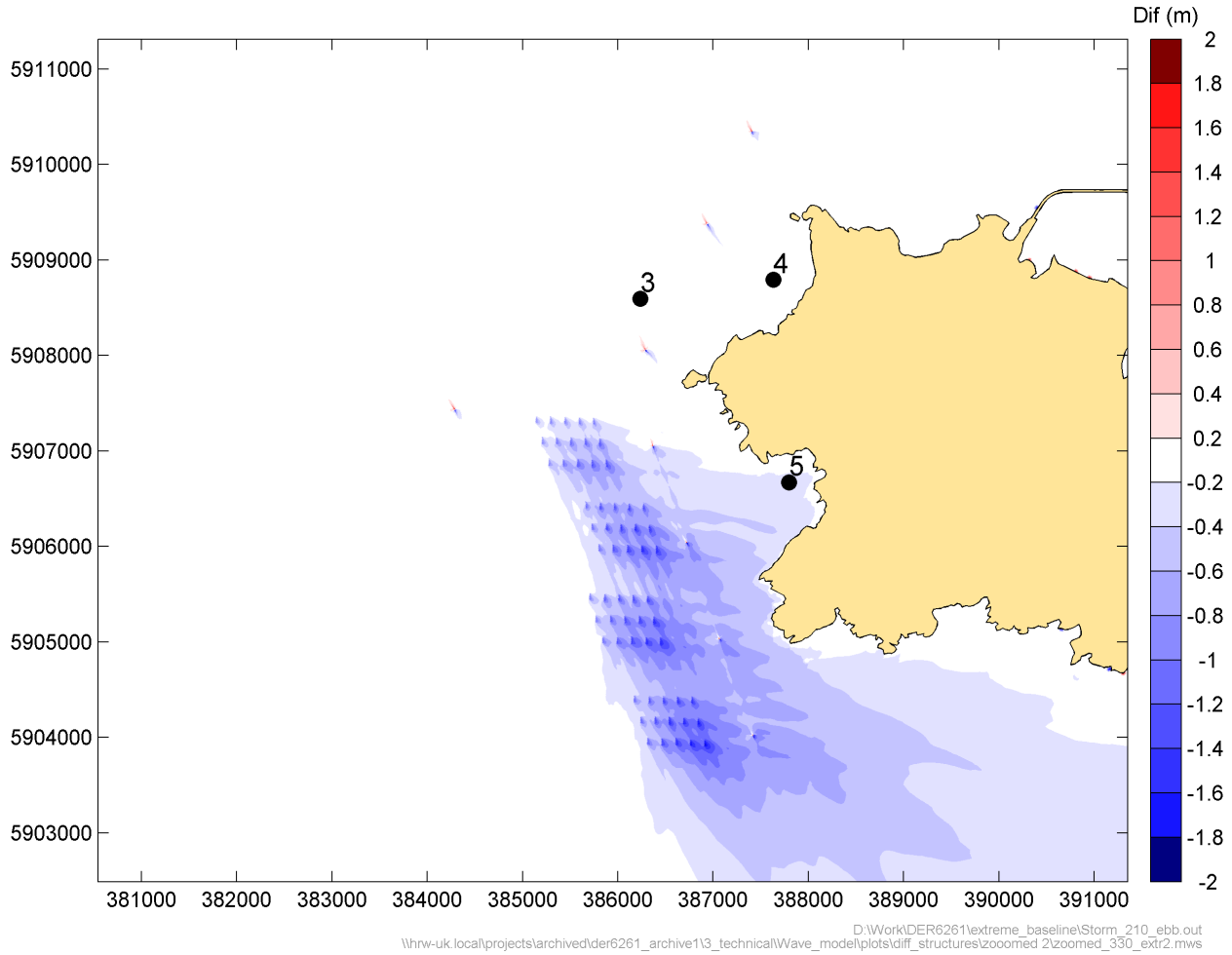

Figure B.10: Difference in wave height from 330°N for an extreme condition

B.2. Waves and tidal currents

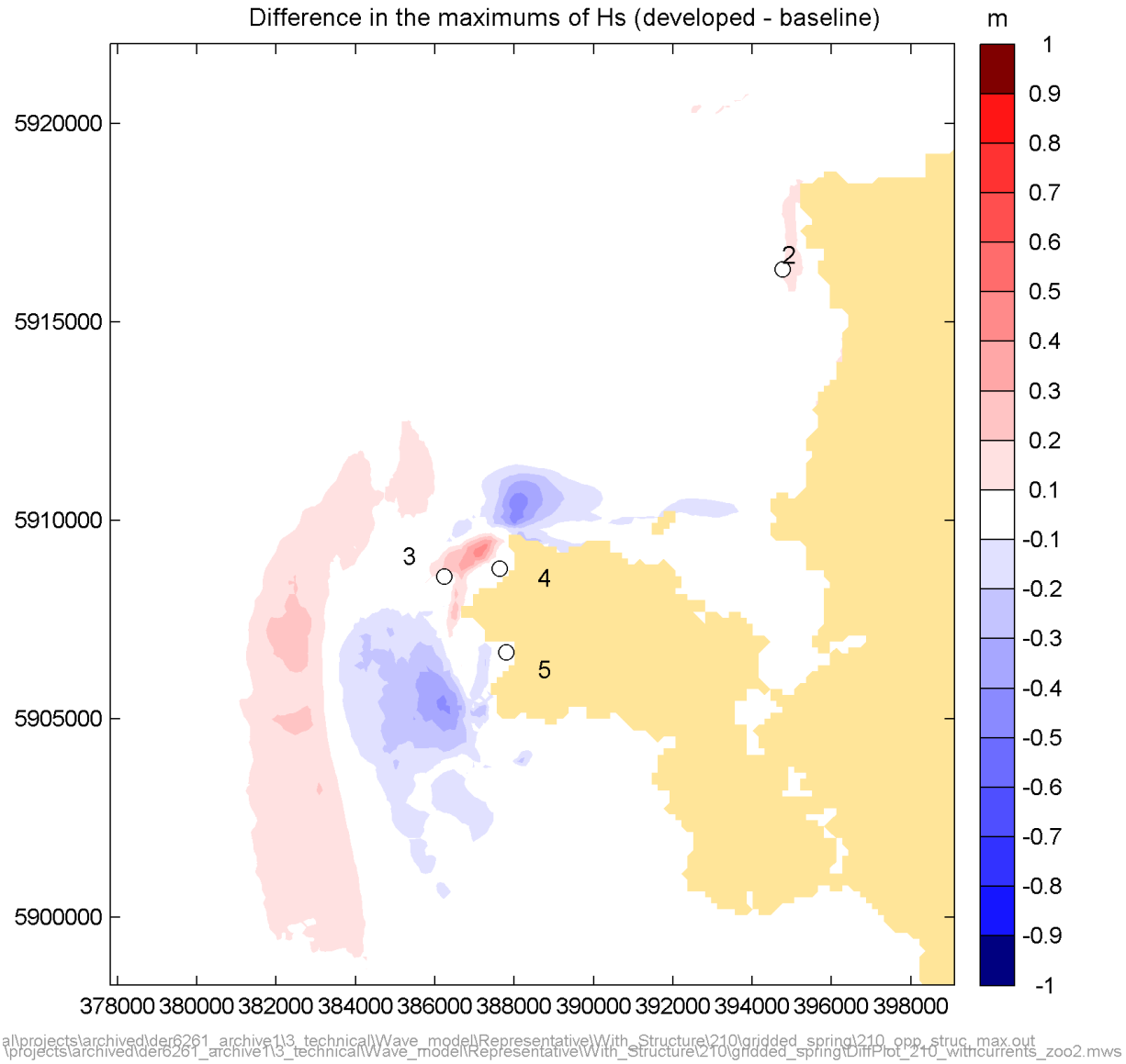

Figure B.11: Difference in the maximum wave height throughout a tidal cycle at each node for a wave direction from 210°N

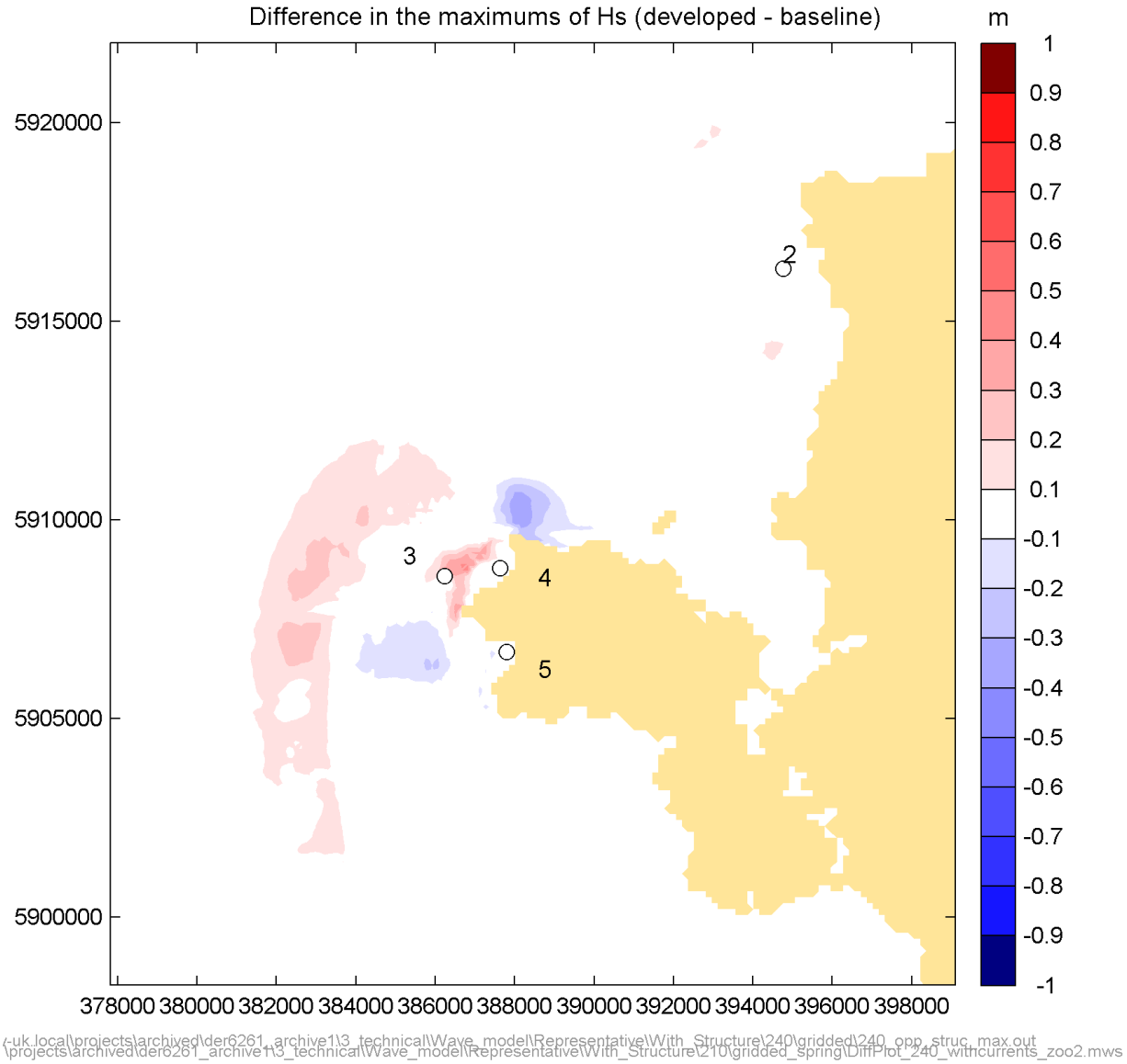

Figure B.12: Difference in the maximum wave height throughout a tidal cycle at each node for a wave direction from 240°N

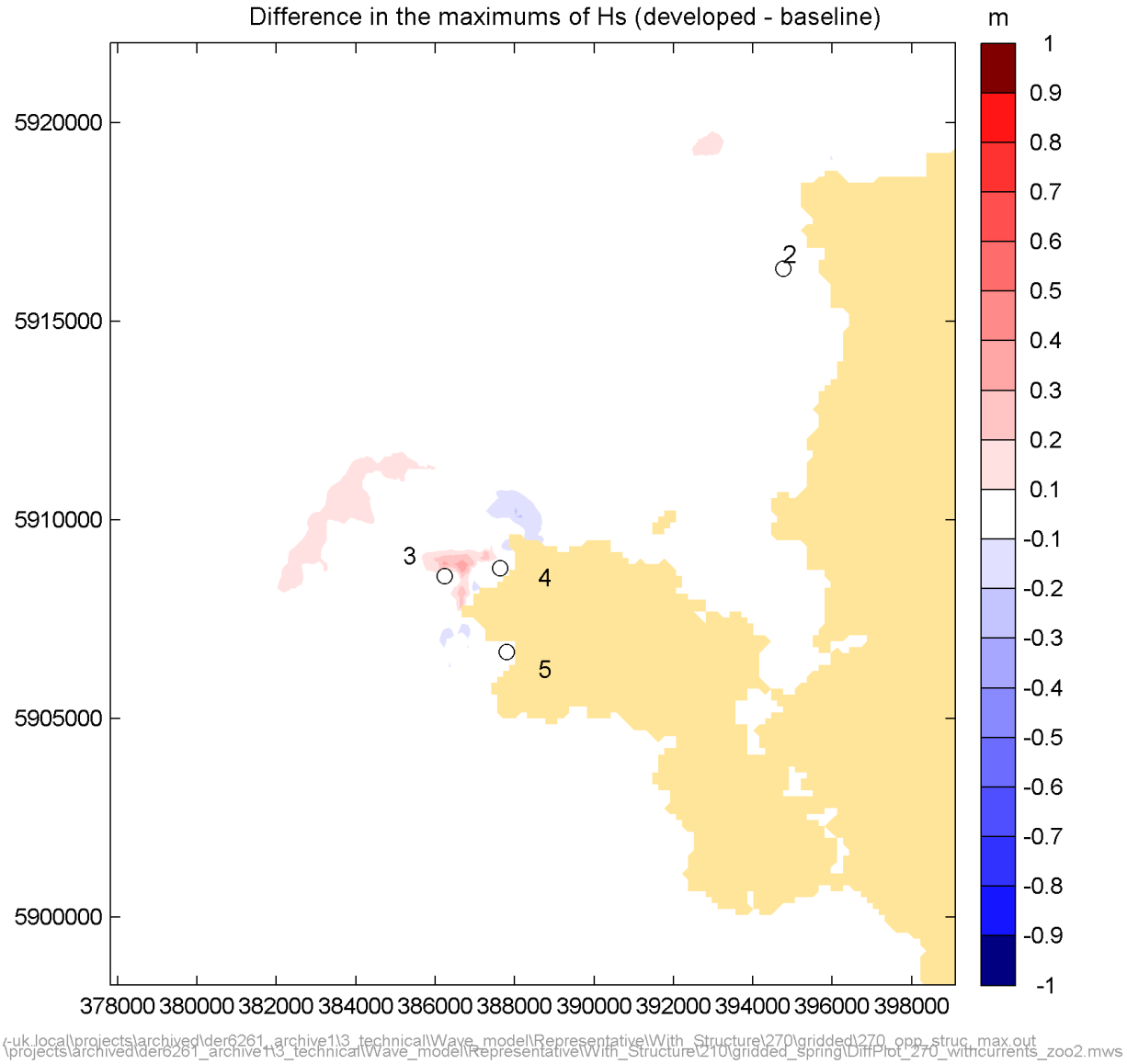

Figure B.13: Difference in the maximum wave height throughout a tidal cycle at each node for a wave direction from 270°N

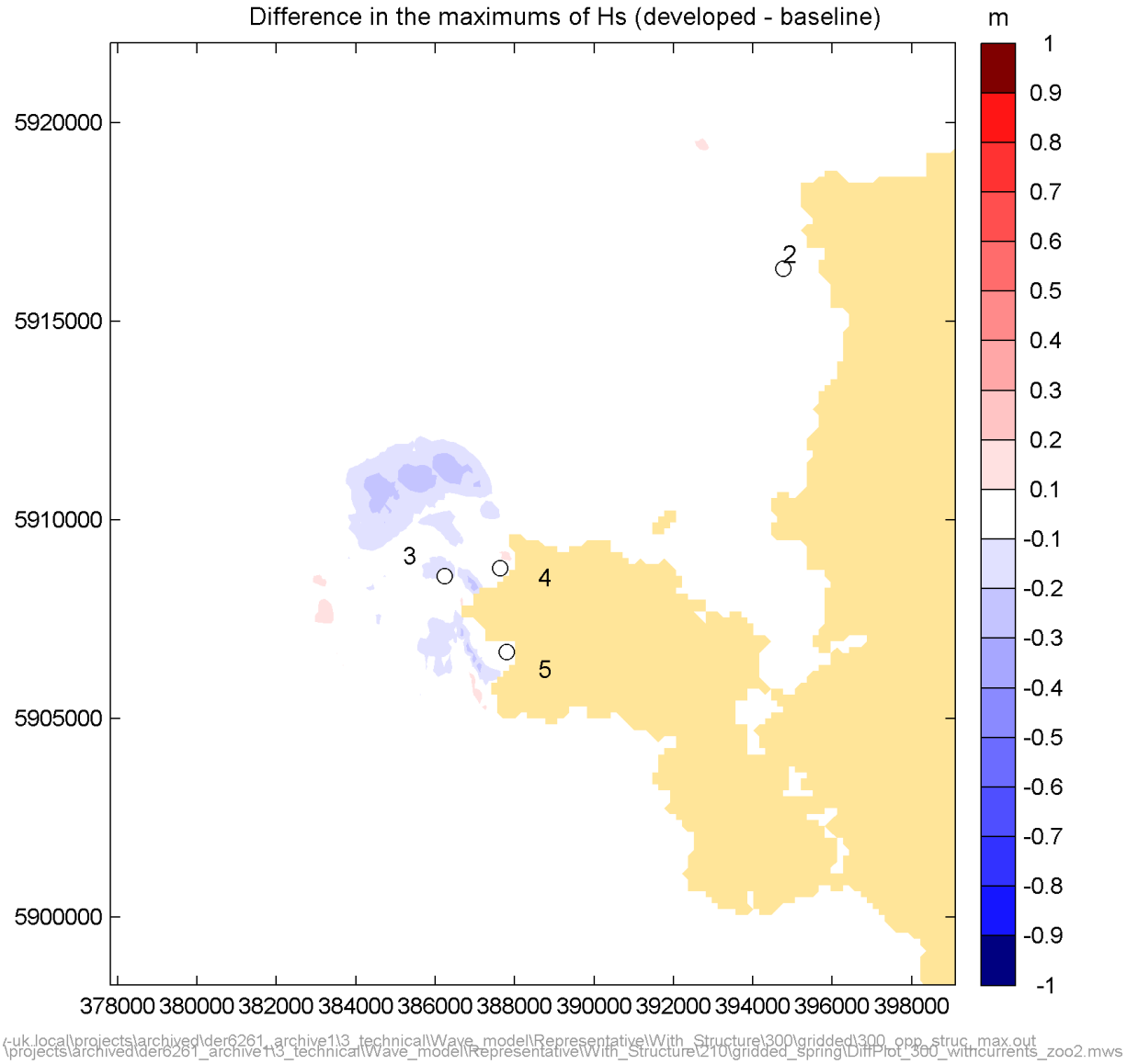

Figure B.14: Difference in the maximum wave height throughout a tidal cycle at each node for a wave direction from 300°N

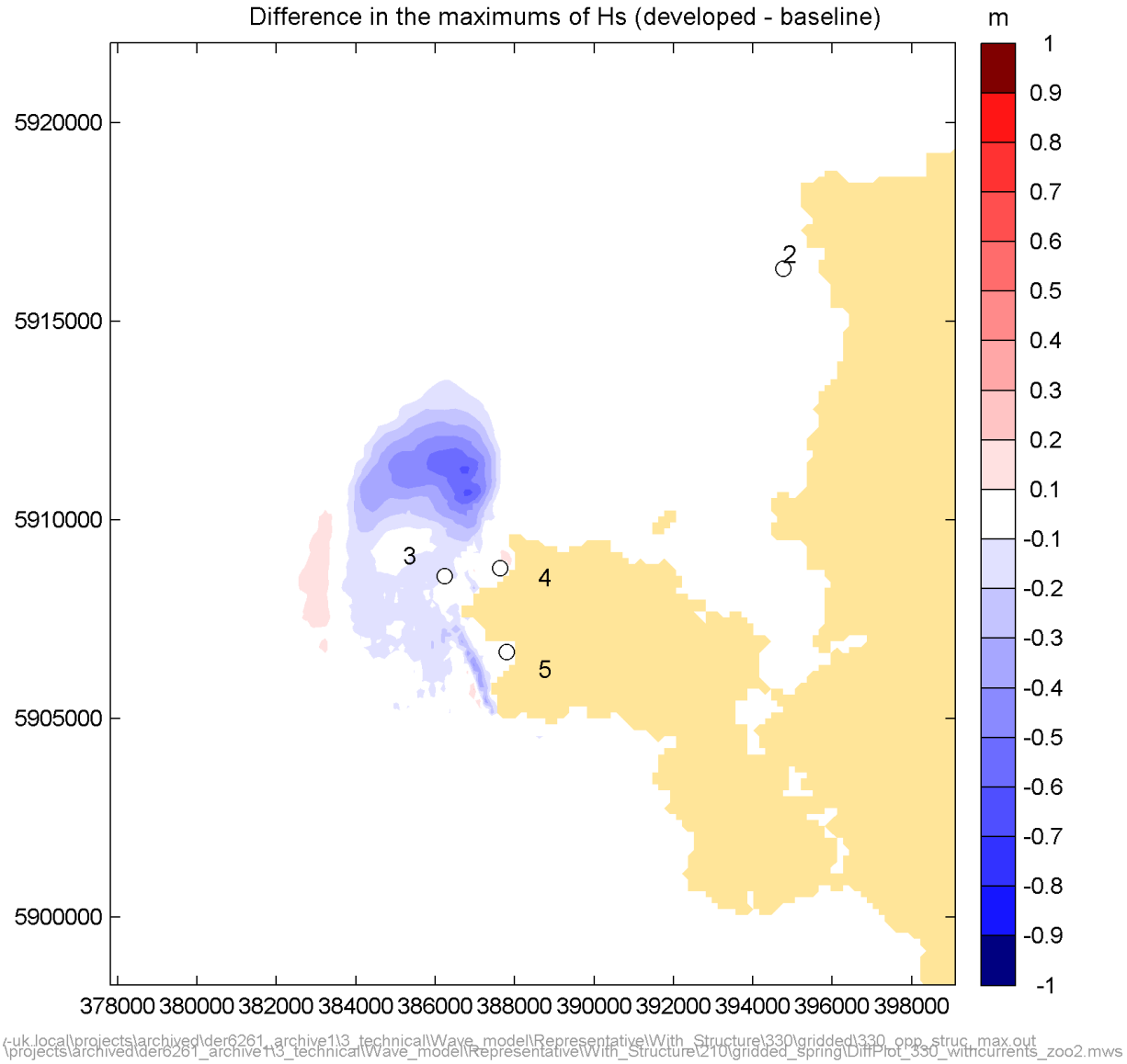

Figure B.15: Difference in the maximum wave height throughout a tidal cycle at each node for a wave direction from 330°N

HR Wallingford
Working with water

HR Wallingford is an independent engineering and environmental hydraulics organisation. We deliver practical solutions to the complex water-related challenges faced by our international clients. A dynamic research programme underpins all that we do and keeps us at the leading edge. Our unique mix of know-how, assets and facilities includes state of the art physical modelling laboratories, a full range of numerical modelling tools and, above all, enthusiastic people with world-renowned skills and expertise.

HR Wallingford, Howbery Park, Wallingford, Oxfordshire OX10 8BA, United Kingdom
tel +44 (0)1491 835381 fax +44 (0)1491 832233 email info@hrwallingford.com
www.hrwallingford.com

FS 516431
EMS 558310
OHS 595357